

# Resistance of cementitious materials to sulfate attack: quantifying performance with a reliable unidirectional approach

Présentée le 23 septembre 2022

Faculté des sciences et techniques de l'ingénieur  
Laboratoire des matériaux de construction  
Programme doctoral en science et génie des matériaux

pour l'obtention du grade de Docteur ès Sciences

par

## Qiao WANG

Acceptée sur proposition du jury

Prof. V. Michaud, présidente du jury  
Prof. K. Scrivener, W. Wilson, directeurs de thèse  
Prof. W. Kunther, rapporteur  
Dr C. Yu, rapporteur  
Dr D. Kulik, rapporteur

# Acknowledgements

Voilà, finalement, I finished this very unforgettable and challenging PhD project at EPFL. I had a very interesting, fantastic, beautiful, but at the same time also a tough four-year-long journey.

The story began with the first meeting with Karen in Wuhan, China in 2018 when there was no Covid yet. I was very happy to be accepted as a PhD student by Karen to join a lovely family, LMC. Of course, I always remembered that moment when I was confirmed to start my brand-new research life in Switzerland. I was worried to meet new people of different nationalities, excited to join a great top laboratory, and looking forward to developing my research competence. Karen, many thanks for your acceptance and your all guidance during the four years. Actually, I learnt things that are way beyond my expectation, I developed my English quite a lot, I can also speak French now (it was a very big issue in the first two years), I developed my patience, I learnt how to slow down to balance the work and life, I learnt new techniques (in research and in life). I am grateful to be a part of the LMC group.

I would like to thank all the jury members (Dr. Yu Cheng, Dr. Dmitrii Kulik, and Prof. Wolfgang Kunther) who attended my thesis defense and gave me constructive suggestions to improve my thesis, and thanks to Prof. Véronique Michaud who presided over my thesis defense.

I am very thankful to be the beneficiary of the China Scholarship Council (File No. 201806050061) and the funding from LMC to support my four years of study in Switzerland. That is quite important base assurance to let me have a steady life to devote to the research.

My co-supervisor, Prof. William Wilson, is of course a very important person whom I am always grateful to meet here. Thanks to your patience, especially at the beginning of my PhD, thanks to your very useful comments on the building journey of my PhD thesis, physically in the seminar room on Monday afternoons as well as the virtual Zoom meeting on Tuesday afternoons (They were in the mornings in Canada time:). I really enjoyed discussing with you every single time, that helped me a lot, no matter on the research, or on the thinking, writing and so on. My thesis would not be made successfully without all your effort and support at any time. I cannot appreciate more your contribution during this fun and long journey. I also would like to take this chance to thank Dr. Dmitrii and Prof. Barbara who helped me with the thermodynamic modelling.

The big family LMC, I will never forget all your lovely faces. First, I have to thank Dr. Sarra who was the first person to give me a hand in the darkness at the beginning, with all the help showing me the road, reminding

me of the registration process, call for me in French whenever it was necessary. All your support that did for me to look for a new apartment, I really appreciated. My first office mates in MXG 241, thanks to all the kind and helpful girls, Natechanok, Mahsa, Solène, I remember all the nice tea breaks that we had together. My second office mate in MXG 235, Franco always offered the “gossip” to add a bit of fun during the lunches and breaks, we had hot-pots (a very spicy one, well done!) and many times Chinese restaurant experiences. We also had a few short-stay people in our office, Eloïse, Dhanush. Andrea, we always encourage each other to continue our PhD when it was tough. Khalil, Maya, we all passed through the very tough Covid time during our PhDs. I will remember all the faces of my sisters and brothers at LMC, thanks to Diana, Emmanuelle, Junjie, Fabien, Yan Yu, Mink, Jinhui, François, Diandian, Shiyu, Meenakshi, Joseph, Beatrice, Lenka, Jinfeng, Hisham, Mai, Chaoqi, Silas, Junmei, Yosra, Julien, Alex Ouzia, Alex Pîrvan... I also need to thank all my students who did great work to help me, Edgar, Charlotte, and Félix.

I am also grateful for all the support from our great secretary staff, Maude and Mirabella always tried to share the information and help me a lot. Fabio, Adrien, Tumasch you are very nice to help whenever I needed. Thanks to John for solving all the computer problems. I cannot accomplish the experimental tasks without the help of Lionel (always transfer the good mood to everyone), Jean, Antonino (merci aussi de m'avoir conduit à Vevey pour mon déménagement).

Last but not least, the support from my family is very important for me to encourage me to move forward. We missed quite a lot of time to be together, but we saw and talked to each other during the weekends. I remember all the laughs and fun that we had in the video calls with my parents and sister, and the cute faces of my nieces. That was a quite strong power behind me. Especially, I need to thank my lovely wife, you are always supportive and kind during the four years. I cannot imagine how could I finish my PhD without your company. You are the best! 感谢我的老婆!

Lausanne, le 2 Septembre 2022

# Abstract

Depending on the environmental conditions, concrete materials can come into contact with sulfate ions which are widely present in rivers, underground water, sewers, seawater and soil. Sulfates can react with the cement paste in concrete and cause damage which impacts the service life of concrete structures. Cement chemistry, transport of sulfate ions, and physical properties of the host material all interact in the complex process of sulfate degradation. Given different conditions of concrete exposure, sulfate attack is commonly divided into “chemical” and “physical” sulfate attack. However, the processes are not fully understood and there is still a need for in-depth investigations of the whole deterioration process.

The current standard testing method is adapted for Portland cement systems affected by the “chemical sulfate attack” in submerged conditions. However, only expansion is monitored, which is not suitable for characterizing the increasingly common usage of supplementary cementitious materials in the cement. Moreover, several key factors (e.g., RH & temperature) are usually overlooked so lab tests do not well represent the field conditions. Particularly, the understanding of the damaging mechanism of “physical sulfate attack” is very limited even if different testing approaches have been established. The division into “chemical” and “physical” attack is in itself misleading. In this context, this research project was launched to establish a uni-directional penetration approach for the in-depth comprehensive investigation of joint sulfate attack mechanisms.

First, the feasibility of this newly established approach was studied for Portland cement mortars and pastes. A high concentration of sulfate solution and a high water-to-cement ratio was chosen to accelerate the degradation and to obtain results in a reasonable period. Results showed that this new concept of combining chemical and physical sulfate attack mechanisms into a single experiment was viable. Moreover, results showed that using cement paste samples can accelerate the degradation, compared to mortar samples. The sulfate degradation process was more rapid with the capillary rise and water evaporation.

A comparison of the macroscopic manifestation of damage (visual appearance and expansion) with the underlying microscopic changes was made considering different key parameters, i.e., water-to-cement ratio, exposure solution concentration, cement type, temperature and humidity conditions (constant or cyclic).

Regarding the different cement types, Ordinary Portland cement pastes and sulfate-resisting cement pastes showed higher expansion and cracking, whereas, spalling damage was more pronounced in blended-cement pastes/mortars (slag Portland cement and limestone calcined clay cement). Damage from the chemical attack

was more extensive and rapid when high concentrations and cyclic exposure conditions were applied. However, lower water-to-cement ratios leading to lower porosity and/or higher mechanical strength could usually reduce the extent of the damage. Thermodynamic modelling was also conducted with GEMS to better explain the pore solution environment and the link between supersaturation and expansion. The interacting factors of porosity and strength were decoupled.

The effect of the curing temperature on the expansion mechanism was also investigated in sulfate-resisting cement mortars under submerged sulfate exposure.

Overall, this thesis presents a more representative and versatile tool to study sulfate attack under conditions similar to field conditions. The mutual influence between chemical and physical attack was explored, and some insights into the salt crystallization mechanism were obtained.

## Keywords

Sulfate Ingress, Sulfate Attack, Unidirectional Penetration Approach, Degradation, Expansion, Spalling, Carbonation, Blended cement, EDXIA, Microstructure Phase Profiles, Thermodynamic modelling.

# Résumé

Selon les conditions environnementales, les matériaux en béton peuvent entrer en contact avec des ions sulfates qui sont largement présents dans les rivières, les eaux souterraines, les égouts, l'eau de mer et le sol. Les sulfates peuvent réagir avec la pâte de ciment du béton et causer des dommages qui ont un impact sur la durée de vie des structures en béton. La chimie du ciment, le transport des ions sulfates et les propriétés physiques du matériau hôte interagissent tous dans le processus complexe de dégradation des sulfates. Compte tenu des différentes conditions d'exposition du béton, l'attaque par les sulfates est communément divisée en attaque "chimique" et "physique". Cependant, les processus ne sont pas entièrement compris et il est encore nécessaire de mener des études approfondies sur l'ensemble du processus de détérioration.

La méthode d'essai standard actuelle est adaptée aux systèmes de ciment Portland affectés par l'"attaque chimique au sulfate" dans des conditions d'immersion. Cependant, seule l'expansion est surveillée, ce qui ne convient pas pour caractériser l'utilisation de plus en plus courante de matériaux cimentaires supplémentaires dans le ciment. En outre, plusieurs facteurs clés (par exemple, l'humidité relative et la température) sont généralement négligés, de sorte que les essais en laboratoire ne représentent pas bien les conditions sur le terrain. En particulier, la compréhension du mécanisme d'endommagement de l'"attaque physique au sulfate" est très limitée, même si différentes approches d'essai ont été établies. La division en attaques "chimiques" et "physiques" est en soi trompeuse. Dans ce contexte, ce projet de recherche a été lancé pour établir une approche de pénétration uniaxiale pour une investigation approfondie des mécanismes d'attaque conjointe par le sulfate.

Tout d'abord, la faisabilité de cette approche nouvellement établie a été étudiée pour les mortiers et les pâtes de ciment Portland. Une concentration élevée de solution de sulfate et un rapport eau/ciment élevé ont été choisis pour accélérer la dégradation et obtenir des résultats dans un délai raisonnable. Les résultats ont montré que ce nouveau concept combinant les mécanismes d'attaque chimique et physique des sulfates en une seule expérience était viable. De plus, les résultats ont montré que l'utilisation d'échantillons de pâte de ciment peut accélérer la dégradation, par rapport aux échantillons de mortier. Le processus de dégradation des sulfates était plus rapide avec la montée capillaire et l'évaporation de l'eau.

Une comparaison de la manifestation macroscopique des dommages (apparence visuelle et expansion) avec les changements microscopiques sous-jacents a été faite en considérant différents paramètres clés, c'est-à-

dire le rapport eau/ciment, la concentration de la solution d'exposition, le type de ciment, la température et les conditions d'humidité (constantes ou cycliques).

En ce qui concerne les différents types de ciment, les pâtes de ciment Portland ordinaire et les pâtes de ciment résistant aux sulfates ont montré une expansion et une fissuration plus importantes, tandis que les dommages dus à l'écaillage étaient plus prononcés dans les pâtes/mortiers de ciment mélangé (ciment Portland au laitier et ciment d'argile calciné au calcaire). Les dommages causés par les attaques chimiques étaient plus étendus et plus rapides lorsque des concentrations élevées et des conditions d'exposition cycliques étaient appliquées. Cependant, des rapports eau/ciment plus faibles conduisant à une porosité plus faible et/ou une résistance mécanique plus élevée pouvaient généralement réduire l'étendue des dommages. Une modélisation thermodynamique a également été réalisée avec GEMS pour mieux expliquer l'environnement de la solution des pores et le lien avec la sursaturation et l'expansion. Les facteurs d'interaction de la porosité et de la résistance ont été découplés.

L'effet de la température de durcissement sur le mécanisme d'expansion a également été étudié dans des mortiers de ciment résistant au sulfate sous une exposition submergée au sulfate.

Dans l'ensemble, cette thèse présente un outil plus représentatif et polyvalent pour étudier l'attaque au sulfate dans des conditions similaires à celles du terrain. L'influence mutuelle entre l'attaque chimique et l'attaque physique a été explorée, et certains aperçus du mécanisme de cristallisation du sel ont été obtenus.

## Mots-clés

Pénétration de sulfate, attaque de sulfate, approche de pénétration uniaxiale, dégradation, expansion, écaillage, carbonatation, ciment mélangé, EDXIA, profils de phase de la microstructure, modélisation thermodynamique.

# 摘要

根据环境条件，混凝土材料可能会接触到广泛存在于河流、地下水、下水道、海水和土壤中的硫酸盐离子。硫酸盐会与混凝土中的水泥净浆发生反应，造成损害，影响混凝土结构的使用寿命。在复杂的硫酸盐降解过程中，水泥的化学性质、硫酸盐离子的传输以及宿主材料的物理特性都会相互影响。鉴于混凝土暴露的条件不同，硫酸盐侵蚀通常被分为"化学"和"物理"硫酸盐侵蚀。然而，这些过程还没有被完全理解，仍然需要对整个退化过程进行深入调查。

目前的标准测试方法适用于受"化学硫酸盐侵蚀"影响的波特兰水泥系统在全浸泡状态下的性能测试。然而，只对膨胀进行监测，这并不适合用来描述水泥中越来越普遍的矿物胶凝材料的使用。此外，一些关键因素（如相对湿度和温度）通常被忽略了，所以实验室测试不能很好地代表现场条件。特别是，即使已经建立了不同的测试方法，对"物理硫酸盐侵蚀"的破坏机理的理解也非常有限。将硫酸盐侵蚀分为"化学"和"物理"侵蚀本身就是一种误导。在这种情况下，本研究项目的启动是为了建立一种单轴穿透法，以深入全面地调查联合硫酸盐侵蚀机理。

首先，研究了这种新建的方法对波特兰水泥砂浆和净浆的可行性。选择了高浓度的硫酸盐溶液和高水灰比来加速降解，并在合理的时间内获得实验结果。结果表明，这种将化学和物理硫酸盐侵蚀机理结合到一个单一实验中的新概念是可行的。此外，与砂浆样品相比，使用水泥浆样品可以加速降解。随着毛细管作用和水份蒸发的结合，硫酸盐的降解过程更加迅速。

考虑到不同的关键参数，即水灰比、浸泡溶液浓度、水泥类型、温度和湿度条件（恒定或循环），对损害的宏观表现（视觉外观和膨胀）与潜在的微观变化进行了比较。

关于不同的水泥类型，普通硅酸盐水泥浆和抗硫酸盐水泥净浆显示出较高的膨胀和开裂，而在混合水泥净浆/砂浆（矿渣硅酸盐水泥和石灰石煅烧粘土水泥）中，表皮剥落损坏更加明显。当采用高浓度和循环暴露条件时，化学侵蚀的破坏更广泛和迅速。然而，较低的水灰比导致较低的孔隙率和/或较高的力学强度通常可以减少破坏的程度。使用 GEMS 进行了热力学建模，以更好地解释孔隙溶液环境以及与过饱和度和膨胀的联系。孔隙率和强度的相互作用因素被解耦。

在全浸泡式硫酸盐暴露条件下，研究了养护温度对抗硫酸盐水泥砂浆膨胀机理的影响。

总的来说，该博士论文提出了一个更具代表性和通用性的工具来研究类似于现场条件下的硫酸盐侵蚀。探讨了化学和物理腐蚀之间的相互影响，并对硫酸盐的结晶机理有了一些深入的了解。



## 关键词

硫酸盐侵入, 硫酸盐腐蚀, 单轴渗透法, 降解, 膨胀, 剥落, 碳化, 复合水泥, EDXIA, 微观结构剖面相貌, 热力学模型。

# Contents

<b>Acknowledgements</b> .....	<b><i>i</i></b>
<b>Abstract</b> <b><i>iii</i></b>	
<b>Résumé</b> <b><i>v</i></b>	
<b>摘要</b> <b><i>vii</i></b>	
<b>List of Figures</b> .....	<b><i>xiii</i></b>
<b>List of Tables</b> .....	<b><i>xviii</i></b>
<b>Glossary</b> <b><i>xix</i></b>	
<b>Chapter 1 Introduction</b> .....	<b><i>21</i></b>
<b>1.1 Background</b> .....	<b><i>22</i></b>
<b>1.2 Motivations of the thesis</b> .....	<b><i>22</i></b>
<b>1.3 Objectives and innovations</b> .....	<b><i>22</i></b>
<b>1.4 Synopsis of the thesis</b> .....	<b><i>23</i></b>
<b>Chapter 2 State of the Art</b> .....	<b><i>24</i></b>
<b>2.1 Introduction</b> .....	<b><i>25</i></b>
<b>2.2 What is sulfate attack ?</b> .....	<b><i>27</i></b>
<b>2.3 External sulfate attack</b> .....	<b><i>31</i></b>
2.3.1 The expansion mechanism .....	<b><i>31</i></b>
2.3.2 The degradation mechanism .....	<b><i>33</i></b>
<b>2.4 Parameters influencing sulfate attack</b> .....	<b><i>40</i></b>
<b>2.5 Current testing methods</b> .....	<b><i>43</i></b>
<b>2.6 Evaluation criteria for sulfate resistance of cementitious materials</b> .....	<b><i>46</i></b>
<b>2.7 Summary and knowledge gaps</b> .....	<b><i>47</i></b>
<b>2.8 Reference</b> .....	<b><i>51</i></b>
<b>Chapter 3 Materials and experimental methods</b> .....	<b><i>55</i></b>
<b>3.1 Materials</b> .....	<b><i>57</i></b>
3.1.1 Cement types .....	<b><i>57</i></b>

3.1.2	Particle size distributions of cements.....	57
<b>3.2</b>	<b>Sample preparation .....</b>	<b>58</b>
3.2.1	Paste samples.....	58
3.2.2	Mortar samples .....	58
<b>3.3</b>	<b>Setups.....</b>	<b>59</b>
3.3.1	Sodium sulfate solution.....	59
3.3.2	Conventional setup for full immersion test.....	59
3.3.3	Unidirectional setup for semi-immersion test .....	59
<b>3.4</b>	<b>Macroscopic observations .....</b>	<b>60</b>
3.4.1	Visual inspections .....	60
3.4.2	Mass change and expansion.....	61
<b>3.5</b>	<b>Microscopic observations .....</b>	<b>62</b>
3.5.1	Scanning Electron microscopy.....	62
3.5.2	X-ray diffraction.....	63
<b>3.6</b>	<b>Mercury intrusion porosimetry .....</b>	<b>64</b>
<b>3.7</b>	<b>Mechanical strength .....</b>	<b>64</b>
<b>3.8</b>	<b>Adsorption and desorption .....</b>	<b>64</b>
<b>3.9</b>	<b>References.....</b>	<b>65</b>
<b>Chapter 4</b>	<b><i>New unidirectional penetration approach.....</i></b>	<b>66</b>
<b>4.1</b>	<b>Introduction .....</b>	<b>68</b>
<b>4.2</b>	<b>Materials and experimental approaches .....</b>	<b>69</b>
4.2.1	Materials and sample preparation .....	69
4.2.2	The new semi-immersion setup .....	70
4.2.3	Expansion measurements .....	71
4.2.4	Scanning electron microscopy (SEM) .....	72
4.2.5	X-ray diffraction (XRD) analyses .....	72
<b>4.3</b>	<b>Results and discussion .....</b>	<b>73</b>
4.3.1	Visual observations .....	73
4.3.2	Expansion as a function of depth and time .....	74
4.3.3	Progress of the degradation processes from the chemical and phase profiles.....	75
4.3.4	Discussion.....	81
<b>4.4</b>	<b>Conclusions.....</b>	<b>85</b>
<b>4.5</b>	<b>References.....</b>	<b>86</b>
<b>Chapter 5</b>	<b><i>Macroscopic and microscopic results – Key variables .....</i></b>	<b>88</b>
<b>5.1</b>	<b>Introduction .....</b>	<b>89</b>
<b>5.2</b>	<b>The effect of the w/c and the sulfate concentration.....</b>	<b>90</b>
5.2.1	Visual inspections .....	90
5.2.2	Expansion and mass gain.....	91
5.2.3	Sulfate ingress as a function of exposure time.....	93
5.2.4	Sulfate ingress rate.....	95

5.2.5	Phase change as a function of depth and time .....	96
<b>5.3</b>	<b>The effect of the cement type .....</b>	<b>98</b>
5.3.1	Chemical properties before sulfate exposure .....	98
5.3.2	Physical changes after sulfate exposure.....	100
5.3.3	Chemical changes after sulfate exposure.....	104
5.3.4	Sulfate ingress as a function of exposure time.....	106
5.3.5	Salt crystallization.....	111
<b>5.4</b>	<b>The comparison of constant and cycling exposure conditions .....</b>	<b>116</b>
5.4.1	Physical behaviours after sulfate exposure.....	116
5.4.2	Chemical changes after sulfate exposure.....	119
<b>5.5</b>	<b>Conclusions.....</b>	<b>129</b>
<b>Chapter 6</b>	<b><i>Chemical thermodynamic modelling .....</i></b>	<b>130</b>
<b>6.1</b>	<b>Introduction .....</b>	<b>132</b>
<b>6.2</b>	<b>The theory of crystallization pressure .....</b>	<b>132</b>
<b>6.3</b>	<b>Thermodynamic modelling .....</b>	<b>135</b>
6.3.1	Thermodynamic calculations in equilibrium conditions.....	135
6.3.2	Saturation index from ettringite.....	140
<b>6.4</b>	<b>Estimation of the crystallization pressure profile of ettringite.....</b>	<b>142</b>
6.4.1	Crystallization pressure from experimental .....	142
6.4.2	Crystallization pressure calculated from saturation index .....	145
6.4.3	The link between crystallization pressure development and macroscopic observations .....	146
<b>6.5</b>	<b>Salt crystallization of sodium sulfate in the carbonated and drying front .....</b>	<b>147</b>
6.5.1	Susceptibility of salt crystallization in Portland cement.....	148
6.5.2	Comparisons between different cement pastes with 50 g/L Na <sub>2</sub> SO <sub>4</sub> in porewater .....	150
<b>6.6</b>	<b>Conclusions.....</b>	<b>152</b>
<b>6.7</b>	<b>References.....</b>	<b>153</b>
<b>Chapter 7</b>	<b><i>Discussion .....</i></b>	<b>154</b>
<b>7.1</b>	<b>Introduction .....</b>	<b>155</b>
<b>7.2</b>	<b>Porosity measured by mercury intrusion porosimetry (MIP) .....</b>	<b>156</b>
<b>7.3</b>	<b>Mechanical strength .....</b>	<b>159</b>
<b>7.4</b>	<b>The interaction between porosity and strength in controlling expansion/cracking.....</b>	<b>162</b>
<b>7.5</b>	<b>Water adsorption and desorption .....</b>	<b>163</b>
7.5.1	Sulfate ingress versus water adsorption .....	165
<b>7.6</b>	<b>The interplay between chemical and physical attack.....</b>	<b>165</b>
<b>7.7</b>	<b>Comments on the observed physical sulfate attack in this project .....</b>	<b>166</b>
<b>7.8</b>	<b>References.....</b>	<b>167</b>
<b>Chapter 8</b>	<b><i>Sulfate-resisting cement mortar in full immersion test .....</i></b>	<b>168</b>
<b>8.1</b>	<b>Introduction .....</b>	<b>170</b>

---

<b>8.2</b>	<b>Materials and methods</b> .....	<b>171</b>
8.2.1	Types of cement.....	171
8.2.2	Methods.....	172
<b>8.3</b>	<b>Results and discussion</b> .....	<b>175</b>
8.3.1	Expansion.....	175
8.3.2	Effect of temperature on initial hydrates and distribution.....	175
8.3.3	Effect of curing temperature on sulfate ingress.....	179
8.3.4	Comparison of C-S-H compositions before and after expansion.....	181
<b>8.4</b>	<b>Conclusions</b> .....	<b>183</b>
<b>8.5</b>	<b>References</b> .....	<b>185</b>
<b>Chapter 9</b>	<b>Conclusions</b> .....	<b>186</b>
9.1	Feasibility of the new unidirectional semi-immersion test (Chapter 4).....	187
9.2	Macroscopic and microscopic findings (Chapter 5 and Chapter 8).....	187
9.3	General discussion (Chapter 6 and Chapter 7).....	189
9.4	Perspectives.....	190
<b>Appendix</b>	<b>191</b>	
<b>Curriculum Vitae</b> .....		<b>192</b>

## List of Figures

Fig. 2-1 Thermodynamic model of hydration of Portland cement [3].	25
Fig. 2-2 Measured concentrations in the pore solutions of sulfate resisting Portland cement (SRPC) hydrated at 5, 20, 50 °C, adapted from [10].	26
Fig. 2-3 Schematic diagram of chemical sulfate attack interactions between sodium sulfate solution and exposed cement pastes [17].	28
Fig. 2-4 Phase assemblage of the mortar samples immersed in A) 4 g/L Na <sub>2</sub> SO <sub>4</sub> and B) 44 g/L Na <sub>2</sub> SO <sub>4</sub> as calculated with GEMS [21].	29
Fig. 2-5 Phase diagram for sodium sulfate, adapted from [11].	30
Fig. 2-6 Spalling damage examples caused by sodium sulfate crystallization: a) Surface scaled on a concrete foundation stem wall coated with latex paint [33], b) A building wall spalled with sodium sulfate deposit, coated with paint found in Pully, Switzerland.	31
Fig. 2-7 The influence of pH on gypsum formation, adapted from [46].	33
Fig. 2-8 Proposed degradation process of sodium sulfate attack, adapted from [15].	35
Fig. 2-9 The relation between expansion and tensile stress, adapted from [40].	37
Fig. 2-10 ESEM image of thenardite on the surface of a cement paste sample [61] (left); thenardite on a decayed limestone spall fragment [24] (middle); and formation of large grape-like mirabilite clusters due to growth of mirabilite on the small thenardite crystallites as nucleation sites in sandstones [30] (right).	38
Fig. 2-11 Solubility of anhydrous sodium sulfate in water as a function of temperature [28].	39
Fig. 2-12 The schematic diagram of semi-immersion test for a concrete block, adapted from [4].	45
Fig. 2-13 Granular disintegration of the salt-contaminated sandstone [30].	45
Fig. 2-14 The schematic of possible evaluations for sulfate resistance.	47
Fig. 3-1 Particle size distribution of raw materials measured by laser diffraction.	58
Fig. 3-2 Full immersion test container with 4 mortar prisms.	59
Fig. 3-3 Experimental set-up for the unidirectional sulfate penetration test: (a) top view of the setup; (b) side view of setup; (c) cement mortar, (d) cement paste.	60
Fig. 3-4 Radial expansion measurement: (a) measure the expansion by using a calliper; (b) steel rings with a thickness of 1mm.	61
Fig. 3-5 The expansion measurement of the mortar prism in the submerge test.	61
Fig. 3-6 The example process of a sample twice impregnation in epoxy: a) the first entire sample impregnation, b) cut perpendicularly into the desired slice of 3 mm thickness, c) the second impregnation with the thin slice.	62
Fig. 3-7 The example of the points selection on the outer C-S-H phase done with paste PC06 at 28 days of hydration.	63
Fig. 3-8 Mortar samples for water adsorption and evaporation testing.	65
Fig. 4-1 Experimental set-up for the unidirectional sulfate penetration test: (a) top view of the setup; (b) side view of setup; (c) cement mortar, (d) cement paste.	71

Fig. 4-2 Radial expansion measurement: (a) measure the expansion by using a calliper; (b) steel rings with a thickness of 1mm.....	72
Fig. 4-3 Visual observations of Portland cement mortar samples after unidirectional exposure to the sulfate solution: (a,b,c) top surface views and (d,e,f) bottom surface views of (a,d) the PC mortar sample at 56d, (b,e) the PC mortar sample at 112d and (c,f) PC mortar sample at 140d. The arrow indicates the capillary rise direction.....	73
Fig. 4-4 Visual observations of Portland cement paste samples after unidirectional exposure to the sulfate solution: (a,b,c) top surface views and (d,e,f) bottom surface views of (a,d) the PC paste sample at 56d, (b,e) the PC paste sample at 91d and (c,f) the PC paste sample at 112d. The arrow indicates the capillary rise direction.....	74
Fig. 4-5 Expansion profiles after exposure: (a) cement mortar & cement paste normalised by 38%; (b) cement paste. .	75
Fig. 4-6 PC paste samples with the entire 5mm-depth profiles after 28 days of exposure: (a) BSE micrograph, (b) sulfur concentration presence, (c) sodium concentration presence, (d) phase distribution, (e) phase profile, (f) phase assemblage profile from XRD.....	77
Fig. 4-7 PC mortar samples with the entire 10mm-depth profiles after exposure: (a) phase distribution after 56 days, (b) phase profiles after 56 days, (c) phase distribution after 112 days, (d) phase profiles after 112 days, (e) phase distribution after 140 days, (f) phase profiles after 140 days. Blue scales on the bottom are recalibrated to 10 mm. ....	80
Fig. 4-8 PC paste samples with the entire 5mm-depth profiles after exposure: (a) phase distribution after 56 days, (b) phase profiles after 56 days, (c) phase distribution after 114 days, (d) phase profiles after 114 days. Blue scales on the bottom are recalibrated to 5 mm. ....	81
Fig. 4-9 Schematic diagram of sulfate attack degradation model on cement mortar and paste. ....	82
Fig. 4-10 The content of Na and S of the entire sample exposed to relative humidity of 55 %, showing signs of thenardite precipitation at 114d: a) profile of Na/S ratio; b) relative content profile of Na and S. Blue scales on the bottom are recalibrated.....	84
Fig. 5-1 Visual inspections of cement pastes with w/c of 0.4 & 0.6 exposed for 91 days (250 days for the w/c ratio of 0.3) to sulfate concentration of 3 & 50 g/L.....	90
Fig. 5-2 Expansion over the depth of the PC pastes at different w/c ratios and sulfate concentrations, a) PC pastes at 3 g/L, b) PC pastes at 50 g/L. ....	92
Fig. 5-3 a) Expansion rate and b) mass variations over time for cement paste samples exposed to different sulfate concentrations. ....	92
Fig. 5-4 Sulfate expansion take-off time as a function of the W/C ratios. The lines only serve as eye guide.....	93
Fig. 5-5 Sulfur profile maps after exposure to different sulfate concentrations with different w/c ratios.....	94
Fig. 5-6 The atomic ratio S/Ca profiles of main hydrates C-S-H based on the long sulfur maps. ....	95
Fig. 5-7 The S ingress depth as a function of days <sup>1/2</sup> for different PC systems with various w/c ratios and solution concentrations. ....	96
Fig. 5-8 Specific phase contents (ettringite, gypsum, portlandite and thenardite, in g/100 g paste) as a function of the depth by sulfate ingress. Lines serve as eye-guide only. ....	97
Fig. 5-9 Hydrates distribution in different cement pastes at w/c 0.6 after 28 days of hydration: a) PC, b) HS, c) SPC, d) LC <sup>3</sup> .....	98

---

Fig. 5-10 Chemical compositions of C-(A)-S-H hydrates in cements: a) PC, b) HS, c) SPC, d) LC <sup>3</sup> -50. Lines serve for eye-guide only.....	99
Fig. 5-11 Phase assemblages before sulfate ingress in for the different cement pastes at w/c ratios of 0.4 and 0.6. ....	100
Fig. 5-12 Visual inspections of cement pastes with w/c of 0.4 & 0.6 and sulfate concentration of 3 and 50 g/L. ....	101
Fig. 5-13 Mass changes and expansion at 0 mm of mortar samples over time for PC, HS and LC <sup>3</sup> systems.....	102
Fig. 5-14 Expansion rate of different cement pastes after sulfate exposure.....	103
Fig. 5-15 Expansion versus AFm hydrate content in cement pastes after 28 days hydration. ....	104
Fig. 5-16 Chemical compositions of C-(A)-S-H hydrates in cement pastes: a) PC, b) HS, c) SPC, d) LC <sup>3</sup> . Lines serve for eye-guide only.....	105
Fig. 5-17 Distribution of hydration products in different cement pastes after sulfate exposure: a) PC, b) HS, c) SPC, d) LC <sup>3</sup> . ....	106
Fig. 5-18 Sulfate profiles of HS cement pastes after sulfate degradation at 50 g/L solution at w/c ratio of 0.6. ....	107
Fig. 5-19 Sulfate and Ca profiles of SPC cement pastes after sulfate exposure in a 50 g/L solution at w/c ratios of 0.4 and 0.6. ....	108
Fig. 5-20 Phase profiles of LC <sup>3</sup> cement pastes after sulfate degradation at 50 g/L solution at w/c of 0.6. ....	110
Fig. 5-21 Sulfate ingress rate of PC and LC <sup>3</sup> cement pastes. ....	111
Fig. 5-22 Salt crystallization damage with the S/Ca and Na/S atomic profiles on the top 2 mm depth of PC and LC <sup>3</sup> mortar samples. ....	113
Fig. 5-23 Alkali content absorbed on C-(A)-S-H gel in PC and LC <sup>3</sup> cement mortars exposed to 50 g/L solution.....	114
Fig. 5-24 Long-term exposed cement pastes samples under a similar exposure condition with 3 g/L sodium sulfate solution: appearance of samples and chemical profiles. ....	115
Fig. 5-25 Visual inspections of cement pastes with w/c 0.6 under constant and cyclic exposure with 3 and 50 g/L sodium sulfate solution. ....	117
Fig. 5-26 Expansion rates of different cement pastes between constant and cyclic exposure regimes.....	118
Fig. 5-27 Mass variations of different cement pastes between constant and cyclic exposure regimes.....	119
Fig. 5-28 Sulfate ingress rate of PC and LC <sup>3</sup> cement pastes under constant and cyclic conditions. ....	120
Fig. 5-29 Profiles of phase distribution and relative phase concentration gradient of PC systems. ....	123
Fig. 5-30 Profiles of phase distribution and relative phase concentration gradient of HS systems. ....	125
Fig. 5-31 Profiles of phase distribution and relative phase concentration gradient of SPC systems.....	127
Fig. 5-32 Profiles of phase distribution and relative phase concentration gradient of LC <sup>3</sup> systems.....	128
Fig. 6-1 A schematic of crystal growing inside a cylindrical pore and link to the macroscopic observations: a) a crystal grows in a relatively large pore under equilibrium, b) a crystal grows in a relatively small pore under non-equilibrium, c) expansion and stress/strain curves after sulfate ingress. Pore radius is $r_p$ , crystal radius is $r_c$ , $r_c \ll r_p$ , $\delta$ is the thickness of the liquid film between the crystal and the pore wall, it is estimated to be 1 nm [8]. ....	134
Fig. 6-2 The schematic diagram of the counter movement of sulfate and hydroxide ions in reality. ....	136
Fig. 6-3 Profiles of phase assemblages and ionic concentrations of the Portland cement paste samples contact with (a) & (b) 50 g/L Na <sub>2</sub> SO <sub>4</sub> and (c) & (d) 10 g/L Na <sub>2</sub> SO <sub>4</sub> solution, CO <sub>2</sub> concentration is 500 ppm for both cases.....	140



---

Fig. 6-4 Simulated phase assemblages and saturation index (blue lines) for a) PC exposed at 3 g/L, b) PC at 50 g/L Na <sub>2</sub> SO <sub>4</sub> solution, ettringite formation is suppressed by upper limit of 0.0030 mol.....	142
Fig. 6-5 Simulated phase assemblages and saturation index (blue lines) for a) PC exposed at 3 g/L, b) PC at 50 g/L Na <sub>2</sub> SO <sub>4</sub> solution, ettringite formation is suppressed by upper limit of 0.040 mol.....	142
Fig. 6-6 Sulfate absorbed on synthetic C-S-H as a function of the sulfate concentration of the solution at 20 and 85 °C, adapted from [21].....	143
Fig. 6-7 Profile of atomic ratio of S/Si on C-S-H gel in the PC06 paste after 148 days exposure to sulfate solution with a concentration of 3 g/L.....	144
Fig. 6-8 The calculated crystallization pressure from ettringite formation by experimental in cement pastes of PC06 exposed to 3 and 50 g/L Na <sub>2</sub> SO <sub>4</sub> solution.....	144
Fig. 6-9 The calculated crystallization pressure from ettringite formation by thermodynamic modelling in Portland cement pastes exposed to 3 and 50 g/L Na <sub>2</sub> SO <sub>4</sub> solution, a) low upper limit 0.003 mol of ettringite, b) high upper limit 0.04 mol of ettringite .....	145
Fig. 6-10 The BSE images from SEM at the different magnification scales from PC pastes, a) before the large macroscopic expansion of PC06-28d, mag × 300, b) after the large macroscopic expansion of PC06-176d, mag × 300, c) before the large macroscopic expansion of PC06-28d, mag × 4000, d) after the large macroscopic expansion of PC06-176d, mag × 4000.....	147
Fig. 6-11 Profiles of phase assemblages and ionic concentrations of the Portland cement paste samples contact with (a) & (b) 50 g/L Na <sub>2</sub> SO <sub>4</sub> and (c) & (d) 3 g/L Na <sub>2</sub> SO <sub>4</sub> solution with an increasing external CO <sub>2</sub> content ingress.....	149
Fig. 6-12 Changes of phase assemblages and pore solution due to carbonation when 50 g/L sulfates are present in various cement pastes, a) and b) for PC paste, c) and d) for LC <sup>3</sup> paste, e) and f) for SPC paste. ....	151
Fig. 7-1 Pore size distribution of different cement pastes with various w/c ratios, a) cumulative porosity, b) differential distribution curves. ....	157
Fig. 7-2 The sulfate penetration graphs and profiles on the bottom layer of depth of ~0-2 mm from Portland cement pastes with different w/c ratios at the same sulfate concentration of 3 g/L. a) PC03-250d, b) PC04-280d, c) PC06-176d, d) sulfate penetration profiles as S/Ca ratios of these three systems.....	158
Fig. 7-3 Compressive and flexural strength at 28 days for mortar samples made with different cements. ....	159
Fig. 7-4 The comparison of cracking extent of the bottom surfaces in PC04 and PC06 pastes after sulfate exposure...160	160
Fig. 7-5 The sulfate penetration graphs and profiles on the bottom layer of depth of ~0-2 mm from Portland cement pastes with different w/c ratios at the same sulfate concentration of 50 g/L. a) PC03-250d, b) PC04-240d, PC06-120d d) sulfate penetration profiles as S/Ca ratios of these three systems.....	161
Fig. 7-6 The depth of sulfate penetration versus the expansion in Portland cement and HS cement pastes at w/c ratios of 0.4 and 0.6. ....	163
Fig. 7-7 Water adsorptive and drying rate of various cement mortars with w/c ratios of 0.4 and 0.6, a) adsorption, b) desorption.....	164
Fig. 8-1 Particle size distribution of the raw materials used in this study.....	171
Fig. 8-2 SEM sample preparation process.....	173
Fig. 8-3 Example of EDS point analysis on outer C-S-H phase for PC mortar sample.....	173

---

<i>Fig. 8-4 Example of stitched long BSE image for PC mortar after sulfate attack with a depth around 10 mm .....</i>	<i>174</i>
<i>Fig. 8-5 Sulfate expansion evolution over time under different curing temperatures of PC and HS mortars. ....</i>	<i>175</i>
<i>Fig. 8-6 Phase contents after hydration after 28 days of curing under different temperatures. ....</i>	<i>176</i>
<i>Fig. 8-7 Phase assemblages of HS and PC cement hydration modelled in CemGEMS under 20 °C and 60 °C cured conditions.....</i>	<i>177</i>
<i>Fig. 8-8 Aluminium-bearing phase segmentation of HS 20 °C mortar by EDXIA: Ms, hydrotalcite, C-A-S-H phases.....</i>	<i>178</i>
<i>Fig. 8-9 BSE maps of a) and c) for PC mortars, b) and d) for HS mortars with AFm phases mapped in cyan and Ht in orange, after 28-day curing at 20 °C and 60 °C.....</i>	<i>179</i>
<i>Fig. 8-10 S/Ca profiles obtained by hyper mappings in C-S-H phase before and after expansion for sample curing at a) 20 °C and b) 60 °C.....</i>	<i>180</i>
<i>Fig. 8-11 S/Ca profiles in C-S-H phase as obtained by hyper mapping before and after expansion for sample curing at a) 20 °C and b) 60 °C.....</i>	<i>181</i>
<i>Fig. 8-12 Atomic ratios of S/Ca versus Al/Ca of the outer C-S-H cluster before and after expansion in PC-20 °C and PC-60 °C at the depth of 0.5mm.....</i>	<i>182</i>
<i>Fig. 8-13 Atomic ratios of S/Ca versus Al/Ca of the outer C-S-H cluster before and after expansion in HS 20 °C and HS-60 °C at the depth of 0.5 mm.....</i>	<i>183</i>

## List of Tables

<i>Table 2-1 The current standard methods for sulfate resistance and prescriptive standards</i> .....	46
<i>Table 2-2 The research history, strategy, interest on sulfate attack of cement and concrete.</i> .....	49
<i>Table 3-1 Chemical composition of cements and admixtures wt.%</i> .....	57
<i>Table 3-2 Phase composition of cements wt.%</i> .....	57
<i>Table 3-3 Equivalent alkali and SO<sub>3</sub> content in cements</i> .....	57
<i>Table 3-4 Times and tolerances for the measurements schedule</i> .....	65
<i>Table 4-1 Chemical composition and phase composition of Portland cement</i> .....	69
<i>Table 4-2 Boundary definition for sulfate attack-related phases in cement-based materials</i> .....	76
<i>Table 6-1 The solid phase assemblages of hydrated PC paste at w/c of 0.6</i> .....	137
<i>Table 6-2 Dissolved element concentrations in aqueous solution.</i> .....	137
<i>Table 6-3 The settings of the salt recipe.</i> .....	137
<i>Table 6-4 The target path of the sulfate ingress process.</i> .....	138
<i>Table 8-1 Chemical composition and phase composition of Portland cement and HS cement.</i> .....	171
<i>Table 9-1 The rankings of sulfate degradation on two aspects – chemical sulfate attack and salt crystallization attack</i> .....	189

# Glossary

## Cement notations

---

C	Calcium oxide - CaO
S	Silica - SiO <sub>2</sub>
A	Alumina - Al <sub>2</sub> O <sub>3</sub>
F	Iron oxide - Fe <sub>2</sub> O <sub>3</sub>
H	Water - H <sub>2</sub> O
\$	Sulfur trioxide - SO <sub>3</sub>
c	Carbonate - CO <sub>3</sub>
C <sub>3</sub> S	Tricalcium silicate (alite) - 3CaO · SiO <sub>2</sub>
C <sub>2</sub> S	Dicalcium silicate (belite) - 2CaO · SiO <sub>2</sub>
C <sub>3</sub> A	Tricalcium aluminate - 3CaO · Al <sub>2</sub> O <sub>3</sub>
C <sub>4</sub> AF	Ferrite - 4CaO · Al <sub>2</sub> O <sub>3</sub> · Fe <sub>2</sub> O <sub>3</sub>
CH	Calcium hydroxide (portlandite) - Ca(OH) <sub>2</sub>
C-(A)-S-H	Calcium (aluminum) silicate hydrates
AFt	Ettringite - 6CaO · Al <sub>2</sub> O <sub>3</sub> · 3SO <sub>3</sub> · 32H <sub>2</sub> O
AFm	Al <sub>2</sub> O <sub>3</sub> · Fe <sub>2</sub> O <sub>3</sub> · mono (OH, SO <sub>3</sub> or CO <sub>3</sub> )
Ms	Monosulfoaluminate – Ca <sub>4</sub> (Fe, Al) <sub>2</sub> (SO <sub>4</sub> )(OH) <sub>12</sub> · 5H <sub>2</sub> O
Hc	Hemicarboaluminate - C <sub>4</sub> Ac0.5H <sub>12</sub>
Mc	Monocarboaluminate - C <sub>4</sub> ACH <sub>11</sub>
Ht	Hydrotalcite – Mg <sub>6</sub> Al <sub>2</sub> (CO <sub>3</sub> )(OH) <sub>16</sub> · 4H <sub>2</sub> O
SRPC	Sulfate-resisting Portland cement
HS	High sulfate-resisting cement
w/c	Mass ratio of water to cement
w/b	Mass ratio of water to binder
Ca/Si	Atomic ratio of Ca to Si in calcium silicate hydrate gel
PC	Portland cement
SPC	Slag Portland cement
SCMs	Supplementary cementitious materials
LC <sup>3</sup>	Limestone calcined clay cement
PSA	Physical sulfate attack
TSA	Thaumasite sulfate attack
ITZ	Interfacial transition zone

---

## Investigation techniques

---

PSD	Particle size distribution or pore size distribution
MIP	Mercury intrusion porosimetry
XRD	X-ray powder diffraction
XRF	X-ray fluorescence
SEM	Scanning electron microscopy
EDS	Energy dispersive spectroscopy
BSE	Back-scattered electron
EDXIA	An image analysis framework for EDS/BSE hyperspectral maps
GEMS	Gibbs energy minimization software for geochemical modeling

---



# Chapter 1 Introduction

## Contents

<b>1.1</b>	<b>Background.....</b>	<b>22</b>
<b>1.2</b>	<b>Motivations of the thesis .....</b>	<b>22</b>
<b>1.3</b>	<b>Objectives and innovations.....</b>	<b>22</b>
<b>1.4</b>	<b>Synopsis of the thesis .....</b>	<b>23</b>

## 1.1 Background

Concrete exposed to environments containing sulfate ions may suffer from “sulfate attack” leading to cracking/spalling damage. Although research has been conducted for decades, most work regarding sulfate attack is not well related to field conditions. The standard approach is to study samples under total immersion in sulfate solutions, whereas cases of damage in the field are almost exclusively in conditions of semi-immersion. Experimental studies demonstrate that under submerged conditions the main mechanism of chemical sulfate attack is the expansion due to the crystallization pressure of the ettringite.

In this thesis, we introduce a new approach designed to improve the understanding of mechanisms occurring in semi-immersion exposure conditions, in a reproducible way. This approach involves unidirectional transport through cementitious samples in contact with the solution on one side and exposed to a controlled relative humidity on the other side.

As supplementary cementitious materials (SCMs) are increasingly used in concrete, a growing number of open questions are raised about their performance in sulfate-rich environments. Testing approaches were developed decades ago and have not been updated to the specificities of blended-cement systems. Furthermore, standard tests only look at expansion under full immersion, which is not representative of most cases of damage in the field. A more comprehensive understanding of the whole degradation process is needed.

## 1.2 Motivations of the thesis

The sulfate degradation process involves many factors, which are still not understood well, despite research over many decades. In particular, capillary rise as a factor contributing to sulfate degradation is underestimated. Most attention has been on expansion-driven damage. However, the understanding of the damage in semi-immersion is needed, as this is the most common form of damage in the field.

The conventional way to study semi-immersion has been to place concrete cylinders vertically with the bottom portion in a sulfate solution, but this configuration does not lead to reproducible results, due to the uncontrolled conditions of evaporation. The motivation of this thesis is to develop a reproducible approach to study sulfate attack under capillary rise.

## 1.3 Objectives and innovations

The objectives of the thesis are to:

- To develop a rigorous and robust investigation approach for sulfate attack;
- To better understand the sulfate degradation processes under capillary rise;
- To clarify the confusion between “chemical” and “physical” sulfate attack;

- To gain insight for future work towards a field-relevant test method.

The innovations of the thesis are:

- To combine for the first time the two aspects of “chemical” and “physical” sulfate attacks into one single practical approach and to investigate their interactions;
- To accelerate the degradation process with the use of cement paste samples;
- To link the macro physical damage with underlying microstructural changes.

## 1.4 Synopsis of the thesis

The thesis is divided in 9 chapters. **Chapter 2** presents a literature review on the sulfate attack in cementitious materials. **Chapter 3** describes experimental methods and materials.

**Chapter 4** presents the unidirectional approach by comparing the degradation behaviors in mortars and pastes. It shows the potential and feasibility to combine the different aspects of sulfate attack into one experimental method.

**Chapter 5** investigates different experimental parameters affecting sulfate damage: w/b ratio and sulfate concentration, cement type, and constant vs cyclic exposure conditions.

**Chapter 6** uses thermodynamic modelling (with GEMS) to better understand the microstructure changes occurring during sulfate attack, especially the role of the pore solution, which cannot be measured directly.

**Chapter 7** discusses the relationship between physical properties of the materials and the observed degradation. Lower concentrations of the external solution led to much less damage in both chemical and physical attack as both are dependent on the high supersaturation with respect to damaging phases (ettringite and thenardite/mirabilite). The relative roles of lower porosity and higher strength at lower w/b are discussed.

**Chapter 8** looks at the study of sulfate resisting (HS) cement with low C<sub>3</sub>A content under full immersion to identify the effect of the curing temperature to the expansion mechanism.

**Chapter 9** summarizes the conclusions of the thesis and the perspectives for future research.



# Chapter 2 State of the Art

## Contents

<b>2.1</b>	<b>Introduction .....</b>	<b>25</b>
<b>2.2</b>	<b>What is sulfate attack ?.....</b>	<b>27</b>
<b>2.3</b>	<b>External sulfate attack .....</b>	<b>31</b>
2.3.1	The expansion mechanism .....	31
2.3.2	The degradation mechanism.....	33
<b>2.4</b>	<b>Parameters influencing sulfate attack .....</b>	<b>40</b>
<b>2.5</b>	<b>Current testing methods .....</b>	<b>43</b>
<b>2.6</b>	<b>Evaluation criteria for sulfate resistance of cementitious materials .....</b>	<b>46</b>
<b>2.7</b>	<b>Summary and knowledge gaps.....</b>	<b>47</b>
<b>2.8</b>	<b>Reference .....</b>	<b>51</b>

## 2.1 Introduction

The process of cement hydration provides the hydrates that may react with sulfate solution leading to degradation and damage of the cement matrix. However, the overall process of degradation due to sulfate ions is not simple, as it involves the different cement hydration products, their relative content and distribution of AFm/AFt in the paste matrix, pore size distribution, porosity and pore solution chemistry. Therefore, it is important to get an understanding of the cement paste microstructure, before discussing the phase alterations and degradation due to the sulfate ingress.

Cement hydration is a dissolution and precipitation process caused by the reaction between clinker phases and water. The four main clinker phases of Portland cement (PC) are tricalcium silicate ( $C_3S$ ), dicalcium silicate ( $C_2S$ ), tricalcium aluminate ( $C_3A$ ) and tetracalcium ferrite ( $C_4AF$ ). The aluminium-containing clinker phases hydrate to produce ettringite (AFt, < 10 wt. %) and AFm phases (< 10 wt. %) monosulfoaluminate and/or hemi- and monocarboaluminate. Hydration of the calcium silicate phases produces portlandite (~10 wt. %) and calcium silicate hydrate (C-S-H, ~50 wt. %). The typical evolution of the hydration products of Portland cement is shown in Fig. 2-1. External sulfate can react with portlandite and AFm phases. This means that the initial phase assemblage can directly influence the final phase alterations, and, hence, the level of damage. The intermixing of the AFt/AFm phases with outer C-S-H can also significantly change the performance [1,2].

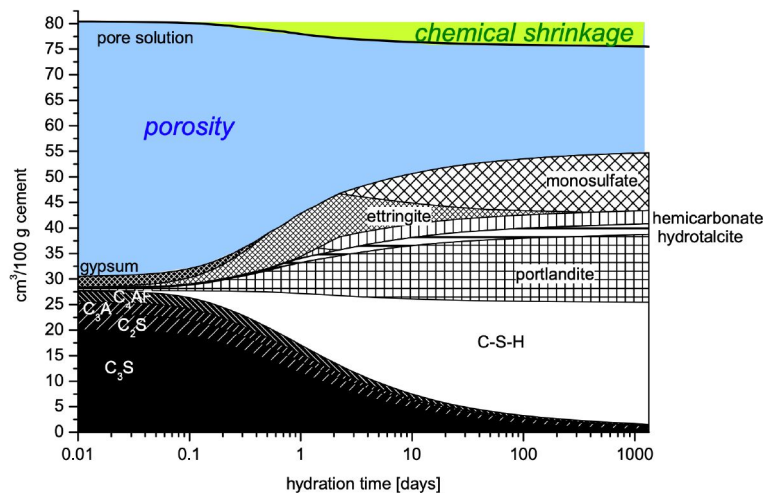


Fig. 2-1 Thermodynamic model of hydration of Portland cement [3].

Cement paste is a heterogeneous and porous material that contains a wide range of pore size distributions from a few nanometres to millimetres. Typically, the total porosity of PC paste is around 10 % to 20 % and determines the permeability and capillary suction of the material. When the external sulfates enter the microstructure, they can react with the aluminium and calcium sources in pores containing water and form ettringite or gypsum. The expansive force can only take place inside the smaller pores as a result of the repulsion exerted between the pore wall and the newly formed crystals [4].

On the other hand, the level of ionic concentration in the pore solution is another key factor that affects sulfate diffusion and phase alterations. The pores are filled with pore solution with a pH of around 13.5 with various concentrations of  $\text{Na}^+$ ,  $\text{K}^+$ ,  $\text{OH}^-$ ,  $\text{SO}_4^{2-}$ ,  $\text{Ca}^{2+}$ ,  $\text{Al}(\text{OH})_4^-$ ,  $\text{SiO}_4^{2-}$ , etc. An example of the ionic concentrations measured in Portland cement pore solution is shown in Fig. 2-2, showing that K and Na concentrations are relatively high above 100 mmol/L as well as high levels of  $\text{OH}^-$  after 1 day of hydration. However, aluminium and iron concentration are much lower, at a level between 0.1 to 0.001 mmol/L. The pH in the pore solution changes the solubility of relevant phases: gypsum tends to form at relatively low pH where leaching is involved [5,6], and ettringite is not stable at pH below 11.5-12 [7,8]. Na and K (intrinsically the NaOH and KOH) content influences the sulfate concentration in pore solutions and also changes the solubility of ettringite. Too high  $\text{OH}^-$  concentration can suppress the ettringite formation, resulting in a sulfate expansion [1,9]. Pore solution chemistry can therefore significantly affect the consequences of sulfate attack.

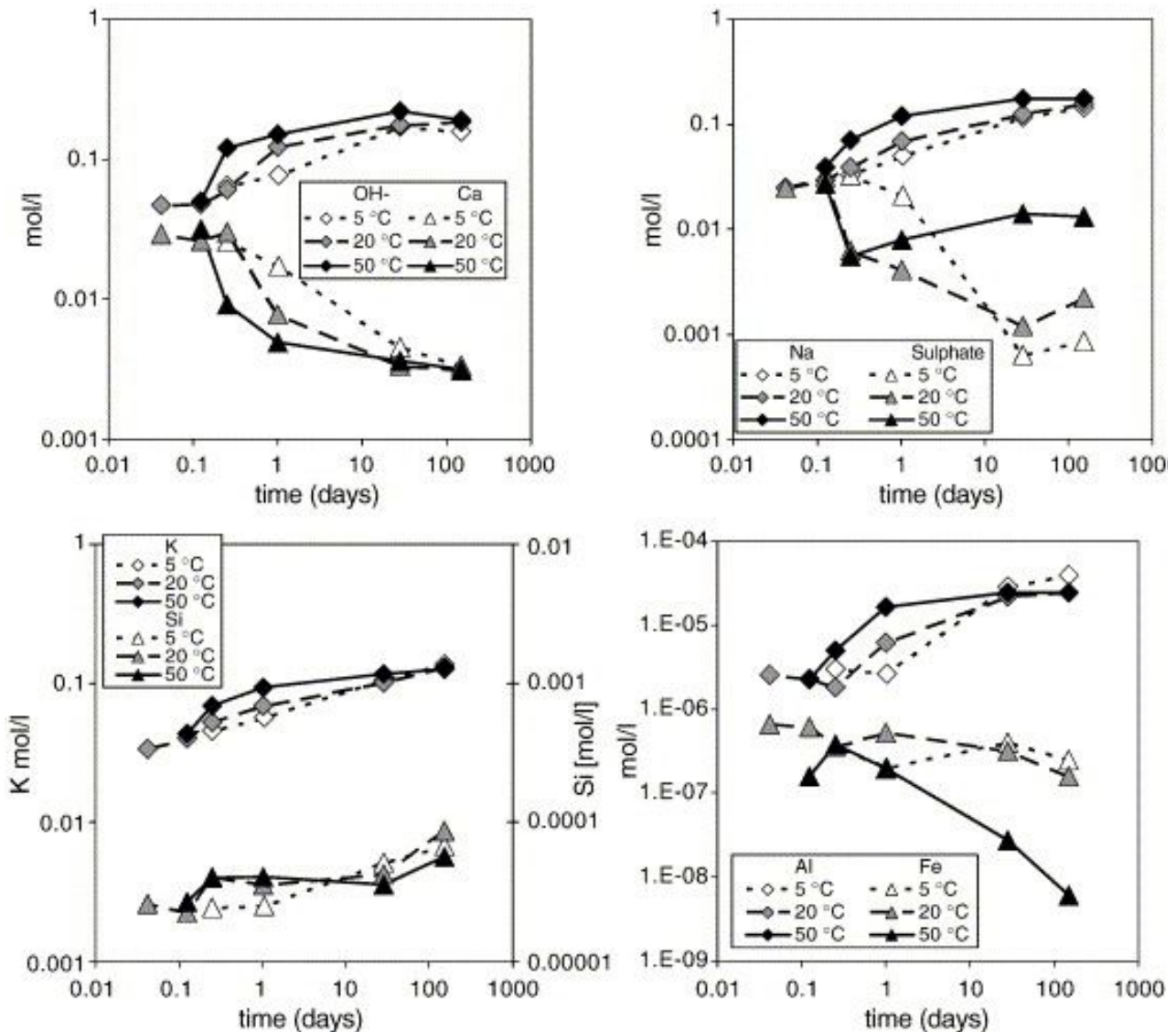


Fig. 2-2 Measured concentrations in the pore solutions of sulfate resisting Portland cement (SRPC) hydrated at 5, 20, 50 °C, adapted from [10].

The physical properties of cement paste, such as mechanical strength, water sorptivity and drying properties, are also important to resist damage. The higher the mechanical strength, the less potential for damage [11].

## 2.2 What is sulfate attack ?

Sulfate attack on concrete has been extensively studied for a long time. Sulfate ions are often present in rivers, underground water, sewers, seawater and soil. When concrete materials come into contact with them, they can react with the cement pastes in concrete and cause damage which impacts the service life of concrete structures [12]. Sulfate attack is commonly divided into chemical and physical sulfate attack. Due to the complex physiochemical reactions within the concrete, given different conditions of climate and exposure, the resulting damage can vary greatly. Sulfate attack on concrete can result in softening, expansion, cracking, disintegration, spalling and delamination.

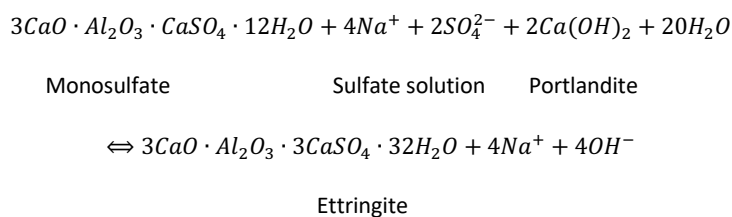
Sulfate attack was first observed in the 1880s [13], but there are still some questions that we do not understand and that needs to be investigated. In particular, it is now more and more common to use supplementary cementitious materials (SCMs) in concrete, such as calcined clay, slag, fly ash, limestone, etc, so it is important to understand how they act upon sulfate attack when incorporated in cement. Moreover, testing approaches must be updated to characterize sulfate attack properly. Existing methods were developed for Portland cement and “chemical sulfate attack” [14], where samples are fully immersed in the solution. Such methods are not necessarily suitable for SCMs-based materials. The so-called “physical sulfate attack” is usually underestimated, and is more common in field conditions. It takes place under conditions where capillary suction is the dominant mechanism. Therefore, physical sulfate attack is also a focus of this work.

### Chemical sulfate attack

Chemical sulfate attack is a process in which diffusion results in a sulfate ingress through the pore solution, and reacts with the aluminium/calcium-bearing phases. Expanding hydrates then cause damage to the cement paste matrix.

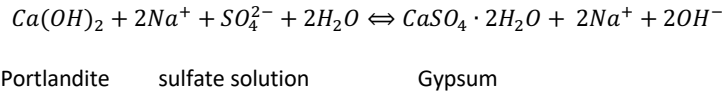
The two main chemical reactions taking place in the chemical sulfate attack process are ettringite formation (Equation 2-1),

Equation 2-1



and gypsum formation (Equation 2-2) under a high sulfate concentration. However, it is believed that gypsum formation does not lead to expansion as it always precipitates inside the pre-existing voids and cracks [2,15].

Equation 2-2



As a consequence of chemical sulfate attack, there is usually a progressive expansion and cracking damage from external surfaces towards the interior part of the concrete. The schematic in Fig. 2-3 can help to understand the dynamic degradation process. The counter-movement of  $\text{SO}_4^{2-}$  and  $\text{Ca}^{2+}/\text{OH}^-$  leads to the distinct zones of degradation from the exposed surface: leached zone at the outermost surfaces; a densified zone with precipitation of ettringite and/or gypsum; a less affected zone and an unaffected zone at the furthest depth from the solution. The most prevalent sulfate source is the sodium sulfate [11,16], therefore, it is the focus of this thesis.

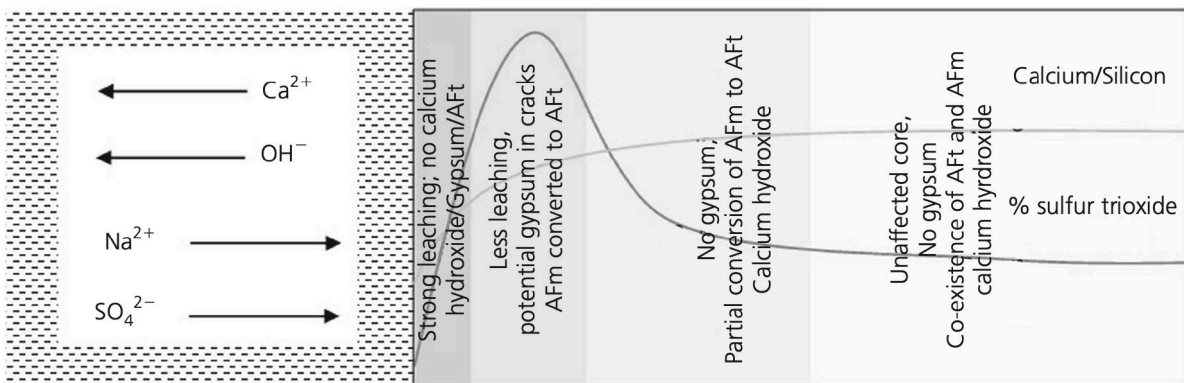


Fig. 2-3 Schematic diagram of chemical sulfate attack interactions between sodium sulfate solution and exposed cement pastes [17].

The phase assemblage under sulfate ingress has been investigated by thermodynamic modelling (GEM-Sel-ektor code was used, <https://gems.web.psi.ch>, [18,19]) with the Cemdata 18 chemical thermodynamic database <https://www.empa.ch/cemdata> [20]. A typical modelled profile is shown in Fig. 2-4 [21]. The results from GEMS are under an equilibrium condition which includes neither an exposure time nor a distance from the exposed surfaces. It is important to note that the degrading, sulfate-rich zone (abundant with ettringite and/or gypsum) moves inwards progressively over time. The degradation is a layer-by-layer process, as previously shown by Gollop and Taylor in the 1990s [22].

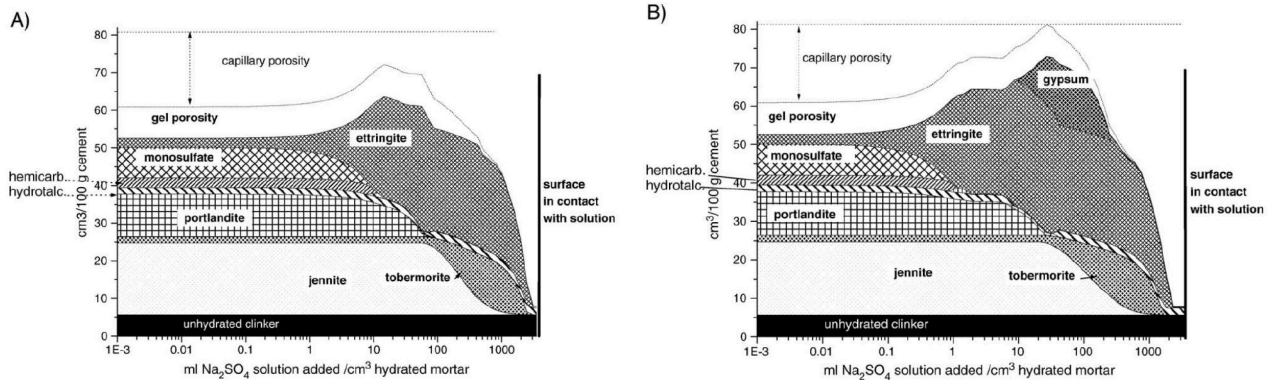
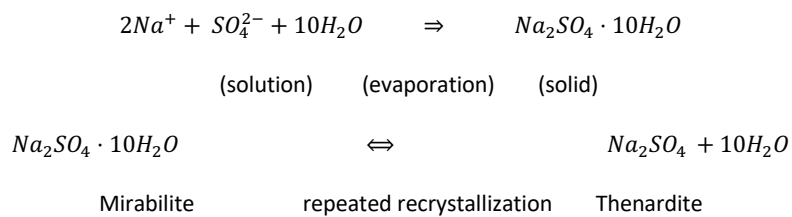


Fig. 2-4 Phase assemblage of the mortar samples immersed in A) 4 g/L Na<sub>2</sub>SO<sub>4</sub> and B) 44 g/L Na<sub>2</sub>SO<sub>4</sub> as calculated with GEMS [21].

### Physical sulfate attack/salt crystallization

Physical sulfate attack is a process in which the capillary suction in concrete is dominant, water evaporates from the surface of concrete and alkali sulfates crystallize near the surface [23,24]. Sometimes the term “salt weathering” is used to describe the more general growth of salt crystals that causes physical disintegration, given a periodic change in temperature and humidity [25,26]. Depending on the relative rate of capillary suction and water evaporation from surfaces, the crystallization may occur inside or outside the materials (subflorescence vs. efflorescence) [23,24]. In this process, the temperature and the relative humidity are very important factors, generating a favorable environment for supersaturation with respect to alkali salts (and the promotion of crystallization). Apart from the sodium sulfate attack, other alkali salts can also cause damage to concrete with a decreasing aggressiveness order to salt crystallization given by Na<sub>2</sub>SO<sub>4</sub> > Na<sub>2</sub>CO<sub>3</sub> > NaCl [23]. Therefore, Na<sub>2</sub>SO<sub>4</sub> salt is the most deleterious form in terms of physical sulfate attack and salt weathering [11,16]. The main chemical reaction involved is the formation of thenardite (Na<sub>2</sub>SO<sub>4</sub>) or mirabilite (Na<sub>2</sub>SO<sub>4</sub> · 10H<sub>2</sub>O) depending on the surrounding environments, as shown in Equation 2-3.

Equation 2-3



To understand these two phases of formation, a phase diagram showing temperature and relative humidity is essential, as demonstrated by Flatt in Fig. 2-5 [11].

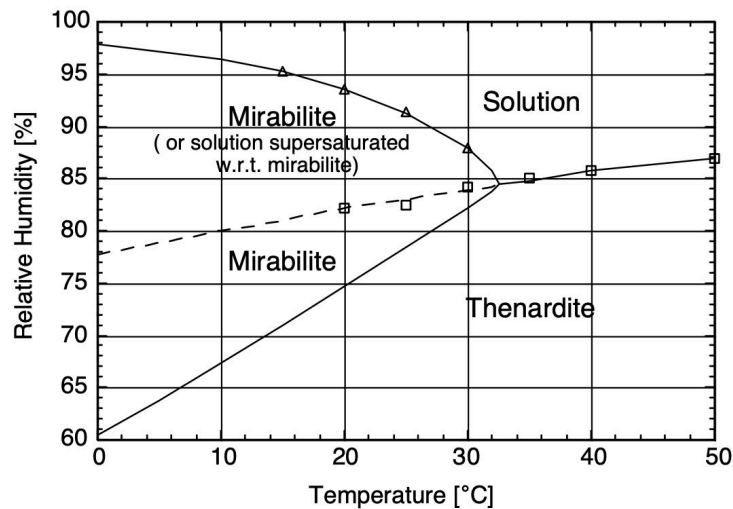


Fig. 2-5 Phase diagram for sodium sulfate, adapted from [11].

It has often been claimed that the spalling damage was from these two phase transformations, as a result of an increase in the solid volume due to the mirabilite formation [12]. However, the empty pores left after degradation in cement pastes indicate that a theory of volume restrictions leading to damage is not convincing [21,27]. Moreover, the hydraulic pressure claimed (i.e., damage from water freezing) is unlikely to cause significant damage as the volume change for sodium sulfate crystallization at 20 °C is much smaller than for the water freezing [11]. In fact, if we consider the liquid phase during the thenardite and mirabilite phase transformation process, the system shrinks by about 5.6 % rather than expanding. Damage is also observed from the NaCl crystallization process which does not have any hydrous phase [28]. There is a series of studies on damaging mechanisms in limestones and sandstones by Flatt and Desarnaud [11,29,30], which suggests that the damage resulted from crystallization pressure rather than volume changes. Damage was observed due to the reprecipitation of mirabilite, where the supersaturation is compensated by the dissolution of thenardite in the pore solution, as the solubility of thenardite was considerably greater than mirabilite at 32 °C. It was demonstrated that mirabilite precipitation alone is sufficient to damage these materials during the rewetting, as the theoretical stress that thenardite might produce is lower than that of the mirabilite [31]. From the experimental study, it was also observed that damage only occurs when mirabilite forms in the rewetting process where the supersaturation is reached by the dissolution of thenardite, rather than in the drying process [11,29].

Another interesting concept is that the expected damage increases substantially once enough salt is present to fill the porous network [29]. This implies that the salt crystallization damage not only depends on the degree of supersaturation but also the pore size distribution and the tensile strength of the materials [4,11]. Supersaturation is a requirement of the thermodynamical reaction with respect to phase formation, but salts forming inside big pores do not cause any damage since the stress generated is below the resistance of the

materials, as discussed in [11]. It was suggested by Scherer that the growth of salt in a single pore is unlikely to cause damage because the volume affected by the stress is too small [32].

Substantial damage can only be observed macroscopically when the individual stresses in small pores are connected in the network of the microstructure, and a threshold is reached [29]. This links the microstructural changes to physical properties. The same concepts can be applied widely to most inorganic building materials and salt crystals.

Typical spalling damage examples of the physical sulfate attack of concrete in the field are shown in Fig. 2-6.

a)



b)



Fig. 2-6 Spalling damage examples caused by sodium sulfate crystallization: a) Surface scaled on a concrete foundation stem wall coated with latex paint [33], b) A building wall spalled with sodium sulfate deposit, coated with paint found in Pully, Switzerland.

## 2.3 External sulfate attack

Sulfate attack is usually broken down into external and internal sulfate attack (also called delayed ettringite formation, DEF). The first case of an external sulfate attack on concrete was found in the field in Paris in 1887 [34]. This type of degradation has been intensively investigated since then by researchers in cement science. Accelerated tests are used in the laboratory, and standard test methods are developed [14]. The mechanisms of expansion and other forms of degradation are reviewed below.

### 2.3.1 The expansion mechanism

#### Ettringite formation

At 20 °C, ettringite precipitates at a sulfate concentration of around 0.4 mmol/L, which is a much lower concentration than the concentration at which gypsum can form (1.4 g/L or 10 mmol/L, a sulfate concentration also occurring in the field) [35]. The expansion phenomenon has been associated with ettringite formation,



since the two conditions for generating crystallization pressures by ettringite formation - confined space and supersaturation - are relatively easily met [36].

However, another factor limiting the ettringite formation is the low Ca concentration in the pore solution of the cement paste. The limited availability of Ca in the small pores limits the supersaturation with respect to ettringite intermixed in outer C-S-H at small scales, especially in blended cement systems [4,37,38]. The ettringite forming inside small pores, which can cause expansion, is largely decreased in the blended cements [39]. In mortar and concrete, ettringite is often found in the interfacial transition zone (ITZ) between the paste and aggregates where the Ca concentration is higher, as portlandite tends to form in ITZ zones [12]. The supersaturation of ettringite is also easily reached in big pores [4,31].

The expansion mechanism of external sulfate attack is very similar to the expansion in DEF (Delayed ettringite formation) except that the source of sulfates is different [1,40]. The accepted theory is that ettringite which forms inside relatively big pores is not expansive, but that ettringite formed in small pores in the C-S-H gel can cause expansion [1]. Some people tried to identify the threshold where S/Ca of C-S-H gel can cause expansion, but there is no established value for the heat-induced DEF [39]. However, the same theory has not been applied to external sulfate attack.

#### Gypsum formation

Gypsum formation usually takes place when the sulfate concentration is high (minimal concentration is 10 mmol/L) and it tends to form inside pre-existed large voids and/or cracks caused by ettringite formation [35,41]. Gypsum can precipitate until pH values as high as 12.9, beyond which even a further increase of sulfate concentration, gypsum cannot form [42]. The solubility of gypsum is shown in Fig. 2-7, which explains the influence of pH. Ettringite is not stable in an environment with pH values below 11.5-12.0. At this relatively low pH for cement pastes, ettringite decomposes and forms gypsum [7,8]. This can perhaps explain why gypsum always prefers to form in the vein-like cracks in leached zones and the ITZ zones in concrete [5] as well as the wet-dry interface of concrete in the field [43]. The  $C_3S/C_2S$  is also an important factor in sulfate attacks, as portlandite is the main source of calcium required to form gypsum [44,45].

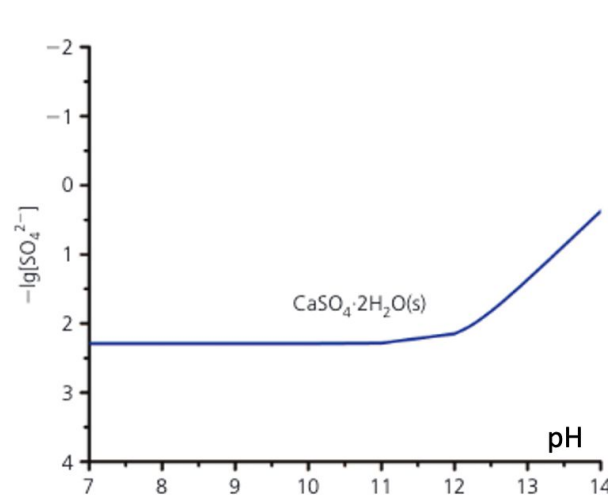


Fig. 2-7 The influence of pH on gypsum formation, adapted from [46].

However, it is not believed that gypsum causes any expansion, it is rather the consequence of expansion/cracking. The real cause for expansion is ettringite formation [2].

### 2.3.2 The degradation mechanism

#### Softening and strength loss

Leaching, combined with the ingress of sulfate solution, can lead to the softening of the material, due to the decalcification of the C-S-H phase and the loss of portlandite. Eventually, the decrease of the pH in the pore solution can destabilize cement hydrates (C-S-H, ettringite, and AFm phases) [47]. The Low Ca/Si ratio of the C-S-H phase is a typical feature of blended cement systems; therefore, it is more easily degraded by decalcification from leaching. The cohesion and binding properties between hydrates are usually decreased, which makes the materials fall apart easily [48,49].

When the Magnesium cation is present in the sulfate solution, M-S-H hydrates can replace C-S-H, and brucite may form by consuming portlandite and  $\text{Mg}^{2+}$  from the solution [50], which leads to a lower pH of the pore solution and therefore an accelerated degradation. In this process, the attack on C-S-H is dominant; eventually, the material disintegrates and loses cohesiveness, rather than any dramatic cracking.

Under field conditions, thaumasite, which is a non-adhesive phase formed by attacking the C-S-H, can also form in the presence of carbonates at low temperatures [44]. Thaumasite formation is believed to be always located on the outer surface of the sample, which implies that it is the last step of degradation in sulfate attack. The thaumasite formation process consumes Si (from decalcified C-S-H gel),  $\text{Ca}^{2+}$ ,  $\text{CO}_3^{2-}$ , and  $\text{SO}_4^{2-}$  (from exposure solution or from the ettringite phase). A low pH environment is often suggested to accelerate the thaumasite attack process [51]. The outcome is that the C-S-H gel is substituted with a non-adhesive thaumasite phase; hence the adhesiveness and mechanical strength of the cementitious material are lost.

### Delamination

Delamination is usually due to extensive layer-by-layer degradation from sulfate attack. The process of this layer damage was first described by Gollop [22] and confirmed by other researchers [15,52,53]. The delamination was then clearly illustrated by Santhanam et al [15]. They demonstrated that the expansion takes place first in the outer skin of the sample, and then leads to the occurrence of cracks in the interior zone, which is unaltered chemically. It means the crack is empty when it appears initially. However, with the continued contact with the sulfate solution, the surface skin is delaminated if the exerted stress is higher than the tensile strength of the materials. The parallel cracks are able to form only when the crystallization pressure from ettringite formation is high enough to initiate the propagation of cracks, which is regarded as the prerequisite of the delamination [15]. The further reaction of hydration products in the cracked regions results in the deposition of hydrates in the cracks (mainly gypsum, as the preferred forming condition is reached in those cracks).

The degraded zone moves again when it triggers the secondary interior cracking, therefore, the damage is a layer-by-layer process. The sample is ultimately disintegrated due to the progressive ingress of the degradation zones.

### Expansion and Cracking

The phenomenon of damage under sulfate attack was illustrated by Santhanam et al [15] (Fig. 2-8). Gypsum can usually form inside the voids and cracks when the sulfate concentration in the pore solution is sufficiently high. But it is the consequence of sulfate attack-induced expansion, rather than the cause of expansion [15,54]. The outer skin is under a compressive force, due to the expansive formation of ettringite, the interior/bulk of the material is subjected to tensile forces which cause cracks. Over time, the surface zone can disintegrate due to the continuous penetration of the solution and the expansion. Once the solution reaches the cracked interior zones, it reacts with hydrates and deposit products inside the voids/cracks. Then this new region eventually expands as the previous outer surface did.

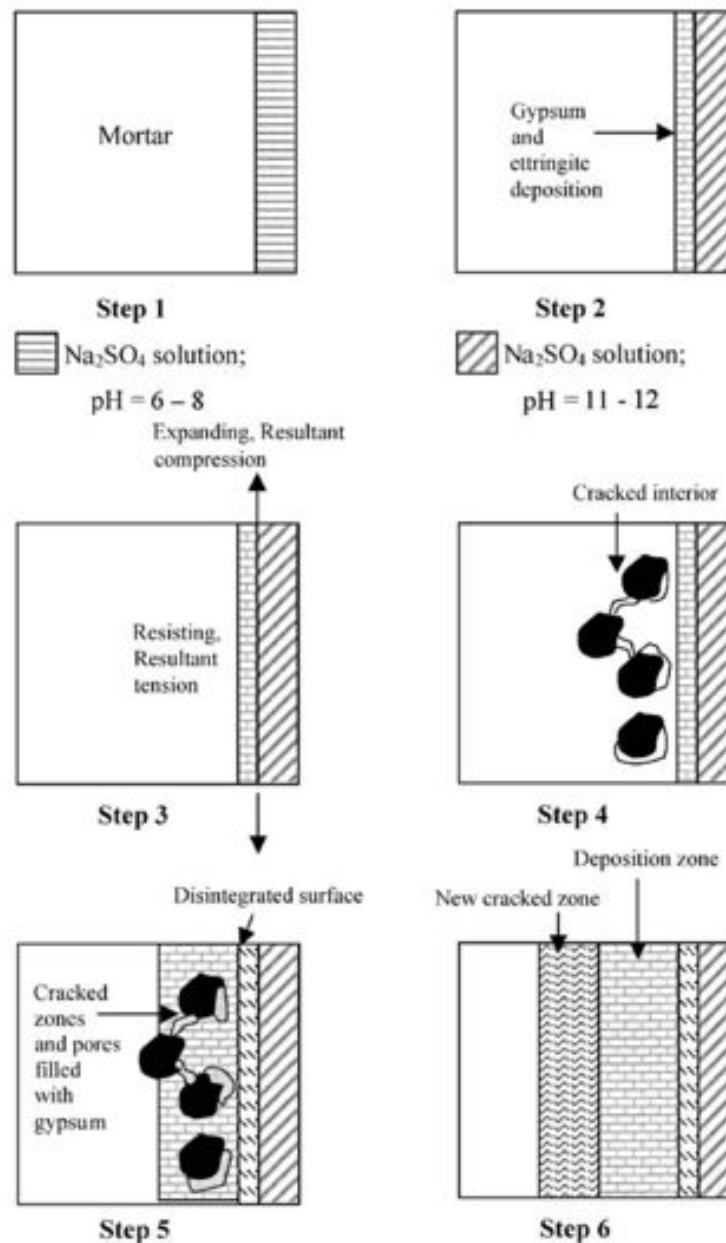


Fig. 2-8 Proposed degradation process of sodium sulfate attack, adapted from [15].

It was first indicated by Gollop and Taylor [22] that cracking is initiated from the outer surface and evolves gradually towards the central zone of the sample. Wang [52] also confirmed the progressive layer damage determined by the layer-by-layer XRD technique which provided the quantitative phase profiles of ettringite, portlandite and gypsum. The cracks are usually parallel to the surface of the sample [33] and filled by gypsum, if sulfate concentration is high enough [42,54]; they are often called vein-like cracks. This period is very much dependent on the sulfate concentration and w/c which control the sulfate ingress rate. This formation of layers upon sulfate attack was also observed in field concrete samples [12,55].

To understand better how the expansion and cracking develop, the link to the mechanical properties is important. As discussed in [36,40], the expansion should be associated with the intrinsic properties of cement

materials, such as porosity and elastic modulus, in Equation 2-4 and Equation 2-5. The crystals talked about here refer to the general situations where the condition is satisfied with any crystal (not only ettringite or sodium sulfate): crystallization pressure can cause expansion. In PC systems, the expansion of concrete is usually accompanied by the development of cracks in the material. If the degradation period is long enough, the sample may be fully disintegrated by the layer-by-layer exfoliation.

Equation 2-4

$$\varepsilon = \frac{\varphi}{E} \frac{RT}{V_{crystal}} \ln \left( \frac{IAP}{K_{s0}} \right)$$

Equation 2-5

$$P = \frac{RT}{V_{crystal}} \ln \left( \frac{IAP}{K_{s0}} \right)$$

Where:  $\varepsilon$  is expansion,  $P$  is the crystallization pressure,  $\varphi$  is porosity,  $E$  is elastic modulus,  $R$  is the molar gas constant,  $T$  is the temperature in K,  $V_{crystal}$  is the molar volume of the crystal (the crystal is ettringite here specifically),  $IAP$  is ionic activity product of ettringite,  $K_{s0}$  is the theoretical equilibrium solubility product of ettringite. The saturation index is defined by the ratio of  $IAP/K_{s0}$ .  $IAP_{Aft}$  is defined by  $(a_{Ca^{2+}})^6 \cdot (a_{Al(OH)_4^-})^2 \cdot (a_{OH^-})^4 \cdot (a_{SO_4^{2-}})^3 \cdot (a_{H_2O})^{26}$ . The equilibrium solubility product for ettringite is  $K_{s0} = 1.25 \times 10^{-45} \text{ M}^{41}$ .

The expansion over time is linked to the strain-stress curve, as shown in Fig. 2-9 adapted from [40]. The latent period of expansion development corresponds to the elastic period, where the expansion/strain  $\varepsilon$  is still very small. When the exerted pressure from ettringite formation is beyond the tensile strength of materials, the cracks occur and the expansion increases drastically. It is important to note that, only comparing the expansion is not accurate in assessing the sulfate resistance, as the expansion varies with the materials' intrinsic properties, i.e., mechanical tensile strength and porosity. The higher tensile strength and the lower porosity result in lower degrees of expansion, even though the same stress is applied to materials. It can be predicted that materials have negligible expansion if there is less exerted pressure than tensile strength.

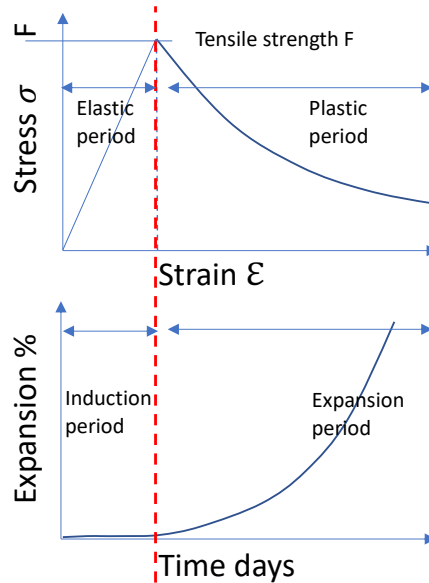


Fig. 2-9 The relation between expansion and tensile stress, adapted from [40].

The latent time is a key indicator associated with sulfate attack resistance: it can last from a few weeks to many decades. Monteiro and Kurtis [56] analysed the data on expansion over forty years of exposure to 2.1 %  $\text{Na}_2\text{SO}_4$  solution. Some concrete samples even underwent a 15.5-year latent period. The latent time is controlled by the factors influencing supersaturation: chemistry of pore solution, external sulfate concentration, and the physical properties of materials influencing the limit of mechanical restraint, tensile strength and sample size [2].

### Spalling

The difference between subflorescence (a soluble salt accumulates under or just beneath the surface of a porous material) generating below concrete surfaces and efflorescence (the migration of a soluble salt to the surface of a porous material, where it forms a coating) forming above concrete surfaces should be carefully addressed, as the consequences are totally different [24]. The relation between the capillary rise rate and the drying rate is of great importance as it can eventually affect the outcome: 1) when the drying rate of materials is faster than the capillary rise rate, subflorescence takes place and may cause spalling; 2) when the drying rate is slower than the capillary rise rate, efflorescence takes place which is generally harmless to concrete materials.

From previous studies [23,57], blended cements systems are more susceptible to spalling damage due to the salt crystallization pressure. “Physical sulfate attack” is usually studied separately from “chemical sulfate attack”, but it is really important to know how the material behaves upon chemical sulfate attack, before the salt crystallization attack, as they interact. A close investigation should be made of how these two processes interplay during the capillary rise action. Although some people state that salt crystallization attacks are more

pronounced in SCM blended-cement systems [17,23,57,58], the reason behind this is still not clear. Exfoliation and spalling are observed, and the damage is often associated with the salt subflorescence, due to the changes in relative humidity and temperature in the above-ground surfaces. It is important to note that the “chemical” and “physical” sulfate attacks are both pore solution chemistry-driven processes, which implies that only if the concentration is sufficiently high can the crystallization take place and cause damage.

The most important phase formation in spalling damage is thenardite/mirabilite crystallization in the sodium sulfate solution. It is believed that the damage is not simply due to the volume changes between these two phases. Salt crystallization pressure with supersaturation seems to be a more convincing explanation [28]. However, understanding this damage mechanism requires more evidence than merely observing the presence of salt and spalling behavior.

It was suggested by Desarnaud that damage in stones is mainly dependent on the kinetics of the crystallization [30,33]. More often, during rewetting (a very fast process of dissolution and recrystallization kinetics) a high supersaturation in the pore solution is reached, due to the dissolution of anhydrous crystals. A similar finding was also presented by Thaulow and Sahu [28], that fast cooling without equilibrium can cause supersaturation and crystallization pressure. The thenardite microcrystallites were observed to act as seeds, forming a large amount of hydrated crystals, creating grape-like mirabilite structures that expand very rapidly [30]. These clusters may generate stresses larger than the tensile strength of the stone, which then leads to damage. The formation of mirabilite/thenardite is heterogeneous in regions where supersaturation occurs so that the spalling always initiates from a localized spot, and then spreads through the contaminated surfaces [59,60]. The formation of sodium sulfate salt observed by SEM is shown in Fig. 2-10. Thenardite is generally precipitated as smaller crystals, of sizes around tens of micrometres, while mirabilite forms with a magnitude of hundreds of micrometres.

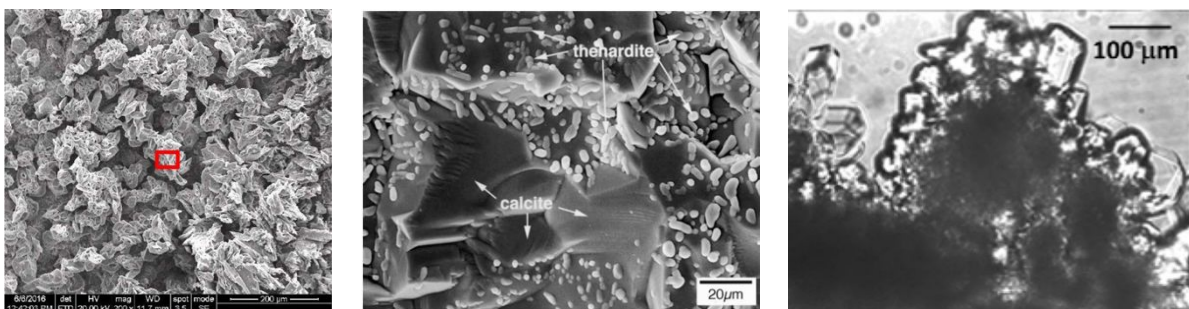


Fig. 2-10 ESEM image of thenardite on the surface of a cement paste sample [61] (left); thenardite on a decayed limestone spall fragment [24] (middle); and formation of large grape-like mirabilite clusters due to growth of mirabilite on the small thenardite crystallites as nucleation sites in sandstones [30] (right).

A latent time is observed in “chemical sulfate attack” before the “take-off” point of significant expansion. A similar latency period (the sulfate accumulation period before damage) in “physical sulfate attack” should analogously exist [60]. Moreover, possible localized chemistry is an inherent feature in the process of non-

homogeneous evaporation in the drying front. The sulfate progress is mainly through capillary porosity, but the ingress rate should be considered as a time-dependent parameter, due to the microstructure changes from the phase alterations. The later microcracking caused by ettringite formation or salt crystallization can further increase the sulfate ingress [44,62,63].

Salts form in the condition when the sulfate is sufficiently high, as seen from the thenardite solubility diagram in Fig. 2-11. This can explain the possible long sulfate accumulation period before we observe the crystallization and, later on, the damage. The high relative humidity is required to form mirabilite as indicated in Fig. 2-5, which makes it more difficult to meet the supersaturation under realistic conditions.

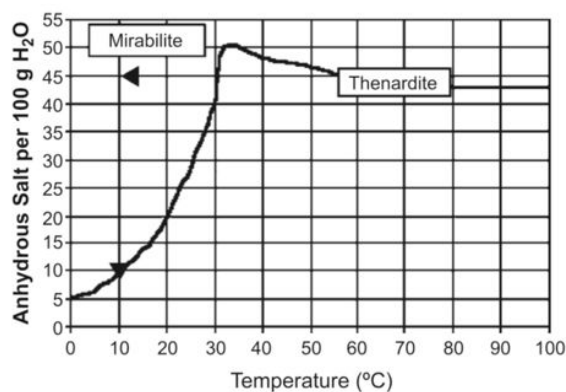


Fig. 2-11 Solubility of anhydrous sodium sulfate in water as a function of temperature [28].

Another important mechanism associated with spalling damage is carbonation. Popcorn calcite was found tightly packed with rosette-like clusters (up to 60  $\mu\text{m}$ ) when the sulfate source was present. They formed in the vicinity of a calcium-depleted highly porous and friable cement paste matrix [64,65]. In this type of carbonated region, spalling can occur when salts crystallize in the weakened cementitious matrix. Moreover, the carbonation can change the chemistry of pore solution, i.e., the decreased free alkali content in pore solution, decreased pH, and changed porosity. All those parameters mentioned above are dependent on the cement types. The consequences of blended cements due to carbonation can be quite different as the  $\text{CO}_2$  buffer capacity is lower than PC, alkali ionic concentration is lower, and the decalcification on C-S-H can be more aggressive. Some researchers showed that concrete with more carbonation could be seen with more physical sulfate attacks resulting in the increased surface scaling [57,66]. As stated above, some researchers have shown that spalling damage is more often observed in blended cements. If we combine these two statements, it seems that the degree of carbonation may be the intrinsic reason for more spalling damage, as the carbonation is more profound in cement systems with SCMs than in PC systems.

Due to its complexity, and despite extensive ongoing studies with various national, international standards and adapted procedures on the stone materials, no common or standard testing method for studying the physical attack of cement-based materials exists, as yet [67]. The most important point to consider in a proper test is to recreate damage found in practice, including damage from the surfaces of concrete. The capillary



rise should be mimicked, for sampling and characterization, and key factors should be controlled. However, the characterization of drying properties is not done adequately, which makes interpretation of the damage mechanism a subtle task.

## 2.4 Parameters influencing sulfate attack

### Cement types

In the first half of the last century, so-called sulfate-resisting cements were developed with low  $C_3A$  content (SRPC, type V cement). These cements have been widely shown to perform better in sulfate solutions. But the role of the  $C_4AF$ -ferrite phase (which also hydrates into the same aluminium-bearing phases as  $C_3A$ : e.g. monosulfate) is playing in the contribution of sulfate degradation has not been much investigated. Some studies have already shown that SRPC cannot prevent sulfate attack completely, but can decrease the kinetics of damage to some extent, so the ferrite seems to be the reason that sulfate attack is still ongoing, with much slower kinetics. High sulfate-resisting cements should be investigated to determine the contribution of the ferrite phase to expansion in full immersion tests.

However, in blended cement materials, the sulfate ingress and damage behaviors are not the same as PC, which also brings up another important aspect of external sulfate attack: salt crystallization attack, or so-called physical sulfate attack.

Blended cements usually show better sulfate resistance to chemical sulfate attacks [38,49,68]. The expansion and large cracks are significantly decreased compared to Portland cement. This is mainly because of the decreased clinker factor, that results from the replacement level of SCMs, and pore refinement which decreases the permeability as well as the pozzolanic consumption of portlandite, which may decrease the ettringite supersaturation.

In the case of slag blended cement systems part of the aluminium is taken up by the hydrotalcite phase, which may not contribute much to the ettringite formation. Aluminium can also be incorporated into C-S-H to become C-A-S-H, which reduces the transformable Al-containing phases (AFms), which can potentially form ettringite to cause expansion [37,39]. Some researchers suggest that slag blended cement tends to soften and cause the loss of adhesiveness rather than expanding due to sulfate attack [48,49]. A thin layer degraded zone is usually found in slag systems, without seeing progressive inwards movement of layers. It suggests that more Ca needed for ettringite formation is coming from the decalcification of C-S-H, which reduces strength. Neither the hydrogarnet-type nor hydrotalcite-type phase appear to contribute to ettringite formation [39].

Cement systems incorporating limestone have been investigated, and an appropriate limestone replacement level is recommended to retain a good sulfate-resistance (It is often suggested around 5 % in standards and maximum 10 % is still to have good performance) [6,44]. A ternary system like limestone calcined clay cements (LC<sup>3</sup>) show good resistance to chemical sulfate attack under full immersion tests [68]. The conversion of carboaluminate to sulfoaluminate in LC<sup>3</sup> requires a sulfate source in addition to the conversion to the ettringite phase, which may require a higher sulfate concentration than in PC systems [68]. Therefore, a minimal expansion (less than 0.05 %) after nearly two years of exposure was observed [69]. It also shows good resistance to thaumasite attack, even though calcite is present in this ternary cement [70].

The modification of C-S-H after sulfate attack should be of concern, as it is the abundant binding hydrate, and is the biggest contributor to the mechanical strength of cement. In particular, disintegration after sulfate attack is dominant in Mg-based sulfate solution [50] (non-adhesive M-S-H is replacing C-S-H) and blended systems [48] generally show reduced expansion, but more transformation of the C-S-H phase).

Studies show that the C-S-H structure is changed due to sulfate attack by decalcification: the average length of C-S-H chains increases [71]. This phenomenon may be more profound in blended systems where the Ca/Si ratio is lower than that in PC systems. There is evidence from nano-indentation tests that lower stiffness C-S-H is generally observed in the blended cement [72]. Therefore, it hints that sulfate ions may attack more on the C-S-H phase in low Ca/Si-based C-S-H containing blends.

It is common to observe the higher susceptibility of surface spalling in SCMs incorporated materials due to salt crystallization [58,73].

#### Water-to-cement ratio (w/c)

Water-to-cement ratio has been investigated extensively as an essential factor, with great influence over the kinetics and the extent of expansion. A low w/c ratio can efficiently extend the latent period before expansion to even more than 10 years [74]. It was recommended already in the 1970s by the technical committee that lower w/c ratios and high-density concrete are imperative at all sulfate levels. Minimum cement content with an appropriate cement type and maximum w/c was recommended [12]. In most standards, the w/c was clearly limited to a certain level (See standards in Table 2-1). Capillary porosity in cement materials is suggested as the intrinsic factor that impacts the expansion rate and latency time [75]. A faster adsorption rate of concrete can carry more salt solution and may also influence the degradation kinetics [62,76]. Cement with lower w/c has less total porosity and pore connectivity, which was also cited as a reason for a better sulfate resistance [5,77]. Studies on the stones and rocks have shown that salt crystallization is closely associated with pores less than 100 nm [16], even though the pore size of natural stones is generally coarser than the concrete (tens of micrometres instead of nanometers) [60].

In terms of the physical aspect, lower w/c ratios of concrete with high mechanical resistance show a different expansion behavior, when compared to sulfate resistance. The expansion is less common in low w/c concrete, as the stress caused by crystallization pressure has to be beyond the tensile strength for large expansion to continue.

#### Cement paste vs mortar or concrete

The different scales of cement paste, mortar and concrete samples were all investigated for sulfate resistance, but only the mortar prism samples were considered as a standard test method in ASTM C1012-18, which only addresses the chemical sulfate attack aspect of PC mortars in an accelerated condition. There are advantages to using paste or concrete samples to characterize the different aspects of sulfate resistance. For example, cement paste samples can largely shorten the testing time, and the analysis of phases in the microstructure is more practical. On the other hand, mortar/concrete samples are closer to real practice. However, sulfate ions only react with cement paste bulk, and aggregates are inert to sulfate.

The ingress of sulfate in mortar is similar to that of cement paste even though aggregates are present. This is confirmed by the experimental observations of the sulfur ingress in the front, as the front is quite flat and evenly distributed at the same level of penetration depth [78].

However, mortar samples are generally larger and this delays the degradation process compared with cement paste [78]. Thus, it requires more time to run experiments by using mortar or concrete samples. The damage behavior is similar no matter the scale of the samples, they all follow the “two-phase” expansion propagation, “latency period” and “fast expansion increasing period”, although the duration of the latent period can be different.

#### Sulfate concentration

Sulfate concentration in the field is usually below 10 mmol/L which is not sufficient to cause gypsum formation [45]. However, higher concentrations are often used in laboratory tests to accelerate the tests.

The concentration can change the expansion rate after the onset of the significant expansion [2,15,79]. However, the sulfate concentration does not significantly change the latent period, according to the initial deposition of attack products[15]. This implies that in this latent period, perhaps ettringite forms mostly in the relatively big pores, where there is less concentration dependence and it can easily take place [9,31]. Once the expansion is initiated, then sulfate concentration takes the main role in establishing supersaturation in the smaller pores [4].

Gypsum and ettringite can only precipitate together in a highly concentrated sulfate solution, and normally it is more aggressive than the case of simple ettringite formation [42]. The presence of gypsum can guarantee the high supersaturation of ettringite that tends to create more expansion [41,80,81].

Gypsum can form in cracks when a sulfate concentration above 10 mmol/L is applied in laboratory experiments [35,82] which is not a realistic case, when compared with field conditions. However, gypsum can still form in field conditions, more often in the wet/dry interfacial zone where the high concentration of sulfate is accumulated [83]. Cracks forming under high sulfate concentration accelerate the penetration of further sulfate ions, and progressive degradation by layers can be triggered. The ultimate damage due to the progressive inward movement of the distinct zones is observed.

### Exposure conditions

Temperature is a very important factor. It can change the reaction rates and thermodynamical parameters [84], such as the capillary rise rate and solubility of ettringite [85] and gypsum. As a consequence, the kinetics of degradation can be accelerated as the latent time is shortened, when the high temperature of solution curing is applied, but similar expansion rates were found no matter what the solution temperature is [84]. However, the expansion rate is increased in blended mortars at low solution temperatures (except metakaolin, as even though thaumasite forms there is not much expansion) [86]. This can be attributed to the fact that the pozzolanic reactions of slag and fly ash mortars are slow at low temperatures, which gives a weak microstructure.

The pH of the sulfate solution is a concern that may influence the Ca leaching, leading to an acceleration of the sulfate ingress and the layer degradation [5,45]. The low pH level (around 6-8) can hence reduce the latent period [87]. Leaching (decalcification and dealumination of C-(A)-S-H) causes the progressive degradation and gypsum/thaumasite formation in a relatively low pH environment [5,6,88].

The presence of cation  $Mg^{2+}$  can decrease the extent of expansion to almost one-third relative to the mortars immersed in the sodium sulfate solution [54]. A rapid brucite layer formation on the surface occurs immediately after the introduction into a solution of magnesium sulfate. A continual expansion increase was observed instead of two-stage expansion, as in sodium sulfate solution. Bicarbonate ions ( $HCO_3^-$ ) in sulfate solution can decrease the expansion [50].

## 2.5 Current testing methods

### Full immersion

The most commonly used test method is ASTM C1012-18a which is summarized in the table of standards in section 2.6. It was modified for cement paste samples [89]. It is a test accelerated by the use of a high sulfate

concentration but is not necessarily representative of field concrete, where chemical sulfate attacks are rarely observed.

### Semi-immersion

Concrete/mortar semi-immersion tests are used for the purpose of investigating physical sulfate attack. However, there is no commonly accepted protocol and guidelines for different laboratories. Scherer [4] conducted the stone experiments inside a humidity controlled (~39 %) box, prismatic stone samples (50 × 50 × 250 mm) were suspended with only the bottom immersed in a solution of sodium sulfate (16 wt.% sodium sulfate). The cracks due to salt crystallization could occur after just 8 days in the limestone samples. However, little damage was observed after 47 days in sandstone. The difference was attributed to the sorptivity (it is defined as a measure of the capacity of the medium to absorb or desorb liquid by capillarity), an order of magnitude smaller of sorptivity for limestone compared to sandstone, which caused more susceptibility to the subflorescence of sodium sulfate below the surface. Nehdi [77] investigated the effect of concrete curing on the degree of damage by salt crystallization. Concrete cylinders (100 × 200 mm) were used in the semi-immersion test, partially immersed in a 5 wt.% sodium sulfate solution with a weekly cycle of temperature and relative humidity. It was found that blended systems with pozzolanic minerals had more surface scaling than plain Portland cement concrete.

At the same time, the influence of the cyclic exposure on the relative rate between evaporation and sorptivity was ignored, which could be the intrinsic mechanism responsible for the increased surface scaling in non-cured concrete and SCMs incorporated concrete. They should have a higher evaporation rate than capillary suction, resulting in subflorescence that potentially causes damage only when the crystallization pressure exceeds the tensile strength of the individual concrete. Liu [61] used another modified protocol adapted from the partial immersion test: cement pastes samples (10 × 40 × 150 mm) were exposed to sodium sulfate solution (10 wt.%). One constant exposure condition (20 ± 2 °C and 60 ± 5 % RH) and another with daily alternate exposure (one day for 30 ± 2 °C and 80 ± 5 % RH, one day for 20 ± 2 °C and 60 ± 5 % RH) were conducted. The damage appeared much earlier in cyclic exposure (only after one cycle) than that in constant conditions (very little damage appeared after 72 days).

The protocols were totally different and modified from different labs, which made the comparison very challenging. Therefore, the results cannot be easily reproduced due to the insufficiently controlled solution level, different sample size, relative humidity and fluctuations above the solution. The biggest drawback of this approach is that to examine physical sulfate attack requires a very particular testing environment. The complex flow (Fig. 2-12) of sulfate solution also complicates the characterization, in particular proper sampling for characterization is problematic. All the details of this semi-immersion approach should be consistent.

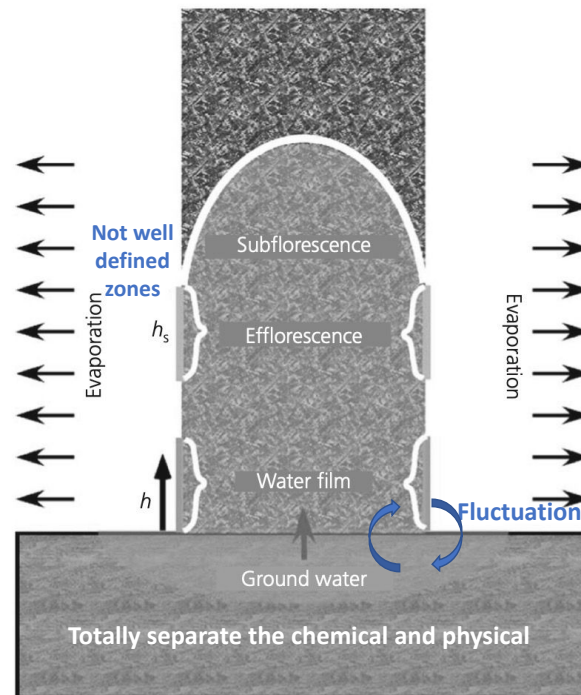


Fig. 2-12 The schematic diagram of semi-immersion test for a concrete block, adapted from [4].

### Drying/wetting cycles

The cyclic drying and wetting method [30] (Fig. 2-13) used for cement-based materials was adapted from the standard test method for natural stones EN 12370. It is not a representative method for most situations found in the field as the sulfate penetration mechanism is not the same, nor are the salt load and temperature. However, the damage mechanism by salt crystallization was found in the rewetting process, in which mirabilite formed, supersaturated from the dissolution of thenardite [4,11,31]. Although the unusually high supersaturation is produced by wetting and drying cycles of exposure environments. The mechanism found as a phase transformation (molar volume increase 314 % from thenardite to mirabilite) causing expansive stress is not sufficiently acceptable [25].



Fig. 2-13 Granular disintegration of the salt-contaminated sandstone [30].

## 2.6 Evaluation criteria for sulfate resistance of cementitious materials

The sulfate attack relevant standards are listed in the Table 2-1 below. It reviews the most important standards in this field, including prescriptive and performance testing standards.

Table 2-1 The current standard methods for sulfate resistance and prescriptive standards

	Items	Year, Ref	Comments
Prescriptive standards	ASTM C150-07	2007 [90]	5 % C <sub>3</sub> A content is limited
	NF EN 206-1	2021 [91]	Limitations on the maximum w/c ratio, minimum cement content, minimum compressive strength. Maximum proportion of fly ash and slag is limited to 15 wt. %
Performance-based standards	PD CEN/TR 15697:2008	2008 [92]	Report contains comprehensive aspects on prescriptions and performance test features
	SIA 262/1	2013 [93]	Accelerated test for concrete samples by drying (50 °C) and wetting (5 % sodium sulfate solution) cycles then expansion track after 8 weeks in 5 % sodium sulfate solution
	ASTM C1012-18a	2018 [14]	Accelerated test for mortar prisms at 50 g/L sulfate solution, w/c=0.485
	ASTM C452-21	2021 [94]	It only applies to determine expansion of Portland cement incorporated with 7 % SO <sub>3</sub>
Standard for natural stones	EN 12370: 2020	2020 [95]	The test procedure is not so representative for common capillary rise situation in practice

The widely involved chemical and physicochemical complexities of the mechanisms in the process of sulfate attack led to the decay of mechanical properties, causing expansion, cracking, spalling, delamination, softening, etc. This very complicated outcome makes the assessment rather challenging.

Fig. 2-14 summarizes the most common manifestations and associated assessments. The different manifestations depend on the exposure conditions. The sensitivity of the techniques also varies depending on the testing procedures and materials. Microstructure analytical methods (i.e., SEM) are quite reliable but it is usually very time-consuming to obtain the results, and it is not possible to apply these in practice.

A more rigorous method needs to be proposed to evaluate the properties after an external sulfate attack, particularly, a fast, robust, and reliable one for practice. Relying on only one method is not enough to cover all the aspects discussed above. Mass loss/gain over time accompanied by expansion and visual inspections can give the most reliable evaluation, as other properties are able to reflect on at least one aspect of the mass changes, expansion or appearance changes.

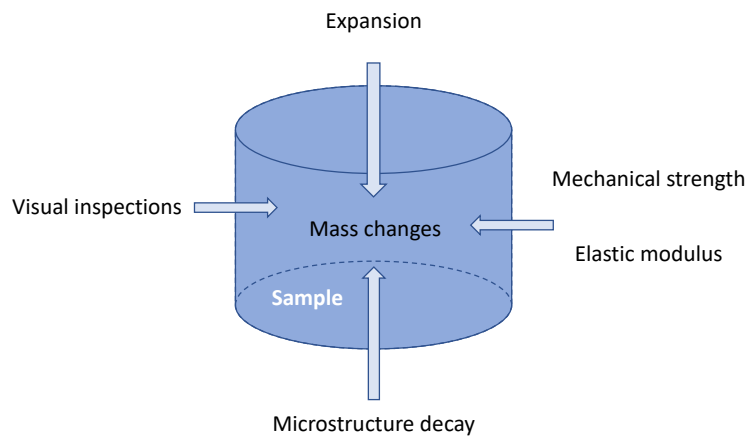


Fig. 2-14 The schematic of possible evaluations for sulfate resistance.

## 2.7 Summary and knowledge gaps

External sulfate attack on concrete has been recognized for 135 years, studies on crystallization in porous materials (stones and concrete) began more than 170 years ago [11]. A review of this research and the key findings should be carried out before any further investigation. From a pragmatic point of view, research helps to solve the real problems in field applications, or guide practical implementations. Therefore, a survey of the research on this topic will be followed.

The purpose of this Table 2-2 is threefold: firstly, it is proof of the benchmarking studies that developed our understanding, step by step over the decades. However, it also shows us how research is connected to real-world cases; secondly, it summarizes in a concise table up-to-date findings and research strategies for the most relevant open questions, which should be a useful reference to those who are interested or investigating this topic, and serves as a beacon showing the researchers the right direction: not only the proper testing method but also the continuous rethinking of the correct research interest; thirdly, to provide recent technical information of the testing for cement paste samples, according to the logic of the research of this thesis.

Many aspects of the scientific topic of sulfate attack on cementitious materials were reviewed in this chapter. Due to its complexity - involving cement chemistry, physiochemical reactions, poromechanics, pore solution and the mechanical/physical properties of the materials - there are many factors that can change the ultimate consequences of sulfate damage if different parameters are applied in the investigating process. The main knowledge gaps that necessarily need to be addressed are as follows:

- The understanding of the degradation mechanisms and the links with the observed manifestations: in particular, the expansion and cracking mechanisms for the innovative, emerging supplementary cementitious materials.
- A proper performance-based characterization method for sulfate attack is necessary to understand and clearly distinguish the sulfate resistance of cement types upon sulfate degradation. Expansion



alone is not a representative evaluation of sulfate resistance. The testing protocol more oriented to realistic field conditions is often neglected in current research.

- The physical sulfate attack is an increasingly hot topic of research, though the damage mechanism is still not well known. A more robust and practical testing approach regarding the mechanism of physical sulfate attack is increasingly demanded. By achieving this, a properly designed approach is needed, to combine the two aspects of sulfate degradation. Capillary suction (which does not feature in past studies) and the sulfate ingress should be taken into account simultaneously, during the exposed conditions.

To tackle these knowledge gaps, and to find answers to some specific research questions, a new approach is needed. There has been a recent development to combine both types of sulfate attack and to avoid the drawbacks present in the current testing approaches and standards [96]. It can be widely applied for relatively small cement paste and mortar samples, showing a well-defined sulfate concentration gradient, with the degradation from chemical and physical attacks shown simultaneously in one single sample. This demonstrates a great potential for studying the sulfate attack. Most importantly, the results are less dependent on the laboratory, with a more accurate, practical, fast and robust approach. It also well represents the field situations that can incur changes in temperature and relative humidity. The details are shown in *Chapter 3*, where technical parts of this approach can be found.

In this thesis, we aim to address the following research questions based on the knowledge gaps:

- What can we learn from the unidirectional penetration approach?
- Can we stop sulfate attack by lowering w/c?
- How long does it take to establish whether degradation is going to occur?
  - What is the critical aspect of degradation?
- How can we accelerate physical sulfate attack resistance testing?
- Is selecting the right binder sufficient to stop sulfate attack?
  - Is cement with low C<sub>3</sub>A content sufficient to prevent sulfate attack?
  - What role does curing temperature have in the degradation process of HS cement mortar?
  - The behavior of blended systems with SCMs?
- What is the damage mechanism of salt crystallization attack?
  - Is cyclic exposure necessary?
- What are the factors beneficial for both the “chemical” and “physical” aspects?

Table 2-2 shown below contains the most important literature published in the last 30 years in the field of sulfate attack on concrete. It shows the research strategy and that over the years cement pastes characterization and physical sulfate attack aspects become more importantly concerned.

Table 2-2 The research history, strategy, interest on sulfate attack of cement and concrete.

Year(s)/Ref	Author(s)	Cement/mortar/concrete	Exposure conditions	Experimental/field studies	Comments
1887 [34]	D.Breyse	Concrete walls interact with gypsum	Field condition	First case of external sulfate attack in <b>Paris</b>	The reaction propagates from the surface towards the concrete core by an external sulfate source.
1949 [97]	Carl W. Correns	Cement pastes	Theory	Theoretical estimation	The first person who estimated the crystallization pressure and derived the equation to calculate the crystallization pressure ( $P_{V_{solid}}=RT\ln C/C_s$ ). The “take off” time is inversely proportional to the fineness of the expansive component (C3A, monosulfate, etc.); The expansion is proportional to the amount of sulfate source.
1983 [98]	M.D. Cohen	Cement pastes	w/c=0.4	Modelling & experimental	High temperature, water, sulfate and aluminum contents of cement, alkali content of concrete is key.
1987 [34]	D.Breyse	Precast concrete on railway tracks	Field condition	First case of internal sulfate attack in <b>Finland</b>	Two conditions are necessary to cause crystallization pressure: 1) confined crystal growth, 2) supersaturation;
1992 [9]	Ping Xie and Beaudoin J. J.	Cement pastes and concretes	Theory	Chemical thermodynamics and experimental	Sulfate expansion is a process in which chemical energy converts into mechanical work to overcome the cohesion of materials. A higher concentration of $Ca^{2+}$ ion in the pore solution is a basic assurance for activation of crystallization pressure from ettringite or gypsum (the former is more easily encountered); It is a universal phenomenon as long as these two conditions are satisfied, such as the expansion from $Mg(OH)_2$ forming in a confined space;
1992 [36]	Ping Xie and Beaudoin J. J.	Cement pastes, mortar and concretes	Theory	Chemical thermodynamics and experimental	The activity of reactants in the pore solution is the key factor to impact sulfate expansion.
1992 [22]	R.S.Gollop and H.F.W.Taylor	Cement pastes, 25mm cubes	0.25 mol/L $Na_2SO_4$ or $MgSO_4$ solution; w/c=0.3 for 6 months	Experimental by SEM/EDS	First time to demonstrate the layer wise degradation from sulfate attack; BSE images showed the layer damage from the surface towards the interior in materials.
1994 [52]	James G. Wang	Cement pastes	Constant pH 6; 5 % $Na_2SO_4$ solution; w/c=0.4, 0.5 and 0.6	Experimental	First time to demonstrate the layer-wise degradation by XRD tests on pastes with different depths from sulfate solution; Low pH can cause leaching of portlandite which influences the mechanical properties of materials.
1995 [99]	C.D. Lawrence	Cement mortar prisms [40×40×160mm] and cement pastes	Elevated curing temperature from 60 to 100 °C; w/c=0.5	Experimental <b>DEF</b>	The cement composition is key to impact expansion due to DEF: such as $MgO$ and $SO_3$ ; The minimum temperature to trigger expansion is above 65 °C; Expansion from DEF can take place in cement pastes without ASR as a precursor.
1995 [100]	R.S.Gollop and H.F.W.Taylor	Sulfate resisting cement paste, 25mm cubes	0.25 mol/L $Na_2SO_4$ or $MgSO_4$ solution; w/c=0.3 for 6 months	Experimental by SEM/EDS	The cracking and mass loss were less profound than PC; Gypsum formation seems less important than ettringite to cause expansion.
1996 [49]	R.S.Gollop and H.F.W.Taylor	70 % replacement by slag, 25mm cement paste cubes	0.25 mol/L $Na_2SO_4$ or $MgSO_4$ solution; w/c=0.3 for 6 months	Experimental by SEM/EDS	The slag blended cement tends to soften and disintegrate rather than expand as a result of sulfate attack; The loss of cohesion and strength to the destruction of C-S-H is the main damage; Ca needed for ettringite formation is partly from CH and the other from decalcification of C-S-H;
1996 [101]	R.Yang, C.D. Lawrence and J.H. Sharp	Cement paste prisms [40×40×160mm]	Curing temperature at 100 °C; w/c=0.45	Experimental <b>DEF</b> by SEM/EDS	Low or even no expansion was detected with slag blended cement. Cement paste samples take more time to reach the onset of the significant expansion than mortar or concrete;

1996 [58]	E.F. Irassar, A. Di Maio and O.R. Batic	Concrete with HS, fly ash, natural pozzolan and slag	Field condition for 5 years, half-buried concrete in sulfate bearing soil; w/c=0.52	Field condition test	<p>The much-delayed expansion (after 2.5 years) may come from the lower w/c in cement paste systems – comment from the writer. Concrete with a higher content of SCMs had the greater surface scaling due to the salt crystallization;</p> <p>Capillary suction is the main mechanism of water and salt transportation in the atmospheric zone.</p> <p>Temperature (above ~70 °C) is a key factor to cause expansion due to DEF;</p> <p>Alkali hydroxide curing solution can inhibit expansion propagation;</p> <p>Sulfate expansion mechanism of DEF is similar with ESA.</p>
2001 [1]	Taylor and Karen	Review paper			<p>Laboratory tests lead to misleading impression on severity of sulfate attack, field cases seldom reported the significant “ettringite” type attack;</p> <p>Large surface to volume ratios accelerates degradation;</p> <p>Only 3 to 5 mm affected depth was observed after 20 years without showing any mechanical strength decrease.</p> <p>A clear damage mechanism model was proposed, three distinct deteriorated zones were discussed;</p> <p>Magnesium sulfate can attack more on C-S-H results in M-S-H.</p>
2002 [33]	Harvey Haynes	Concrete		Laboratory vs field experience	<p>The damage of sodium sulfate is from the rewetting process where mirabilite crystallizes; The extensive damage occurs once no longer possibilities of salts growing further as there is a salt content threshold in porosity.</p> <p>Experimental study and theoretical analysis showed the crystallization of sodium sulfate formation is the driving force to cause damage.</p> <p>A simple conceptual model for the development of salt damage was proposed: “induction phase” to accumulate the salts in the pores without causing any detectable damage, and the “propagation phase” to initiate the fast degradation.</p>
2003 [15]	Santhanam	Mortar	Full immersion	Laboratory test	<p>A sulfate concentration gradient transfer occurs but rapidly end up with only the sulfate accumulation on surfaces;</p> <p>Ettringite can form from the aluminum incorporated in C-S-H;</p> <p>C-S-H chain is extended due to decalcification.</p>
2003 [29]	Tsui, Flatt and Scherer	Limestone	Wetting and drying cycles	Laboratory test	<p>Limestone contributes to a faster deterioration of cement paste;</p> <p>Mechanical properties drop significantly tested by nanoindentation;</p> <p>Three distinct layers of brucite, gypsum and leached cement matrix consist a deterioration front.</p>
2004 [28]	Thaulow and Sahu	Sodium sulfate dissolution and precipitation	Change temperature and humidity	Laboratory test	
2017 [60]	Flatt, Nevin, Francesco, et al.	Natural stones	Semi-immersion	Laboratory test	
2019 [5]	Rim Ragoug et. al	CEMI Cement paste cylinders w/c ratios of 0.45 & 0.6 [D=10cm, H=5cm]	Constant pH (8 ± 0.1) of sodium sulfate solution (15 g/L); Semi-immersion T= 5 ± 1°C for 6 months	ICP-AES; TGA; ESEM; XRD; NMR	
2021 [6]	Sotiriadis et. al	Portland-limestone cement paste cylinders [D=21mm, H=42mm]	MgSO <sub>4</sub> solution [5.1 g/L Mg <sup>2+</sup> and 20 g/L SO <sub>4</sub> <sup>2-</sup> ]; w/c=0.45; full immersion except the surface in contact with the container	μ-computed T; Solid state NMR spectroscopy; Nanoindentation; Thermodynamic modelling	

## 2.8 Reference

- [1] H.F.W. Taylor, C. Famy, K.L. Scrivener, Delayed ettringite formation, *Cement and Concrete Research*. 31 (2001) 683–693. [https://doi.org/10.1016/S0008-8846\(01\)00466-5](https://doi.org/10.1016/S0008-8846(01)00466-5).
- [2] C. Yu, W. Sun, K. Scrivener, Mechanism of expansion of mortars immersed in sodium sulfate solutions, *Cement and Concrete Research*. 43 (2013) 105–111. <https://doi.org/10.1016/j.cemconres.2012.10.001>.
- [3] B. Lothenbach, G. Le Saout, E. Gallucci, K. Scrivener, Influence of limestone on the hydration of Portland cements, *Cement and Concrete Research*. 38 (2008) 848–860. <https://doi.org/10.1016/j.cemconres.2008.01.002>.
- [4] G.W. Scherer, Stress from crystallization of salt, *Cement and Concrete Research*. 34 (2004) 1613–1624. <https://doi.org/10.1016/j.cemconres.2003.12.034>.
- [5] R. Ragoug, O.O. Metalssi, F. Barberon, J.-M. Torrenti, N. Roussel, L. Divet, J.-B. d’Espinoze de Lacaillerie, Durability of cement pastes exposed to external sulfate attack and leaching: Physical and chemical aspects, *Cement and Concrete Research*. 116 (2019) 134–145. <https://doi.org/10.1016/j.cemconres.2018.11.006>.
- [6] K. Sotiriadis, M. Hlobil, A. Viani, P. Mácová, M. Vopálenský, Physical-chemical-mechanical quantitative assessment of the microstructural evolution in Portland-limestone cement pastes exposed to magnesium sulfate attack at low temperature, *Cement and Concrete Research*. 149 (2021) 106566. <https://doi.org/10.1016/j.cemconres.2021.106566>.
- [7] M. Santhanam, M.D. Cohen, J. Olek, Sulfate attack research — whither now?, *Cement and Concrete Research*. 31 (2001) 845–851. [https://doi.org/10.1016/S0008-8846\(01\)00510-5](https://doi.org/10.1016/S0008-8846(01)00510-5).
- [8] P.K. Mehta, SULFATE ATTACK ON CONCRETE: SEPARATING MYTHS FROM REALITY A critical look at the seriousness of this problem, *CONCRETE INTERNATIONAL -DETROIT-*. 22 (2000) 57–61.
- [9] X. Ping, J.J. Beaudoin, Mechanism of sulphate expansion I. Thermodynamic principle of crystallization pressure, *Cement and Concrete Research*. 22 (1992) 631–640. [https://doi.org/10.1016/0008-8846\(92\)90015-N](https://doi.org/10.1016/0008-8846(92)90015-N).
- [10] B. Lothenbach, F. Winnefeld, C. Alder, E. Wieland, P. Lunk, Effect of temperature on the pore solution, microstructure and hydration products of Portland cement pastes, *Cement and Concrete Research*. 37 (2007) 483–491. <https://doi.org/10.1016/j.cemconres.2006.11.016>.
- [11] R.J. Flatt, Salt damage in porous materials: how high supersaturations are generated, *Journal of Crystal Growth*. 242 (2002) 435–454. [https://doi.org/10.1016/S0022-0248\(02\)01429-X](https://doi.org/10.1016/S0022-0248(02)01429-X).
- [12] Jan Skalny, Jacques Marchand, Ivan Odler, *Sulfate Attack on Concrete*, London and New York, 2002. [https://www.bookdepository.com/Sulfate-Attack-on-Concrete-J.-Marchand/9780419245506?redirected=true&utm\\_medium=Google&utm\\_campaign=Base5&utm\\_source=CH&utm\\_content=Sulfate-Attack-on-Concrete&selectCurrency=CHF&w=AF72AU9SLSQSCQA803VV&pdg=pla-293946777986:kwd-293946777986:cmp-1578060869:adg-65091841852:crv-296436506046:pid-9780419245506:dev-c&gclid=EA1aIqobChMizbvA6M-a4gIViuR3Ch0tjw8TEAYYASA-BEgJUXPD\\_BwE](https://www.bookdepository.com/Sulfate-Attack-on-Concrete-J.-Marchand/9780419245506?redirected=true&utm_medium=Google&utm_campaign=Base5&utm_source=CH&utm_content=Sulfate-Attack-on-Concrete&selectCurrency=CHF&w=AF72AU9SLSQSCQA803VV&pdg=pla-293946777986:kwd-293946777986:cmp-1578060869:adg-65091841852:crv-296436506046:pid-9780419245506:dev-c&gclid=EA1aIqobChMizbvA6M-a4gIViuR3Ch0tjw8TEAYYASA-BEgJUXPD_BwE) (accessed May 14, 2019).
- [13] W. Michaelis, THE BEHAVIOUR OF PORTLAND CEMENT IN SEA-WATER., *Minutes of the Proceedings of the Institution of Civil Engineers*. 107 (1892) 370–376. <https://doi.org/10.1680/imotp.1892.20314>.
- [14] Standard Test Method for Length Change of Hydraulic-Cement Mortars Exposed to a Sulfate Solution, *ASTM C1012-18a*, 2018. [https://compass.astm.org/EDIT/html\\_annot.cgi?C1012+18b](https://compass.astm.org/EDIT/html_annot.cgi?C1012+18b) (accessed February 12, 2020).
- [15] M. Santhanam, M.D. Cohen, J. Olek, Mechanism of sulfate attack: a fresh look: Part 2. Proposed mechanisms, *Cement and Concrete Research*. 33 (2003) 341–346. [https://doi.org/10.1016/S0008-8846\(02\)00958-4](https://doi.org/10.1016/S0008-8846(02)00958-4).
- [16] S. Yu, C.T. Oguchi, Complex relationships between salt type and rock properties in a durability experiment of multiple salt-rock treatments, *Earth Surface Processes and Landforms*. 34 (2009) 2096–2110. <https://doi.org/10.1002/esp.1904>.
- [17] M. Whittaker, L. Black, Current knowledge of external sulfate attack, *Advances in Cement Research*. 27 (2015) 532–545. <https://doi.org/10.1680/adcr.14.00089>.
- [18] D.A. Kulik, T. Wagner, S.V. Dmytrieva, G. Kosakowski, F.F. Hingerl, K.V. Chudnenko, U.R. Berner, GEM-Selektor geochemical modeling package: revised algorithm and GEMS3K numerical kernel for coupled simulation codes, *Comput Geosci*. 17 (2013) 1–24. <https://doi.org/10.1007/s10596-012-9310-6>.
- [19] T. Wagner, D.A. Kulik, F.F. Hingerl, S.V. Dmytrieva, GEM-SELEKTOR GEOCHEMICAL MODELING PACKAGE: TSolMod LIBRARY AND DATA INTERFACE FOR MULTICOMPONENT PHASE MODELS, *The Canadian Mineralogist*. 50 (2012) 1173–1195. <https://doi.org/10.3749/canmin.50.5.1173>.
- [20] B. Lothenbach, D.A. Kulik, T. Matschei, M. Balonis, L. Baquerizo, B. Dilnesa, G.D. Miron, R.J. Myers, Cemdata18: A chemical thermodynamic database for hydrated Portland cements and alkali-activated materials, *Cement and Concrete Research*. 115 (2019) 472–506. <https://doi.org/10.1016/j.cemconres.2018.04.018>.
- [21] B. Lothenbach, B. Bary, P. Le Bescop, T. Schmidt, N. Letierrier, Sulfate ingress in Portland cement, *Cement and Concrete Research*. 40 (2010) 1211–1225. <https://doi.org/10.1016/j.cemconres.2010.04.004>.
- [22] R.S. Gollop, H.F.W. Taylor, Microstructural and microanalytical studies of sulfate attack. I. Ordinary portland cement paste, *Cement and Concrete Research*. 22 (1992) 1027–1038. [https://doi.org/10.1016/0008-8846\(92\)90033-R](https://doi.org/10.1016/0008-8846(92)90033-R).
- [23] N. Ghafoori, I. Batilov, M. Najimi, Influence of Nanosilica on Physical Salt Attack Resistance of Portland Cement Mortar, *MJ*. 117 (2020) 67–80. <https://doi.org/10.14359/51725779>.
- [24] C. Rodriguez-Navarro, E. Doehne, E. Sebastian, How does sodium sulfate crystallize? Implications for the decay and testing of building materials, *Cement and Concrete Research*. 30 (2000) 1527–1534. [https://doi.org/10.1016/S0008-8846\(00\)00381-1](https://doi.org/10.1016/S0008-8846(00)00381-1).
- [25] C. Rodriguez-Navarro, E. Doehne, Salt weathering: influence of evaporation rate, supersaturation and crystallization pattern, *Earth Surface Processes and Landforms*. 24 (1999) 191–209. [https://doi.org/10.1002/\(SICI\)1096-9837\(199903\)24:3<191::AID-ESP942>3.0.CO;2-G](https://doi.org/10.1002/(SICI)1096-9837(199903)24:3<191::AID-ESP942>3.0.CO;2-G).

- [26] D.H. Yaalon, SALT WEATHERINGSalt weathering, in: M. Schwartz (Ed.), *Beaches and Coastal Geology*, Springer US, New York, NY, 1984: pp. 708–709. [https://doi.org/10.1007/0-387-30843-1\\_384](https://doi.org/10.1007/0-387-30843-1_384).
- [27] W. Kunther, B. Lothenbach, K.L. Scrivener, On the relevance of volume increase for the length changes of mortar bars in sulfate solutions, *Cement and Concrete Research*. 46 (2013) 23–29. <https://doi.org/10.1016/j.cemconres.2013.01.002>.
- [28] N. Thaulow, S. Sahu, Mechanism of concrete deterioration due to salt crystallization, *Materials Characterization*. 53 (2004) 123–127. <https://doi.org/10.1016/j.matchar.2004.08.013>.
- [29] N. Tsui, R.J. Flatt, G.W. Scherer, Crystallization damage by sodium sulfate, *Journal of Cultural Heritage*. 4 (2003) 109–115. [https://doi.org/10.1016/S1296-2074\(03\)00022-0](https://doi.org/10.1016/S1296-2074(03)00022-0).
- [30] J. Desarnaud, F. Bertrand, N. Shahidzadeh-Bonn, Impact of the Kinetics of Salt Crystallization on Stone Damage During Wetting/Drying and Humidity Cycling, *Journal of Applied Mechanics*. 80 (2013). <https://doi.org/10.1115/1.4007924>.
- [31] A. La Iglesia, V. González, V. López-Acevedo, C. Viedma, Salt crystallization in porous construction materials I Estimation of crystallization pressure, *Journal of Crystal Growth*. 177 (1997) 111–118. [https://doi.org/10.1016/S0022-0248\(96\)01072-X](https://doi.org/10.1016/S0022-0248(96)01072-X).
- [32] G.W. Scherer, Crystallization in pores, *Cement and Concrete Research*. 29 (1999) 1347–1358. [https://doi.org/10.1016/S0008-8846\(99\)00002-2](https://doi.org/10.1016/S0008-8846(99)00002-2).
- [33] H. Haynes, Sulfate Attack on Concrete: Laboratory vs Field Experience, *CI*. 24 (2002) 64–70.
- [34] D. Breyse, 3 - Deterioration processes in reinforced concrete: an overview, in: C. Maierhofer, H.-W. Reinhardt, G. Dobmann (Eds.), *Non-Destructive Evaluation of Reinforced Concrete Structures*, Woodhead Publishing, 2010: pp. 28–56. <https://doi.org/10.1533/9781845699536.1.28>.
- [35] R. Barbarulo, H. Peycelon, S. Leclercq, Chemical equilibria between C–S–H and ettringite, at 20 and 85 °C, *Cement and Concrete Research*. 37 (2007) 1176–1181. <https://doi.org/10.1016/j.cemconres.2007.04.013>.
- [36] X. Ping, J.J. Beaudoin, Mechanism of sulphate expansion II. Validation of Thermodynamic Theory, *Cement and Concrete Research*. 22 (1992) 845–854. [https://doi.org/10.1016/0008-8846\(92\)90109-9](https://doi.org/10.1016/0008-8846(92)90109-9).
- [37] B. Lothenbach, K. Scrivener, R.D. Hooton, Supplementary cementitious materials, *Cement and Concrete Research*. 41 (2011) 1244–1256. <https://doi.org/10.1016/j.cemconres.2010.12.001>.
- [38] M.M.A. Elahi, C.R. Shearer, A. Naser Rashid Reza, A.K. Saha, M.N.N. Khan, M.M. Hossain, P.K. Sarker, Improving the sulfate attack resistance of concrete by using supplementary cementitious materials (SCMs): A review, *Construction and Building Materials*. 281 (2021) 122628. <https://doi.org/10.1016/j.conbuildmat.2021.122628>.
- [39] T. Ramlochan, M.D.A. Thomas, R.D. Hooton, The effect of pozzolans and slag on the expansion of mortars cured at elevated temperature: Part II: Microstructural and microchemical investigations, *Cement and Concrete Research*. 34 (2004) 1341–1356. <https://doi.org/10.1016/j.cemconres.2003.12.026>.
- [40] Y. Gu, P. Dangla, R.-P. Martin, O. Omikrine Metalssi, T. Fen-Chong, Modeling the sulfate attack induced expansion of cementitious materials based on interface-controlled crystal growth mechanisms, *Cement and Concrete Research*. 152 (2022) 106676. <https://doi.org/10.1016/j.cemconres.2021.106676>.
- [41] M.A. González, E.F. Irassar, Ettringite formation in low C3A Portland cement exposed to sodium sulfate solution, *Cement and Concrete Research*. 27 (1997) 1061–1071. [https://doi.org/10.1016/S0008-8846\(97\)00093-8](https://doi.org/10.1016/S0008-8846(97)00093-8).
- [42] F.E. -mail: frank bellmann@bauing uni-weimar de Bellmann, B. Moeser, J. Stark, Influence of sulfate solution concentration on the formation of gypsum in sulfate resistance test specimen, *Cement and Concrete Research*. 36 (2006). <https://doi.org/10.1016/J.CEMCONRES.2005.0>.
- [43] The damage mechanism and failure prediction of concrete under wetting–drying cycles with sodium sulfate solution, *Construction and Building Materials*. 264 (2020) 120525. <https://doi.org/10.1016/j.conbuildmat.2020.120525>.
- [44] E.F. Irassar, Sulfate attack on cementitious materials containing limestone filler — A review, *Cement and Concrete Research*. 39 (2009) 241–254. <https://doi.org/10.1016/j.cemconres.2008.11.007>.
- [45] E. Rozière, A. Loukili, R. El Hachem, F. Grondin, Durability of concrete exposed to leaching and external sulphate attacks, *Cement and Concrete Research*. 39 (2009) 1188–1198. <https://doi.org/10.1016/j.cemconres.2009.07.021>.
- [46] K. Liu, M. Deng, L. Mo, Influence of pH on the formation of gypsum in cement materials during sulfate attack, *Advances in Cement Research*. 27 (2015) 487–493. <https://doi.org/10.1680/jadcr.14.00076>.
- [47] K. Natkunarajah, K. Masilamani, S. Maheswaran, B. Lothenbach, D.A.S. Amarasinghe, D. Attygalle, Analysis of the trend of pH changes of concrete pore solution during the hydration by various analytical methods, *Cement and Concrete Research*. 156 (2022) 106780. <https://doi.org/10.1016/j.cemconres.2022.106780>.
- [48] C. Yu, W. Sun, K. Scrivener, Degradation mechanism of slag blended mortars immersed in sodium sulfate solution, *Cement and Concrete Research*. 72 (2015) 37–47. <https://doi.org/10.1016/j.cemconres.2015.02.015>.
- [49] R.S. Gollop, H.F.W. Taylor, Microstructural and microanalytical studies of sulfate attack. IV. Reactions of a slag cement paste with sodium and magnesium sulfate solutions, *Cement and Concrete Research*. 26 (1996) 1013–1028. [https://doi.org/10.1016/0008-8846\(96\)00089-0](https://doi.org/10.1016/0008-8846(96)00089-0).
- [50] W. Kunther, Investigation of Sulfate Attack by Experimental and Thermodynamic Means, PhD Thesis, EPFL, 2012. <https://doi.org/10.5075/epfl-thesis-5263>.
- [51] J. Bensted, Thaumasite — background and nature in deterioration of cements, mortars and concretes, *Cement and Concrete Composites*. 21 (1999) 117–121. [https://doi.org/10.1016/S0958-9465\(97\)00076-0](https://doi.org/10.1016/S0958-9465(97)00076-0).
- [52] J.G. Wang, Sulfate attack on hardened cement paste, *Cement and Concrete Research*. 24 (1994) 735–742. [https://doi.org/10.1016/0008-8846\(94\)90199-6](https://doi.org/10.1016/0008-8846(94)90199-6).
- [53] D. Planel, J. Sercombe, P. Le Bescop, F. Adenot, J.-M. Torrenti, Long-term performance of cement paste during combined calcium leaching–sulfate attack: kinetics and size effect, *Cement and Concrete Research*. 36 (2006) 137–143. <https://doi.org/10.1016/j.cemconres.2004.07.039>.

- [54] M. Santhanam, M.D. Cohen, J. Olek, Mechanism of sulfate attack: A fresh look: Part 1: Summary of experimental results, *Cement and Concrete Research*. 32 (2002) 915–921. [https://doi.org/10.1016/S0008-8846\(02\)00724-X](https://doi.org/10.1016/S0008-8846(02)00724-X).
- [55] D.A. St John, An unusual case of ground water sulphate attack on concrete, *Cement and Concrete Research*. 12 (1982) 633–639. [https://doi.org/10.1016/0008-8846\(82\)90025-4](https://doi.org/10.1016/0008-8846(82)90025-4).
- [56] P.J.M. Monteiro, K.E. Kurtis, Experimental Asymptotic Analysis of Expansion of Concrete Exposed to Sulfate Attack, *ACI Materials Journal*. 105 (2008) 62–71.
- [57] Effect of carbonation on physical sulfate attack on concrete by Na<sub>2</sub>SO<sub>4</sub>, *Construction and Building Materials*. 193 (2018) 211–220. <https://doi.org/10.1016/j.conbuildmat.2018.10.191>.
- [58] E.F. Irassar, A. Di Maio, O.R. Batic, Sulfate attack on concrete with mineral admixtures, *Cement and Concrete Research*. 26 (1996) 113–123. [https://doi.org/10.1016/0008-8846\(95\)00195-6](https://doi.org/10.1016/0008-8846(95)00195-6).
- [59] Z. Liu, W. Hu, M. Pei, D. Deng, The role of carbonation in the occurrence of MgSO<sub>4</sub> crystallization distress on concrete, *Construction and Building Materials*. 192 (2018) 167–178. <https://doi.org/10.1016/j.conbuildmat.2018.10.127>.
- [60] R. Flatt, N.A. Mohamed, F. Caruso, H. Derluyn, J. Desarnaud, B. Lubelli, R.M.E. Marzal, L. Pel, C. Rodriguez-Navarro, G.W. Scherer, N. Shahidzadeh, M. Steiger, Predicting salt damage in practice: A theoretical insight into laboratory tests., *RILEM Technical Letters*. 2 (2017) 108–118. <https://doi.org/10.21809/rilemtechlett.2017.41>.
- [61] Liu Zanqun, Hou Le, Hu Wenlong, Zhang Fengyan, Deng Dehua, Na<sub>2</sub>SO<sub>4</sub> Salt Weathering of Calcium Sulfoaluminate Cement Paste Partially Immersed in a Na<sub>2</sub>CO<sub>3</sub> Solution, *Journal of Materials in Civil Engineering*. 30 (2018) 04017309. [https://doi.org/10.1061/\(ASCE\)MT.1943-5533.0002198](https://doi.org/10.1061/(ASCE)MT.1943-5533.0002198).
- [62] Z. Zhang, Y. Zou, J. Yang, J. Zhou, Capillary rise height of sulfate in Portland-limestone cement concrete under physical attack: Experimental and modelling investigation, *Cement and Concrete Composites*. 125 (2022) 104299. <https://doi.org/10.1016/j.cemconcomp.2021.104299>.
- [63] T. Ikumi, S.H.P. Cavalaro, I. Segura, The role of porosity in external sulphate attack, *Cement and Concrete Composites*. 97 (2019) 1–12. <https://doi.org/10.1016/j.cemconcomp.2018.12.016>.
- [64] P. Hagelia, R.G. Sibbick, Thaumassite Sulfate Attack, Popcorn Calcite Deposition and acid attack in concrete stored at the «Blindtarmen» test site Oslo, from 1952 to 1982, *Materials Characterization*. 60 (2009) 686–699. <https://doi.org/10.1016/j.matchar.2009.01.007>.
- [65] T. Sibbick, D. Fenn, N. Crammond, The occurrence of thaumasite as a product of seawater attack, *Cement and Concrete Composites*. 25 (2003) 1059–1066. [https://doi.org/10.1016/S0958-9465\(03\)00128-8](https://doi.org/10.1016/S0958-9465(03)00128-8).
- [66] Z. Liu, F. Zhang, D. Deng, Y. Xie, G. Long, X. Tang, Physical sulfate attack on concrete lining—A field case analysis, *Case Studies in Construction Materials*. 6 (2017) 206–212. <https://doi.org/10.1016/j.cscm.2017.04.002>.
- [67] B. Lubelli, V. Cnudde, T. Diaz-Goncalves, E. Franzoni, R.P.J. van Hees, I. Ioannou, B. Menendez, C. Nunes, H. Siedel, M. Stefanidou, V. Verges-Belmin, H. Viles, Towards a more effective and reliable salt crystallization test for porous building materials: state of the art, *Material Struct*. 51 (2018) 55. <https://doi.org/10.1617/s11527-018-1180-5>.
- [68] Z. Shi, S. Ferreira, B. Lothenbach, M.R. Geiker, W. Kunther, J. Kaufmann, D. Herfort, J. Skibsted, Sulfate resistance of calcined clay – Limestone – Portland cements, *Cement and Concrete Research*. 116 (2019) 238–251. <https://doi.org/10.1016/j.cemconres.2018.11.003>.
- [69] M.F. Suma, M. Santhanam, Y. Dhandapani, Sulphate resistance of limestone calcined clay cement, 2017.
- [70] A. Skaropoulou, K. Sotiriadis, G. Kakali, S. Tsvivilis, Use of mineral admixtures to improve the resistance of limestone cement concrete against thaumasite form of sulfate attack, *Cement and Concrete Composites*. 37 (2013) 267–275. <https://doi.org/10.1016/j.cemconcomp.2013.01.007>.
- [71] X. Liu, P. Feng, W. Li, G. Geng, J. Huang, Y. Gao, S. Mu, J. Hong, Effects of pH on the nano/micro structure of calcium silicate hydrate (C-S-H) under sulfate attack, *Cement and Concrete Research*. 140 (2021) 106306. <https://doi.org/10.1016/j.cemconres.2020.106306>.
- [72] A review on the mechanical properties of cement-based materials measured by nanoindentation, *Construction and Building Materials*. 90 (2015) 80–90. <https://doi.org/10.1016/j.conbuildmat.2015.05.008>.
- [73] A. Chabreliè, Mechanisms of degradation of concrete by external sulfate ions under laboratory and field conditions, PhD Thesis, EPFL, 2010. <https://infoscience.epfl.ch/record/143041> (accessed February 21, 2019).
- [74] P.J.M. Monteiro, Scaling and saturation laws for the expansion of concrete exposed to sulfate attack, *Proc. Natl. Acad. Sci. U.S.A.* 103 (2006) 11467–11472. <https://doi.org/10.1073/pnas.0604964103>.
- [75] Tixier Raphaël, Mobasher Barzin, Modeling of Damage in Cement-Based Materials Subjected to External Sulfate Attack. I: Formulation, *Journal of Materials in Civil Engineering*. 15 (2003) 305–313. [https://doi.org/10.1061/\(ASCE\)0899-1561\(2003\)15:4\(305\)](https://doi.org/10.1061/(ASCE)0899-1561(2003)15:4(305)).
- [76] N.M. Alderete, Y.A. Villagrán Zaccardi, N. De Belie, Mechanism of long-term capillary water uptake in cementitious materials, *Cement and Concrete Composites*. 106 (2020) 103448. <https://doi.org/10.1016/j.cemconcomp.2019.103448>.
- [77] M.L. Nehdi, A.R. Suleiman, A.M. Soliman, Investigation of concrete exposed to dual sulfate attack, *Cement and Concrete Research*. 64 (2014) 42–53. <https://doi.org/10.1016/j.cemconres.2014.06.002>.
- [78] Q. Wang, W. Wilson, K. Scrivener, Unidirectional penetration approach for characterizing sulfate attack mechanisms on cement mortars and pastes, (n.d.).
- [79] T. Schmidt, B. Lothenbach, M. Romer, J. Neuenschwander, K. Scrivener, Physical and microstructural aspects of sulfate attack on ordinary and limestone blended Portland cements, *Cement and Concrete Research*. 39 (2009) 1111–1121. <https://doi.org/10.1016/j.cemconres.2009.08.005>.
- [80] W. Kunther, B. Lothenbach, K. Scrivener, Influence of bicarbonate ions on the deterioration of mortar bars in sulfate solutions, *Cement and Concrete Research*. 44 (2013) 77–86. <https://doi.org/10.1016/j.cemconres.2012.10.016>.

- [81] W. Kunther, B. Lothenbach, Improved volume stability of mortar bars exposed to magnesium sulfate in the presence of bicarbonate ions, *Cement and Concrete Research*. 109 (2018) 217–229. <https://doi.org/10.1016/j.cemconres.2018.04.022>.
- [82] Z. Liu, D. Deng, G. De Schutter, Does concrete suffer sulfate salt weathering?, *Construction and Building Materials*. 66 (2014) 692–701. <https://doi.org/10.1016/j.conbuildmat.2014.06.011>.
- [83] J. Ren, Y. Lai, R. Bai, Y. Qin, The damage mechanism and failure prediction of concrete under wetting–drying cycles with sodium sulfate solution, *Construction and Building Materials*. 264 (2020) 120525. <https://doi.org/10.1016/j.conbuildmat.2020.120525>.
- [84] M. Santhanam, M.D. Cohen, J. Olek, Modeling the effects of solution temperature and concentration during sulfate attack on cement mortars, *Cement and Concrete Research*. 32 (2002) 585–592. [https://doi.org/10.1016/S0008-8846\(01\)00727-X](https://doi.org/10.1016/S0008-8846(01)00727-X).
- [85] R.B. Perkins, C.D. Palmer, Solubility of ettringite ( $\text{Ca}_6\text{Al}(\text{OH})_6\text{J}_2(\text{SO}_4)_3 \cdot 26\text{H}_2\text{O}$ ) at 5–75°C, *Geochimica et Cosmochimica Acta*. 63 (1999) 1969–1980. [https://doi.org/10.1016/S0016-7037\(99\)00078-2](https://doi.org/10.1016/S0016-7037(99)00078-2).
- [86] A.M. Hossack, M.D.A. Thomas, The effect of temperature on the rate of sulfate attack of Portland cement blended mortars in  $\text{Na}_2\text{SO}_4$  solution, *Cement and Concrete Research*. 73 (2015) 136–142. <https://doi.org/10.1016/j.cemconres.2015.02.024>.
- [87] K.L. Scrivener, J.F. Young, eds., *Mechanisms of Degradation of Portland Cement-based Systems by Sulfate Attack*, in: *Mechanisms of Chemical Degradation of Cement-Based Systems*, CRC Press, 1997.
- [88] G. Zhang, C. Wu, D. Hou, J. Yang, D. Sun, X. Zhang, Effect of environmental pH values on phase composition and microstructure of Portland cement paste under sulfate attack, *Composites Part B: Engineering*. 216 (2021) 108862. <https://doi.org/10.1016/j.compositesb.2021.108862>.
- [89] L. Caneda-Martínez, W. Kunther, C. Medina, M.I. Sánchez de Rojas, M. Frías, Exploring sulphate resistance of coal mining waste blended cements through experiments and thermodynamic modelling, *Cement and Concrete Composites*. 121 (2021) 104086. <https://doi.org/10.1016/j.cemconcomp.2021.104086>.
- [90] Standard Specification for Portland Cement, ASTM C150-07, n.d.
- [91] Béton - Spécification, performances, production et conformité, NF EN 206+A2, n.d. <https://www.boutique.afnor.org/fr-fr/norme/nf-en-206-a2/beton-specification-performances-production-et-conformite/fa201846/238491> (accessed May 1, 2022).
- [92] PD CEN/TR 15697:2008 - Cement. Performance testing for sulfate resistance. State of the art report, (n.d.). <https://shop.bsigroup.com/ProductDetail/?pid=000000000030164792> (accessed February 19, 2019).
- [93] SIA 262/1 Appendix D: sulfate resistance, SIA Zürich, 2013.
- [94] Standard Test Method for Potential Expansion of Portland-Cement Mortars Exposed to Sulfate, (n.d.). <https://www.astm.org/c0452-21.html> (accessed May 8, 2022).
- [95] Natural stone test methods – Determination of resistance to salt crystallisation, 2020.
- [96] Q. Wang, W. Wilson, K. Scrivener, Investigating Dual Sulfate Attack Mechanisms using Unidirectional Penetration Approach, *SP*. 349 (2021) 623–628.
- [97] C.W. Correns, Growth and dissolution of crystals under linear pressure, *Discuss. Faraday Soc.* 5 (1949) 267–271. <https://doi.org/10.1039/DF9490500267>.
- [98] M.D. Cohen, Modeling of expansive cements, *Cement and Concrete Research*. 13 (1983) 519–528. [https://doi.org/10.1016/0008-8846\(83\)90011-X](https://doi.org/10.1016/0008-8846(83)90011-X).
- [99] C.D. Lawrence, Mortar expansions due to delayed ettringite formation. Effects of curing period and temperature, *Cement and Concrete Research*. 25 (1995) 903–914. [https://doi.org/10.1016/0008-8846\(95\)00081-M](https://doi.org/10.1016/0008-8846(95)00081-M).
- [100] R. Gollop, H. Taylor, Microstructural and microanalytical studies of sulfate attack III. Sulfate-resisting portland cement: Reactions with sodium and magnesium sulfate solutions, (1995). [https://doi.org/10.1016/0008-8846\(95\)00151-2](https://doi.org/10.1016/0008-8846(95)00151-2).
- [101] R. Yang, C.D. Lawrence, J.H. Sharp, Delayed ettringite formation in 4-year old cement pastes, *Cement and Concrete Research*. 26 (1996) 1649–1659. [https://doi.org/10.1016/S0008-8846\(96\)00161-5](https://doi.org/10.1016/S0008-8846(96)00161-5).

# Chapter 3 Materials and experimental methods

## **Abstract**

This chapter describes the cement materials used in this whole project: Portland cement (PC), sulfate-resisting cement (HS), slag Portland cement (SPC) and limestone calcined clay cement (LC<sup>3</sup>). Conventional submerge and unidirectional semi-immersion testing approaches are introduced to reveal some specific open questions. The experimental part of the thesis was based on the analytical methods described in this chapter. The macroscopic degradation was monitored by expansion measurements and mass changes. Visual inspections of the appearance of degraded samples give an overview of the damage caused by chemical or physical sulfate attack. To link with the macroscopic observations, profiles of phase distributions were obtained qualitatively and quantitatively by Scanning Electron Microscopy and X-ray diffraction techniques, respectively. Some other relevant physical properties of cement pastes or mortars before sulfate exposure were also characterized: porosity of cement paste measured by mercury intrusion porosimetry, mortar mechanical strength, and water adsorption/desorption.



## Contents

<b>3.1</b>	<b>Materials .....</b>	<b>57</b>
3.1.1	Cement types .....	57
3.1.2	Particle size distributions of cements.....	57
<b>3.2</b>	<b>Sample preparation .....</b>	<b>58</b>
3.2.1	Paste samples .....	58
3.2.2	Mortar samples .....	58
<b>3.3</b>	<b>Setups.....</b>	<b>59</b>
3.3.1	Sodium sulfate solution.....	59
3.3.2	Conventional setup for full immersion test.....	59
3.3.3	Unidirectional setup for semi-immersion test .....	59
<b>3.4</b>	<b>Macroscopic observations .....</b>	<b>60</b>
3.4.1	Visual inspections .....	60
3.4.2	Mass change and expansion.....	61
<b>3.5</b>	<b>Microscopic observations .....</b>	<b>62</b>
3.5.1	Scanning Electron microscopy.....	62
3.5.2	X-ray diffraction.....	63
<b>3.6</b>	<b>Mercury intrusion porosimetry .....</b>	<b>64</b>
<b>3.7</b>	<b>Mechanical strength .....</b>	<b>64</b>
<b>3.8</b>	<b>Adsorption and desorption .....</b>	<b>64</b>
<b>3.9</b>	<b>References.....</b>	<b>65</b>

## 3.1 Materials

### 3.1.1 Cement types

CEM I, Portland cement, is used as reference cement. Sulfate-resisting cement is a Portland based cement with around 17 % clinker replacement by blast furnace slag. Slag Portland cement consists of 70 % slag and 30 % Portland cement. Limestone calcined clay cement consists of 50 % Portland cement, 30 % calcined clay, 15 % limestone and 5 % gypsum. The chemical compositions of all raw materials are shown in Table 3-1. The phase compositions of CEM I and HS cement are shown in Table 3-2.

For each cement system, the equivalent metal alkali ( $\text{Na}_2\text{O}$  and  $\text{K}_2\text{O}$ ) and  $\text{SO}_3$  content are calculated as shown in Table 3-3.

Table 3-1 Chemical composition of cements and admixtures wt.%

Materials	$\text{SiO}_2$	$\text{Al}_2\text{O}_3$	$\text{Fe}_2\text{O}_3$	$\text{CaO}$	$\text{MgO}$	$\text{SO}_3$	$\text{Na}_2\text{O}$	$\text{K}_2\text{O}$	$\text{TiO}_2$	$\text{P}_2\text{O}_5$	LOI
CEM I	20.4	5.1	1.9	64.2	1.0	2.9	0.4	0.7	0.2	0.2	1.7
HS	24.3	6.5	2.7	54.9	3.7	4.6	0.3	0.9	0.4	0.2	1.3
Slag	35.4	11.8	0.8	41.1	7.0	1.5	0.3	0.3	0.5	0.01	
Calcine clay	56.1	36.7	3.4	0.2	0	0.1	0.1	0.2	2.4		0.5
Limestone	0.1			55	0.2		0.1				42.6

Table 3-2 Phase composition of cements wt.%

Phase composition wt.%	CEM I	HS
$\text{C}_3\text{S}$	63.8	49.5
$\text{C}_2\text{S}$	13.9	13.1
$\text{C}_3\text{A}$	10.6	3.3
$\text{C}_4\text{AF}$	1.9	6.9
Anhydrite	4	1.3
Calcite	5.2	0.6
Gypsum	0.6	8.3
Slag		17

Table 3-3 Equivalent alkali and  $\text{SO}_3$  content in cements

Cements	Equivalent alkali content in cements wt. %	Total $\text{SO}_3$ content wt. %
PC	1.10	2.90
HS	1.13	4.61
SPC	0.75	1.92
$\text{LC}^3$	0.66	4.4

### 3.1.2 Particle size distributions of cements

Fig. 3-1 shows the particle size distribution of the different cement powders used in this study, obtained by laser diffractometry. 0.1 g cement was dispersed in 50 ml isopropanol to avoid possible hydration during the measurement. The suspension was placed in an ultrasonic probe for 15 minutes and kept it stirred with a magnetic stirrer. After the suspension was ready, a pipette was used to transfer the solution into the measuring zone which was also rinsed with isopropanol three times, the transfer was carried out slowly until a 12

% obscuration was reached. The distribution curve was finally obtained by an average of three measurements.

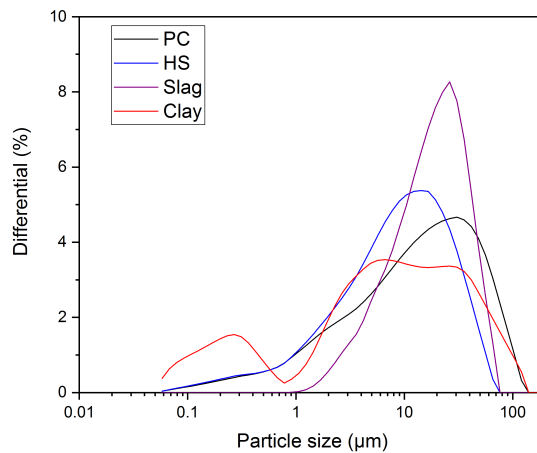


Fig. 3-1 Particle size distribution of raw materials measured by laser diffraction.

## 3.2 Sample preparation

### 3.2.1 Paste samples

Cement pastes were prepared at w/c of 0.6 and 0.4. The pastes were mixed with distilled water using a shear mixer for 120 s at a speed of 1600 rpm. Then, the paste was cast in cylindrical plastic containers with a diameter of 33 mm and a length of 60 mm. After one day, paste samples were demoulded and cured in a slightly bigger container for 28 days with a small amount of water to avoid leaching (samples were fully submerged in the water). After removing about 3 mm at the two ends of each sample, the samples were cut into slices with a thickness of 5 mm. The slices were then installed in the semi-immersion setup, as described below. The cement paste samples were then mounted in the test setup; the details can be found in *Chapter 4*.

The samples with a high w/c ratio of 0.6 were treated differently due to the higher water content. After mixing the cement paste was immediately transferred into the plastic container which was completely filled. The air bubbles were removed then the surface was covered by a rigid piece of plastic which filled exactly the gap between the plastic lid and the cement paste. This procedure helped to seal the container without introducing any new air bubbles during rotation. Bleeding was avoided by rotating about 5 rpm during the first 24 hours of hardening. To avoid the minor effect of the centrifugal force introduced by the rotating process, 5 mm slices were removed from the two surfaces after another 27 days of curing, so only the central portion was taken for the experiments.

### 3.2.2 Mortar samples

Cement mortars were prepared according to EN 196-1 with w/c of 0.4 and 0.6. For each mix, 1 part cement (491 g) to 2.75 parts of sand (1350 g) by mass was used. Samples were cast in the same container as cement

paste used for unidirectional exposure but cut with a thickness of 10 mm after 28 days of curing under distilled water. Some mortar samples were cut for the water adsorption and desorption test that is described in more detail in the section 3.8.

Mortar samples were also cast in the steel moulds (to produce mortar prism bar with the dimension of  $40 \times 40 \times 160$  mm) for the conventional full-immersion exposure. The samples were cured under the saturated lime solution for 28 days with different temperatures of  $20^\circ\text{C}$ ,  $40^\circ\text{C}$  and  $60^\circ\text{C}$ . For each system, three mortar prisms with the studs adhered on the two ends for expansion test and one prism for microstructural test were prepared.

### 3.3 Setups

#### 3.3.1 Sodium sulfate solution

A chemical grade pure salt containing more than 99 %  $\text{Na}_2\text{SO}_4$  solid was used as the external sulfate source. A solution of 3 and 50 g/L of  $\text{Na}_2\text{SO}_4$  was prepared for exposure of the samples. The solution was changed periodically once per month for both full and unidirectional exposure conditions.

#### 3.3.2 Conventional setup for full immersion test

The mortar samples were immersed under  $\text{Na}_2\text{SO}_4$  solution (see Fig. 3-2) with a concentration of 50 g/L as indicated by the standard [1] and the solution was refreshed every month to control the sufficient constant sulfate concentration. The setup was kept at room temperature around  $20^\circ\text{C}$ .



Fig. 3-2 Full immersion test container with 4 mortar prisms.

#### 3.3.3 Unidirectional setup for semi-immersion test

A new partial immersion configuration was designed as shown in Fig. 3-3 (a) & (b). A plastic container was employed to contain the sulfate solution. In each container, 16 samples (cement mortar and/or paste) were fixed with red silicone moulds (Fig. 3-3 (c) & (d)) on a plastic support plate installed at the middle height of

the container. The ratio of the exposed sample surface area to solution volume was  $\sim 38 \text{ cm}^2/\text{L}$ . With this setup, the sulfate solution is in contact only with the bottom surface of the samples and it penetrates inwards only in one direction. On the other side, the top surface is exposed to an environment-controlled room with a constant condition of relative humidity of 55 %, a temperature of  $20 \pm 2 \text{ }^\circ\text{C}$  and a weekly cycling condition of relative humidity of 78 %, temperature of  $20 \pm 2 \text{ }^\circ\text{C}$  and relative humidity of 33 %, temperature of  $40 \pm 2 \text{ }^\circ\text{C}$ . At each testing age, one mortar sample or two cement paste samples were sacrificed for analysis. One sample is cut vertically to obtain the phase distribution profiles by SEM-EDS. A second sample is ground parallel to the exposed surface to obtain phase assemblage by XRD (only done with cement paste samples).

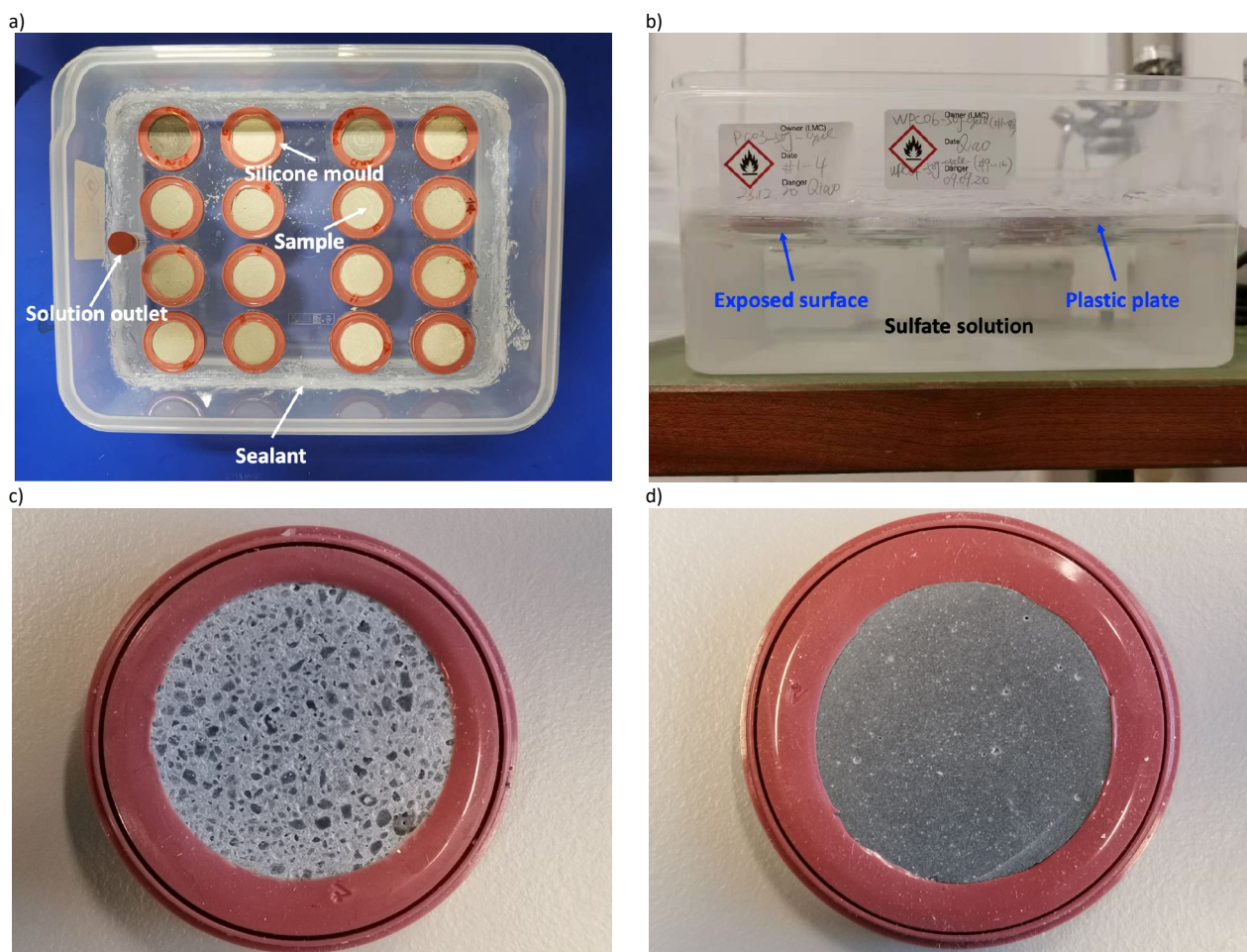


Fig. 3-3 Experimental set-up for the unidirectional sulfate penetration test: (a) top view of the setup; (b) side view of setup; (c) cement mortar, (d) cement paste.

## 3.4 Macroscopic observations

### 3.4.1 Visual inspections

The appearance of mortar and paste samples was photographed after a certain time of sulfate exposure. The bottom and top surfaces were taken respectively to monitor the degradation process as a function of time.

The occurrence of cracking/spalling and efflorescence can be compared between different systems and different exposure conditions.

### 3.4.2 Mass change and expansion

The mass of the sample was measured right after the removal from the setup, in the surface-dry state. Later the diameter was measured in the direction parallel to the degradation front (parallel to the exposed surface). The measurement was carried out as shown in Fig. 3-4 (a), using a digital slide calliper and stacked 1-mm thick hollowed steel rings (Fig. 3-4 (b)). Therefore, the expansion can be measured at each mm. The measurements were done with the same points before and after expansion.

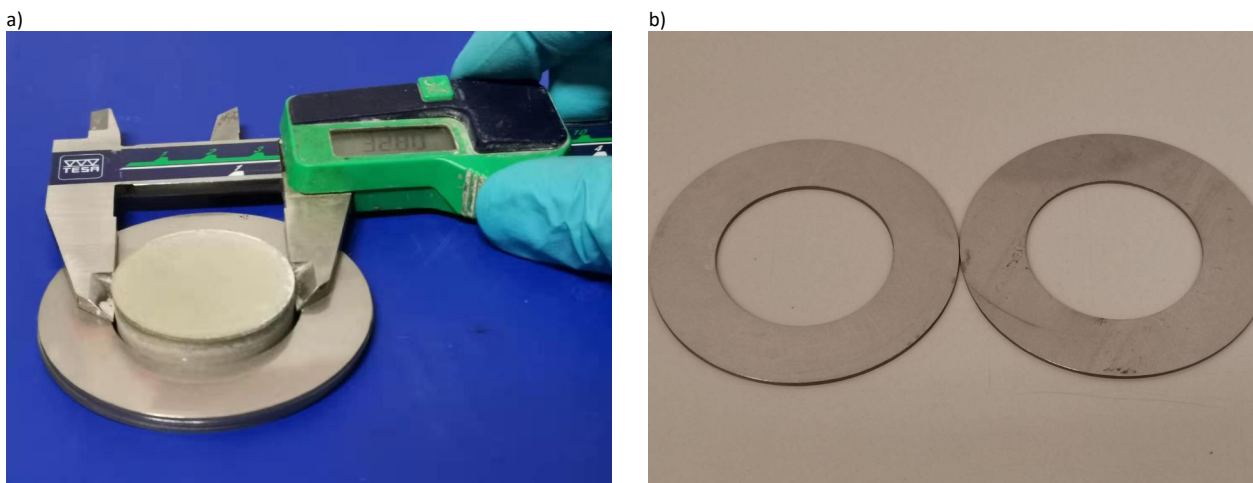


Fig. 3-4 Radial expansion measurement: (a) measure the expansion by using a calliper; (b) steel rings with a thickness of 1mm.

Expansion of the mortar prism was conducted every two weeks according to the standard method [1]. The measurement example is shown in Fig. 3-5.



Fig. 3-5 The expansion measurement of the mortar prism in the submerge test.

## 3.5 Microscopic observations

### 3.5.1 Scanning Electron microscopy

Sections were cut perpendicular to the exposed surface and polished progressively to 1  $\mu\text{m}$  with diamond pastes. Sometimes, the extra step of a second epoxy impregnation before polishing was necessary to prepare the extensively deteriorated sample as shown in Fig. 3-6.

The paste and mortar samples were coated with carbon and then examined by scanning electron microscopy (FEI Quanta 200) with backscattered electron imaging (BSE) and elemental hyper mapping as well as point analysis from energy dispersive spectroscopy (EDS). The accelerating voltage was 15.0 kV and a working distance of 12.5 mm.

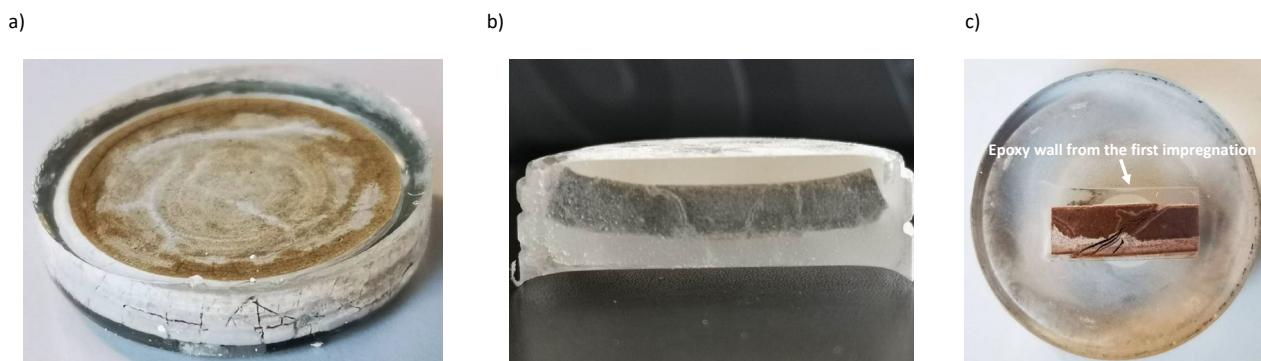


Fig. 3-6 The example process of a sample twice impregnation in epoxy: a) the first entire sample impregnation, b) cut perpendicular to the exposed surface into the desired slice of 3 mm thickness, c) the second impregnation with the thin slice.

#### Point analysis on outer C-S-H gel

The points were selected carefully from the outer C-S-H phase of cement paste parts for analysis. It needs the operator's expertise in cement science, to select the points apart from portlandite, ettringite, AFm and aggregates. A cluster of outer C-S-H phase intermixed with fine AFm and ettringite should be expected, and the example of the points selection is shown in Fig. 3-7. More detail on proper point selection from a typical BSE image was discussed in the previous paper published by our group [2]. A magnification of 2000  $\times$  was used to get a clear picture of the C-S-H gel zone. 200 points of each sample were taken to plot the graph of atomic ratios.

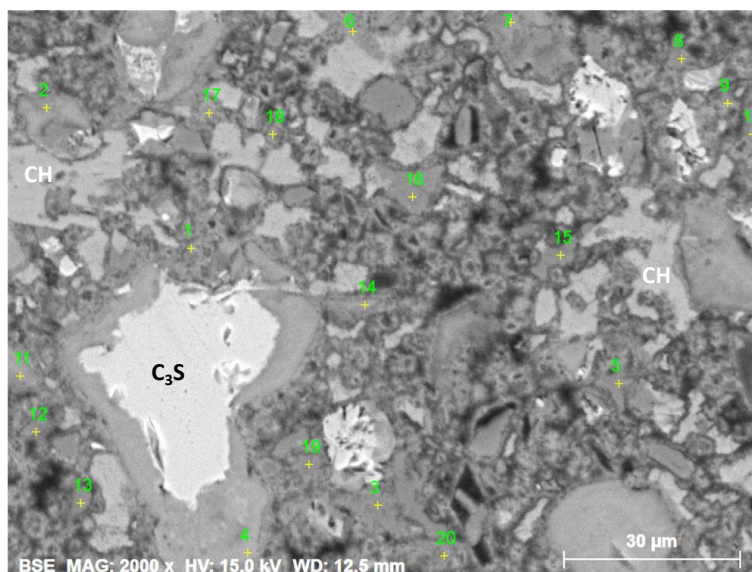


Fig. 3-7 The example of the points selection on the outer C-S-H phase done with paste PC06 at 28 days of hydration.

### Mappings

For hyper mapping, a line scan from the sulfate exposed surface (initial position) to the inner part was set at the beginning of the program with a given step and mapping overlap value. Each mapping area along the line for the pastes was about  $860 \times 645 \mu\text{m}$  (magnification  $300 \times$ ) with a resolution of  $1000 \times 750$  pixels. The mappings for mortar samples were done instead with a magnification of  $150 \times$  which compromised the sand aggregate size and the paste bulk. Esprit 1.9 software was used to quantify the hypermaps after calibration with standards for each element of interest. After processing, the mappings were quantitatively analysed by using the EDXIA approach developed by Georget et al [3]. The 8-10 individual maps were stitched together by ImageJ [4]. Eventually, a long BSE and elemental map over the analysed depth was obtained.

### 3.5.2 X-ray diffraction

X-ray diffraction (XRD) analyses were done with a Philips X'Pert Pro PANalytical ( $\text{CuK}\alpha$ ,  $\lambda = 1.54$ ) working in Bragg–Brentano geometry over a  $2\theta$ -range of  $5\text{--}65^\circ$ . Quantitative Rietveld analyses were made with the HighScore Plus software and with the external standard method (titanium dioxide as crystalline standard, rutile Kronos 2300).

### Phase assemblages

The fresh paste slice 2 mm thick was cut after 28 days of hydration. A 15-minute scan was done to get the XRD pattern. The initial phase content in different cement pastes was obtained which can be treated as the reference before the sulfate ingress.

### Degradation profiles



X-ray diffraction on fresh cement paste slices after exposure was made on successive parallel sections, with manual grinding between each scan to reach the desired depth into the discs and provide quantitative phase assemblage profiles. The evolution of the hydrated phase assemblage with depth from the solution exposed surface to the top surface was tracked over time. Slices were analysed at distances from the surface of 0, 1, 2, 3, 4, 5 mm (or specific depths of interest based on SEM observations).

### 3.6 Mercury intrusion porosimetry

The porosity of the pastes was analysed by mercury intrusion porosimetry (MIP) (Porotec GmbH Pascal 140–440 instruments) at 28 days hydration. Slices 2 mm thick were cut and then immersed in isopropanol for a week to stop the hydration. During this time the isopropanol was renewed after one hour, 1 day and 3 days until 7 days. They were then dried in a vacuumed desiccator for two days. The paste was crushed into pieces, about 1.5 g and 3-5 pieces were placed in a glass dilatometer. A contact angle of  $140^\circ$  was assumed.

### 3.7 Mechanical strength

The mortar samples with w/c ratios of 0.4 and 0.6 were prepared followed by the EN 196-1 standard to measure the compressive and flexural strength of PC, HS, SPC and LC<sup>3</sup> systems. Cement mortars were then cured in a humid chamber for 28 days before the mechanical test.

### 3.8 Adsorption and desorption

For the adsorption test, mortar samples were prepared instead of concrete followed by the ASTM C1585-13 standard but adapted to the sample size of the current research. In parallel, the samples for measuring the drying rate were cut and cured under distilled water for 28 + 18 days (18 days refers to the sample preconditioning time required for the adsorption test). The mass change due to water adsorption or drying was measured over 8 days. The measuring interval time (as shown in Table 3-4) of water evaporation was taken the same as prescribed in the water adsorption test. Both measurements were conducted under exactly the same environments as the next sulfate exposure experiments: temperature  $20 \pm 2^\circ\text{C}$ , relative humidity 55%. Data were collected for up to 8 days to get a linear increasing water gain/loss as a function of the square root of seconds. Testing samples are shown in Fig. 3-8.

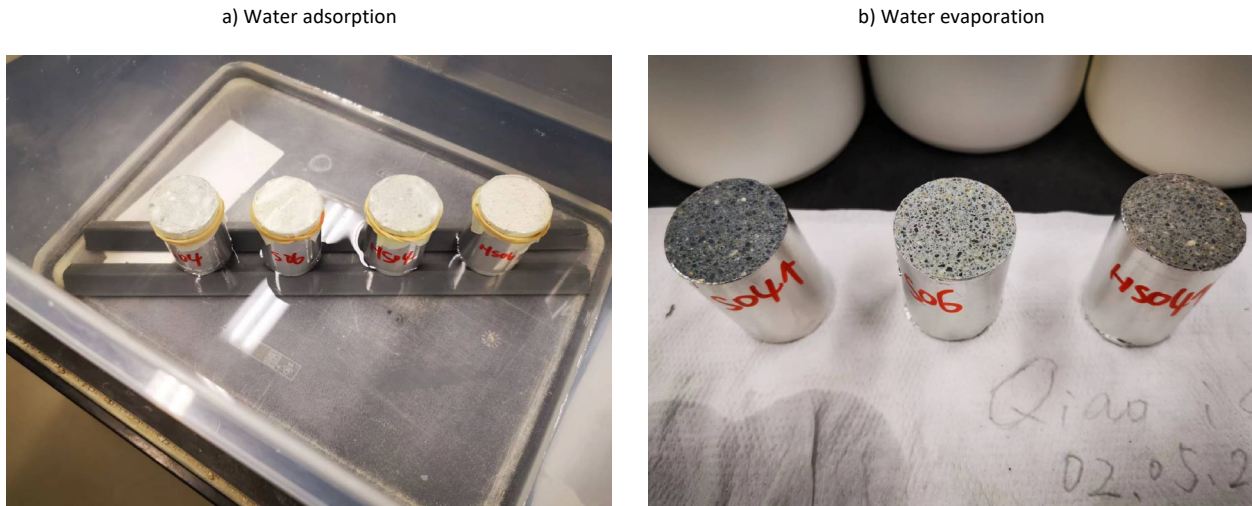


Fig. 3-8 Mortar samples for water adsorption and evaporation testing.

Table 3-4 Times and tolerances for the measurements schedule

Time	60 s	5 min	10 min	20 min	30 min	60 min	Every hour up to 6 h	Once a day up to 3 days	Day 4 to 74 to 7 3 measurements 24 h apart	Day 7 to 9 1 measurement
Tolerance	2 s	10 s	2 min	2 min	2 min	2 min	5 min	2 h	2 h	2 h

### 3.9 References

- [1] C01 Committee, Test Method for Potential Expansion of Portland-Cement Mortars Exposed to Sulfate, ASTM International, 2019. <https://doi.org/10.1520/C0452-19>.
- [2] C. Yu, W. Sun, K. Scrivener, Mechanism of expansion of mortars immersed in sodium sulfate solutions, *Cement and Concrete Research*. 43 (2013) 105–111. <https://doi.org/10.1016/j.cemconres.2012.10.001>.
- [3] F. Georget, W. Wilson, K.L. Scrivener, edxia: Microstructure characterisation from quantified SEM-EDS hypermaps, *Cement and Concrete Research*. 141 (2021) 106327. <https://doi.org/10.1016/j.cemconres.2020.106327>.
- [4] S. Preibisch, S. Saalfeld, P. Tomancak, Globally optimal stitching of tiled 3D microscopic image acquisitions, *Bioinformatics*. 25 (2009) 1463–1465. <https://doi.org/10.1093/bioinformatics/btp184>.

# Chapter 4 New unidirectional penetration approach

**Note:** This chapter is based on a journal paper submitted to the journal of <cement and concrete research>.

Contribution of the doctoral candidate: conceptualization, writing of the first manuscript, investigation, review & editing.

**Submission title: Unidirectional penetration approach for characterizing sulfate attack mechanisms on cement mortars and pastes**

*Qiao Wang, William Wilson, Karen Scrivener*

## **Abstract**

Degradation of cementitious materials by sulfate ions is commonly classified into chemical and physical sulfate attacks. So-called “physical” attack dominates in many field situations, but laboratory testing focuses on “chemical” attack under full immersion. This paper presents a new setup which looks at sulfate ion ingress under unidirectional capillary action, as a first approach to field conditions. Here, a high concentration of sulfate ions and w/c and Portland cement were used to accelerate degradation to see if the approach is feasible. The radial expansion and appearance of mortar and paste samples were tracked over time. Periodically, profiles of sulfate ingress and phase assemblage were studied in the SEM and by X-ray diffraction. The results show that physical and chemical sulfate attack occur in different areas of the same sample. The approach shows the potential to uncover the mechanisms involved in sulfate attack including both “chemical” and “physical” aspects of the degradation process.

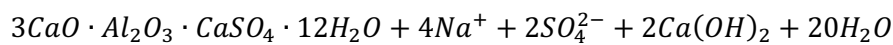
## Contents

<b>4.1</b>	<b>Introduction .....</b>	<b>68</b>
<b>4.2</b>	<b>Materials and experimental approaches .....</b>	<b>69</b>
4.2.1	Materials and sample preparation .....	69
4.2.2	The new semi-immersion setup .....	70
4.2.3	Expansion measurements .....	71
4.2.4	Scanning electron microscopy (SEM) .....	72
4.2.5	X-ray diffraction (XRD) analyses .....	72
<b>4.3</b>	<b>Results and discussion .....</b>	<b>73</b>
4.3.1	Visual observations .....	73
4.3.2	Expansion as a function of depth and time .....	74
4.3.3	Progress of the degradation processes from the chemical and phase profiles.....	75
4.3.4	Discussion .....	81
<b>4.4</b>	<b>Conclusions.....</b>	<b>85</b>
<b>4.5</b>	<b>References.....</b>	<b>86</b>

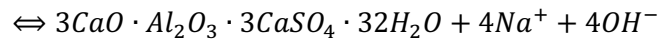
## 4.1 Introduction

Sulfate ions, which are sometimes present in groundwater, can be deleterious to concrete when they penetrate and react with the hydration products of the cement paste. Sulfate attack causes different forms of degradation, including expansion, cracking, softening, spalling, and eventually disintegration of concrete structures. Sulfate attack is generally classified into “physical sulfate attack” and “chemical sulfate attack”. Although ground waters may contain different cations, the most prevalent sodium sulfate is the most widely studied in the laboratory. The most important reactions of sulfate ions with cement hydrates are:

### Ettringite formation



monosulfate



ettringite

Gypsum may also form under a high sulfate concentration but it is believed to have no contribution to expansion as it always precipitates inside the pre-existed voids and cracks [1,2].

Sulfate attack may cause expansion, delamination and cracking of concrete due to the crystallization pressure of ettringite. However, if the water evaporates from the surface of concrete whose pore solution is highly concentrated with alkali sulfates, the salt crystallization by capillary rise and diffusion may take place in areas close to the surface which is termed a “physical sulfate attack”. At the drying front crystallization pressure may be generated, causing spalling surfaces as often seen in field concretes. However, the thermal cycling between thenardite and mirabilite has also been implicated. Thermal cycling was not investigated in this preliminary study.

Although both “chemical” and “physical” sulfate attacks often occur together in the field, indeed the degradation due to physical attack may be more implicated in real cases. The most common occurrence of damage in the field is when concrete structures are partially immersed in sulfate-bearing soil or water, where damage is usually concentrated just above the soil or water level [3–5]. However existing test methods only look at chemical sulfate attacks under full immersion. Expansion is related to the crystallization pressure of ettringite forming under supersaturated and restrained conditions (small pores  $< \sim 50$  nm) [2]. It cannot be related simply to the amount of ettringite formed as ettringite may precipitate in pre-existing pores without generating a pressure [2,6–8]. Macroscopic damage is complicated by gradients in concentration and the formation of ettringite created as the sulfate ions ingress from a surface. This explains the size dependence of mortar

bar expansion due to relative amounts of expanding surface restrained by the non-expanding core [2,9,10]. As sulfate ions penetrate radially inwards, surface-parallel cracks occur [11–13].

Different immersion regimes have been explored. The main approaches investigated have been full immersion, partial immersion and wetting/drying cycles [2,3,14–20]. Partial immersion and wetting/drying cycles are very dependent on parameters such as sample size and circulation of air in the laboratory, which makes it difficult to compare results between laboratories, and probably explains why these approaches have not been developed into test methods.

This paper reports a novel unidirectional semi-immersion approach to investigate the mechanisms responsible for both “chemical” and “physical” sulfate attacks, by considering the degradation process as a whole. To verify the applicability of the setup, PC mortar and paste systems with a w/c ratio of 0.6 were investigated. After several months of exposure, the distribution of sulfate and sodium ions in both mortars and pastes were mapped by SEM-EDS and the phase assemblages of hydration products were analysed by X-ray diffraction based on the paste samples. In parallel, the radial expansion for both mortars and pastes was tracked over time. The mechanisms of sulfate ions ingress and their contribution to damage on both sides of the sample were further investigated. The results show that the setup is very promising for studying simultaneously both “physical” and “chemical” sulfate attacks in mortars, and can also be used on pastes.

## 4.2 Materials and experimental approaches

### 4.2.1 Materials and sample preparation

#### Cement

A Portland cement CEM I 42.5 was used. The chemical composition and main clinker phases according to Rietveld analysis are shown in Table 4-1.

Table 4-1 Chemical composition and phase composition of Portland cement

Chemical compositions wt.%		Phase composition wt.%	
SiO <sub>2</sub>	20.4	C <sub>3</sub> S	63.8
Al <sub>2</sub> O <sub>3</sub>	5.1	C <sub>2</sub> S	13.9
Fe <sub>2</sub> O <sub>3</sub>	1.9	C <sub>3</sub> A	10.6
CaO	64.2	C <sub>4</sub> AF	1.9
MgO	1.0	Anhydrite	4
SO <sub>3</sub>	2.9	Calcite	5.2
Na <sub>2</sub> O	0.4	Gypsum	0.6
K <sub>2</sub> O	0.7		
TiO <sub>2</sub>	0.2		
P <sub>2</sub> O <sub>5</sub>	0.2		
LOI	1.67		

### Sample preparation

Cement mortars were prepared according to EN 196-1 with a w/c of 0.6. For each mix, 1 part cement (491 g) to 2.75 parts of sand (1350 g) by mass was used. Samples were cast in cylindrical plastic containers with a diameter of 33 mm and a length of 60 mm. Cement pastes with w/c of 0.6 were mixed with distilled water using a high shear mixer for 120 s at a speed of 1600 rotations per minute. Then, the pastes were cast in containers of the same size. After one day, both mortar and paste samples were demoulded and cured in slightly bigger containers for 28 days fully immersed in a small amount of water to avoid desiccation and leaching. After removing about 3 mm at the ends of each sample, the samples were cut into slices with a thickness of 5 or 10 mm. The slices were then installed in the semi-immersion setup, as described below.

### Sodium sulfate solution

A chemical grade pure salt containing more than 99 % Na<sub>2</sub>SO<sub>4</sub> solid was used as the external sulfate source. A solution of 50 g/L of Na<sub>2</sub>SO<sub>4</sub> was prepared for exposure of the samples. The solution was changed periodically once per month.

#### 4.2.2 The new semi-immersion setup

A new partial immersion configuration was designed as shown in Fig. 4-1 (a) & (b). A plastic container was employed to contain the sulfate solution. In each container, 16 samples (cement mortar and/or paste) were fixed with red silicone moulds (Fig. 4-1 (c) & (d)) on a plastic support plate installed at the middle height of the container. The ratio of the sample surface to solution volume was 38 cm<sup>2</sup>/L. With this setup, the sulfate solution is in contact only with the bottom surface of the samples and it penetrates inwards only in one direction. On the other side, the top surface is exposed to an environment-controlled room with a relative humidity of ~55 %, and a temperature of 20 ± 2 °C. At each testing age, one mortar sample or two cement paste samples were sacrificed for analysis. One sample is cut vertically to obtain the phase distribution profiles by SEM-EDS. A second sample is ground parallel to the exposed surface to obtain phase assemblage by XRD (only done with cement paste samples).

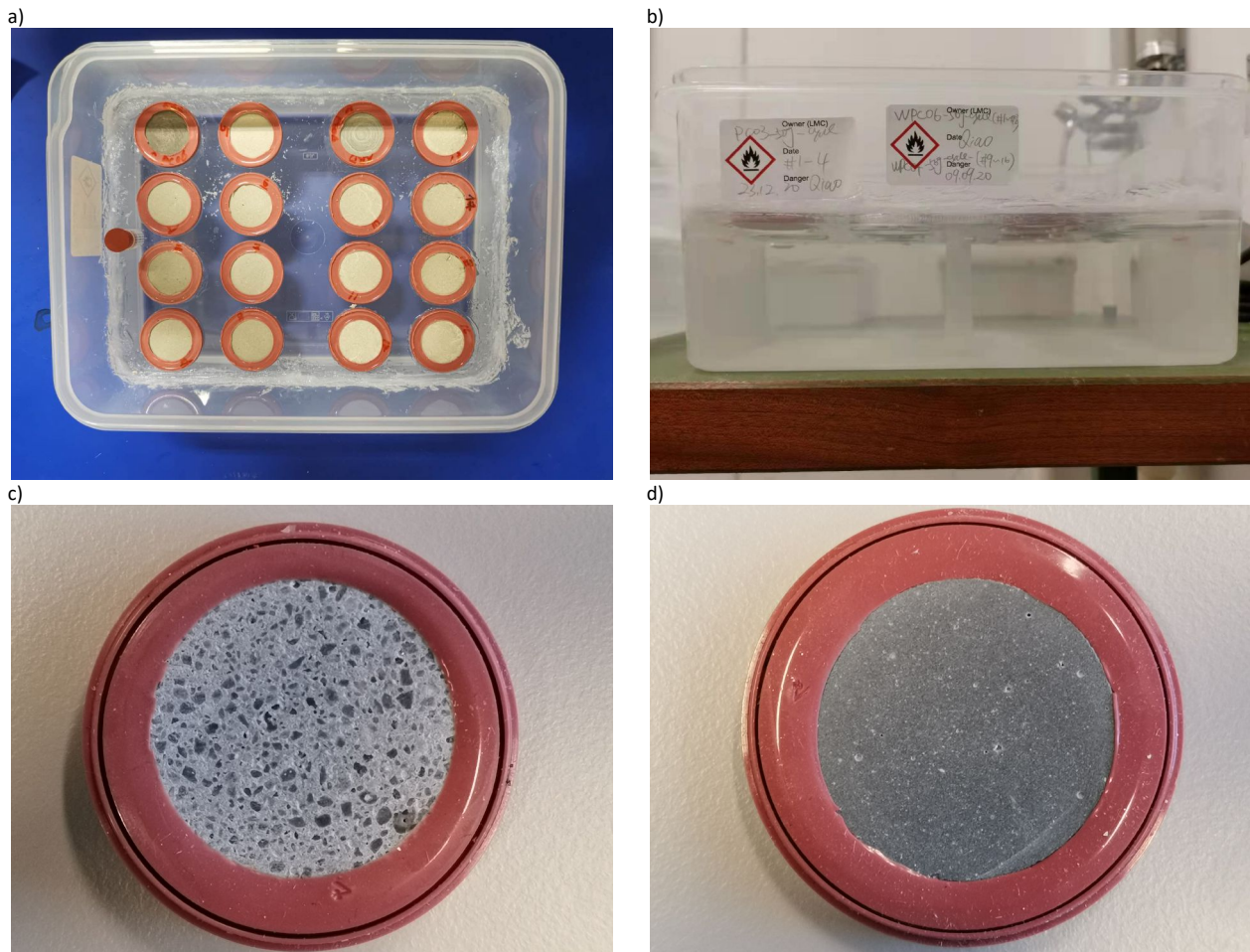


Fig. 4-1 Experimental set-up for the unidirectional sulfate penetration test: (a) top view of the setup; (b) side view of setup; (c) cement mortar, (d) cement paste.

### 4.2.3 Expansion measurements

The radial expansion was measured parallel to the degradation front (parallel to the exposed surface). The measurement was carried out as shown in Fig. 4-2 (b), using a digital slide calliper and stacked 1-mm thick hollowed steel rings (Fig. 4-2 (a)). Therefore, the expansion can be measured at each mm. The measurements were done with the same points before and after expansion measurements. A radial expansion profile is then obtained as a function of depth from the sulfate solution. To do so, the expansion at each mm can be tracked over time. There is some distance between the measuring point and the steel plate, so the measurements need to be offset by  $\sim 0.49$  mm. The representative error is indicated in Fig. 4-5, which is from the two different samples.



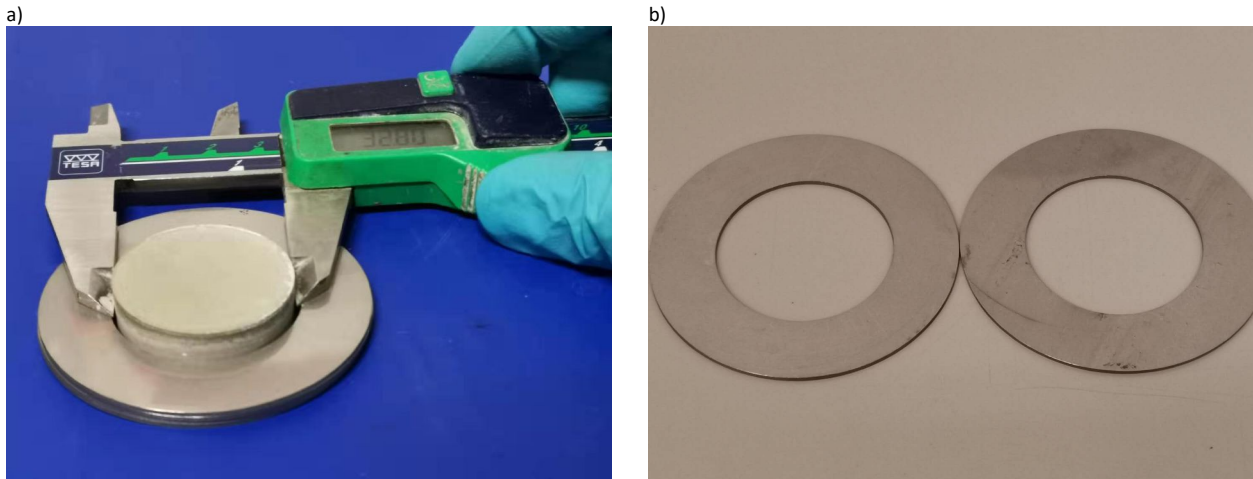


Fig. 4-2 Radial expansion measurement: (a) measure the expansion by using a calliper; (b) steel rings with a thickness of 1mm.

#### 4.2.4 Scanning electron microscopy (SEM)

Sections were cut perpendicular to the exposed surface and polished progressively to 1  $\mu\text{m}$  with diamond pastes. The cement paste samples were examined by scanning electron microscopy (FEI Quanta 200) using backscattered electron imaging (BSE) and elemental hyper mapping from energy dispersive spectroscopy (EDS). The accelerating voltage was 15.0 kV, with a working distance of 12.5 mm. Esprit 1.9 software was used to quantify the hypermaps after calibration with standards for each element of interest. The mapping area for the pastes was about  $860 \times 645 \mu\text{m}$  (nominal magnification  $300\times$ ) with a resolution of  $1000 \times 750$  pixels and a 2 times larger area for the mortars with the same pixel resolution. After processing, the mappings were quantitatively analysed using the EDXIA approach developed by Georget et al.[21].

#### 4.2.5 X-ray diffraction (XRD) analyses

X-ray diffraction (XRD) analyses were done with a Philips X'Pert Pro PANalytical ( $\text{CuK}\alpha$ ,  $\lambda = 1.54 \text{ \AA}$ ) working in Bragg–Brentano geometry over a  $2\theta$ -range of  $5\text{--}65^\circ$ . Quantitative Rietveld analyses were made with the HighScore Plus software and with the external standard method (titanium dioxide as crystalline standard, rutile Kronos 2300). X-ray diffraction was made on successive parallel sections of fresh cement paste slices, with manual grinding between each scan to reach the desired depth into the discs and provide quantitative phase assemblage profiles. The evolution of the hydrated phase assemblage with depth from the solution exposed surface to the top surface was tracked over time. Slices were analysed at distances from the surface of 0, 1, 2, 3, 4, 5 mm (or specific depths of interest based on SEM observations).

## 4.3 Results and discussion

### 4.3.1 Visual observations

The mortar samples after different exposure times are shown in Fig. 4-3. Generally, mortar samples stayed intact with no obvious cracks through the sample. Significant macroscopic damage was not observed until 112 days of exposure (Fig. 4-3 a, d and b, e). There was no efflorescence on the upper surface because the thicker mortar samples required a longer time before sulfate reached the top surface. At 140 days (Fig. 4-3 c, f) the samples started to have visible transversal cracks and flaking on the bottom surface. The side view of the samples illustrates that external sulfate attack is a process that progresses into the samples layer by layer, as further described in the following sections. With the mortar samples, there is a long delay before seeing any manifestations of sulfate attack even though the degradation of the bottom surface is quite profound. As an option to accelerate the visual evidence of the degradation process, cement paste samples were also investigated.

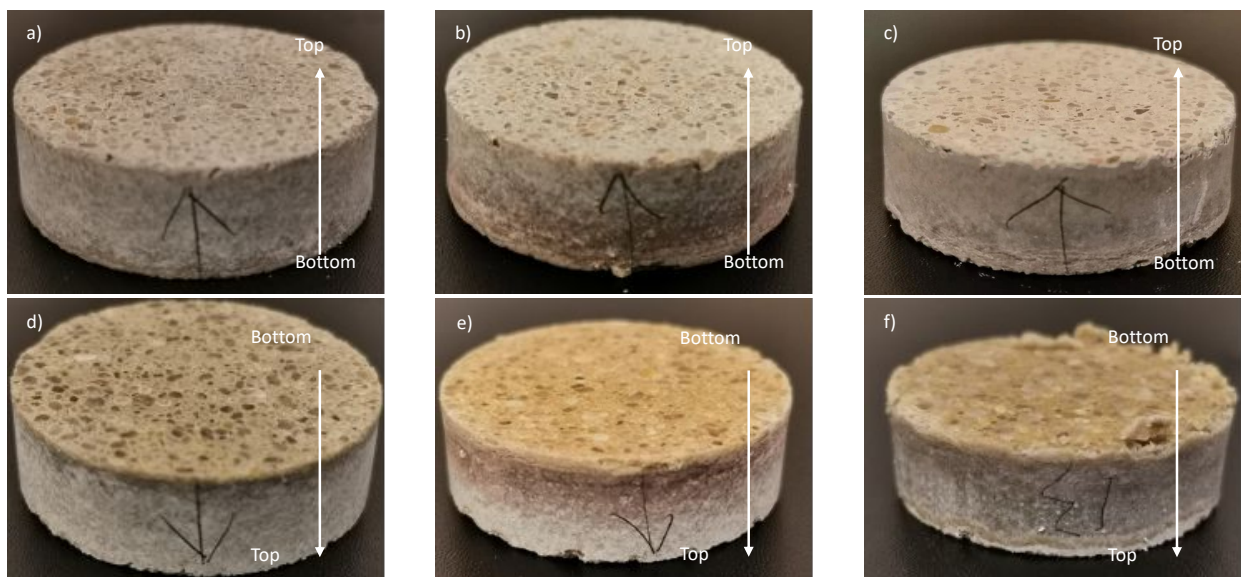


Fig. 4-3 Visual observations of Portland cement mortar samples after unidirectional exposure to the sulfate solution: (a,b,c) top surface views and (d,e,f) bottom surface views of (a,d) the PC mortar sample at 56d, (b,e) the PC mortar sample at 112d and (c,f) PC mortar sample at 140d. The arrow indicates the capillary rise direction.

Fig. 4-4 shows the appearance of the cement paste samples after different durations of exposure to sulfate solutions. The side views in Fig. 4-4 (b, e) show a trapezoid shape already after 91 days of exposure resulting from the unidirectional sulfate ingress (from bottom to top) with the main degraded area near the bottom. Paste samples have no aggregates and a smaller thickness so that efflorescence around cracks on the top surface can be observed from 91 days. This indicates that the samples were fully penetrated by sulfate ions due to capillary rise and concentrated in the regions where the water evaporated (Fig. 4-4 c, f). The paste sample was intact at 56 days (Fig. 4-4 a, d), but by 91 days of exposure extensive degradation and even cracks throughout the whole sample were observed. The damage was most extensive near the bottom of the

sample in contact with the sulfate solution. The degradation process is more evident and disruptive in paste samples because there are no aggregates present to dilute the paste volume, the extra space available for precipitation in the interfacial transition zone (ITZ) is not present, and paste samples are more brittle than mortar samples.

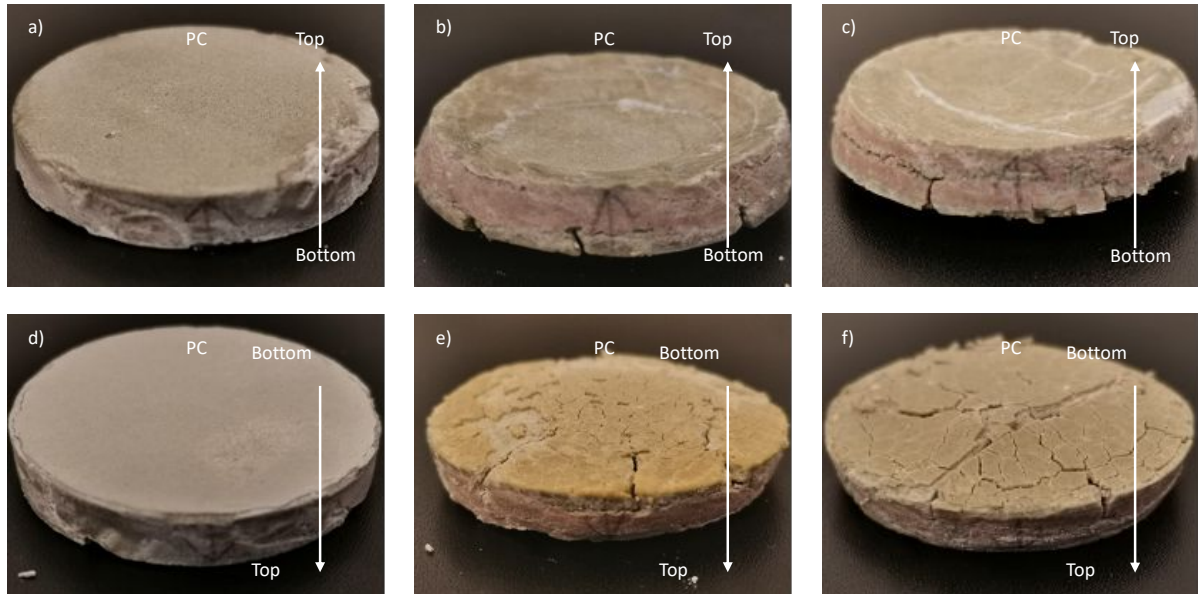


Fig. 4-4 Visual observations of Portland cement paste samples after unidirectional exposure to the sulfate solution: (a,b,c) top surface views and (d,e,f) bottom surface views of (a,d) the PC paste sample at 56d, (b,e) the PC paste sample at 91d and (c,f) the PC paste sample at 112d. The arrow indicates the capillary rise direction.

#### 4.3.2 Expansion as a function of depth and time

Expansion measurement is the simplest quantitative method to follow the deterioration process due to the chemical reactions that take place when the sulfates migrate into cement matrix. In this new approach, the lateral expansion is measured at different depth, rather than a single longitudinal one under conventional mortar ponding tests. Although the expansion measurements by this method are not as precise as those on long bars with measurement studs, the general trend is clear and the lack of precision is outweighed by the more detailed insight into the relation between expansion and alterations in the microstructure. Expansion profiles over the depth of the sample were followed as a function of exposure time, as shown in Fig. 4-5. The expansion was highest either at the directly exposed surface or 1–2 mm from bottom surface for both mortar and paste samples. The expansion increased as exposure time increased but the magnitude of the mortar expansion was much less than paste samples as shown in Fig. 4-5 b). The difference in magnitude between mortar and paste expansion is much more than could be explained by the lower volume of paste in the mortar (the paste is about 38% of the volume in mortar). In Fig. 4-5 a) the paste curves normalized by 38% are superposed. For example, the normalized expansion of cement paste at 56 days is similar to the expansion of mortar samples at 112 days. As will be discussed significant expansion results in extensive cracking, so the

lower relative expansion of the mortar can be due to the greater thickness of the mortar samples (by providing more restraint) and perhaps the possibility for ettringite to precipitate harmlessly in the more porous ITZ.

The expansion was minimal at the top surface. At an early age, there was some shrinkage at the top of the sample because of drying due to the low relative humidity of 55 %. The trend of expansion with time indicates that it is only a matter of time to observe the expansion of the top side because expansion propagates from the bottom upwards. There is no indication that the deposits seen as efflorescence contribute to expansion in the top zone.

The trend in the expansion curves suggests the attack mechanisms are similar between PC mortars and pastes, but the damage is more extensive in the cement paste, and once cracks form the ingress of sulfates is much faster. This suggests that the use of pastes rather than mortars may be a good way of accelerating the degradation.

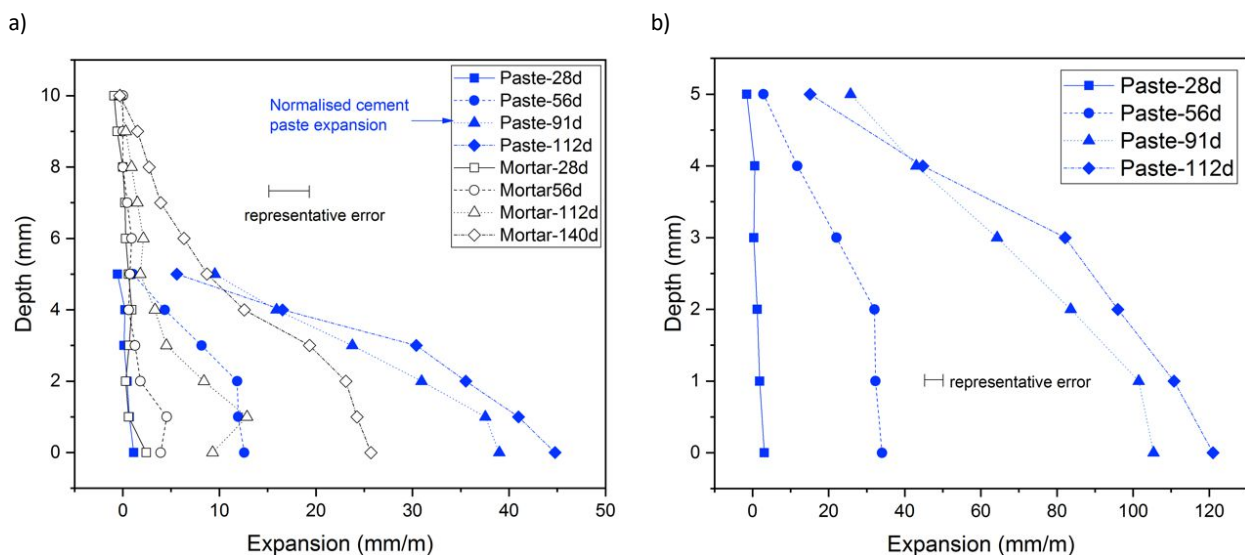


Fig. 4-5 Expansion profiles after exposure: (a) cement mortar & cement paste normalised by 38%; (b) cement paste.

### 4.3.3 Progress of the degradation processes from the chemical and phase profiles

#### Methodology to identify chemical and phase profiles

In the newly established unidirectional semi-immersion approach, sulfate ions ingress by capillary rise and/or diffusion then react only within the cement paste. To investigate further the attack mechanisms, the alterations in microstructure were studied in detail. In this section we describe the methodology developed to study the chemical and phase profiles through the sample with different analytical techniques. Fig. 4-6 illustrates this for a cement paste sample.

First, the porosity and degradation profiles can be obtained from the BSE image which was stitched together from 9 images covering the entire depth. The sulfate and sodium penetration can be visualised either by the

elemental maps (Fig. 4-6 b) and Fig. 4-6 c)) or more quantitatively in the concentration profiles (Fig. 4-6 e)). The carbonation depth can also be qualified. To get the phase profiles, EDXIA [21] was used to segment all the phases of interest in terms of sulfate attack. For different phases, specific atomic ratios were applied to select the relevant clusters which are then overlaid on the BSE images (full details of the algorithm are explained in [21]). The specific atomic ratios used to distinguish the different phases are given in Table 4-2 and ref [21]. The approximate volume fractions of different phases are estimated from pixels at each depth: this is a semi-quantitative estimation for comparative purposes. The weight fractions from XRD measurements at various depths of the same sample are also shown on the same depth scale.

Table 4-2 Boundary definition for sulfate attack-related phases in cement-based materials

Phases	Si/Ca	Al/Ca	BSE peak	Others
Portlandite	<0.2	<0.2	Hydrate	Na/Ca, K/Ca
Calcite	<0.2	<0.2	Hydrate	Na/Ca, K/Ca
Carbonated gel			Hydrate	Na/Ca, K/Ca
Gypsum			Hydrate	S/Ca→1
Ettringite			Hydrate mixes with C-S-H	S/Ca→0.5, Al/Ca→0.33
C-S-H matrix	Variable	Variable	Hydrate	Depends on cement types
Thenardite			Hydrate	Na/S→2

The example shows the cement paste sample after 28 days of exposure, a densified layer has formed at the bottom around 2 mm thick as seen in the BSE micrographs in Fig. 4-6 (a), this may be attributed to the formation of new phases filling voids. The sulfur and sodium concentration gradient maps shown in Fig. 4-6 (b), (c) trace the penetration of sodium sulfate solution. It is seen by EDS and XRD profiles in Fig. 4-6 (d), (e) and (f), that the main products from sulfate attack are ettringite (with a decreasing concentration of this phase from the bottom moving into the sample) and gypsum filling the cracks caused by the expansion. At 1 mm depth, the phase composition in the exposed sample is similar to that of the reference sample (stored in pore solution) (shown at the centre of Fig. 4-6 (f)) and indicates the depth of penetration of the sulfate solution at this time. The information from SEM and XRD is very consistent, but the identification of AFm phases is rather challenging by EDXIA due to the fine intermixing of these phases and the quantification by XRD is likely to be an underestimate due to their poor crystallinity. Therefore, in the following sections, AFm phases were not segmented by EDXIA. Carbonation occurred on the upper side of the samples. XRD measurements for mortar samples are not very accurate as the minerals in the sand (mainly quartz) dilute other phases). So the phase maps from EDXIA analysis are the main tool used to study mortars.

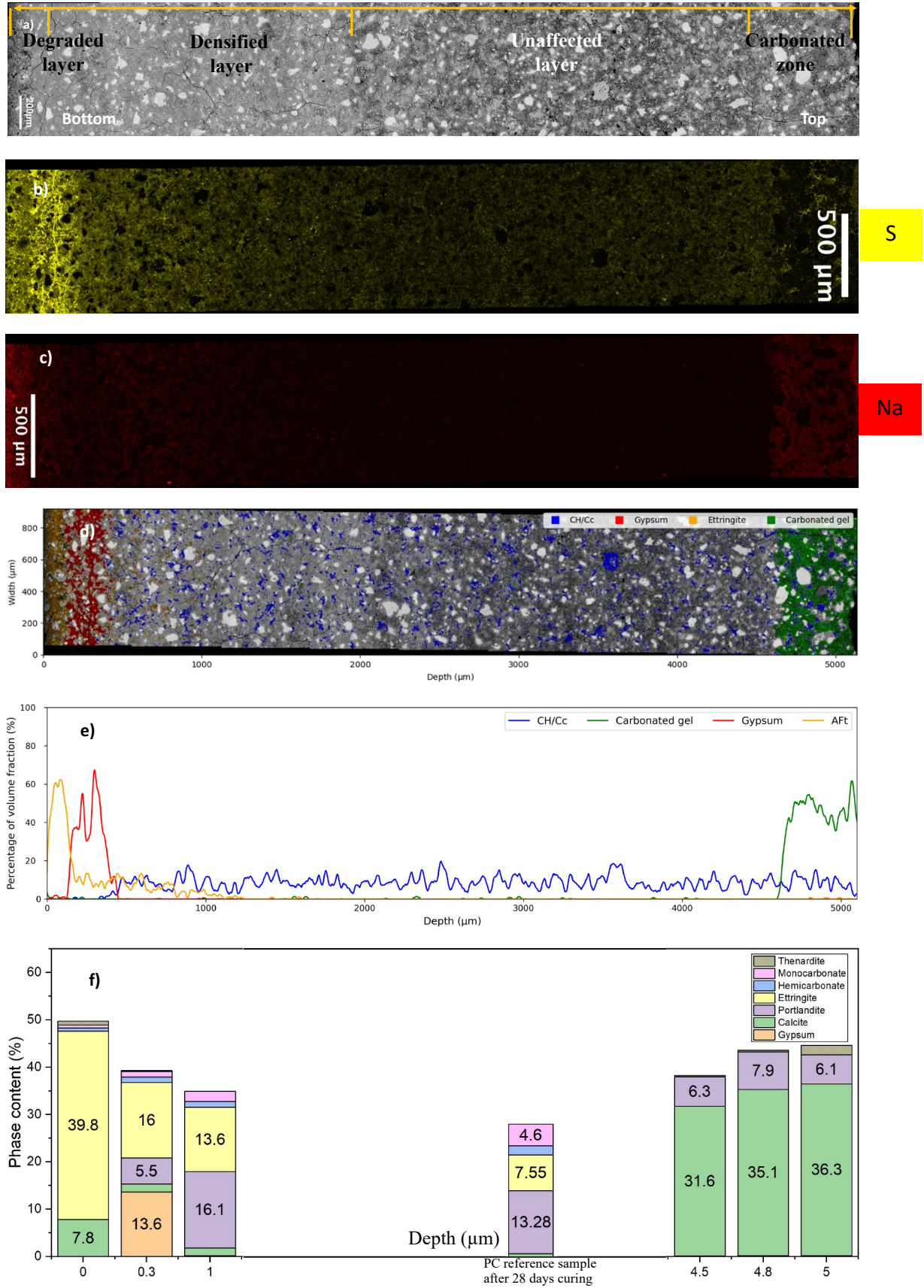


Fig. 4-6 PC paste samples with the entire 5mm-depth profiles after 28 days of exposure: (a) BSE micrograph, (b) sulfur concentration presence, (c) sodium concentration presence, (d) phase distribution, (e) phase profile, (f) phase assemblage profile from XRD.

### Degradation process in mortars

To better understand the mechanism of sulfate attack for the more realistic mortar samples, the results from 56 days up to 140 days are shown in Fig. 4-7. The figure shows the BSE plots, overlain by the main phases identified by EDXIA and the semi-quantitative fractions of these phases below. The combination of leaching and sulfate attack softens the bottom surface and around 0.5 mm was lost during cutting to prepare the SEM samples in the case of 56 days and 112 days as indicated in the plots. Above this leached zone, there is a zone, dominated by gypsum, which is mainly precipitated in the interface between cement paste and aggregates. Expansion of the pastes, due to ettringite formation, causes the paste fraction to expand and open gaps around the aggregates where the gypsum precipitates [22]. In this layer, the sand particles were completely decoupled from the cement matrix big cracks formed in this and the leached layer below. This layer, dominated by gypsum, moves up from the bottom surface with time. Interestingly, the gypsum front is quite flat, with little apparent influence of the aggregates.

Above the gypsum layer, there is a layer in which ettringite has formed, where expansion occurs. This zone of ettringite formation can be linked to the expansion profiles shown previously. The amount of ettringite in this layer and the thickness of the layer, where ettringite is identified, increases with time. The ettringite front stops at around 3 and 4 mm at the ages of 56 days and 112 days respectively. By 140 days ettringite has formed throughout the thickness of the sample. At this time expansion started to speed up as shown in Fig. 4-5 and thenardite is formed near the top surface where water has evaporated from the pore solution in Fig. 4-7 (f). In this central part, the microstructure appears denser due to ettringite filling pores.

In parallel, a carbonated layer forms at the top surface. The carbonated layer also grows with time.

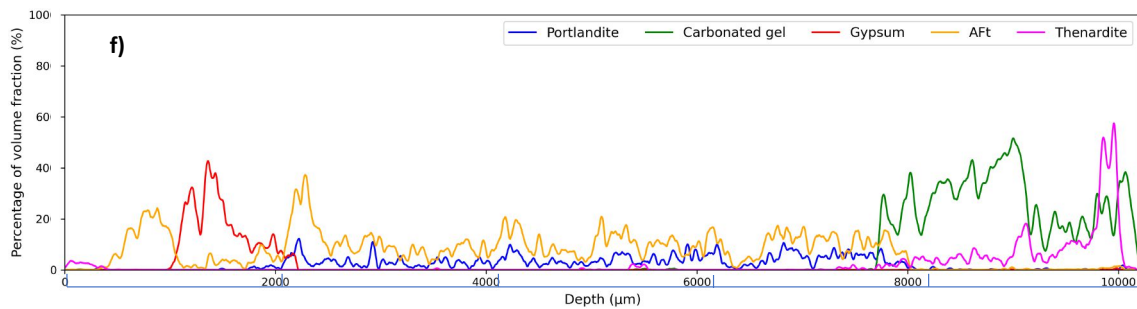
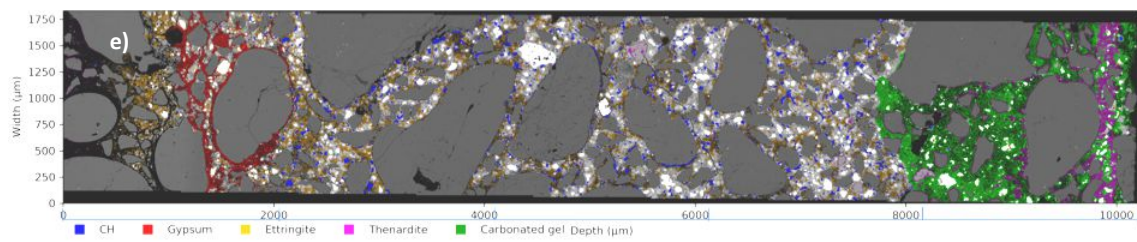
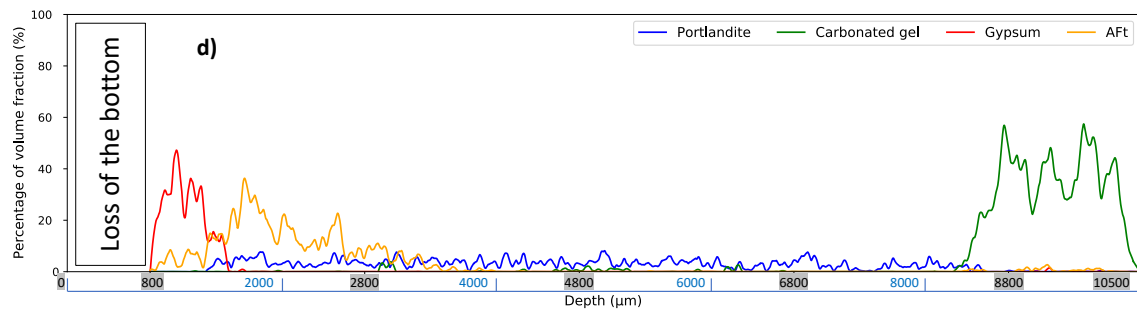
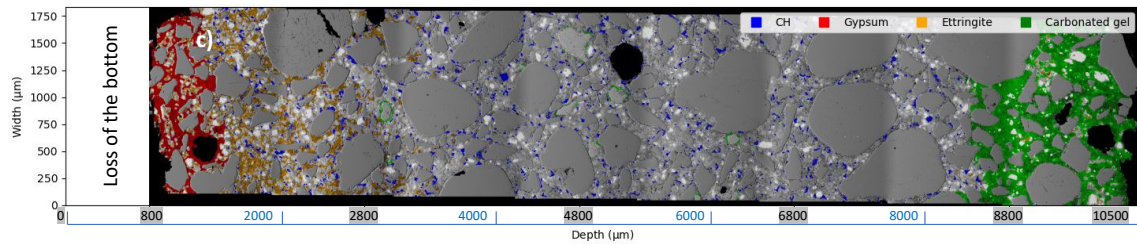
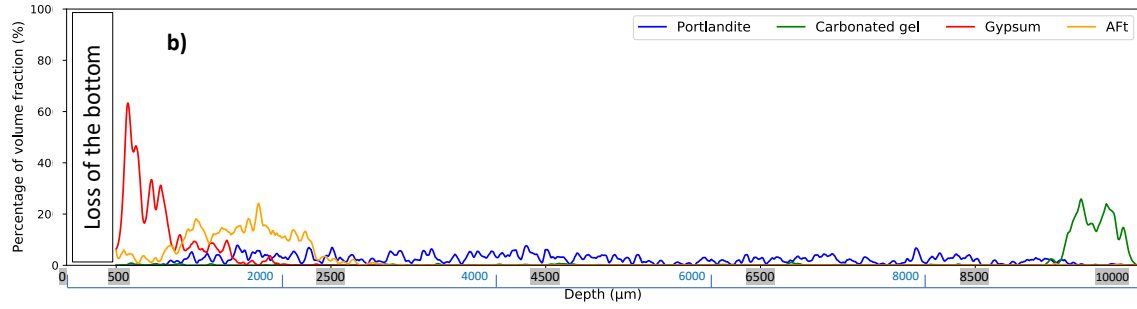
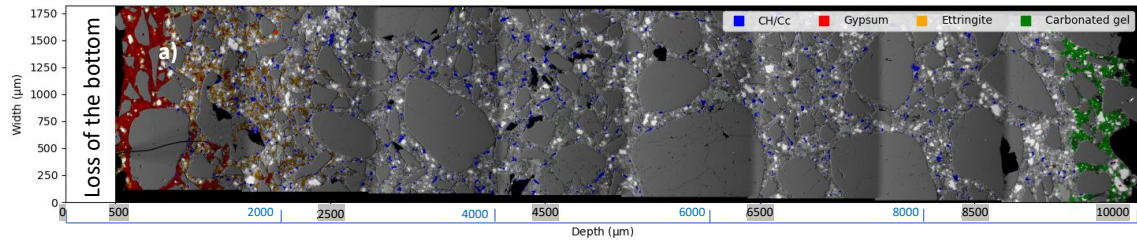




Fig. 4-7 PC mortar samples with the entire 10mm-depth profiles after exposure: (a) phase distribution after 56 days, (b) phase profiles after 56 days, (c) phase distribution after 112 days, (d) phase profiles after 112 days, (e) phase distribution after 140 days, (f) phase profiles after 140 days. Blue scales on the bottom are recalibrated to 10 mm.

### Degradation process in pastes

The results from pastes at 56 and 114 days are shown in Fig. 4-8. As already seen by visual observation and expansion measurements, the degradation advanced much faster in the pastes and more extensive damage was observed. Nevertheless, the broad pattern of microstructural changes was similar to that in mortars. A highly leached and degraded layer forms at the bottom surface. Above this, is a layer dominated by gypsum precipitation. However, as there are no aggregates, the expansion process now leads to the formation of mainly surface subparallel cracks in which the gypsum precipitates. Above this expanded and cracked layer with gypsum precipitation, is a layer in which ettringite can be identified. At 28 days, shown in section 3.3.1 the depth of extra ettringite formation extends to about 1 mm, but by 56 days ettringite formation is seen throughout the whole depth. Microcracks can be seen throughout the samples which probably percolate through the whole depth as the paste sample is more brittle than mortars, this will facilitate the ingress of sulfate.

The expansion also speeds up at 56 days and is similar to the mortar sample at 112 days if we compare the paste sample normalized by 38 %. Gypsum is not only precipitated in cracks close to the bottom but also can be found in the wet/dry interface zone close to the top surface in pastes. But it disappears as the carbonation advances deeper into the evaporation zone.

Thenardite can be seen at 114 days of exposure which is around one month earlier, than in the thicker mortar samples. After both systems have been thoroughly penetrated, the ettringite volume can be estimated, it is around 10 vol.% in both pastes (normalized by 38 %) and mortars which indicate chemical changes are similar in the two systems.

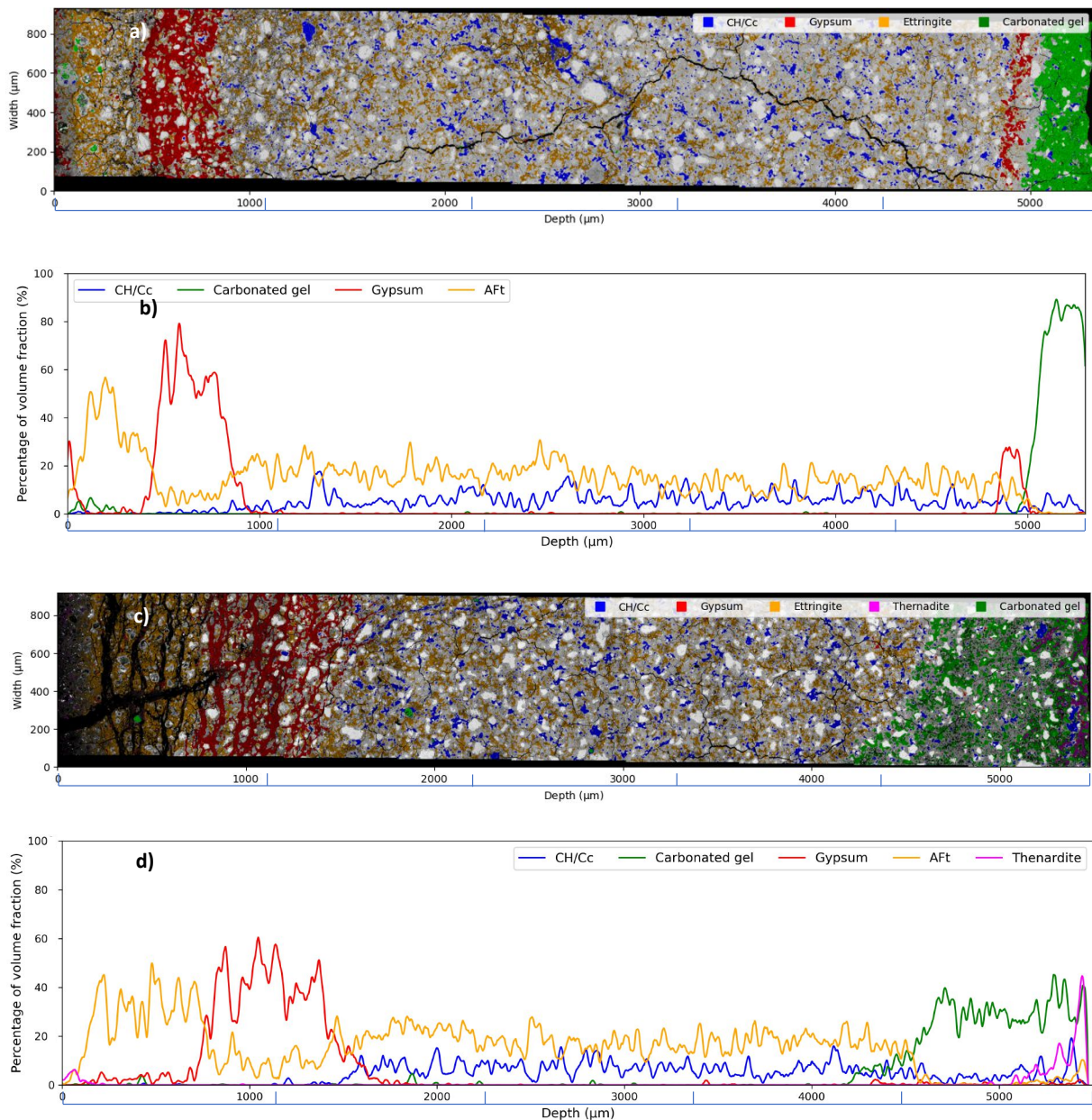


Fig. 4-8 PC paste samples with the entire 5mm-depth profiles after exposure: (a) phase distribution after 56 days, (b) phase profiles after 56 days, (c) phase distribution after 114 days, (d) phase profiles after 114 days. Blue scales on the bottom are recalibrated to 5 mm.

#### 4.3.4 Discussion

##### Global damage model for sulfate attack

The first investigations involving the proposed unidirectional approach confirm previous work [2,12,13,23–25] that external sulfate attack is a layer-by-layer degradation process. Sulfate ions move inwards by diffusion and capillary action and then react with paste. The formation of ettringite in confined conditions leads to expansion and cracking. Once cracks percolate through the whole sample, the ingress of sulfate through the cracks is rapidly leading to degradation throughout the sample.

Fig. 4-9 Shows the process schematically, including a hypothetical indication of how expansion and crystallization pressure may vary through the sample. In all the samples different zones can be identified as described below:

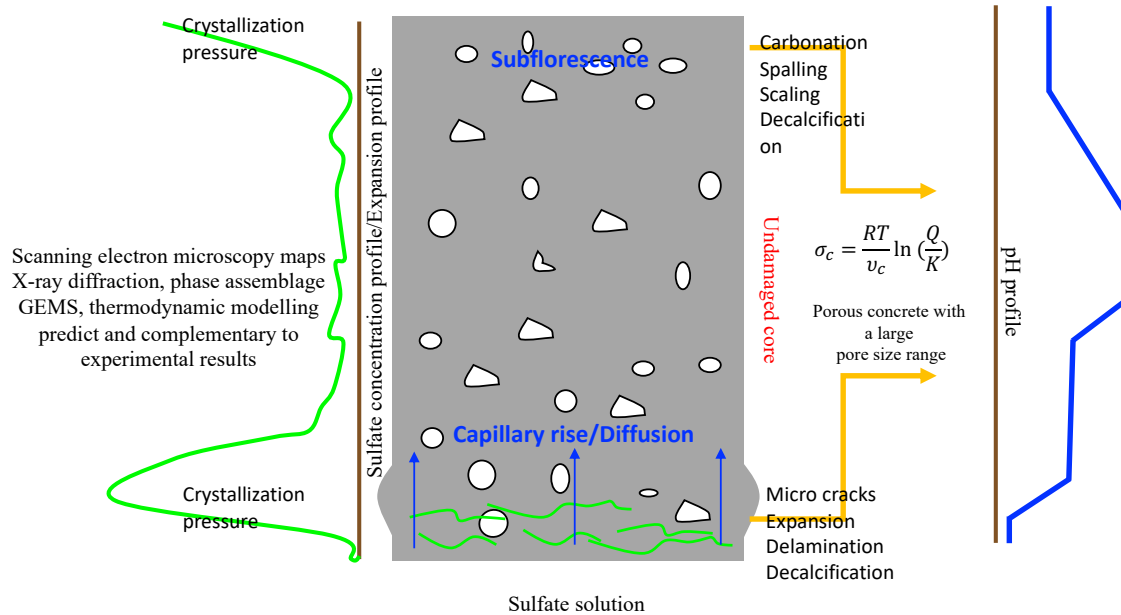


Fig. 4-9 Schematic diagram of sulfate attack degradation model on cement mortar and paste.

**Central Zone:** We start with the central zone as this has the microstructure which has undergone the least change and is most similar to the starting microstructure. However, the appearance of this zone progressively “densifies”. As the sulfate ions ingress, they react with the large clusters of freely transformable AFm phases to form ettringite. This formation of ettringite is in larger pores and so does not cause expansion.

**Bottom Subsurface Zone:** Once the freely transformable AFm phases have reacted, the sulfate concentration in the solution can build up. This creates the conditions of supersaturation necessary for ettringite to form from the submicron AFm phases within the C-S-H, which causes expansion. This expansion causes cracking according to the conditions of constraint in the sample. In mortars, gaps open up around aggregates, while in paste cracks form subparallel to the surface. Gypsum precipitates in these gaps and cracks, but does not contribute directly to the expansion as the conditions of supersaturation and constraint with respect to this phase are not sufficient.

**Bottom leached zone:** At the bottom surface, in contact with the solution, a heavily leached zone forms. It is a thin and soft layer of amorphous material with extensive leaching and cracking. Ettringite (which may be leached as well in the later stages) and calcite are the main phases apart from the large proportion of amorphous phases. The expansion is highest in this zone and it is heavily cracked due to the disintegration of hydrates.

In these 3 zones “chemical” sulfate attack occurs. As the subsurface zone progresses into the sample it eventually causes cracking through the whole sample.

**Top zone:** In the top zone, two processes occur. First carbonation is due to contact with the atmosphere. Secondly, once the freely transformable AFm phases in the central region have reacted, the sulfate ions penetrate the sample and may precipitate as thenardite. Although this phase is associated with a “physical sulfate attack”, it did not seem to be associated with any damage in the samples studied here, perhaps because hydraulic and/or thermal cycling are needed to cause damage.

With the combination of analytical techniques used, it was possible to characterize the changes occurring throughout the whole depth of the sample and follow their evolutions with exposure time.

#### Salt crystallization

The salt crystallisation in the upper part of the cement paste sample can give information on “physical sulfate attack”. For the cement paste sample at 114 days (Fig. 4-10) a relatively large “Na/S” ratio is detected from SEM–EDS in the evaporation/carbonation zone, which suggests that the salt crystallization attack potentially takes place there.

The characteristic high sodium and depleted sulfate content of the carbonation zone found here agrees with modelling predictions [26] and was also previously seen experimentally in PC systems [27]. The high Na/S ratio is a consequence of the combination processes of carbonation and accumulation of Na ions due to the evaporation of water at the top surface. Specifically, Alkalis (Na and K) are present in the pore solution after the hydration of the cement paste moved up through the sample.

The decrease of sulfate ions in the carbonated zone is due to the high solubility of gypsum in the pore solution of the carbonated zone. Therefore, it is likely that when thenardite precipitation is detected by XRD (far right in Fig. 4-6 f), the Na/S ratio could be much higher than the value ( $\text{Na/S}=2$  for  $\text{Na}_2\text{SO}_4$  or  $\text{Na}_2\text{SO}_4 \cdot 10\text{H}_2\text{O}$  salts) due to excess Na in the surrounding matrix.

So even though, precipitation of thenardite is associated with “physical sulfate attack”, it is a chemical-based process which indicates the confused nomenclature currently employed.

In this study, we do not see any visible damage from the subflorescence in either mortar or pastes this may be because cycles of temperature and humidity and changes between thenardite and mirabilite are needed to produce damage [16].

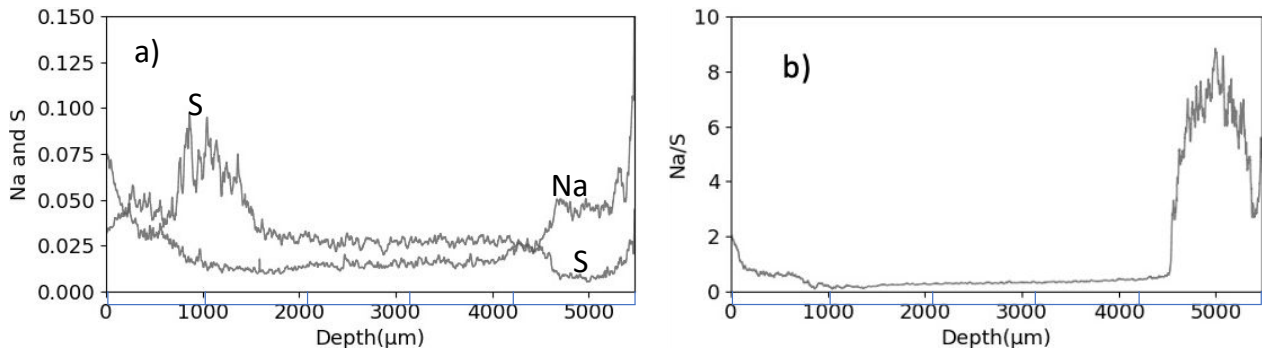


Fig. 4-10 The content of Na and S of the entire sample exposed to relative humidity of 55 %, showing signs of thenardite precipitation at 114d: a) profile of Na/S ratio; b) relative content profile of Na and S. Blue scales on the bottom are recalibrated.

### Perspectives for the approach

This study shows the feasibility of a unidirectional approach. In this first study, we chose a high  $\text{Na}_2\text{SO}_4$  concentration, high water-to-cement ratio and OPC, to maximise the chances to observe degradation in a reasonably short time. It is likely that the mortar samples have less evident degradation due to the greater thickness, necessary to accommodate the larger sand particles and the changes in pore structure due to the presence of the ITZ. It was already shown in [2] that in conditions of full immersion thicker samples expanded slower and had a longer latency period before the expansion started to become significant. A major factor is the constraint provided by the non-expanding part of the sample. In addition, the higher porosity of the ITZ may also give more space for precipitation of ettringite without expansion.

The time required to get both “chemical” and “physical” sulfate attack on mortar samples is still quite long, 6 months or even more. It seems that paste samples, provide a good option to speed up the degradation process. This is mainly because it is possible to prepare thinner representative samples, but also because pastes are more brittle and cracking speeds up the ingress of sulfate. This brings down the time needed to see degradation for the same material by two months or more.

This new unidirectional approach is a comprehensive method for investigating the sulfate attack degradation process on mortars and pastes, which integrates both “chemical sulfate attack” and “physical sulfate attack”. Compared with conventional full or partial immersion approaches, the same sample can be precisely characterized over the full depth including both types of sulfate attacks.

Importantly, this novel semi-immersion approach can also contribute to eliminating the confusing and misleading concept of separating sulfate attack into “chemical sulfate attack” and “physical sulfate attack”. The interaction between these different reactions can also be easily studied by varying experimental parameters, such as the relative humidity and temperature conditions, the concentration of the sulfate solution, the binder types and the water-to-binder ratio of the investigated systems. More work is needed to study the influence of different parameters, such as solution concentration and water-to-cement ratio, but eventually,

we think such a uni-directional set-up could provide the basis for a new approach to testing which reflects better the phenomena of importance in the field. Of course, a test method should not require complex SEM investigations, but the understanding brought by these investigations is important to verify the link between degradation and the mechanisms. More work is needed to establish simple reproducible failure criteria, which do not rely on time-consuming microscopical observations.

The set-up also provides a means to get better insights into other outstanding questions. Such as the effects of wet/dry cycles, particularly concerning the damage caused by the salt crystallization [28–32].

## 4.4 Conclusions

This study demonstrates the feasibility of a new unidirectional testing approach to study sulfate attack processes as a whole. This contributes to understanding the fundamental mechanisms and eliminating the confusion between “chemical” and “physical” sulfate attacks. With the new set up it is possible to study both the effects of ettringite formation (so-called “chemical attack”) and the effects of sodium sulfate salt precipitation (thenardite and/or mirabilite) (so-called “physical attack”) in the same mortar or paste sample. The complementary in-depth characterization with XRD (phase assemblage profiles), SEM (pore structures), and EDXIA (chemical and phase profiles) provides new insights to understand sulfate attack degradation processes.

- The study confirms the layer-by-layer process first reported by Taylor and Gollop [11–13] and for which the link to the expansion process was established by Yu et al [2]. In this methodology 4 zones can be identified in both PC cement mortars and pastes: three “chemical” sulfate attack zones including a central zone without visible damage, a bottom subsurface zone and a bottom leached zone. A top zone is carbonated and susceptible to salt crystallization attack.
- The comparison between Portland cement mortars and pastes shows that degradation follows a very similar pattern in both cases, but larger thickness, lower paste volume and aggregates present in the former compensate for the stress exerted from crystallization pressure due to ettringite formation.
- Paste samples can be used to accelerate the degradation process.

Finally, the proposed unidirectional testing approach has shown great potential in this first study. Mechanisms happening in both cement mortar and paste materials are the same which can allow us to focus on the more rapidly deteriorating paste samples in future explorations. On-going work is looking at different systems and experimental conditions (e.g., sulfate-resisting cement, or limestone calcined clay cement, with variations of w/c, solution concentration, relative humidity, etc.).

## 4.5 References

- [1] B. Lothenbach, B. Bary, P. Le Bescop, T. Schmidt, N. Leterrier, Sulfate ingress in Portland cement, *Cement and Concrete Research*. 40 (2010) 1211–1225. <https://doi.org/10.1016/j.cemconres.2010.04.004>.
- [2] C. Yu, W. Sun, K. Scrivener, Mechanism of expansion of mortars immersed in sodium sulfate solutions, *Cement and Concrete Research*. 43 (2013) 105–111. <https://doi.org/10.1016/j.cemconres.2012.10.001>.
- [3] A.R.S. M.L. Nehdi, A.M. Soliman, Investigation of concrete exposed to dual sulfate attack, *Cement and Concrete Research*. 64 (2014) 42–53. <https://doi.org/10.1016/j.cemconres.2014.06.002>.
- [4] M. Whittaker, L. Black, Current knowledge of external sulfate attack, *Advances in Cement Research*. 27 (2015) 532–545. <https://doi.org/10.1680/adcr.14.00089>.
- [5] PD CEN/TR 15697:2008 - Cement. Performance testing for sulfate resistance. State of the art report, (n.d.). <https://shop.bsigroup.com/ProductDetail/?pid=000000000030164792> (accessed February 19, 2019).
- [6] A. Chabrelie, Mechanisms of degradation of concrete by external sulfate ions under laboratory and field conditions, PhD Thesis, EPFL, 2010. <https://infoscience.epfl.ch/record/143041> (accessed February 21, 2019).
- [7] W. Kunther, Investigation of Sulfate Attack by Experimental and Thermodynamic Means, PhD Thesis, EPFL, 2012. <https://doi.org/10.5075/epfl-thesis-5263>.
- [8] W. Kunther, B. Lothenbach, K.L. Scrivener, On the relevance of volume increase for the length changes of mortar bars in sulfate solutions, *Cement and Concrete Research*. 46 (2013) 23–29. <https://doi.org/10.1016/j.cemconres.2013.01.002>.
- [9] Z. Shi, S. Ferreira, B. Lothenbach, M.R. Geiker, W. Kunther, J. Kaufmann, D. Herfort, J. Skibsted, Sulfate resistance of calcined clay – Limestone – Portland cements, *Cement and Concrete Research*. 116 (2019) 238–251. <https://doi.org/10.1016/j.cemconres.2018.11.003>.
- [10] T. Schmidt, B. Lothenbach, M. Romer, J. Neuenschwander, K. Scrivener, Physical and microstructural aspects of sulfate attack on ordinary and limestone blended Portland cements, *Cement and Concrete Research*. 39 (2009) 1111–1121. <https://doi.org/10.1016/j.cemconres.2009.08.005>.
- [11] R.S. Gollop, H.F.W. Taylor, Microstructural and microanalytical studies of sulfate attack. I. Ordinary portland cement paste, *Cement and Concrete Research*. 22 (1992) 1027–1038. [https://doi.org/10.1016/0008-8846\(92\)90033-R](https://doi.org/10.1016/0008-8846(92)90033-R).
- [12] R.S. Gollop, H.F.W. Taylor, Microstructural and microanalytical studies of sulfate attack III. Sulfate-resisting portland cement: Reactions with sodium and magnesium sulfate solutions, *Cement and Concrete Research*. 25 (1995) 1581–1590. [https://doi.org/10.1016/0008-8846\(95\)00151-2](https://doi.org/10.1016/0008-8846(95)00151-2).
- [13] R.S. Gollop, H.F.W. Taylor, 21 SOME CHEMICAL AND MICROSTRUCTURAL ASPECTS OF CONCRETE DURABILITY, in: CRC Press, 1997.
- [14] M.T. Bassuoni, M.L. Nehdi, Durability of self-consolidating concrete to different exposure regimes of sodium sulfate attack, *Mater Struct*. 42 (2009) 1039–1057. <https://doi.org/10.1617/s11527-008-9442-2>.
- [15] Crystallization of sodium sulfate phases in porous materials: The phase diagram Na<sub>2</sub>SO<sub>4</sub>–H<sub>2</sub>O and the generation of stress, *Geochimica et Cosmochimica Acta*. 72 (2008) 4291–4306. <https://doi.org/10.1016/j.gca.2008.05.053>.
- [16] N. Tsui, R.J. Flatt, G.W. Scherer, Crystallization damage by sodium sulfate, *Journal of Cultural Heritage*. 4 (2003) 109–115. [https://doi.org/10.1016/S1296-2074\(03\)00022-0](https://doi.org/10.1016/S1296-2074(03)00022-0).
- [17] J. Desarnaud, S. Noushine, STUDY OF KINETICS OF SALT CRYSTALLIZATION DURING REWETTING DRYING AND HUMIDITY CYCLING, 2012.
- [18] H. Derluyn, Salt transport and crystallization in porous limestone: Neutron-X-ray imaging and poromechanical modeling, Doctoral Thesis, ETH Zurich, 2012. <https://doi.org/10.3929/ethz-a-007578301>.
- [19] Z. Liu, D. Deng, G. De Schutter, Does concrete suffer sulfate salt weathering?, *Construction and Building Materials*. 66 (2014) 692–701. <https://doi.org/10.1016/j.conbuildmat.2014.06.011>.
- [20] The damage mechanism and failure prediction of concrete under wetting–drying cycles with sodium sulfate solution, *Construction and Building Materials*. 264 (2020) 120525. <https://doi.org/10.1016/j.conbuildmat.2020.120525>.
- [21] F. Georget, W. Wilson, K.L. Scrivener, edxia: Microstructure characterisation from quantified SEM-EDS hypermaps, *Cement and Concrete Research*. 141 (2021) 106327. <https://doi.org/10.1016/j.cemconres.2020.106327>.
- [22] Jan Skalny, Jacques Marchand, Ivan Odler, Sulfate Attack on Concrete, London and New York, 2002. [https://www.bookdepository.com/Sulfate-Attack-on-Concrete-J.-Marchand/9780419245506?redirected=true&utm\\_medium=Google&utm\\_campaign=Base5&utm\\_source=CH&utm\\_content=Sulfate-Attack-on-Concrete&selectCurrency=CHF&w=AF72AU9SLSQSCQA803VV&pdg=pla-293946777986:kwd-293946777986:cmp-1578060869:adg-65091841852:crv-296436506046:pid-9780419245506:dev-c&gclid=EAlalQobChMizbvA6M-a4glViuR3Ch0tjw8TEAYASA-BEgJUXPD\\_BwE](https://www.bookdepository.com/Sulfate-Attack-on-Concrete-J.-Marchand/9780419245506?redirected=true&utm_medium=Google&utm_campaign=Base5&utm_source=CH&utm_content=Sulfate-Attack-on-Concrete&selectCurrency=CHF&w=AF72AU9SLSQSCQA803VV&pdg=pla-293946777986:kwd-293946777986:cmp-1578060869:adg-65091841852:crv-296436506046:pid-9780419245506:dev-c&gclid=EAlalQobChMizbvA6M-a4glViuR3Ch0tjw8TEAYASA-BEgJUXPD_BwE) (accessed May 14, 2019).
- [23] M. Santhanam, M.D. Cohen, J. Olek, Mechanism of sulfate attack: a fresh look: Part 2. Proposed mechanisms, *Cement and Concrete Research*. 33 (2003) 341–346. [https://doi.org/10.1016/S0008-8846\(02\)00958-4](https://doi.org/10.1016/S0008-8846(02)00958-4).
- [24] J.G. Wang, Sulfate attack on hardened cement paste, *Cement and Concrete Research*. 24 (1994) 735–742. [https://doi.org/10.1016/0008-8846\(94\)90199-6](https://doi.org/10.1016/0008-8846(94)90199-6).
- [25] D. Planel, J. Sercombe, P. Le Bescop, F. Adenot, J.-M. Torrenti, Long-term performance of cement paste during combined calcium leaching–sulfate attack: kinetics and size effect, *Cement and Concrete Research*. 36 (2006) 137–143. <https://doi.org/10.1016/j.cemconres.2004.07.039>.
- [26] F. Georget, J.H. Prevost, B. Huet, Impact of the microstructure model on coupled simulation of drying and accelerated carbonation, *Cement and Concrete Research*. 104 (2018) 1–12. <https://doi.org/10.1016/j.cemconres.2017.11.008>.
- [27] W. Soja, Carbonation of low carbon binders, PhD Thesis, EPFL, 2019. <https://doi.org/10.5075/epfl-thesis-9400>.

- [28] R.J. Flatt, G.W. Scherer, Hydration and Crystallization Pressure of Sodium Sulfate: a Critical Review, *MRS Online Proceedings Library Archive*. 712 (2002). <https://doi.org/10.1557/PROC-712-II2.2>.
- [29] G.W. Scherer, Crystallization in pores, *Cement and Concrete Research*. 29 (1999) 1347–1358. [https://doi.org/10.1016/S0008-8846\(99\)00002-2](https://doi.org/10.1016/S0008-8846(99)00002-2).
- [30] C. Rodriguez-Navarro, E. Doehne, E. Sebastian, How does sodium sulfate crystallize? Implications for the decay and testing of building materials, *Cement and Concrete Research*. 30 (2000) 1527–1534. [https://doi.org/10.1016/S0008-8846\(00\)00381-1](https://doi.org/10.1016/S0008-8846(00)00381-1).
- [31] C. Rodriguez-Navarro, E. Doehne, Salt weathering: influence of evaporation rate, supersaturation and crystallization pattern, *Earth Surface Processes and Landforms*. 24 (1999) 191–209. [https://doi.org/10.1002/\(SICI\)1096-9837\(199903\)24:3<191::AID-ESP942>3.0.CO;2-G](https://doi.org/10.1002/(SICI)1096-9837(199903)24:3<191::AID-ESP942>3.0.CO;2-G).
- [32] S. Chatterji, N. Thaulow, Unambiguous demonstration of destructive crystal growth pressure, *Cement and Concrete Research*. 27 (1997) 811–816. [https://doi.org/10.1016/S0008-8846\(97\)00078-1](https://doi.org/10.1016/S0008-8846(97)00078-1).



# Chapter 5 Macroscopic and microscopic results – Key variables

## Contents

<b>5.1</b>	<b>Introduction .....</b>	<b>89</b>
<b>5.2</b>	<b>The effect of the w/c and the sulfate concentration.....</b>	<b>90</b>
5.2.1	Visual inspections .....	90
5.2.2	Expansion and mass gain.....	91
5.2.3	Sulfate ingress as a function of exposure time.....	93
5.2.4	Sulfate ingress rate.....	95
5.2.5	Phase change as a function of depth and time .....	96
<b>5.3</b>	<b>The effect of the cement type .....</b>	<b>98</b>
5.3.1	Chemical properties before sulfate exposure .....	98
5.3.2	Physical changes after sulfate exposure.....	100
5.3.3	Chemical changes after sulfate exposure.....	104
5.3.4	Sulfate ingress as a function of exposure time.....	106
5.3.5	Salt crystallization.....	111
<b>5.4</b>	<b>The comparison of constant and cycling exposure conditions .....</b>	<b>116</b>
5.4.1	Physical behaviours after sulfate exposure.....	116
5.4.2	Chemical changes after sulfate exposure.....	119
<b>5.5</b>	<b>Conclusions.....</b>	<b>129</b>

## 5.1 Introduction

This chapter uses the newly established unidirectional approach (see *Chapter 4*) to investigate three important aspects influencing the degradation of different cement pastes:

- 1) the effect of the w/c and the sulfate concentration;
- 2) the effect of the cement type;
- 3) the comparison of constant and cycling exposure conditions.

First, w/c ratios of 0.3, 0.4 and 0.6 are investigated, as well as solution concentrations of 3 g/L and 50 g/L, to understand the effect of those parameters on the degradation of Portland cement pastes. The exposure was conducted under constant conditions of 20 °C and 55 % RH.

Second, the different degradation behaviours were compared under constant exposure conditions (20 °C and 55 % RH) on cement pastes made with four types of cement: Portland cement (PC), sulfate-resisting cement (HS), slag Portland cement (SPC), and limestone calcined clay cement (LC<sup>3</sup>).

Third, selected cement systems were analysed by the comparison between constant and cycling exposures. The constant condition was controlled at 20 °C and 55 % RH and the cycling exposure condition was a weekly displacement of samples between a humid room of 20 °C and 78 % RH and a drying room of 40 °C and 33 % RH.

## 5.2 The effect of the w/c and the sulfate concentration

### 5.2.1 Visual inspections

Fig. 5-1 shows the appearance of paste samples with different w/c ratios exposed to two different sulfate concentrations for 91 days of exposure. Overall, the samples with lower w/c ratios and the samples exposed to lower sulfate concentration show less damage. On the one hand, the sample with w/c of 0.6 and exposed to the 50 g/L solution is the most extensively degraded, which shows the kind of typical results from laboratory accelerated experiments. On the other hand, the sample with w/c of 0.3–0.4 and exposed to the 3 g/L solution is the least degraded, which shows more realistic conditions representative of field exposure.

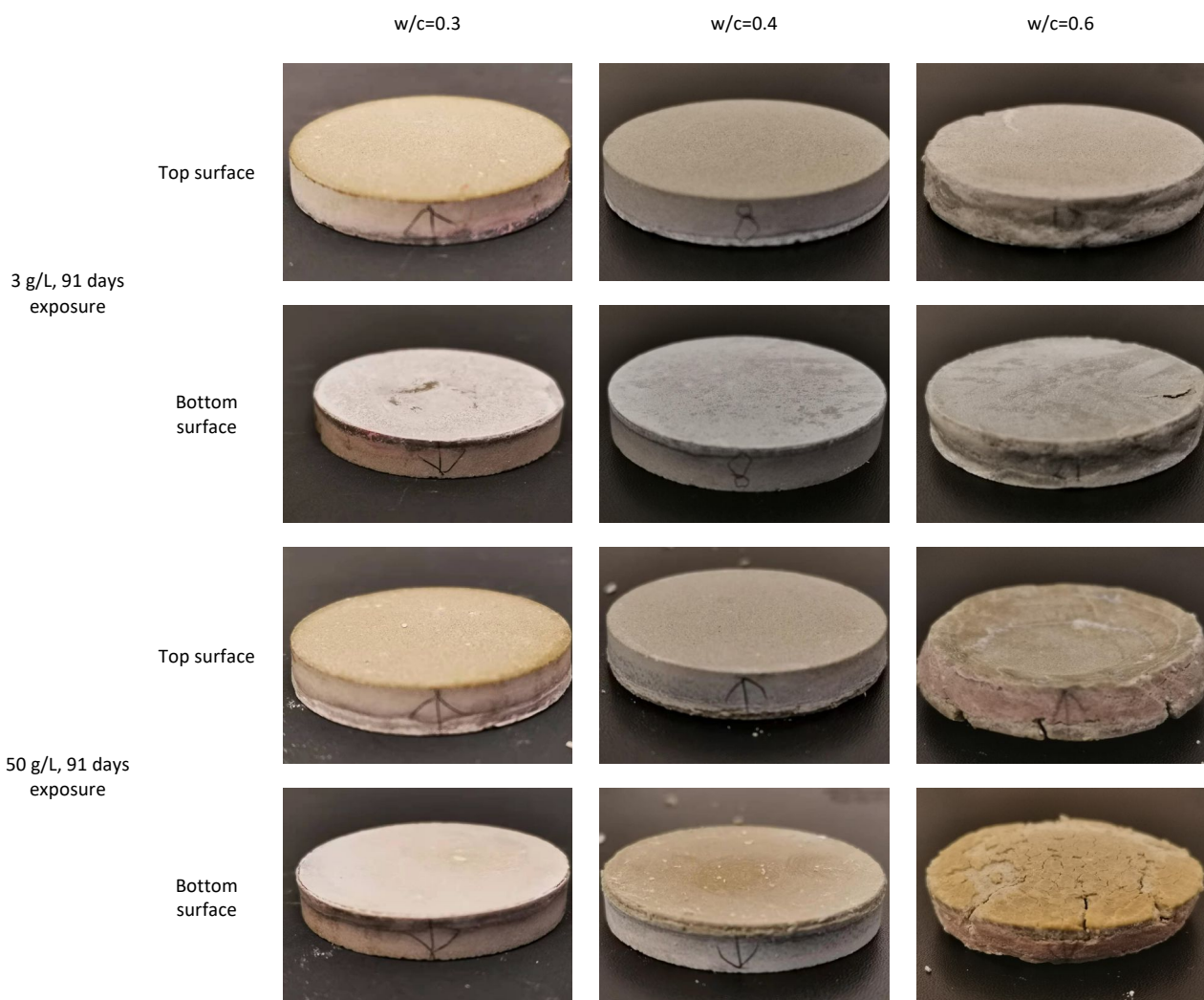


Fig. 5-1 Visual inspections of cement pastes with w/c of 0.4 & 0.6 exposed for 91 days (250 days for the w/c ratio of 0.3) to sulfate concentration of 3 & 50 g/L.

### 5.2.2 Expansion and mass gain

Fig. 5-2 shows the expansion of PC paste samples with different w/c ratios and after exposure to different sulfate concentrations. Generally, the samples with lower w/c ratios show less expansion and the samples exposed to lower sulfate concentration show less expansion.

As a first interpretation, the lower expansion for samples with a lower w/c ratio can be linked to the higher mechanical restraint and a lower capillary porosity for the movement of sulfates which is discussed specifically in *Chapter 7*. The comparison of Fig. 5-2 (a) and (b) shows that a higher sulfate concentration causes a higher expansion, which is believed to be caused by a higher crystallization pressure. Furthermore, samples with a w/c ratio of 0.3 showed much lower degradation but still started expanding at high sulfate concentration. However, the samples with a w/c ratio of 0.3 under the exposure of 3 g/L do not show no expansion until 250 days of exposure.

Another representation of the results of Fig. 5-2 is to plot the expansion at depth 0 mm (i.e., at the exposed surface) as a function of time, as shown in Fig. 5-3 (a). In addition, the mass variations of cement paste specimens were monitored over time, as shown in Fig. 5-3 (b). The same trends were observed in both graphs, a latency period (where the expansion is small) occurs before large expansion, which corresponds to a slight mass loss period before the mass gain. During that negative mass gaining period, the overall mass loss may come from a higher water loss due to drying than the mass gain due to the formation of new hydrates (ettringite & gypsum).

The mass gain is 0 when the dynamic equilibrium between mass loss and gain is reached, i.e., the newly formed phases are exactly equivalent to the water lost from drying. Eventually, the solution can penetrate more easily (cracks may appear with high expansion) and react with cement paste phases to form new hydrates, then the gain of mass surpasses the mass lost by drying.

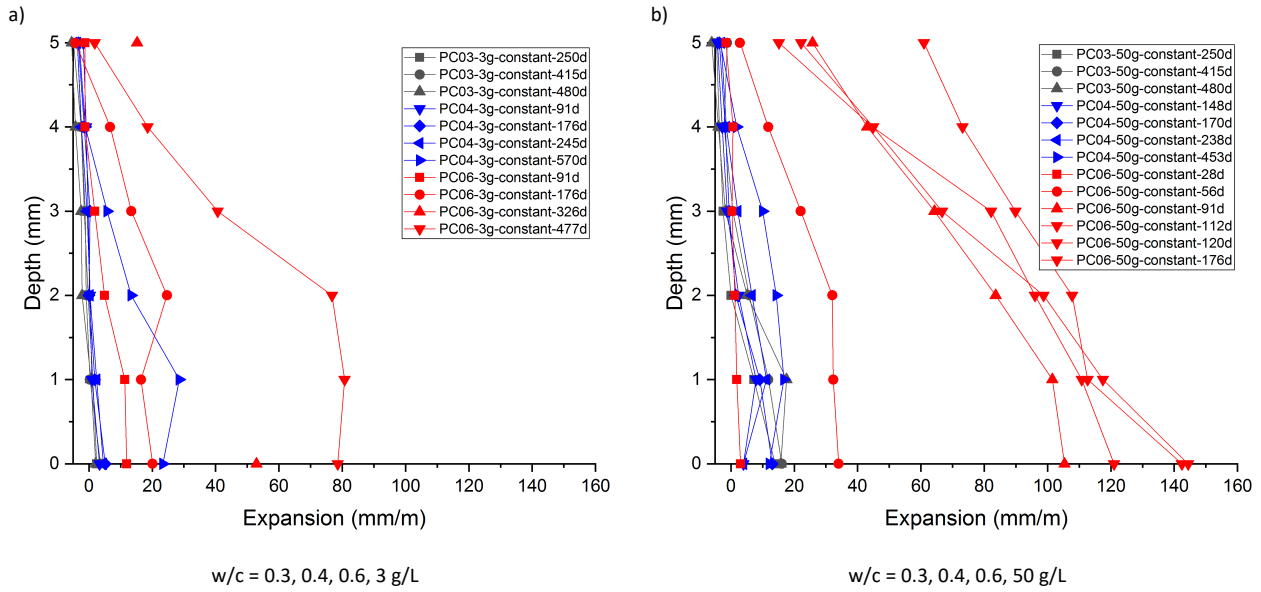


Fig. 5-2 Expansion over the depth of the PC pastes at different w/c ratios and sulfate concentrations, a) PC pastes at 3 g/L, b) PC pastes at 50 g/L.

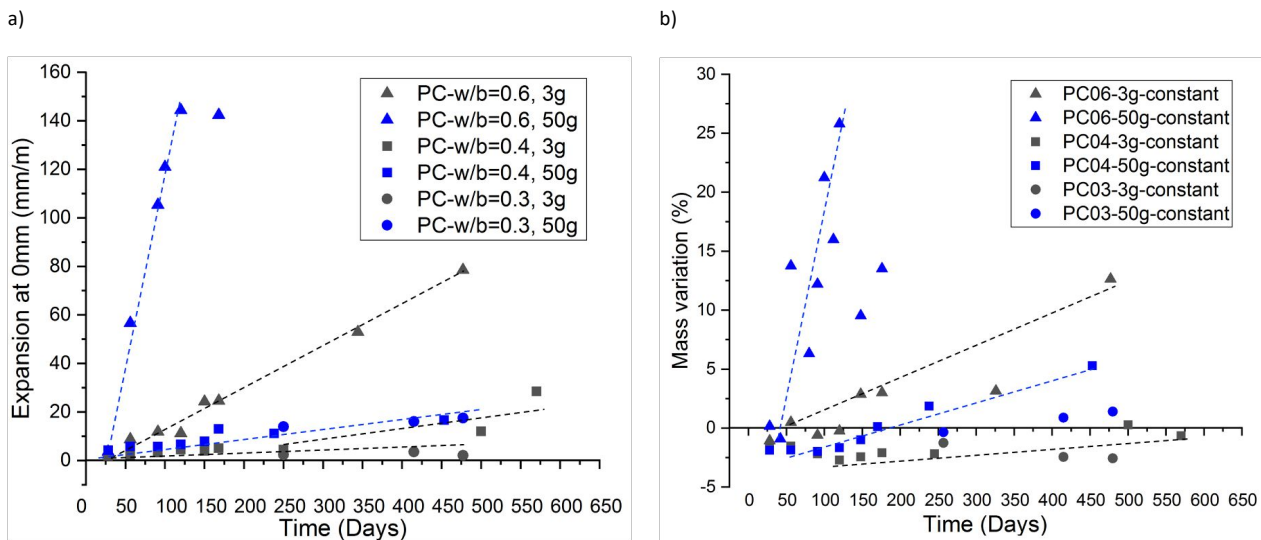


Fig. 5-3 a) Expansion rate and b) mass variations over time for cement paste samples exposed to different sulfate concentrations.

Fig. 5-4 presents the take-off time, defined as the transition time between the latency period of lower expansion and the fast expansion period, as a function of the w/c and the concentration of the exposure solution. Lower w/c samples require more time before take-off and the difference can be more than a year between w/c ratios of 0.4 and 0.6. To get a better complete trend of these relationships, the w/c of 0.5 was added and mortar samples were also added to the graph. As expected, the take-off time of samples with w/c of 0.5 is located between w/c ratios of 0.4 and 0.6.

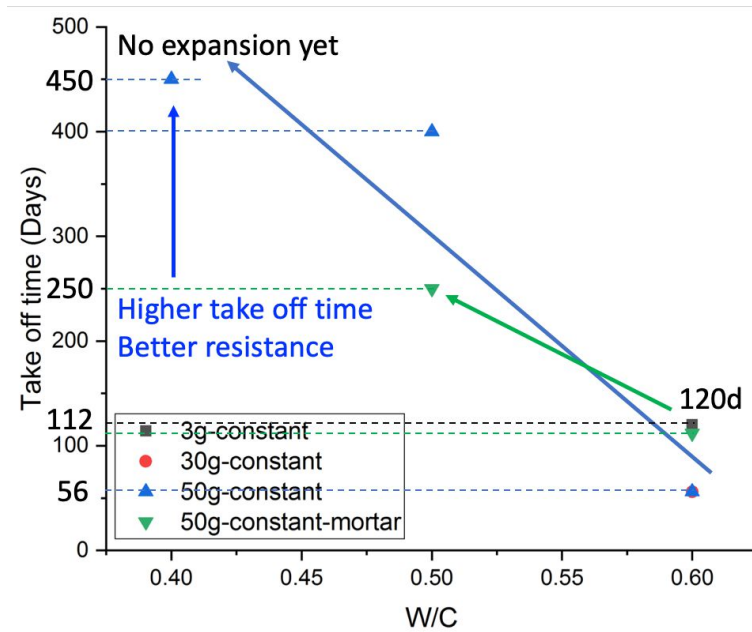


Fig. 5-4 Sulfate expansion take-off time as a function of the W/C ratios. The lines only serve as eye guide.

### 5.2.3 Sulfate ingress as a function of exposure time

#### *Chemical mappings of sulfate concentration*

In Fig. 5-5, the sulfur profile maps of concentration gradient are compared for various w/c ratios and solution concentrations. As described in *Chapter 4*, the main sulfate-containing hydrates are ettringite and gypsum, which are in the brighter zones of sulfur maps. Ettringite forms in the pores and within the C-S-H gel due to the transformation from the finely mixed AFm. Gypsum mainly forms inside the newly formed vein-like cracks parallel to the surface and in cavities. The phase verification (the segmentation of C-S-H, gypsum, ettringite, etc.) through the EDXIA strategy was discussed previously in *Chapter 4*.

The comparison of the different conditions indicates that although the sulfate ingress is only slightly more advanced at 50 g/L, the cracking is much more extensive compared to the rare occurrence of cracks at 3 g/L. As an example, in the paste with w/c=0.3, the sulfate ingress depth is similar for both exposure conditions, but the extensive cracking can be only observed at 50 g/L.

All the samples show the sulfate ingress moving inwards progressively over time, similarly for the different w/c ratios but at a different pace. With the increases of w/c, more extensive cracks and phase alterations can be observed. At w/c=0.6 sulfate reached the top zone of the sample after less than 120 days of exposure. Moreover, vertical cracks also appeared and connected the different depths for the sample PC06-50 g/L.

At 3 g/L, a slower sulfate penetration is governed by diffusion and sulfate mappings show fewer occurrence of cracks. Due to the much lower porosity in the sample at w/c=0.3, sulfate diffusion is rather slow and there is nearly no phase change or cracks, which explains that no expansion was detected for this sample.

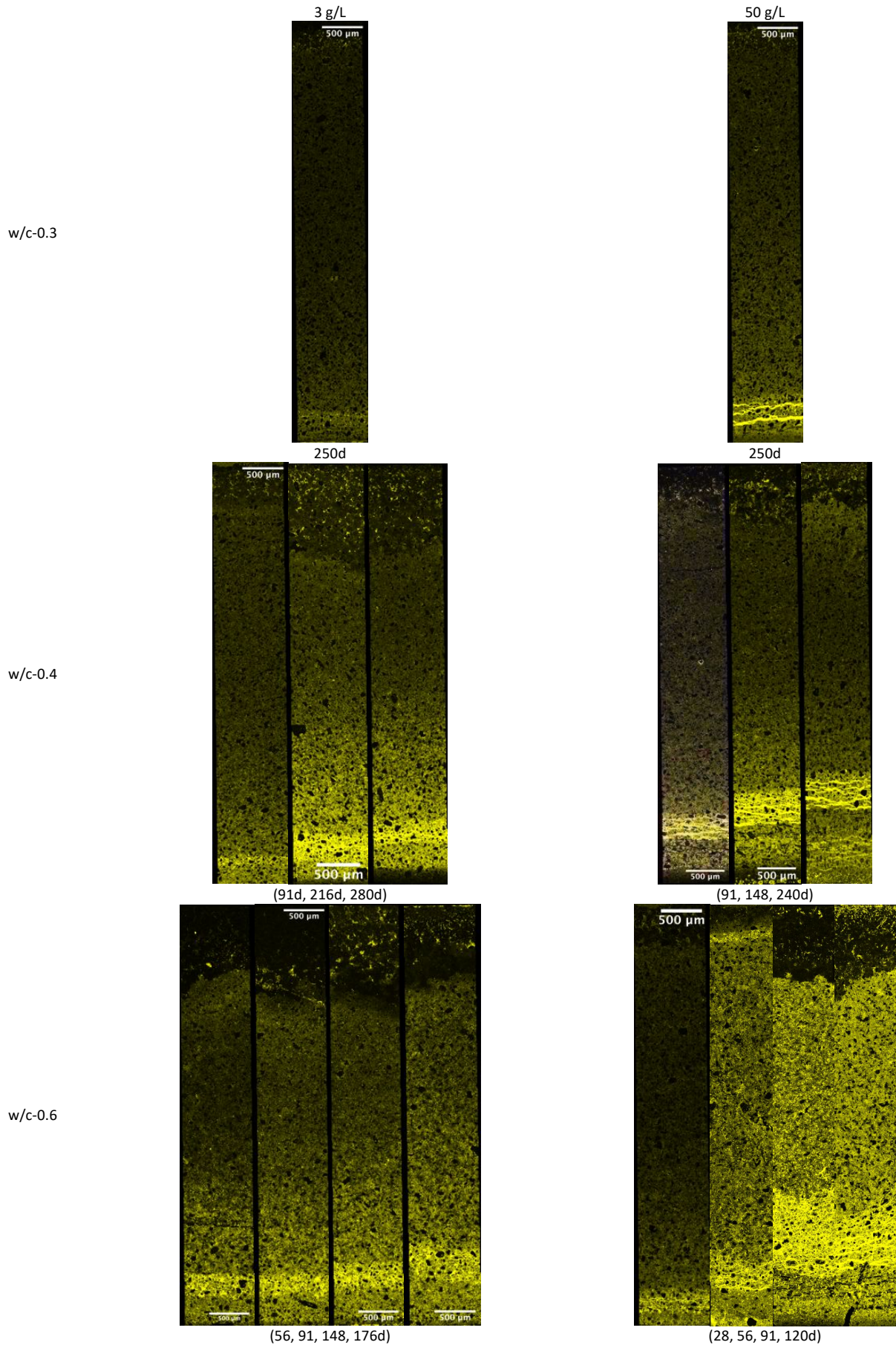


Fig. 5-5 Sulfur profile maps after exposure to different sulfate concentrations with different w/c ratios.

### 5.2.4 Sulfate ingress rate

Upon sulfate ingress, ettringite forms and intermixes with C-S-H, which can increase the relative sulfate concentration in the C-S-H gel. The segmentation of the C-S-H with EDXIA enables plotting the S/Ca profile of the C-S-H over the depth of the sample, as shown in Fig. 5-6. Then, the sulfur ingress depth can be estimated by comparing the profile with the initial S/Ca before exposure (i.e., the grey baseline).

The sulfate ingress depth for a given sample is defined as the depth where the S/Ca ratio decreases to the baseline of the reference C-S-H for the same sample without exposure to sulfate. Fig. 5-6 shows the S/Ca profile for system PC06 after 148 days of exposure to 3 g/L sulfate solution, along with the baseline of S/Ca 0.038 obtained for the PC06 paste after 28 days of hydration. This example shows an S ingress depth of 2.8 mm.

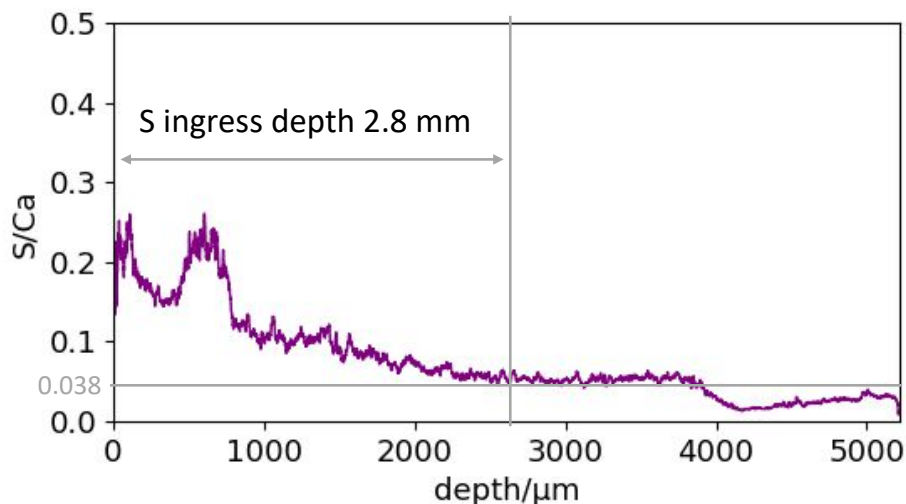


Fig. 5-6 The atomic ratio S/Ca profiles of main hydrates C-S-H based on the long sulfur maps.

Similar S/Ca profiles were analysed for all the investigated samples, and the S ingress depth as a function of exposure time is shown in Fig. 5-7. The sulfate ingress is slightly faster in the samples with higher w/c ratios, likely because of a higher capillary porosity that increases the capillary rise action. High S ingress was also observed in high concentration cases, e.g., for PC04, the slope is  $0.15 \text{ mm/d}^{1/2}$  in high concentration versus  $0.12 \text{ mm/d}^{1/2}$  in low concentration. Note that the sulfate ingress value for PC06-50g may not be as high as in Fig. 5-7, because the points do not follow a linear trend as there is a sudden increase of sulfate ingress after 56 days, which may be due to the appearance of connected cracks that accelerate the sulfate ingress. Nevertheless, Fig. 5-7 shows that the sulfate ingress is higher for a concentration of 50 g/L than that 3 g/L, as validated by the linear relationships obtained for PC04 samples. In sound cement materials, the sulfate ingress depth seems to be governed by diffusion (and capillary rise) as the increase of the ingress depth was found to be linear with the square root of time.



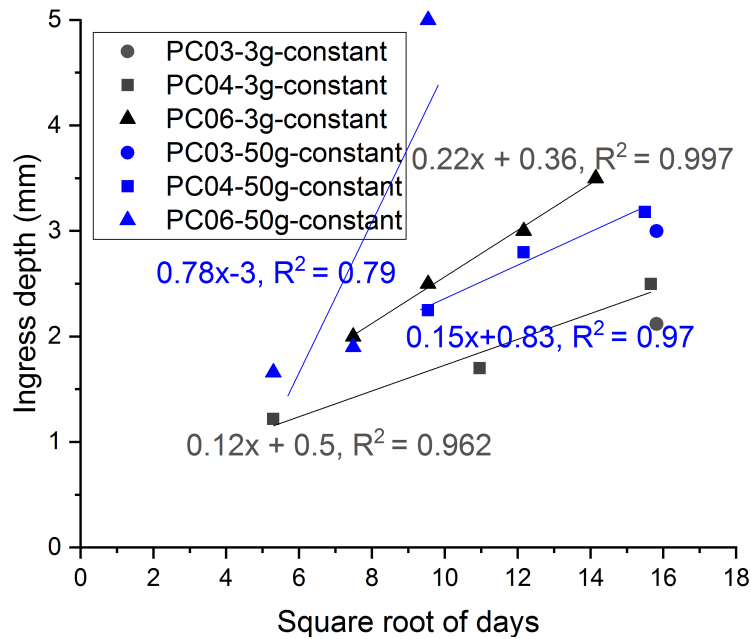


Fig. 5-7 The S ingress depth as a function of days<sup>1/2</sup> for different PC systems with various w/c ratios and solution concentrations.

### 5.2.5 Phase change as a function of depth and time

The phase concentration gradient qualitatively identified with the SEM-EDS sulfur maps is verified in this section with quantitative X-ray diffraction using the Rietveld method with an external standard. As shown in Fig. 5-8, our relevant hydrates were quantified: ettringite, gypsum, portlandite and thenardite. Ettringite forms preferentially near the exposed surface (depth = 0 mm) and decreases with increasing depths. Gypsum occurs in a narrow band above the exposed surface (in the cracks, as shown by SEM-EDS mappings). Portlandite profiles show evidence of Ca<sup>2+</sup> leaching and carbonation, on the surfaces of samples exposed to the sulfate solution and to the air, respectively. Thenardite is potentially formed in the drying front as a subflorescence and it is also mainly precipitated as efflorescence outside the sample (it is consistent with the slow drying feature of the PC pastes, as discussed in *Chapter 7*). A higher sulfate concentration of the exposure solution leads to higher thenardite contents near the surface exposed to air. Based on the results of SEM-EDS mappings, thenardite generally occurs as subflorescence only in specific conditions for a limited period of time and then occurs as non-harmful efflorescence (not shown here by the XRD test). The quantitative phase profiles support the progressive layered sulfate degradation presented in *Chapter 4*.

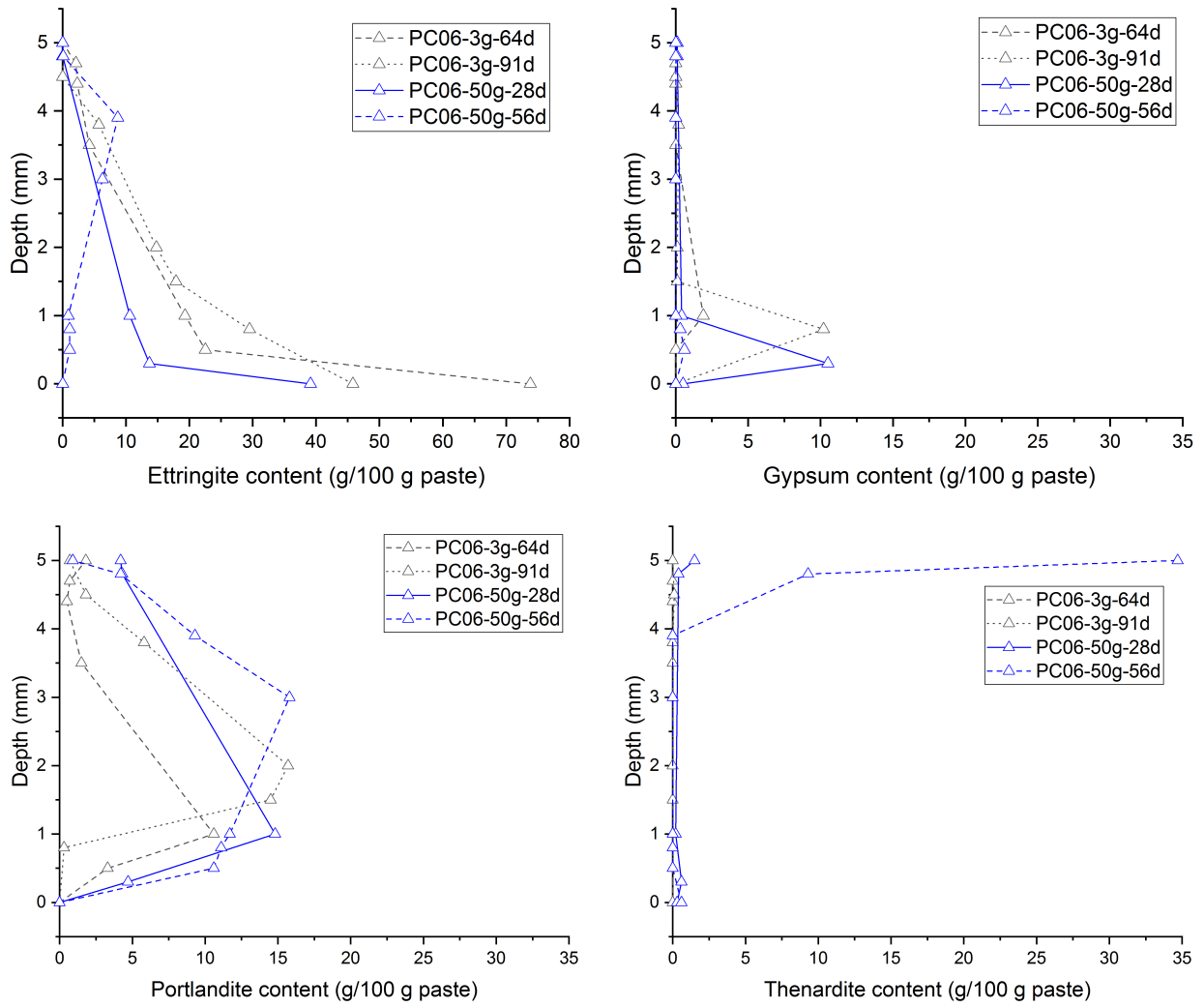


Fig. 5-8 Specific phase contents (ettringite, gypsum, portlandite and thenardite, in g/100 g paste) as a function of the depth by sulfate ingress. Lines serve as eye-guide only.

## 5.3 The effect of the cement type

### 5.3.1 Chemical properties before sulfate exposure

#### *Distribution of hydrates by image analysis*

Fig. 5-9 shows the hydrates distribution for the investigated cement pastes after 28 days of hydration under distilled water at ambient temperature. In the PC paste, abundant portlandite is mixed with outer C-(A)-S-H gel but AFm is not observed (at the resolution of Fig. 5-9). Nevertheless, small-sized AFm may be intermixed in the C-(A)-S-H gel (as shown in the next chemical composition analysis of C-(A)-S-H). In the HS paste, a few AFm grains is observed on a size scale of 5-10  $\mu\text{m}$ . Ettringite is also present in the mixture (relatively big grains with a cracked morphology) which can consume a part of the aluminium source before sulfate ingress. In the SPC paste, a more heterogenous paste matrix is observed and AFm size is less than 5  $\mu\text{m}$ . Portlandite is not that widely present due to the pozzolanic reaction by slag. In the LC<sup>3</sup>-50 paste, AFm is present with a big size of 10-20  $\mu\text{m}$ , mainly monocarbonate/hemicarbonate. Portlandite can be found in the mixture of hydrates, along with clays and some other impurities closely bonded with the main hydrates.

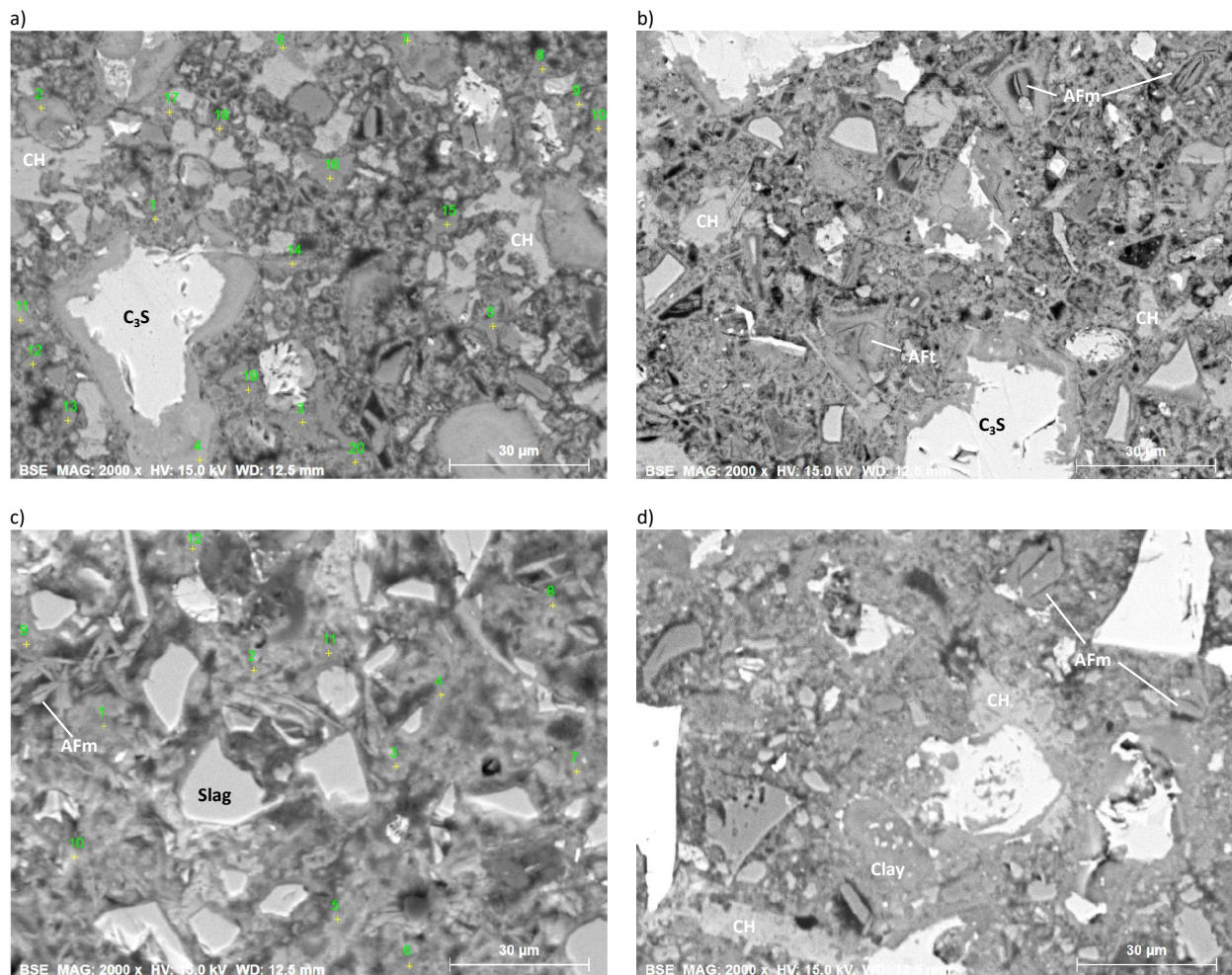


Fig. 5-9 Hydrates distribution in different cement pastes at w/c 0.6 after 28 days of hydration: a) PC, b) HS, c) SPC, d) LC<sup>3</sup>.

### Chemical composition of the C-(A)-S-H hydrates

The C-(A)-S-H compositions are obtained by SEM-EDS point analyses, as shown in the atomic ratio plots in Fig. 5-10. In each subplot, the S/Ca baseline of the reference sample is a constant value that represents the initial  $\text{SO}_3$  content in raw materials. In the HS paste, the background of S/Ca is the biggest and the ettringite mixed with C-(A)-S-H is already present before sulfate ingress. In the PC system, there is a clear trend that monosulfate and monocarbonate/hemicarbonate are present which can somehow indicate the potential of AFm transformation into ettringite which causes expansion. In SPC and  $\text{LC}^3$  cements, the points are more scattered (big size of AFm which does not contribute to expansive force) rather than centred towards either AFm or ettringite. Higher Al/Ca ratios are observed in SPC and  $\text{LC}^3$  as Al is incorporated into the C-(A)-S-H phase becoming C-A-S-H.

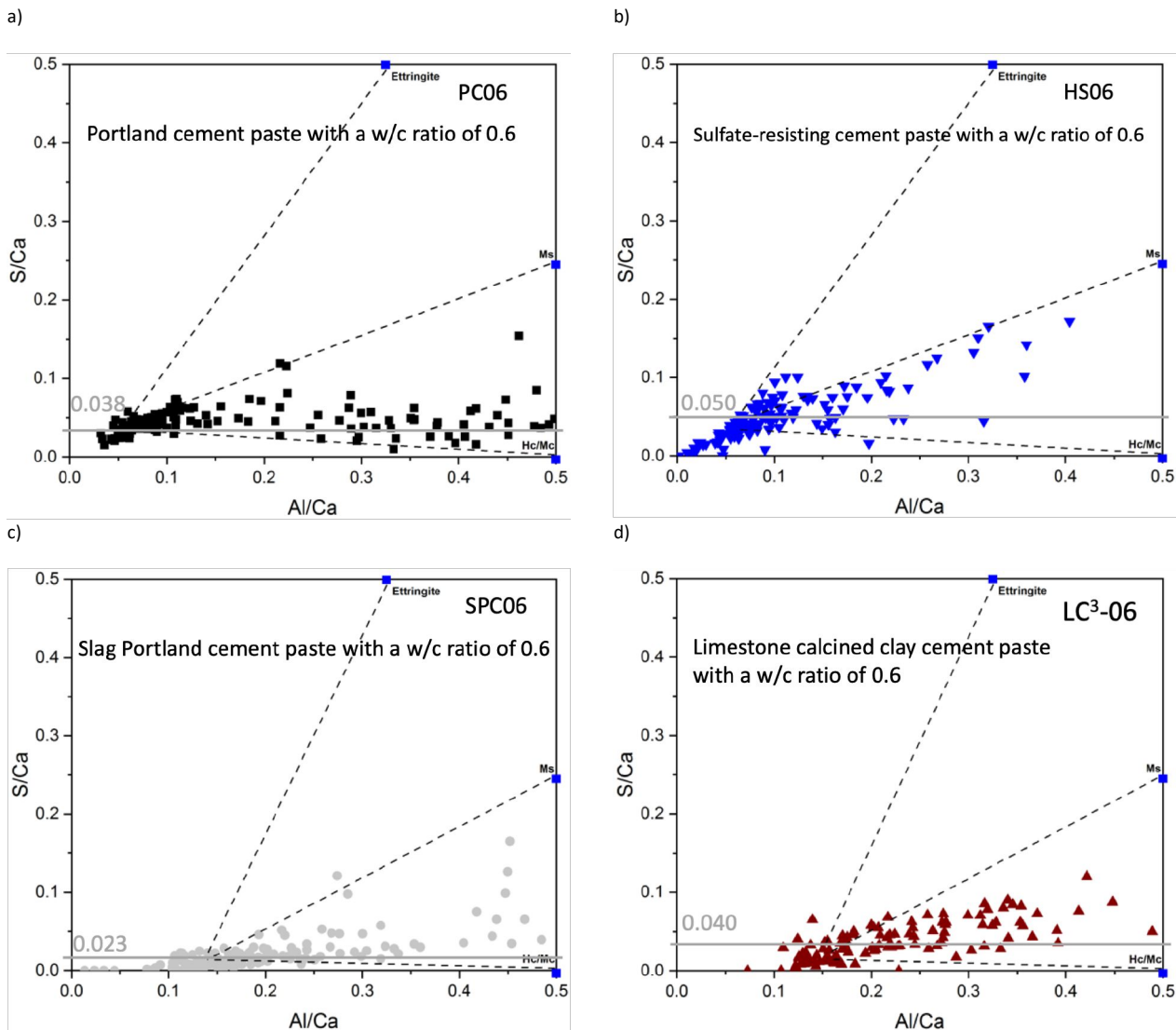


Fig. 5-10 Chemical compositions of C-(A)-S-H hydrates in cements: a) PC, b) HS, c) SPC, d)  $\text{LC}^3$ -50. Lines serve for eye-guide only.

### Phase assemblages

The initial phase assemblage after 28 days of hydration is given in Fig. 5-11 for the four investigated systems, as measured with the XRD-Rietveld method. In HS systems, the content of ettringite for both w/c ratios is higher than for the PC systems. The AFm phase was present according to EDS analysis, but no AFm phases were detected by XRD. In the SPC pastes, the AFm is not that abundant in big size nor mixed with C-(A)-S-H. LC<sup>3</sup> cement paste consists of the high amount of AFm, but nearly no AFm is intermixed with C-(A)-S-H. That means in SPC and LC<sup>3</sup> cement pastes, there are less transformable AFm present in smaller spaces to cause any detectable expansion from ettringite crystallization pressure. In LC<sup>3</sup> materials, an important feature is the much-reduced portlandite content, AFm is mainly in Hc and Mc due to the presence of excess limestone.

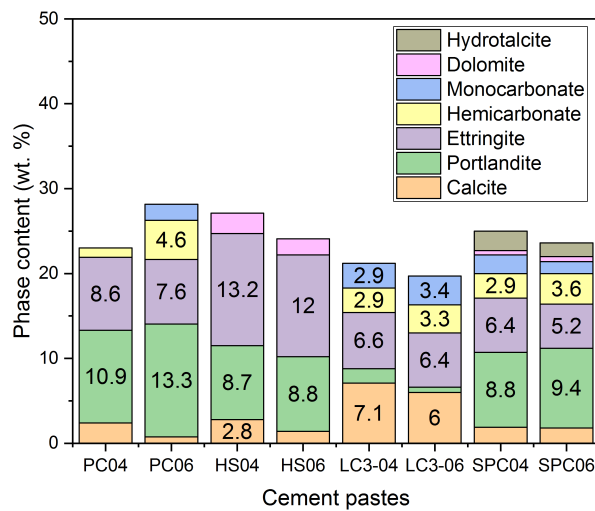


Fig. 5-11 Phase assemblages before sulfate ingress in for the different cement pastes at w/c ratios of 0.4 and 0.6.

### 5.3.2 Physical changes after sulfate exposure

#### Appearance

As shown in Fig. 5-12, the damage varies depending on the cement type. The cracking of the bottom surfaces is mainly observed in PC based cement materials (PC and HS). The expansion of these surfaces can even lead to the peeling of the whole samples and reflect on the other side with a vertical crack showing up. However, the top surfaces of PC and HS samples are not spalled, even if the chemical sulfate attack moves quite far through the whole samples, with an abundant efflorescence on the top surface (efflorescence was removed before taking photos). For the SPC and LC<sup>3</sup> cements pastes, no cracks are observed on the bottom surfaces but the top surfaces are more prone to spalling, particularly in the high sulfate concentration cases. The damage extent was related to the high sulfate concentration, which leads more rapidly to supersaturation causes salt crystallization hence high pressures. Spalling initiates when the pressure is higher than the tensile strength of the material, hence the extent of damage is lower with a lower w/c ratio of 0.4.

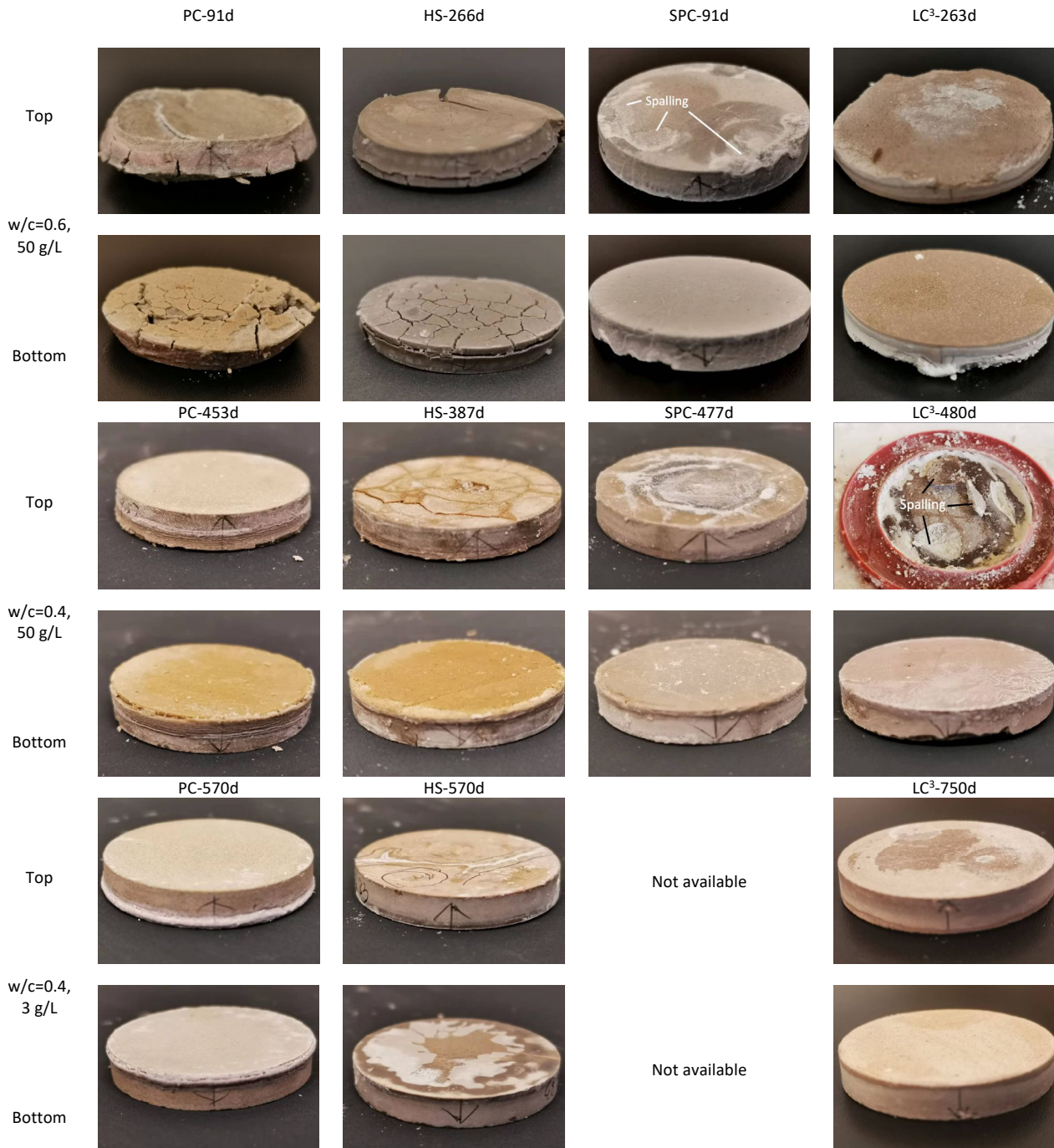


Fig. 5-12 Visual inspections of cement pastes with w/c of 0.4 & 0.6 and sulfate concentration of 3 and 50 g/L.

Although spalling occurs at a high sulfate concentration, the LC<sup>3</sup> materials do not show any cracking or spalling at a low sulfate concentration of 3 g/L, even after 2 years of exposure. The only concern is the appearance that can be affected by the efflorescence, which may occur in realistic situations. With the same w/c ratio of 0.4, the LC<sup>3</sup> cement paste has a higher capillary porosity than the other cement types (see *Chapter 7*), which leads to full-depth penetration of sulfate but no damage at 3 g/L. In comparison, PC is affected in those conditions with an expansion of the bottom of the sample, and HS shows efflorescence. On the other hand, the relatively high resistance against chemical sulfate attack perhaps plays a role in facilitating the ingress of

sulfates in HS and LC<sup>3</sup> systems. As sulfates are not consumed by the chemical attack, they can penetrate further towards the upper side of the sample. Thus, the interplay between chemical and physical seems to be an important aspect, which will be discussed further later in the thesis. The chemistry details of full profiles can be found in the next section, which better explain the mechanism of layered degradation.

### Expansion and mass gain

Fig. 5-13 shows the mass changes and expansion of mortar samples prepared with the different types of cement investigated in this study. The mass variation plot in Fig. 5-13 a) shows that HS and LC<sup>3</sup> systems have very little mass gain (or even mass loss due to some drying). The extensive mass loss is of the LC<sup>3</sup> sample after 600 days is due to spalling of surfaces in the drying front. For PC systems, a mass gain is detected due to the new hydrate precipitation in the pores or cracks, i.e., ettringite and gypsum. A similar trend is observed in the expansion plot: PC-based materials show significant expansion, whereas HS and LC<sup>3</sup> mortars show a very good resistance against expansion even after long-term exposure (until 650 days).

Therefore, if we link the mass gain and expansion, we can see that the mass gain is probably due to the new hydrates formation which causes high expansion. Almost zero mass gain implies that there is a small amount of new hydrates forming inside the materials which perhaps exactly compensates for the mass of water loss in the evaporation front. A significant mass loss is related to the surface scaling due to the high salt crystallization pressure near the surface exposed to air. For PC systems, there seem to be an upper limit on the mass gain, which also corresponds to the maximum expansion plateau observed after 280 days.

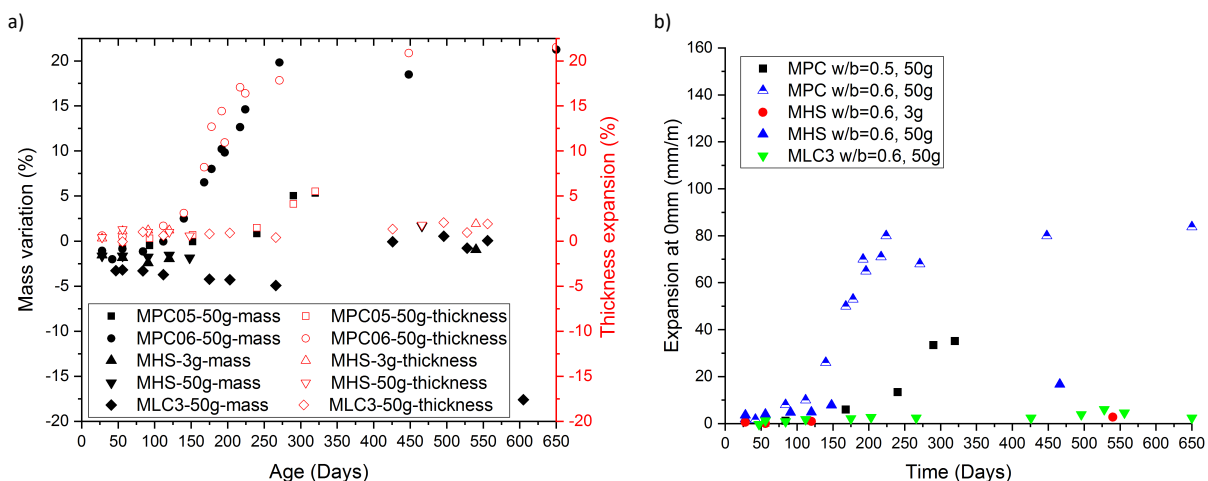


Fig. 5-13 Mass changes and expansion at 0 mm of mortar samples over time for PC, HS and LC<sup>3</sup> systems.

Fig. 5-14 shows the expansion of cement pastes, with trend similar to those observed in mortars. Expansion takes place in PC and HS sooner or later, depending on the applied parameters. SPC and LC<sup>3</sup> cement pastes show expansion below 20 mm/m, pointing out that the expansion is not the feature of the reaction of the blended cements upon sulfate exposure, and that a mere expansion evaluation may give a confusing impression on the sulfate resistance. Thus, expansion is a necessary but not sufficient indicator for a poor sulfate-

resistant cement, because expansion only reflects the behaviour of materials under high humidity or in a fully wet condition (i.e., the resistance against chemical sulfate attack).

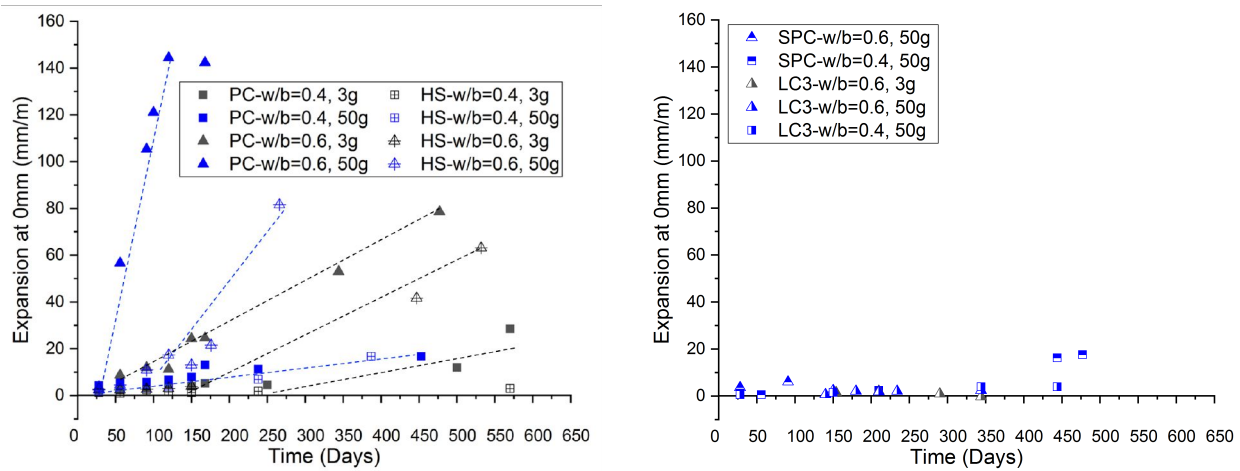


Fig. 5-14 Expansion rate of different cement pastes after sulfate exposure.

#### *The relationship between AFm content and expansion*

The  $C_3A$  content of clinker is usually regarded as a critical parameter for sulfate attack, because  $C_3A$  hydrates into AFm phases which can later transform into deleterious ettringite upon exposure to external sulfates. Fig. 5-15 shows the detected expansion in the investigated systems as a function of the initial AFm content.

Interestingly, low AFm content cannot completely stop sulfate attack in HS cement pastes, although the AFm content is quite low at about 1.5 wt. %. On the other hand, the  $LC^3$  paste has around 6.5 wt. % but does not expand at all. SPC has a good sulfate resistance with 6.6 wt. % of AFm. Thus, only considering the amount of AFm (or  $C_3A$  content of clinker) is not a good strategy to control sulfate expansion.

The expansion degree being not completely dependent on the AFm content in the cement paste, the location and size of the AFm should be investigated more precisely, as the distribution of aluminium hydrates and AFm within the C-(A)-S-H transformable into ettringite may be better indicators.



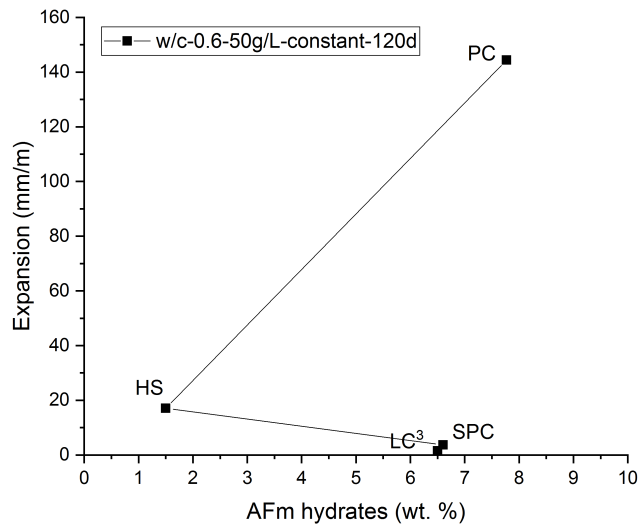


Fig. 5-15 Expansion versus AFm hydrate content in cement pastes after 28 days hydration.

### 5.3.3 Chemical changes after sulfate exposure

#### *Changes in chemical compositions of C-(A)-S-H hydrates*

In Fig. 5-16, the phase composition of C-(A)-S-H is measured after sulfate ingress, at the depth of degradation front at 0.3-1.0 mm from the exposed surface (the depth was selected for each sample depending on the degradation front). In PC and HS systems, the AFm intermixed within C-(A)-S-H transformed to ettringite at the depth of 0.5 mm, as shown by the cluster of points extending towards AFm in the reference that shifts towards ettringite after expansion. The main C-(A)-S-H cluster is also shifted towards higher S content, located above the reference baseline of S/Ca. Even gypsum points can be observed at the depth of 1 mm in PC cement where the cluster extend towards a very high S content. These points were taken in the vicinity of the gypsum band, and thus, they may include mixtures between C-(A)-S-H and small-sized gypsum.

The phenomena in SPC and LC<sup>3</sup> cements are different. The sulfate content of C-(A)-S-H is clearly also increased, even in LC<sup>3</sup> cement where the S/Ca can reach 0.3. However, the main cluster still extends towards the monosulfate composition instead of that of ettringite. This shows that the ettringite formation in a confined space (the small porosity within C-(A)-S-H gel) is not occurring. This is also consistent with the initial C-(A)-S-H compositions of SPC and LC<sup>3</sup> cements, C-(A)-S-H is less intermixed with AFm which consequently gives much less potential to have phase transformation inside the C-(A)-S-H structure. It can to some extent explain the lower expansion detected in these two blended cements, the confined ettringite precipitation (only this type of ettringite can cause expansion) is not sufficient although the ettringite is present in big size which can be detected by SEM technique. It is discussed more specifically in the next section.

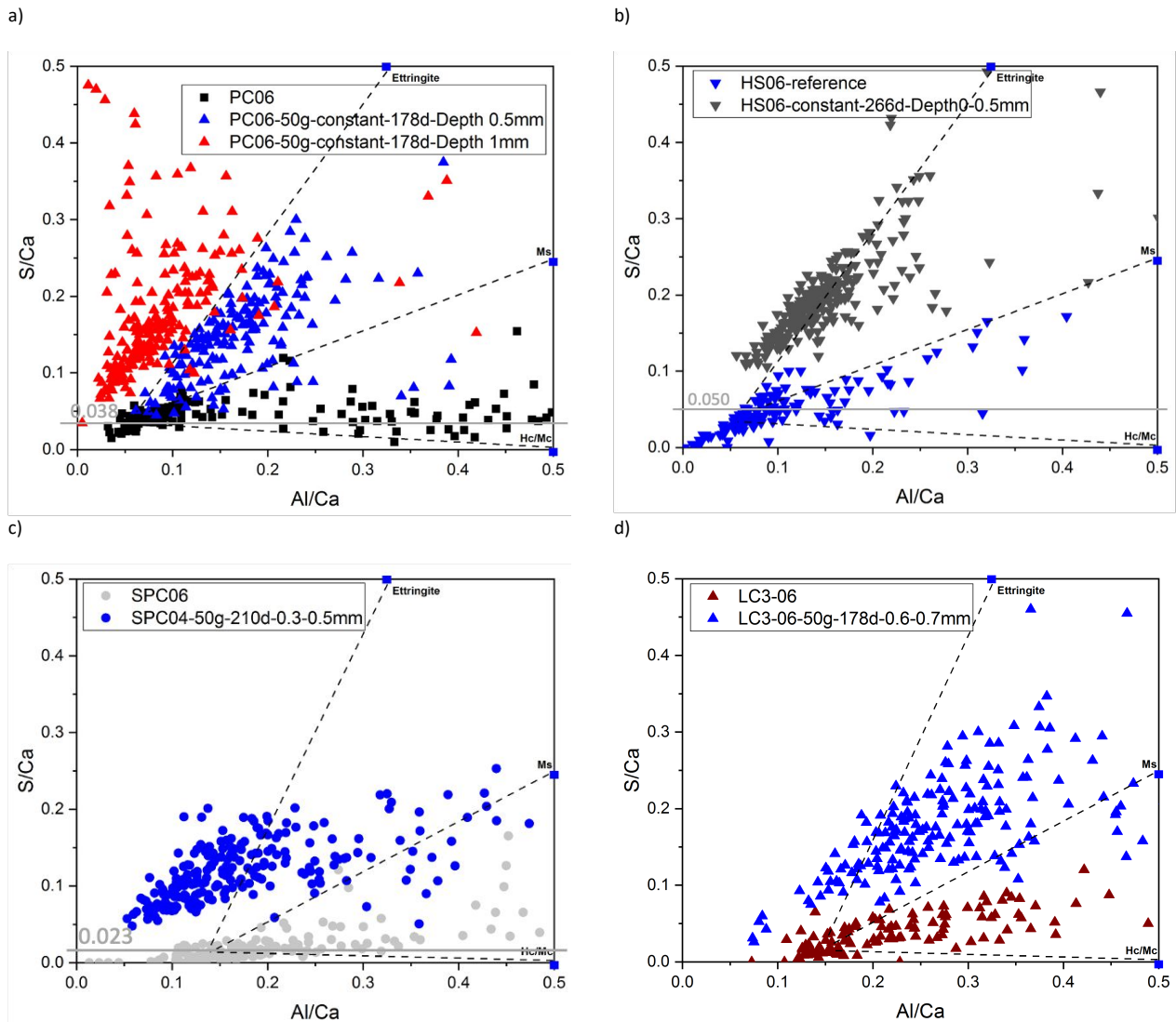


Fig. 5-16 Chemical compositions of C-(A)-S-H hydrates in cement pastes: a) PC, b) HS, c) SPC, d) LC<sup>3</sup>. Lines serve for eye-guide only.

### Hydrates distribution

In Fig. 5-17, the phase alterations are compared between various cement pastes after sulfate ingress. The images were taken at the same depth and exposure ages as for Fig. 5-16. The morphology of hydrates and porosity suggest that cement pastes are getting denser due to the continuous hydration and extra ettringite from external sulfate reactions with hydrates, both of which densify the microstructures. However, an important difference between Portland cement and blended cement is observed: secondary ettringite with microcracks are seen in the PC and HS cement pastes; while more AFm are formed in SPC and LC<sup>3</sup> cement pastes. This is a very important finding because the AFm formation or very little ettringite transformation is not causing any expansive force in terms of sulfate degradation. Still, the large size of ettringite outside of C-(A)-S-H can be found but it does not cause expansion.

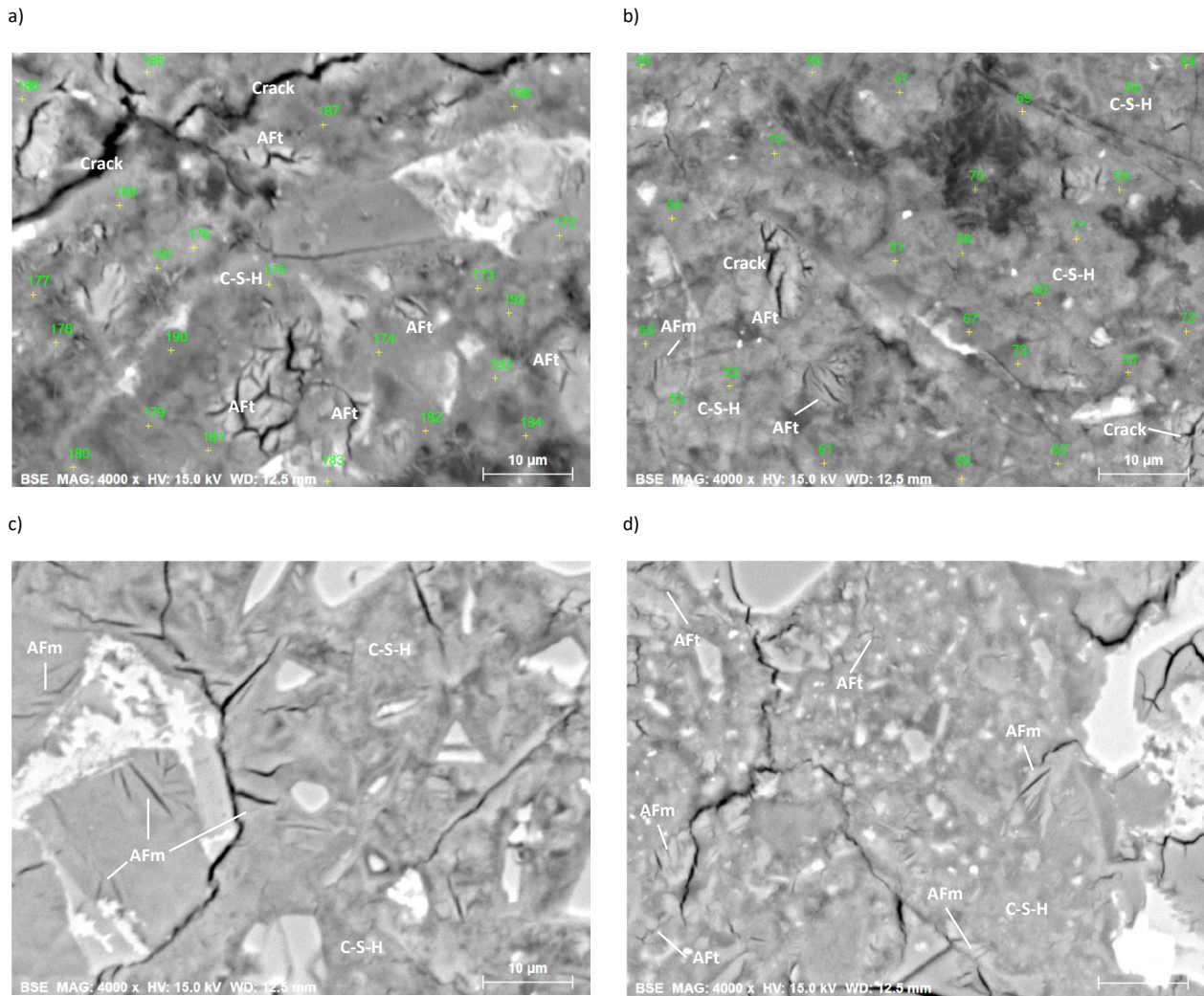


Fig. 5-17 Distribution of hydration products in different cement pastes after sulfate exposure: a) PC, b) HS, c) SPC, d) LC<sup>3</sup>.

### 5.3.4 Sulfate ingress as a function of exposure time

#### *Degradation fronts*

Degradation fronts of PC cement pastes were already described in *Chapter 4*, and in the previous section where the w/c ratios and sulfate concentrations were discussed based on PC pastes. Therefore, the degradation of PC pastes is not discussed here.

The same methodology applied for PC pastes is reproduced below for HS pastes. Fig. 5-18 shows the sulfate profiles of HS06 Portland cement paste at different ages of exposure. Ettringite and gypsum are still the main sulfate-rich phases formed after sulfate exposure. The sulfate penetration trend is similar as in PC pastes, the sulfate front depth increases over time. Parallel cracks filled with gypsum started appearing at 56 days and propagated further at 266 days.

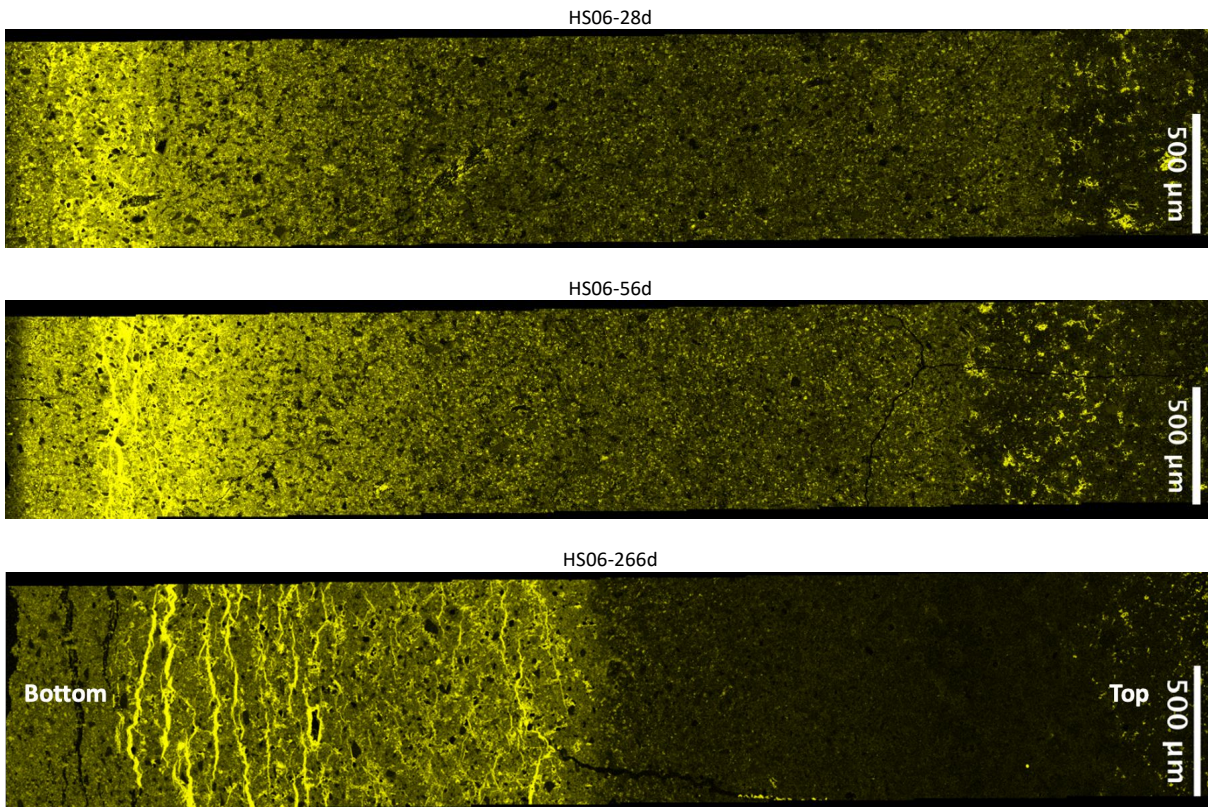


Fig. 5-18 Sulfate profiles of HS cement pastes after sulfate degradation at 50 g/L solution at w/c ratio of 0.6.

For SPC and LC<sup>3</sup> pastes, differentiating the sulfate ingress fronts in the sulfate profiles is more challenging. Therefore, a different methodology is used with *edxia*: phase profiles are shown instead to compare the degradation fronts. The phase profiles can also provide more information on the sodium sulfate crystallization in the drying front.

Fig. 5-19 shows the degradation by phase distribution in the SPC systems at w/c ratios of 0.4 and 0.6 exposed to a 50 g/L solution. There are no cracks in the bottom zones thus no gypsum is observed, and the ettringite zones do not advance much in SPC04 even after 210 days. These results indicate that the damage from the chemical attack is much suppressed. Nevertheless, ettringite forms in the interlayer in the evaporation front showing that the Ca source from the decalcified C-(A)-S-H is sufficient for the ettringite precipitation with a reduced relative humidity. The Ca profile shows a decrease in the interfacial zone and then stabilizes above it, which agrees well with the ettringite front in the evaporation zone.

Although it is quite early at 28 days (the sample was gone after 91 days) at the case of w/c 0.6, the thenardite-like phase forms on the other side below the surface which causes a small spalling that is observed in the degradation profiles (a fractured surface indicates the initiation of spalling). There is no spalling occurring at all for SPC04-50g-210d when the thenardite is also found in the drying front which is perhaps due to the

higher mechanical strength than the possible salt crystallization pressure. Moreover, the concentration of thenardite is lower.

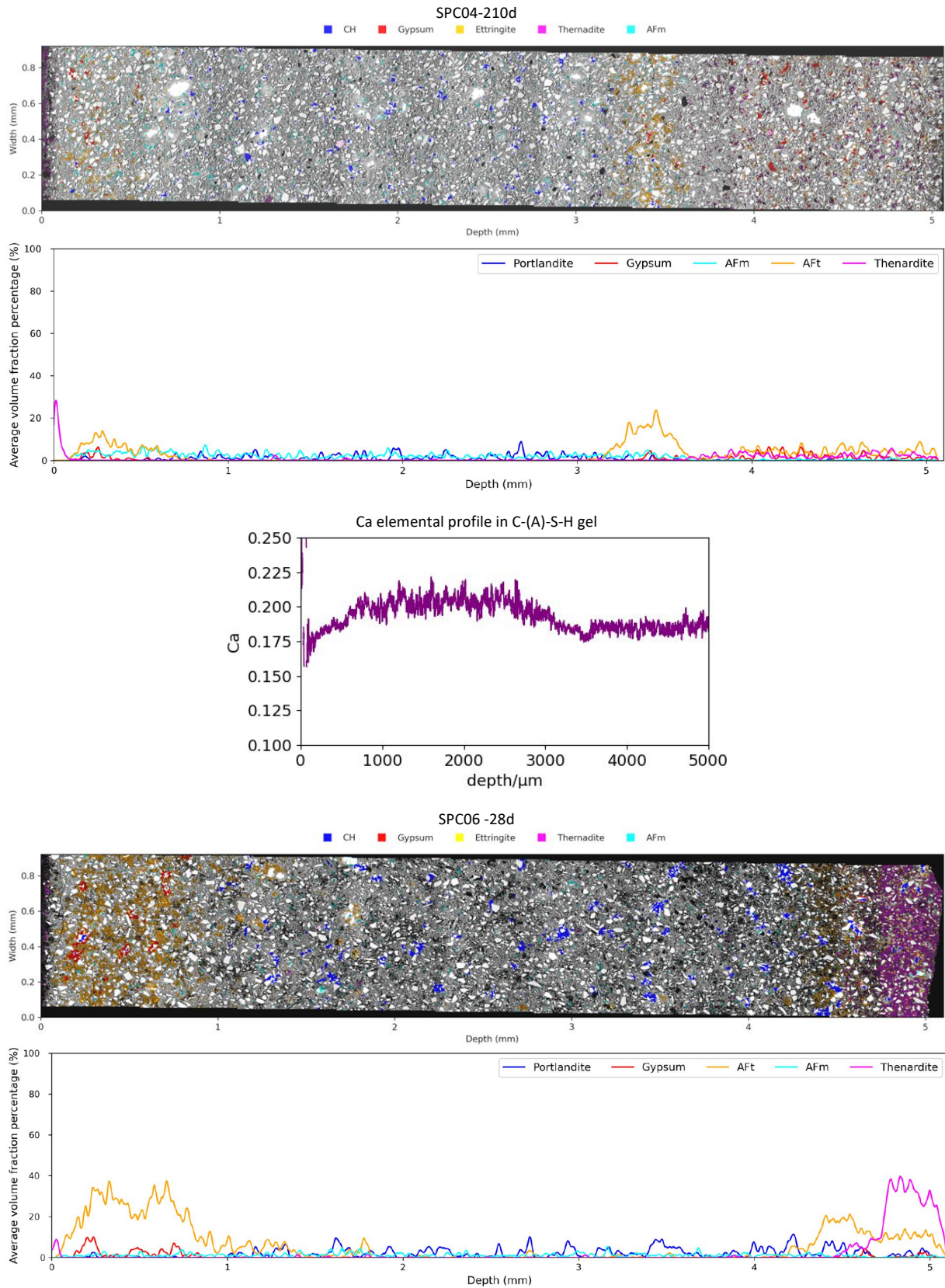


Fig. 5-19 Sulfate and Ca profiles of SPC cement pastes after sulfate exposure in a 50 g/L solution at w/c ratios of 0.4 and 0.6.

In LC<sup>3</sup> pastes shown in Fig. 5-20, the portlandite content is lower due to the low clinker factor and Ca consumption by pozzolanic reactions. However, the lack of gypsum formation in the bottom layers is not only attributed to the shortage of portlandite, but also to the low crystallization pressure that leads to the absence of cracks to be filled with gypsum. This interpretation is supported by the delayed gypsum formation of gypsum at 263 days. In addition, the ettringite formation in the top zone may indicate where the wet/dry interface is inside the sample .

A higher extent of expansion is observed in the systems which contain the gypsum formation in the phase profiles. Usually, the band where gypsum with ettringite co-exist move inwards progressively due to the leaching. The leached zone previously filled with ettringite and/or gypsum is then left with porosity mainly. Specifically, the ettringite front can go to a maximum depth about 1.5 mm then the ettringite stops moving inwards again.

With respect to the top surface, thenardite forms slightly in a narrow region in SPC pastes which is already enough to cause spalling to SPC06-50g sample at 28 days of exposure as shown in Fig. 5-19. The abundant thenardite found in LC<sup>3</sup> samples causes even more extensive spalling damage at 237 and 263 days. At 263 days in Fig. 5-20, thenardite spreads all the depth above the bottom ettringite layer and shows a concentration gradient increasing from the lower depth to the upper outer surface. Cracks appear in the region where the highest concentration of thenardite is found. Along all the depth of the thenardite profile, ettringite is also present which may be transformed from gypsum. The result indicates that spalling damage appears along with the formation of detectable thenardite which can create the crystallization pressure above the strength of materials. For example, the LC<sup>3</sup> with w/c 0.6 have a relatively lower flexural strength which cannot resist the crystallization pressure. Salt crystallization is discussed in more details in the next section.

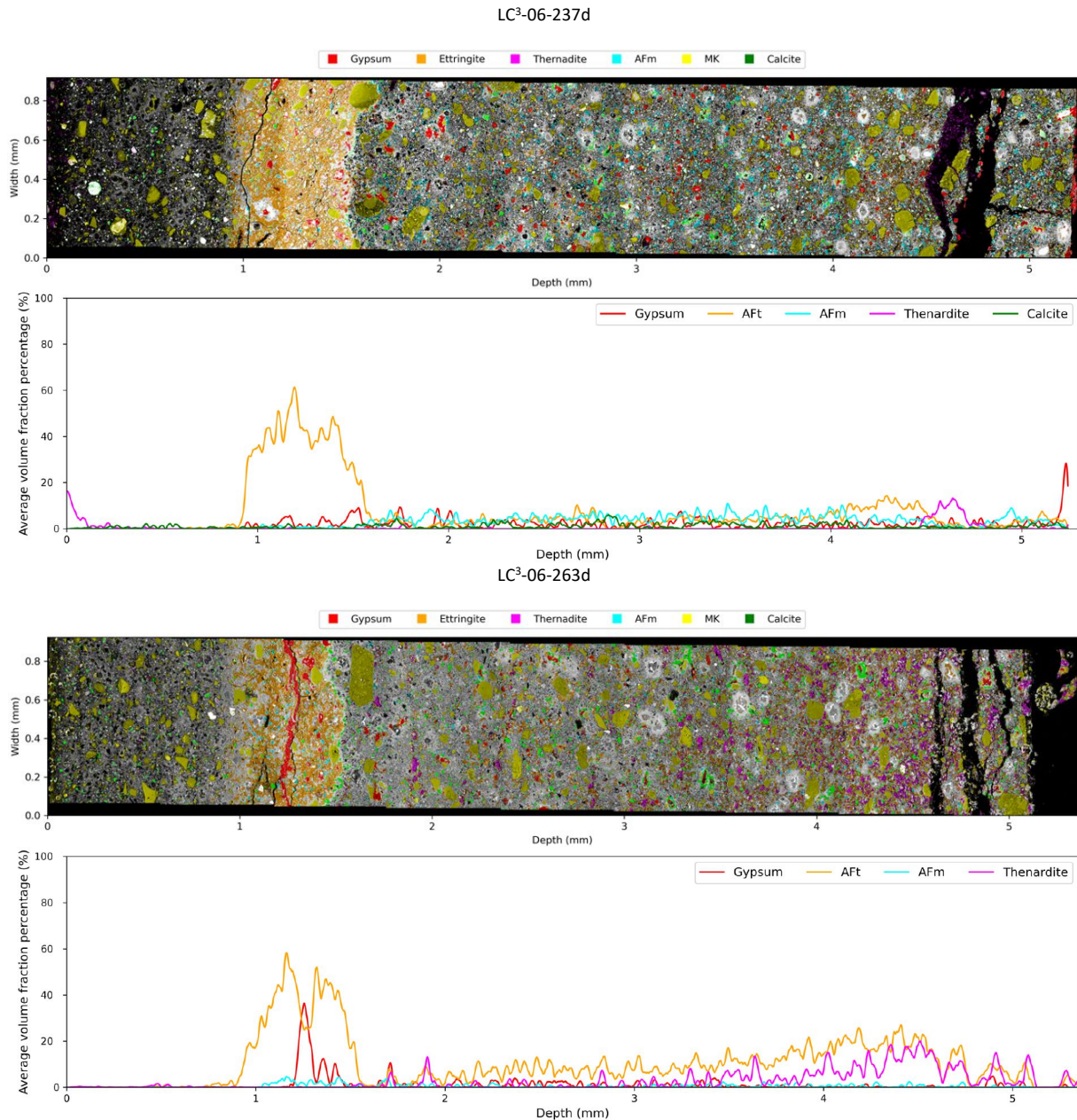


Fig. 5-20 Phase profiles of LC<sup>3</sup> cement pastes after sulfate degradation at 50 g/L solution at w/c of 0.6.

### Sulfate ingress rate

The sulfate ingress rate is obtained based on the approach presented in section 5.2.1. The ingress rate is illustrated with PC and LC<sup>3</sup> cements in Fig. 5-21. LC<sup>3</sup> cement pastes show a higher sulfate ingress rate than PC pastes. With the same exposure time for PC and LC<sup>3</sup> cement pastes, LC<sup>3</sup> pastes allow a higher sulfate ingress than PC.

SPC cement systems are expected to behave similarly as LC<sup>3</sup>, because the high chemical resistance is sufficient to satisfy the favourable conditions of ionic diffusion through the materials. It is confirmed by the

chemical phase profiles presented in the following sections: thenardite can form in LC<sup>3</sup> systems, which potentially results in visible spalling damage. Therefore, sulfate ingress rate is dependent on the extent of chemical reaction with sulfates (which depends on the cement type and porosity).

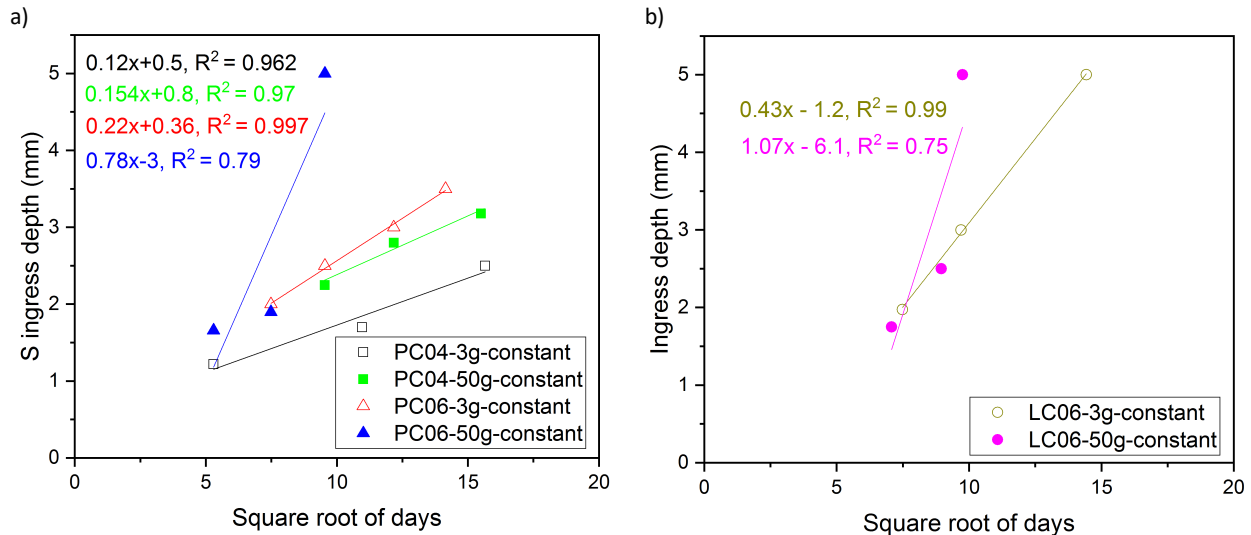


Fig. 5-21 Sulfate ingress rate of PC and LC<sup>3</sup> cement pastes.

### 5.3.5 Salt crystallization

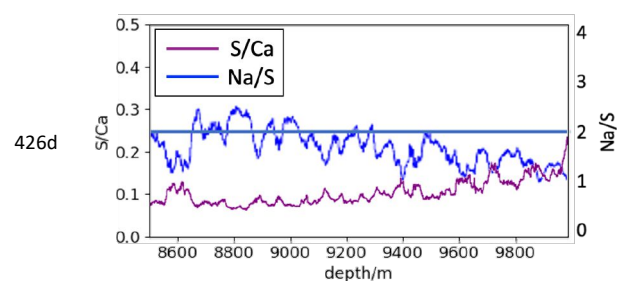
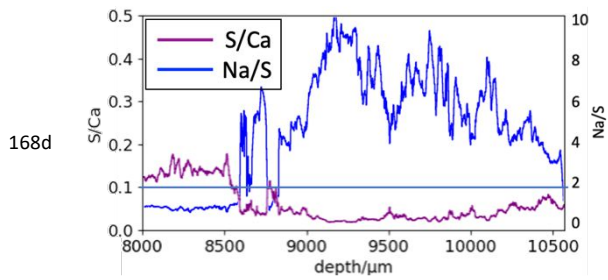
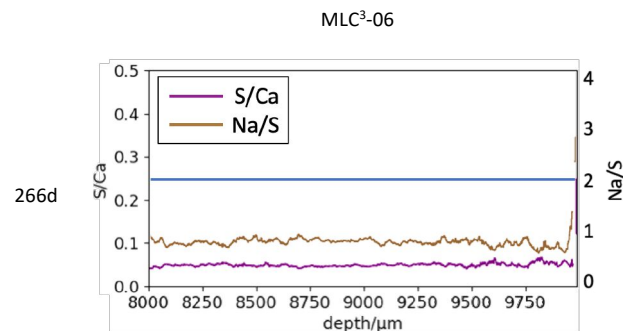
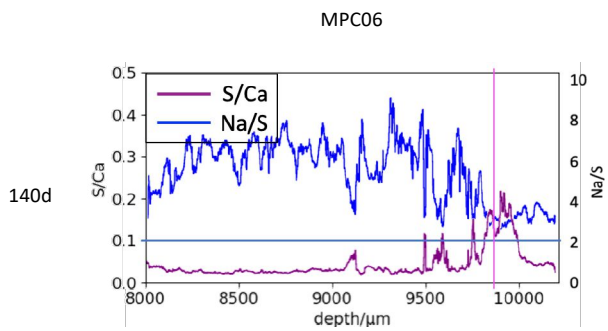
This section investigates the origin of salt crystallization. The discussion is based on PC and LC<sup>3</sup> mortars, with figures to link with the visual observations with the profiles of Na/S and S/Ca, see Fig. 5-22. Profiles of atomic ratios for the top 2 mm were obtained from hyper mappings by SEM-EDS processed by EDXIA. The profiles carry the information representative for the bulk paste of mortars (aggregates and pores were excluded). A Na/S ratio of 2 can indicate the formation of thenardite (Na<sub>2</sub>SO<sub>4</sub>) or mirabilite (Na<sub>2</sub>SO<sub>4</sub>·10H<sub>2</sub>O). S/Ca can suggest the sulfate concentration level which results from the external sulfate solution.

In Portland cement mortar samples, subflorescence appears at 140 days in the region 0 – 0.5 mm from the top surface which is accompanied with an increase of S/Ca. At this time, no damage appears because the thenardite formation is relatively new and thenardite precipitated mostly outside the materials (i.e., as efflorescence) on the mortar sample at 168 days. Therefore, Na/S becomes much higher than 2 because there is not much sulfate bonded in solids, but with the concentration of Na in Portland cement is high. It seems sodium sulfate solution can penetrate through the sample without causing damage in the drying front. The increased S/Ca is believed to be due to the progressive layer degradation from ettringite/gypsum in the region below the drying front. Efflorescence presence can explain this non-harmful flow of sulfate through the samples.

In LC<sup>3</sup> cement mortars, the phenomenon is totally different. The S/Ca ratio is low as there is no sulfate ingress to the top subsurface zone yet at 266 days. Na/S profile is below the line of 2 because the alkali content in



LC<sup>3</sup> raw materials is about half that of Portland cement. When the efflorescence starts to appear at 426 days, the sulfate concentration is also increased to  $S/Ca \approx 0.1$ . The local chemistry is satisfied with thenardite formation as the  $Na/S$  reaches to  $\sim 2$ . As the crystallization pressure reach a certain level beyond the strength of the material, cracks appear as seen at 496 days. The spalling damage continues to propagate deeper and the materials above are disintegrated into pieces. A possible interpretation is that the drying rate is faster than the capillary rise action in blended systems, as seen from adsorption and drying test results (see *Chapter 7*). As a consequence salts precipitate inside the materials leading to crystallization pressures.



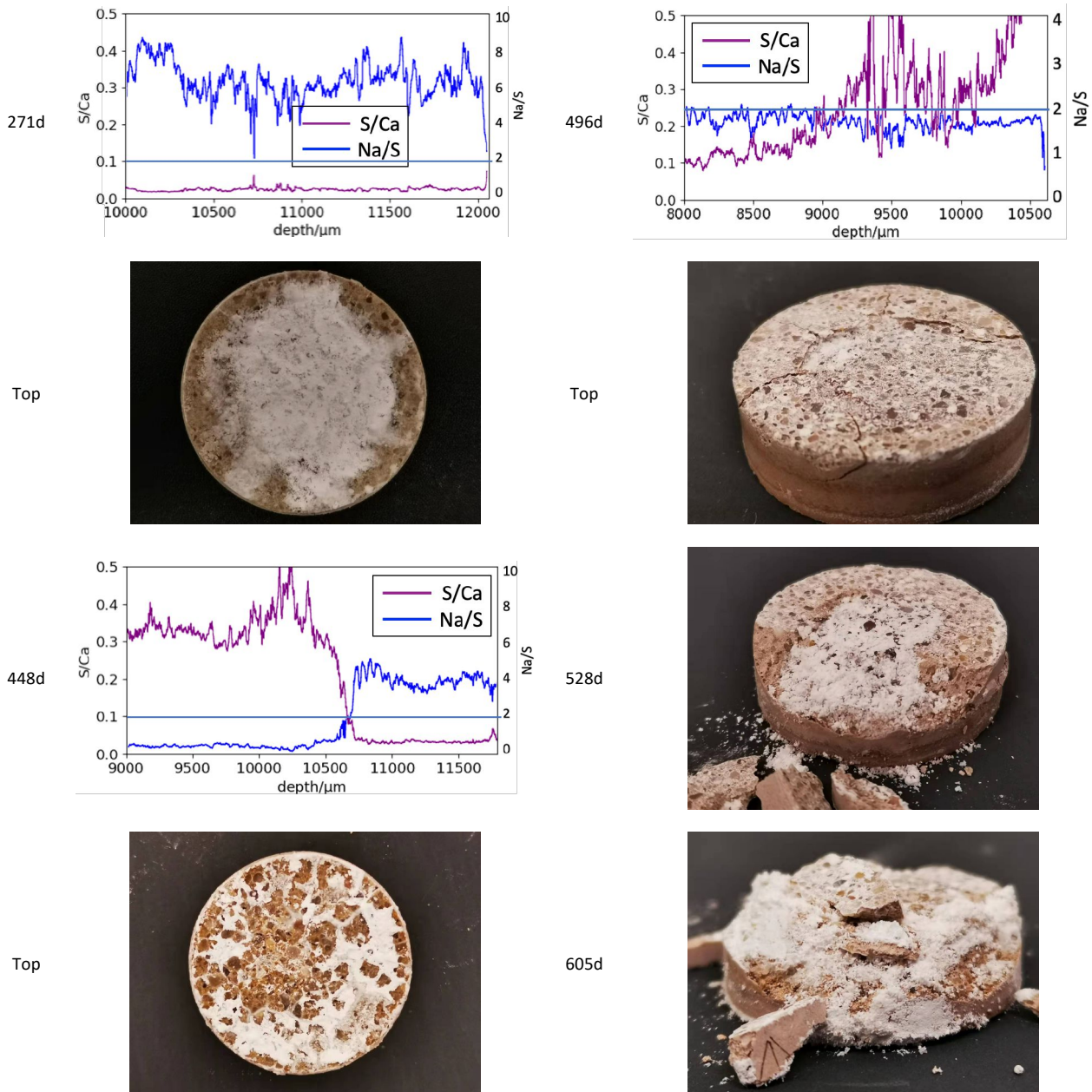


Fig. 5-22 Salt crystallization damage with the S/Ca and Na/S atomic profiles on the top 2 mm depth of PC and LC<sup>3</sup> mortar samples.

Another explanation of salt crystallization is the effect of alkali content and alkali absorptivity on C-(A)-S-H gel.

In Fig. 5-23, Na/Si in alkali silica gel (top zone, where the C-(A)-S-H is decalcified due to the carbonation) is quite different in PC and LC<sup>3</sup> which perhaps explain the environment for thenardite formation in LC<sup>3</sup> is more favourable. H<sub>2</sub>Na<sub>2</sub>SiO<sub>4</sub> is the possible analogue in nature with the Na/Si ratio of 2 observed in LC<sup>3</sup>, HNaSi<sub>2</sub>O<sub>5</sub>·3H<sub>2</sub>O (mineral name: Kanemite) could be the natural analogue hydrate that observed in PC with a Na/Si ratio of 0.5.

Na is more incorporated in decalcified C-(A)-S-H in LC<sup>3</sup> than that in PC which gives the totally different local chemistry in pore solution, in LC<sup>3</sup> the stoichiometric of thenardite is preferentially met. It is very similar with the sulfate accumulation in the drying front: alkali can accumulate at the beginning of the efflorescence appearing period in PC systems, later on it is decreased to a level nearly to the original Na/Si < 0.5. However, in LC<sup>3</sup> mortars, the higher alkali accommodation ability is clear from 426 days as the whole depth above ettringite zone (~ 2 mm) is translated to a double fold than that at 266 days. This high alkali content in C-(A)-S-H tendency is increased over Na/Si = 0.5 at 496 days and afterwards the cracking appears at the depth around 9 mm where the Na/Si reaches higher than 1. The trend is similar in SPC cement systems which is not discussed here in detail. Overall, the capacity of alkali absorption on C-(A)-S-H is higher in SCMs blended cements.

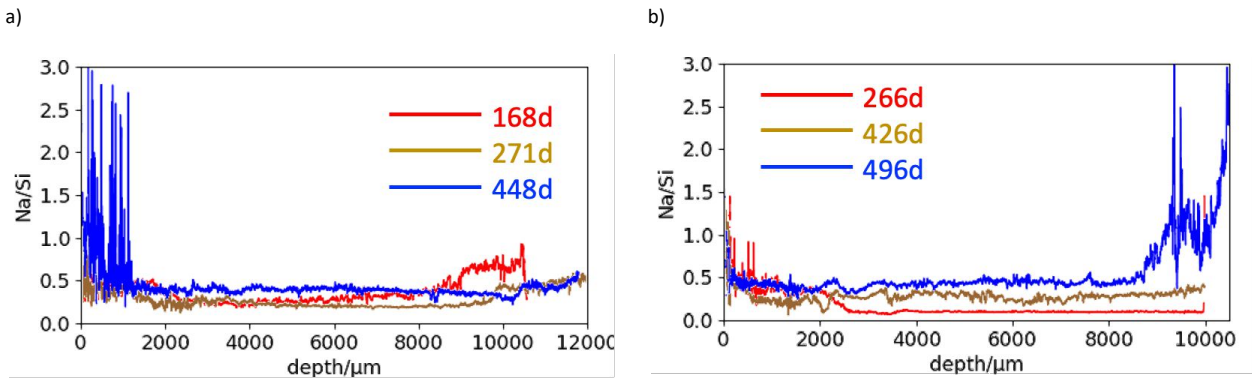


Fig. 5-23 Alkali content absorbed on C-(A)-S-H gel in PC and LC<sup>3</sup> cement mortars exposed to 50 g/L solution.

Fig. 5-24 shows a very long-term example from LC06-3g and PC06-3g samples to show there is no problem at all for salt crystallization attack as the local chemistry is not sufficient to reach high supersaturation, and it stays the high constant Na/S and low S/Ca in the drying front which means the S cannot accumulate sufficiently anyway no matter how long the sample is in contact with sulfate, in both cement pastes. In this case, only S concentration is essential for the degree of supersaturation that sodium sulfate can form. The sodium sulfate salt does form inside the LC06, but it is not sufficient to cause any damage, while, in PC, there is not much salt that can crystallize inside the material due to its intrinsic water adsorption and drying property. We do observe the cracks occurring on the surface of PC paste but it is due to the chemical sulfate attack and damage propagated easily to the top surfaces as the sample is relatively thin.

The results of sulfate ingress and absorptivity can support it. We can only observe the sulfate dynamic ingress current which results in efflorescence without any damage taking place. Efflorescence of PC06 occurs as sulfate solution reaches the top surface without the process of subflorescence as that in LC06, although the ultimate manifestation is the same, the mechanism is different.

Therefore, the important point of the mechanism of salt crystallization attack contact with sulfate solution is that nearly no similar damage should be expected in realistic situations because the sulfate concentration is much lower than the one used (50 g/L) in this study which shows the damage. In the one (3 g/L) close to field condition, we do not and possibly will not see any damage from merely sodium sulfate crystallization. The spalling damage from the field cases should be concerned also with the tidal flush force, wind, rain and temperature changes which are probably also contributing to the eventual manifestations.

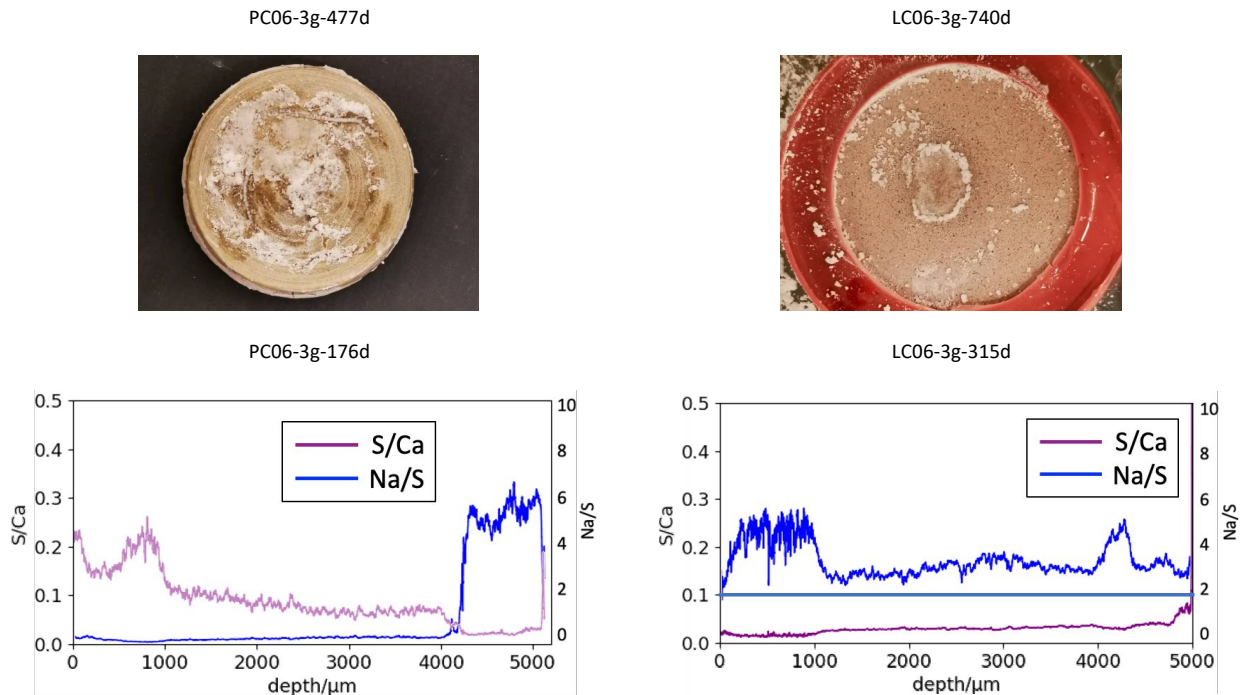


Fig. 5-24 Long-term exposed cement pastes samples under a similar exposure condition with 3 g/L sodium sulfate solution: appearance of samples and chemical profiles.

## 5.4 The comparison of constant and cycling exposure conditions

### 5.4.1 Physical behaviours after sulfate exposure

#### *Appearance*

The damage degree of cement paste samples is different between constant and cyclic exposures as shown in Fig. 5-25. The damage from high sulfate concentration is more extensive than that in low concentration, no matter the ettringite-induced cracking or the thenardite-induced spalling damage. In the cracking-dominated Portland-based cement pastes, cracking and bottom layers detaching is more extensive in cyclic exposure. However, the spalling-dominated damage in SPC and LC<sup>3</sup> samples more extensively appeared in constant exposure, although cyclic exposure shows a significant efflorescence increase. The bottom surfaces of SPC and LC<sup>3</sup> samples are not damaged at all but only with the softening effect from the leaching.

Under low sulfate concentration conditions, cracking from chemical attack cannot be totally avoided, but spalling damage is not likely to occur. This manifestation difference demonstrates that the necessary sulfate concentration is more relevant in a physical attack than that in a chemical attack to initiate the degradation. It shows a significant impact of the exposure regime on the appearance of spalling damage, which contradicts the traditional impression that physical attack should be more intense in varied environments of temperatures and relative humidities. The damage is not initiated even after ~ 2.5 years in LC06-3g samples under both constant and cyclic exposure.

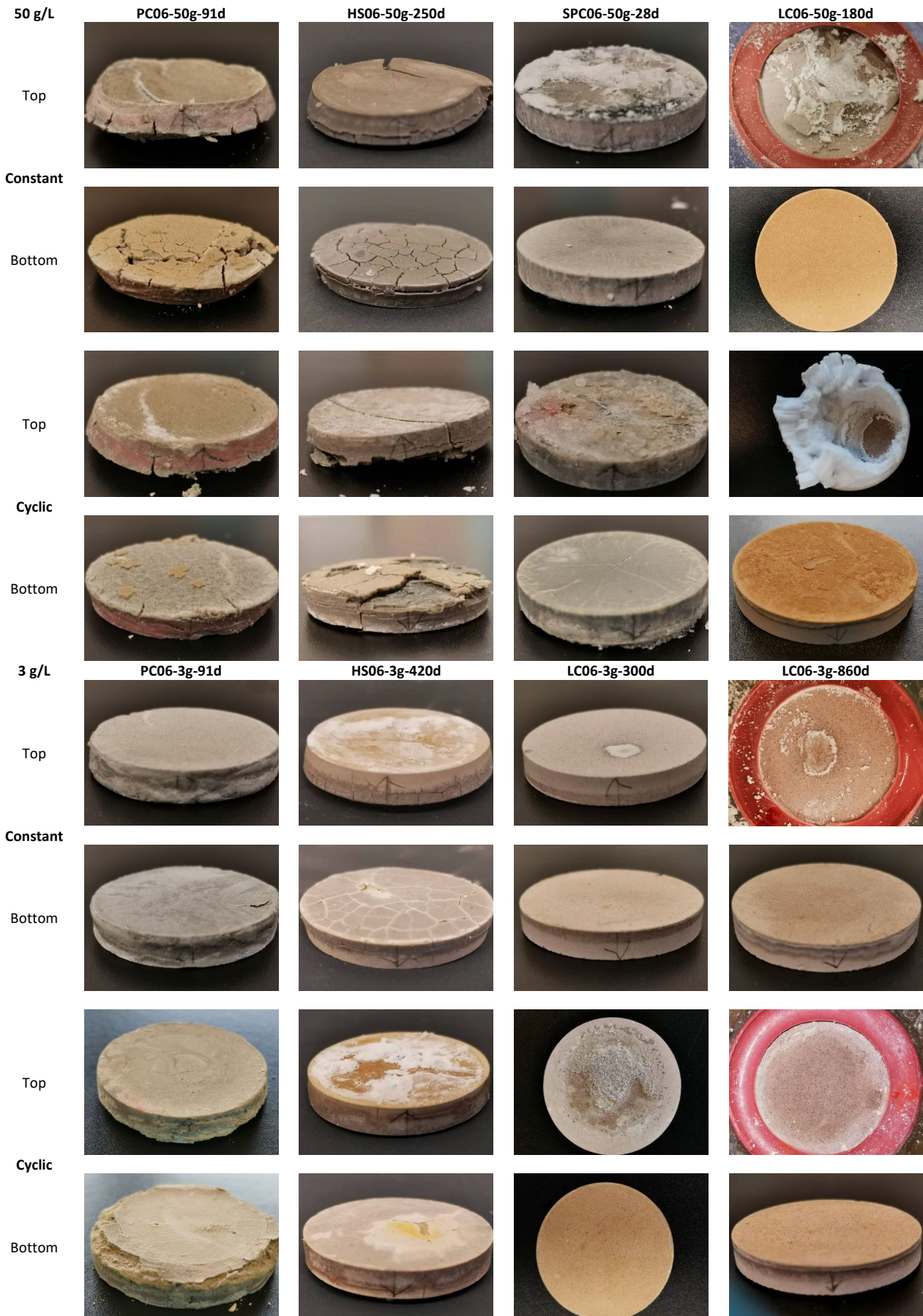


Fig. 5-25 Visual inspections of cement pastes with w/c 0.6 under constant and cyclic exposure with 3 and 50 g/L sodium sulfate solution.

### Expansion and mass gain

Expansion developments over time under constant and cyclic exposure conditions are shown in Fig. 5-26. The expansion is only increasingly detectable in PC and HS systems, while expansion in SPC and LC<sup>3</sup> pastes are not that visible and are mostly below 20 mm/m. Expansion propagates similarly under both constant and cyclic exposure conditions which imply the low sensitivity of expansion measurements, although the expansion of LC<sup>3</sup> and SPC under cyclic exposure is slightly increased. SPC samples were quickly damaged due to their low mechanical strength resistance and low degree of hydration only with 28 days of curing, so the expansion data for SPC was limited.

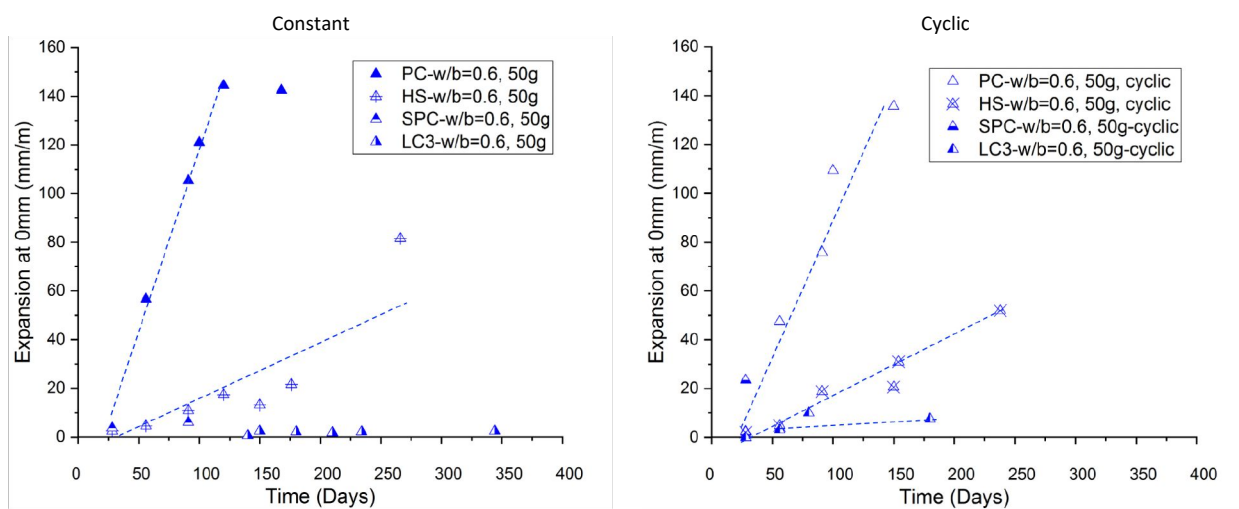


Fig. 5-26 Expansion rates of different cement pastes between constant and cyclic exposure regimes.

Another aspect of the degree of sulfate resistance is to measure the mass changes over time as shown in Fig. 5-27. Mass gain mainly takes place in PC and HS cement pastes corresponding to an expansion increase that shows that the expansion is due to the newly formed hydrates in the small voids and/or cracks. Whereas, the mass loss or very little mass gain is observed under the constant condition in SPC and LC<sup>3</sup> shows possible spalling of surfaces instead of any expansion. The initial mass loss of HS cement pastes shows the water evaporation is not yet compromised by the capillary rise before sulfate reaches the drying front and parallel cracks appear. Mass changes can help to discriminate the different cements and the potential damage modes. Mass changes follow the same rule as expansion propagation in PC and HS samples. While low mass changes correspond to low expansion in blended cement pastes. It is evident that expansion alone is not sufficient to characterize the sulfate resistance as the spalling of surfaces can induce mass loss without any expansion detected.

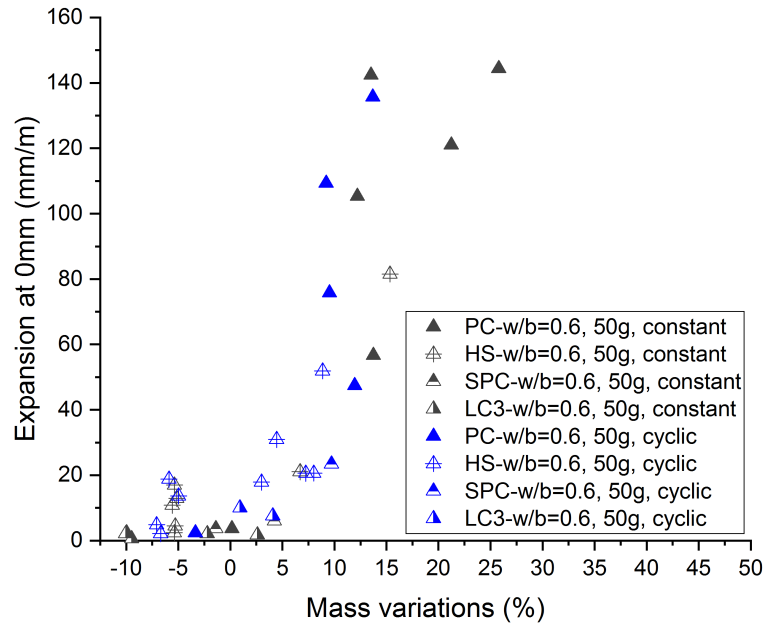


Fig. 5-27 Mass variations of different cement pastes between constant and cyclic exposure regimes.

## 5.4.2 Chemical changes after sulfate exposure

### *Effect of exposure condition on sulfate ingress rate*

For the expansion behaviour mentioned before, not much difference that can be found between constant and cyclic exposures. However, the chemical sulfate ingress should be addressed particularly since temperature and relative humidity can change the sulfate ingress and drying kinetics.

In this section PC and LC<sup>3</sup> samples with w/c=0.6 are compared in terms of sulfate ingress rate as shown in Fig. 5-28. Sulfate ingress is increased under the cyclic condition where the sulfate may reach faster to the other side of samples and hence cause possibly salt crystallization either inside or outside the samples depending on the varied drying properties of both PC and LC<sup>3</sup> systems. This can only be confirmed by the presence of salts which is discussed in the next part of the chemical profiles. One thing is clear that cyclic can accelerate the sulfate ingress in both systems. One example of w/c of 0.4 is compared between constant and cyclic conditions by HS cement, cyclic exposure enhances the sulfate ingress.



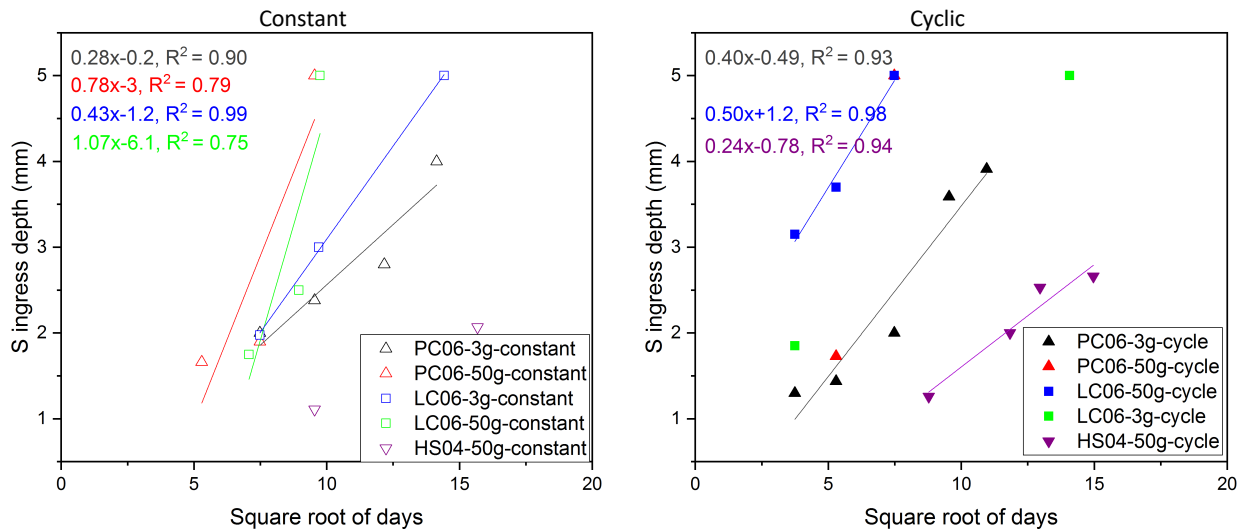


Fig. 5-28 Sulfate ingress rate of PC and LC<sup>3</sup> cement pastes under constant and cyclic conditions.

### Phase profiles

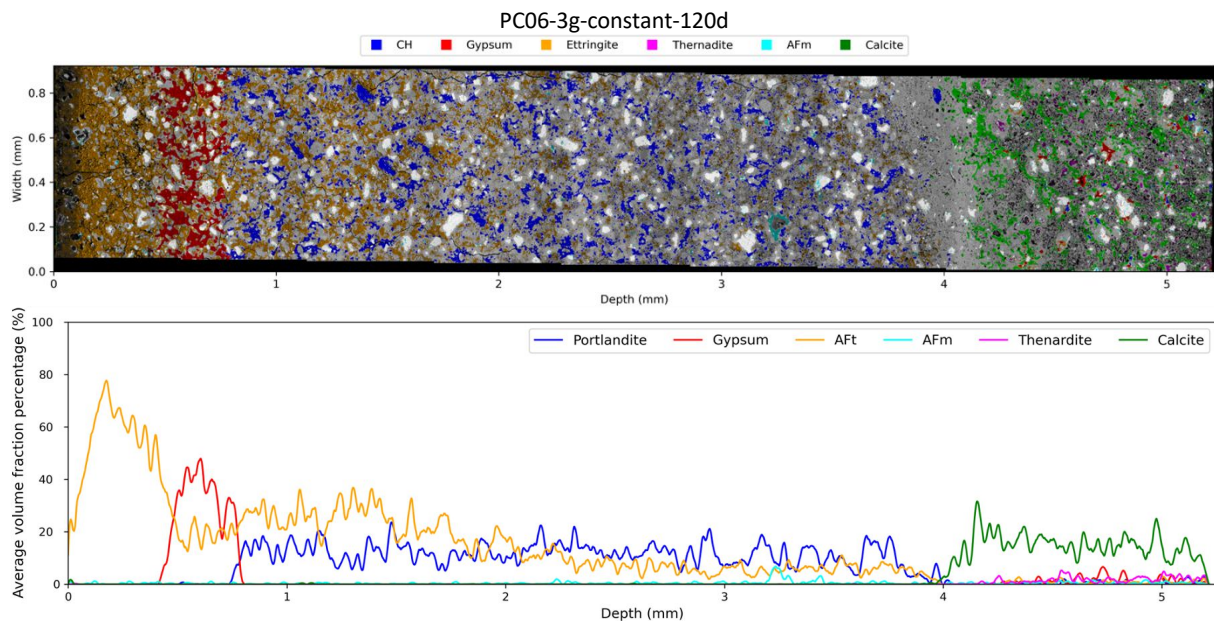
In this section, the degradation profiles of four cement systems under constant and cyclic exposures are compared. The degradation is significantly dependent on the exposure condition which changes the capillary rise as well as drying property, accordingly sulfate ingress rate and susceptibility of salt precipitation are totally changed. As a result, the ultimate degradation and speed of deterioration might be completely different with different exposure conditions.

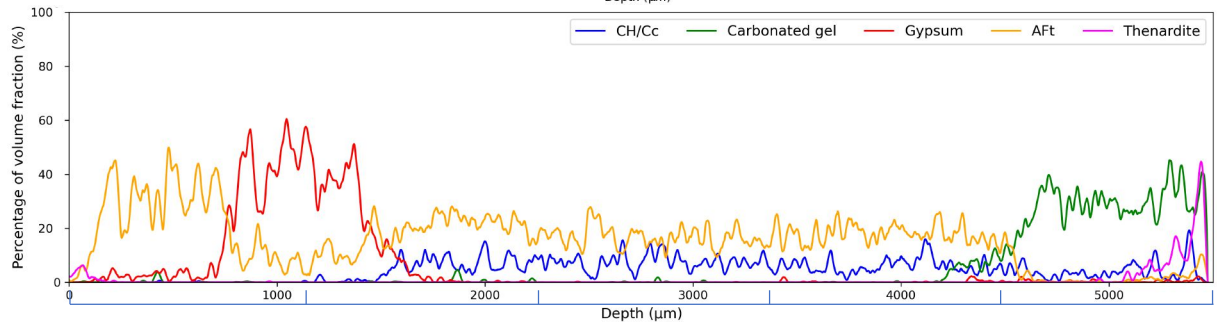
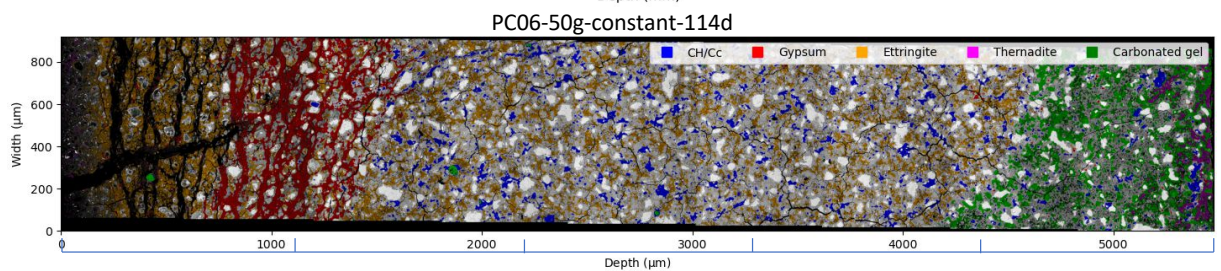
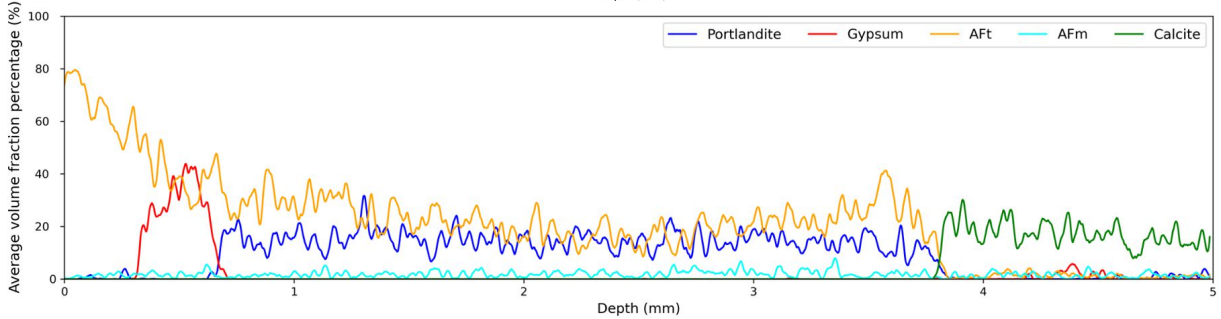
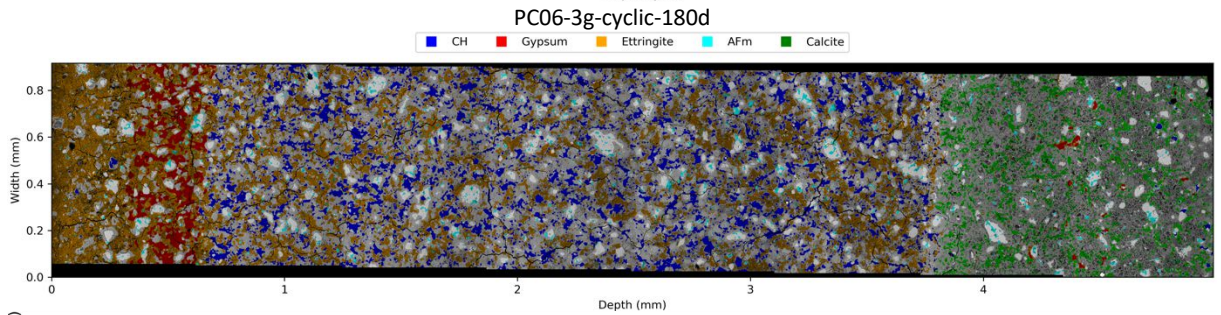
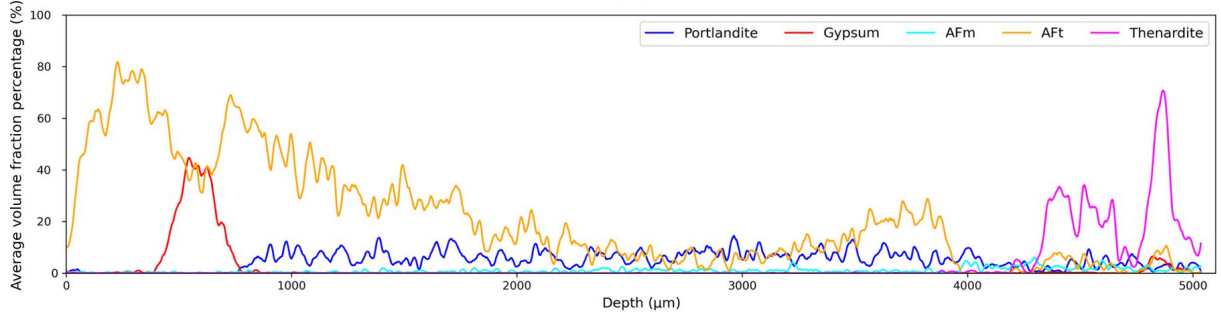
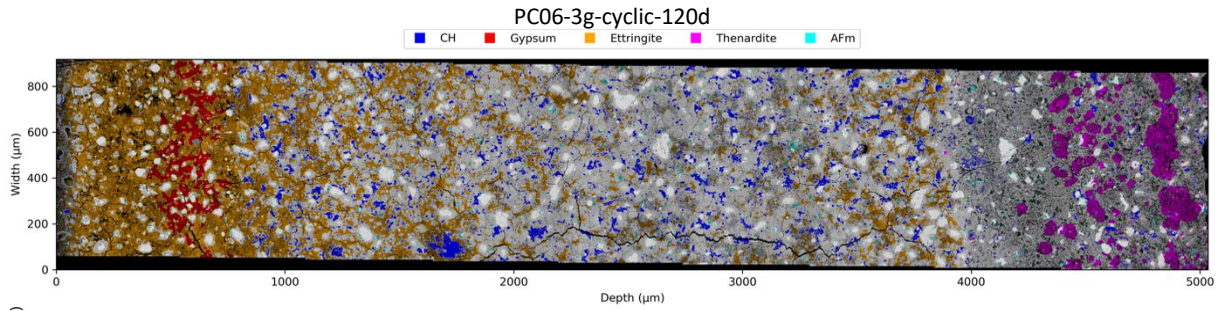
First of all, PC systems are compared with different exposure parameters in Fig. 5-29. Generally, the sulfate ingress and damage can be accelerated by cyclic exposure in terms of ettringite-type attack. The cyclic condition does not help much on the diffusion as the quite constant ettringite fronts are still the same over time compared with the constant condition. However, advection of external solution is accelerated under cyclic conditions, and it shows the evidence on the other side of the sample, that ettringite precipitates there as the sulfate concentration grows. If the condition of supersaturation and confined space is met, theoretically expansion can take place in the interface zone.

From the eventual salts presence behaviours, the capillary rise may be accelerated up to a level that is much faster than the evaporation rate, which can only give a short period of subflorescence or efflorescence in the cyclic exposure. Like in PC06-3g-cyclic-120d, where the thenardite-like phase is formed, but there is no damage. The subflorescence disappears with longer exposure at 180 days, which demonstrates the subflorescence is only present in the temporarily satisfied condition where the evaporation rate is faster than capillary rise. With the same exposure time, it is obvious that sulfate ingress is slower under constant conditions, and there is no ettringite hump in the interface and no thenardite-like phase forming in the drying front.

In the high concentration situations, the ettringite concentration gradient is more homogenized (more advanced ettringite front by capillary rise) in the middle zone without observing the typical two hump ettringite. A tiny region of the thenardite phase forms near the top surface under constant conditions, while under the cyclic condition, the chemical sulfate attack is much more extensive as the gypsum and cracks can form on the other side in the interlayer zone. However, in this cracked sample at 120 days, there is no thenardite formation though it shows the same degradation phenomenon as the cracking damage on the bottom zone in the sample of PC06-50g-cyclic-120d.

Water evaporation rate in PC06 systems is much slower than water sorptivity which does not provide the condition that salts form inside the paste; in cyclic conditions, the situation is still the same or with a short period of thenardite presence, even though water evaporation may be accelerated by the lower relative humidity. But finally, the results show that the drying speed is not fast enough to force salts forming inside.





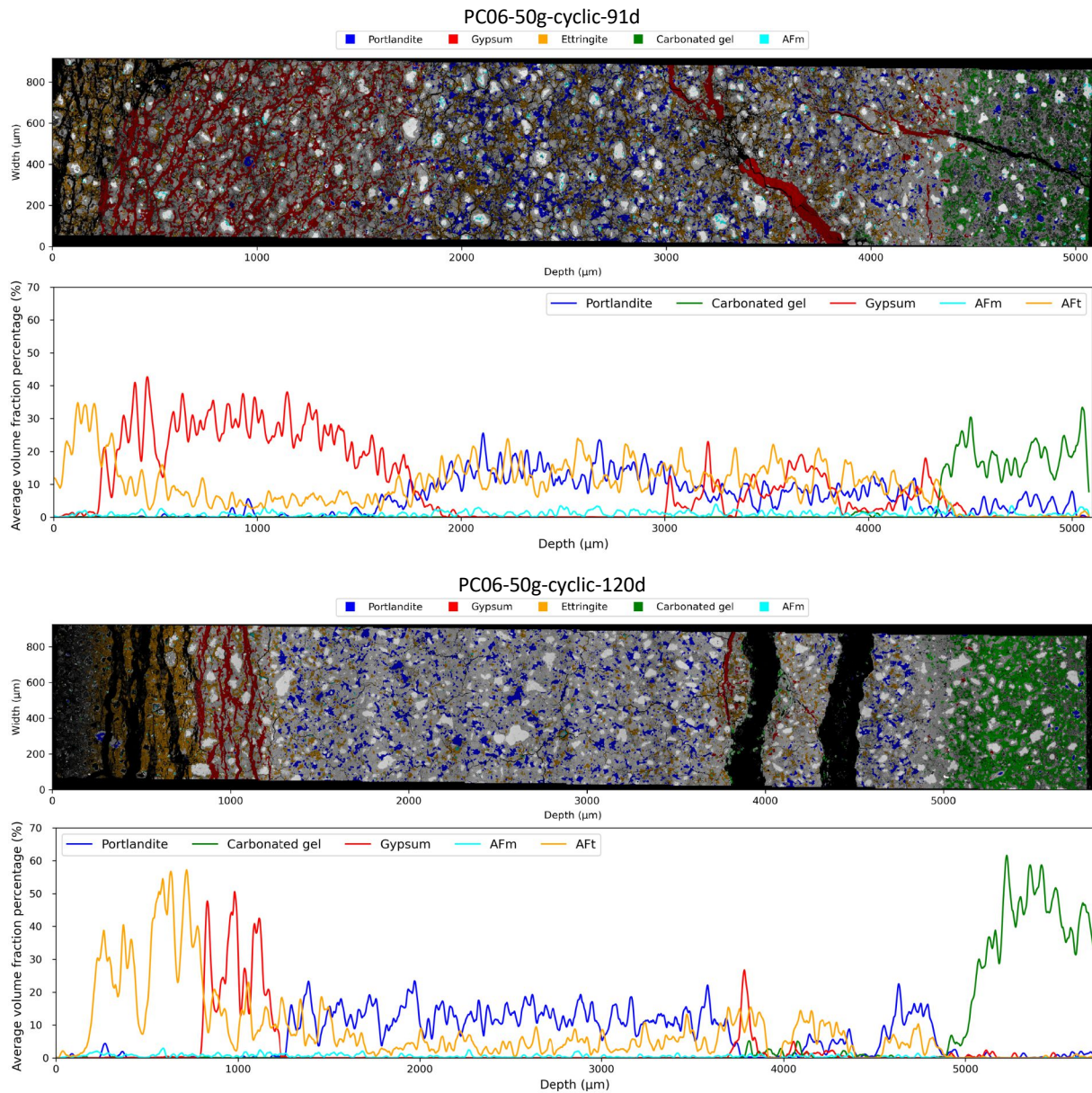
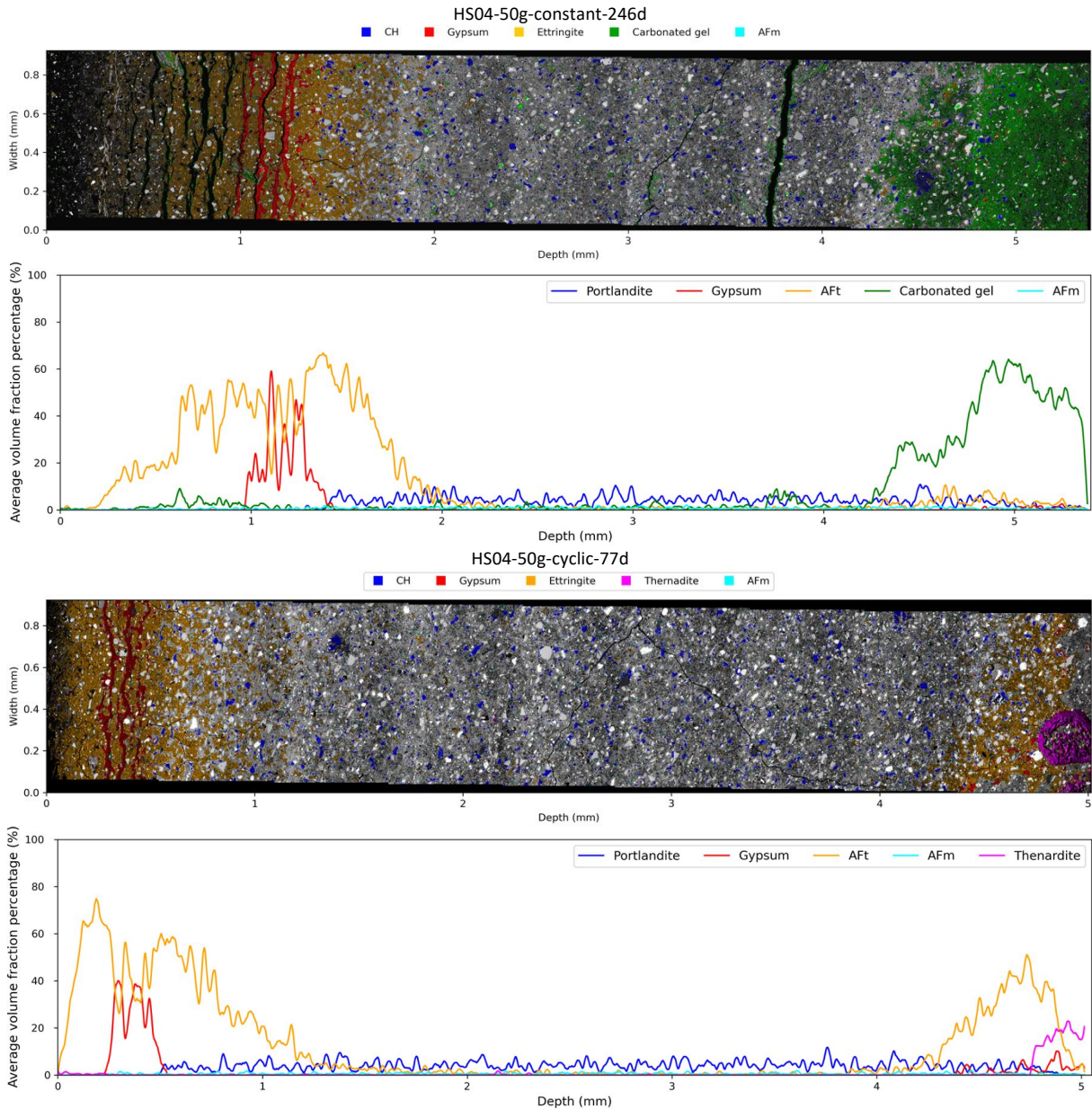


Fig. 5-29 Profiles of phase distribution and relative phase concentration gradient of PC systems.

In Fig. 5-30, the HS cement paste systems show a more obvious effect of exposure conditions. Thenardite starts to form after 77 days under cyclic exposure and it can last until 300 days. It appears in a very localised place, and only concentrates near the surface, which causes the local spalling damage. The characteristic of the carbonation front is not flat, showing the heterogeneous paste matrix, hence the local chemistry is possible for salt crystallization. The fast-drying property can explain the precipitation inside the HS paste samples. A slightly higher evaporation rate than capillary rise determines the location of thenardite presence that cannot move deeply.

Under the constant condition, it does not show any thenardite formation until 246 days, but may come later as the sulfate ingress is theoretically slower than under cyclic condition. And the appearance of a similar spalling phenomenon under constant exposure is discussed in the appendix. Therefore, cyclic exposure does

not seemly change the susceptibility of salt crystallization damage, but can obviously accelerate the damage process in HS systems. The long-time presence of thenardite (from 77 days to 300 days) reveals that the accumulation of salts inside the paste is retained, and that is probably important to cause any detectable damage. No visible damage is observed since the mechanical strength of HS04 is probably higher than the exerted stress. Therefore, it is a totally different phenomenon than in PC systems. Even though thenardite is present in both systems, it forms in PC paste only within a short period, then disappears and forms outside.



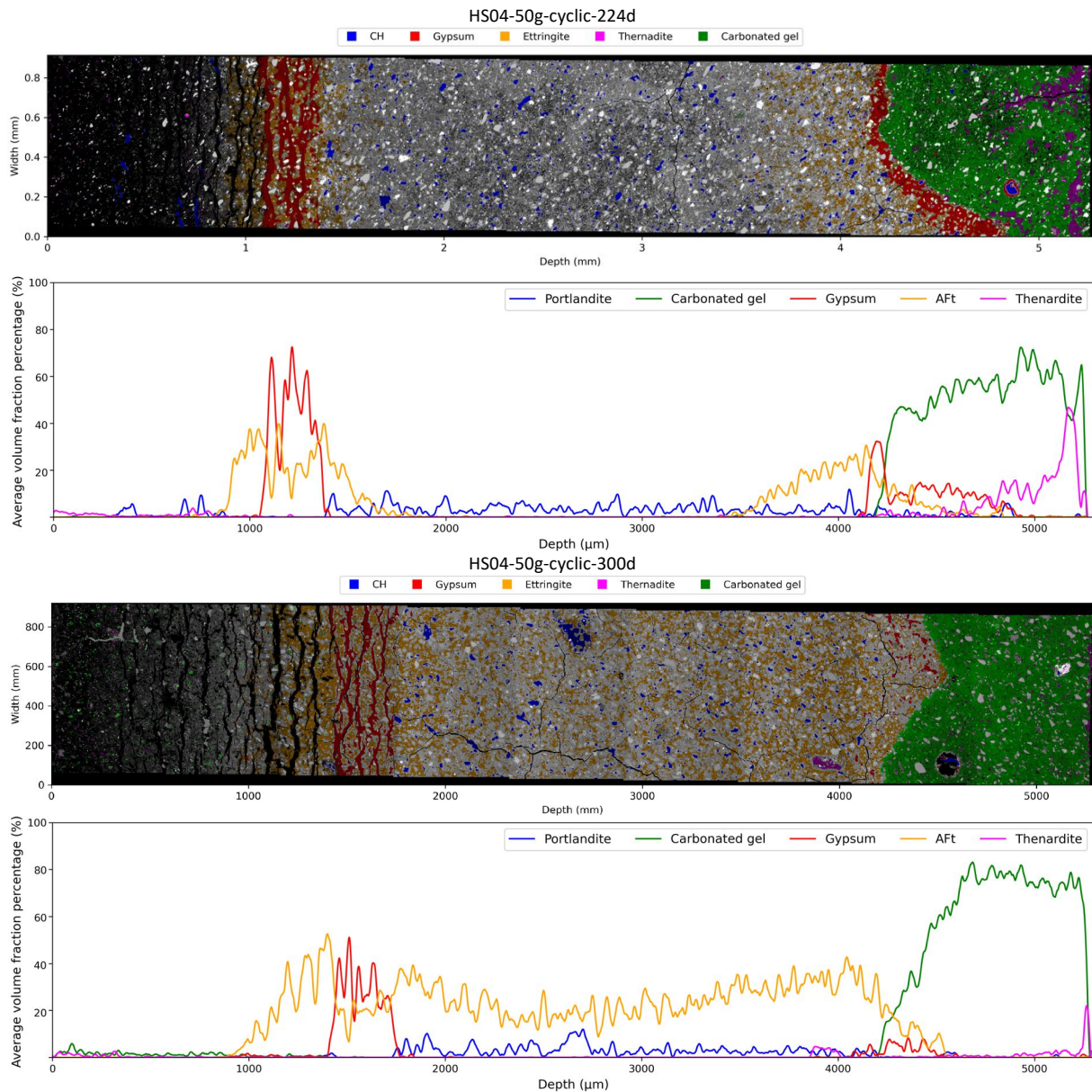
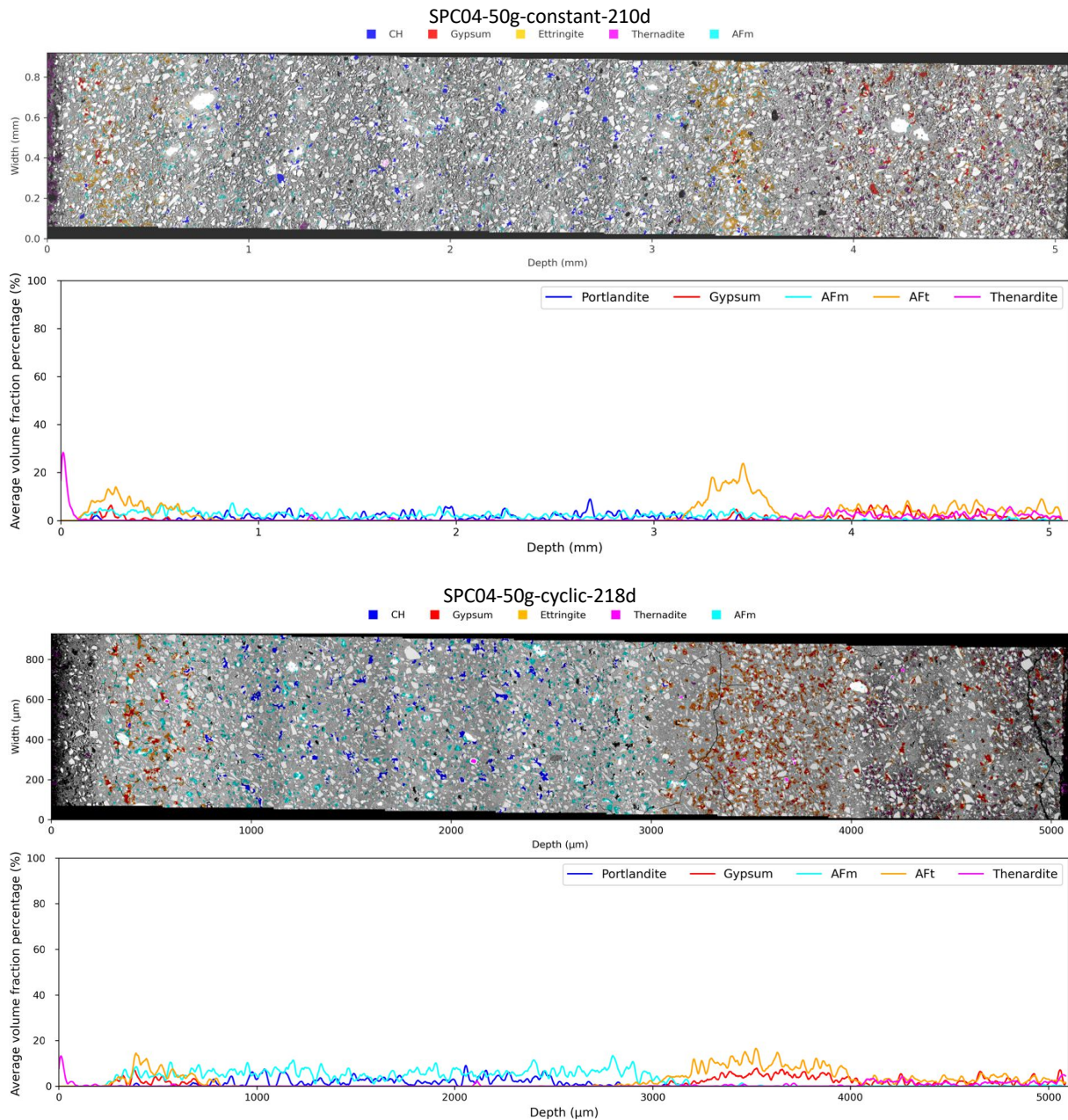


Fig. 5-30 Profiles of phase distribution and relative phase concentration gradient of HS systems.

In Fig. 5-31, the degradation of SPC systems is compared between different w/c ratios of 0.4 and 0.6. The system of SPC06 was destroyed quickly only after 28 days due to its weakness from relatively low strength. For further analysis of the progressive degradation mechanism of the SPC system, SPC04 was added to obtain chemical profiles and degradation fronts.

The spalling damage takes place at 28 days of SPC06 under constant condition, there is a layer around 0.3 mm from the top surface rich with thenardite. The residence time of thenardite in SPC06 is relatively short before it causes damage which is attributed to lower strength than HS. However, in SPC04 systems, thenardite forms in a very small amount and is scattered, which cannot cause damage as the strength are higher than

SPC06. The much-reduced chemical sulfate attack may contribute to the more extensive physical sulfate attack. The ettringite front on the bottom surface is limited to  $\sim 0.5$  mm either under constant or cyclic exposure after 210 days, and there is no parallel crack which accommodates further the sulfates. Reduced chemical sulfate attack and fast drying property potentially lead to the physical sulfate attack. It reveals the mutual influence between chemical and physical sulfate attack, it is a relationship when one is rising (severe), and the other is falling (less severe).



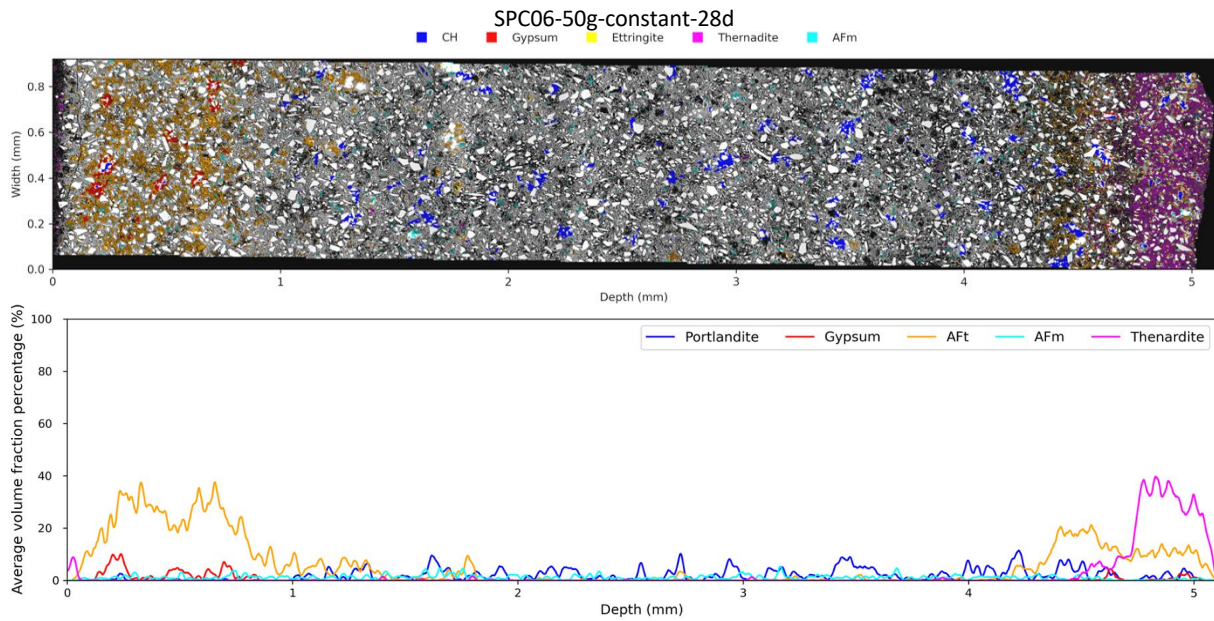


Fig. 5-31 Profiles of phase distribution and relative phase concentration gradient of SPC systems.

In Fig. 5-32, LC<sup>3</sup> systems show a completely different physical damage phenomenon than others. Spalling is more profound in constant conditions, and the thenardite front moves to the zone exactly above the ettringite-rich zone close to the bottom surface. The cracks appear at 180 days and move deep progressively, the thenardite is dominantly present around the cracks. Gypsum and ettringite presence in the vicinity reveals the high concentration is ensured for thenardite crystallization pressure.

However, under the cyclic condition, no visible damage is observed, accompanied by a limited amount of thenardite. Constant condition is more likely to retain longer faster evaporation than capillary rise with the less ettringite-type favourable attack, hence more sulfate can ingress to the evaporation zone.

The chemical attack is similarly progressed with SPC systems, as there is a limited maximum depth of 1.5 mm to the ettringite-rich layer, while the further movement of this layer is somehow inhibited by the advanced carbonation from the other side. The combined effect of the continuous leaching and the stopped ettringite further movement shortens the thickness of the preformed ettringite layer. Ettringite formation in SPC and LC<sup>3</sup> systems cannot cause large expansion and crack as is already proven in section 5.2.2, therefore, thenardite/mirabilite crystallization pressure is the only reasonable mechanism causing spalling damage in the drying front. After all, the ettringite amount is largely decreased in the drying front. Cyclic exposure may accelerate more prominently the capillary rise than drying which reduces the possibility of salt crystallization inside the sample. Only a very narrow area of thenardite formation below the surface shows evidence of less susceptibility.



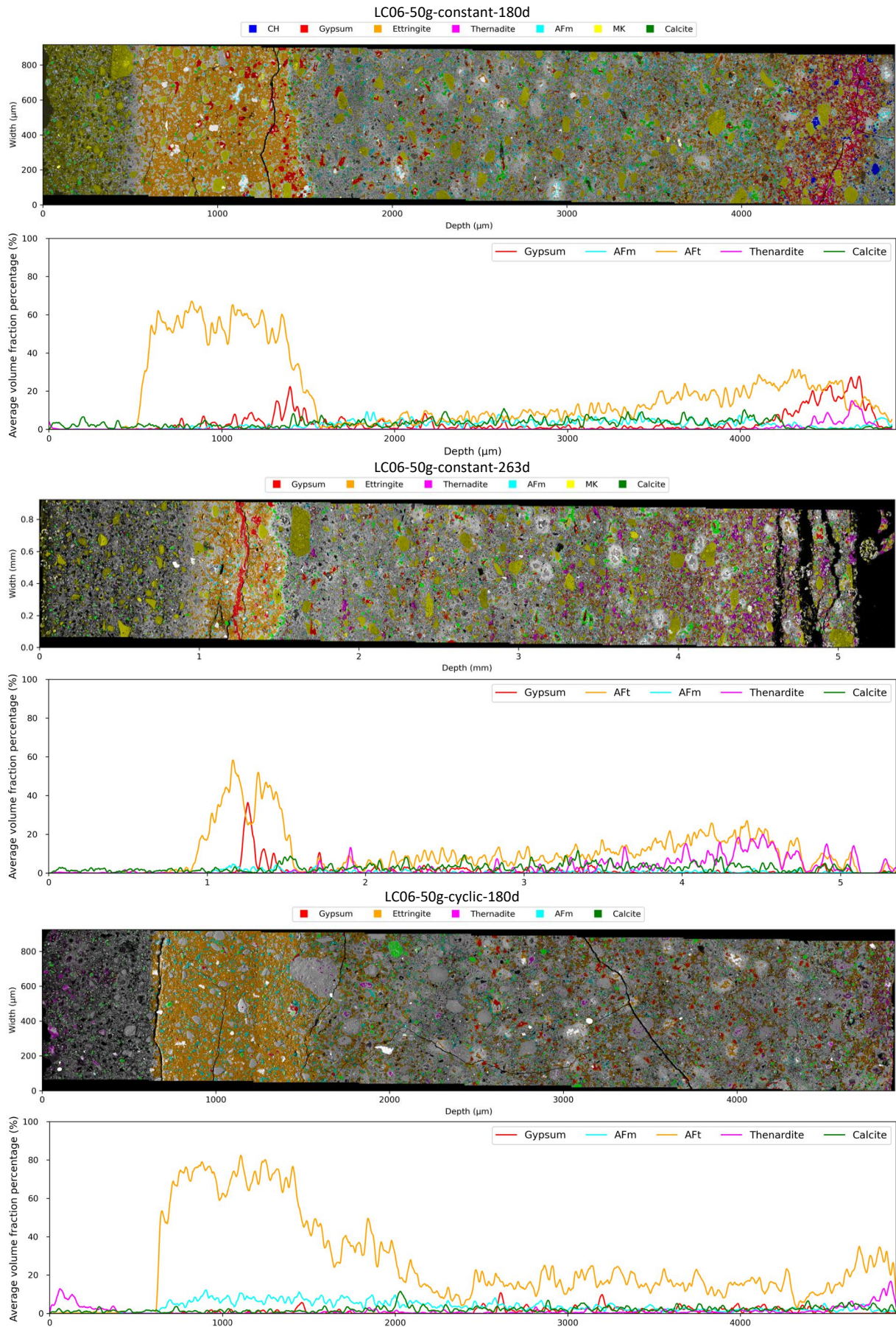


Fig. 5-32 Profiles of phase distribution and relative phase concentration gradient of LC<sup>3</sup> systems.

## 5.5 Conclusions

1. A lower w/c ratio of 0.3/0.4 shows less extensive expansion/cracking; the sulfate ingress depth (i.e., the depth of S/Ca in C-(A)-S-H above the reference) follows a linear relationship with the square root of exposure time. The sulfate ingress rate increases with the increase of the concentration of the exposure solution and the w/c ratios, LC<sup>3</sup> shows higher sulfate ingress than PC and cyclic exposure accelerates sulfate ingress.
2. No significant expansion and degradation were observed under the exposure of 3 g/L solution and a w/c ratio of 0.3 after exposure for 250 days. The w/c ratio shows a great impact on the expansion take-off time. At high concentrations, even PC systems at w/c of 0.3 expanded after 250 days of exposure.
3. The expansion is initiated as fine ettringite forms from the AFms transformation within C-(A)-S-H gel. The expansion increases as the solution concentration and w/c increase. SPC and LC<sup>3</sup> cement pastes indicate negligible expansion as there is no ettringite transformation within C-(A)-S-H.
4. Spalling damage happens more preferentially in SPC and LC<sup>3</sup> cement systems under sulfate concentration of 50 g/L in constant conditions.
5. Parallel cracking forms with gypsum filling can be treated as a macroscopic indicator to initiate a progressively degraded layer from sulfate attack.
6. No damage by sodium sulfate crystallization pressure is observed under a low sulfate concentration (3 g/L) in LC<sup>3</sup> cement pastes until nearly 2.5 years of sulfate exposure.

# Chapter 6 Chemical thermodynamic modelling

## **Abstract**

Thermodynamic modelling can simulate cement hydration, calculate phase assemblages, and assess the ingress of deleterious ions ( $\text{CO}_2$ , sulfate, chloride, etc.). In this chapter, thermodynamic modelling of the investigated cement pastes was done with variations in exposure conditions (sulfate concentration,  $\text{CO}_2$  content for carbonation), to get insight into the changes in phase assemblage and ionic concentrations in the pore solution. Two main aspects are addressed in this chapter: (1) estimation of the ettringite crystallization pressure from chemical sulfate attack; (2) the susceptibility of salt crystallization of sodium sulfate at the drying front by investigating the pore solution chemistry. The modelling results give a further understanding of the pore solution environment of the occurrence of phase precipitation, which can directly link with the experimental results, from which the likely conditions existing in the real samples are discussed.

## Contents

<b>6.1</b>	<b>Introduction .....</b>	<b>132</b>
<b>6.2</b>	<b>The theory of crystallization pressure .....</b>	<b>132</b>
<b>6.3</b>	<b>Thermodynamic modelling .....</b>	<b>135</b>
6.3.1	Thermodynamic calculations in equilibrium conditions.....	135
6.3.2	Saturation index from ettringite.....	140
<b>6.4</b>	<b>Estimation of the crystallization pressure profile of ettringite .....</b>	<b>142</b>
6.4.1	Crystallization pressure from experimental .....	142
6.4.2	Crystallization pressure calculated from saturation index .....	145
6.4.3	The link between crystallization pressure development and macroscopic observations .....	146
<b>6.5</b>	<b>Salt crystallization of sodium sulfate in the carbonated and drying front .....</b>	<b>147</b>
6.5.1	Susceptibility of salt crystallization in Portland cement.....	148
6.5.2	Comparisons between different cement pastes with 50 g/L Na <sub>2</sub> SO <sub>4</sub> in porewater .....	150
<b>6.6</b>	<b>Conclusions.....</b>	<b>152</b>
<b>6.7</b>	<b>References.....</b>	<b>153</b>

## 6.1 Introduction

Expansion is significantly influenced by the sulfate concentration, as discussed previously in *Chapter 5*. There are several mechanisms (solid volume increase, swelling of colloidal ettringite and topochemical reactions) proposed trying to explain the cause of the expansion over the last decades [1–4]. However, the crystallization pressure theory is increasingly recognized as the most plausible nowadays to explain the expansive force that exerts from ettringite formation in confined pores as well as supersaturation [1,5–7]. However, the understanding is still limited because the supersaturation cannot be directly measured from experiments that limit the understanding of the relationship between the crystallization pressure and the expansion and later on cracking.

Although the chemistry in pore solution at a specific depth in a thin sample cannot be directly obtained from experiments, through thermodynamic modelling, it is possible to simulate the phase assemblage profiles and the pore solution in equilibrium conditions which was already explored [7]. Less commonly, to estimate the upper limit of supersaturation from ettringite, the calculation can be done in a non-equilibrium condition where the formation of ettringite is suppressed (only monosulfate and gypsum are present) by limiting the quantity equivalent to the initial amount before the exposure to sulfate solution [5].

Modelling the pore solutions gives a way to estimate the saturation index and then calculate the crystallization pressure. Two external sulfate concentrations were considered according to the experimental approach, 3 and 50 g/L.

Simulating the salt crystallization process under a relatively low RH is more challenging as the low relative humidity cannot be modelled in GEMS (some thermodynamic data is still missing), so the supersaturation with respect to sodium sulfate salt from evaporation-driven is not possible to be calculated. However, the pore solution information at the drying front of the paste sample is missing, which is the key to explain the driving force of salt crystallization pressure in various cement pastes. Here GEMS modelling is attempted to simulate the changes of ionic concentrations in the pore solution of the paste or mortar due to carbonation and the presence of sulfate. It is analysed and combined with the experimental results to infer the susceptible environment for salt crystallization damage.

## 6.2 The theory of crystallization pressure

Crystals growing in an equilibrium condition in big pores do not cause any stress (as we observe the normal hydration process), and the pressure can be exerted under the confined space where the supersaturation is in charge of the crystal growing under a non-equilibrium condition. This process can convert chemical energy into mechanical work that causes damage to the pore walls [8]. Supersaturation determines the upper limit of the pressure that is potentially able to form, while curvature determines the lower limit that the maximum

pore size can generate the damageable stress. A common tensile strength of the concrete is taken as 4 MPa, and the maximum pore size in a cylindrical shape is a diameter of 100 nm. The pressure can only occur when the confined pores are fully filled by the crystals [9,10]. It implies that in the latent period, big pores are filled which is under unconfined growth.

A schematic illustration of the crystal growth in pores and its possible relation to the macroscopic behaviour during the whole sulfate ingress process is shown in Fig. 6-1. The case of only cylindrical pores is considered (the curvature is  $2/r_p$ ). First of all, the physical meaning of crystallization pressure should be highlighted here: the pressure needed to stop the growth of crystals in equilibrium with a supersaturated solution. Two cases of crystal growing inside the pores are discussed, 1) a crystal grows in a large pore (unconfined space), and 2) a crystal grows in a small pore (confined space).

In the case of a large pore in Fig. 6-1 a), the radius of the crystal  $r_c$  is much smaller than the radius of the pore  $r_p$ . There is no stress from the pore wall applied to the crystal as it is freely growing. The supersaturation is not that significant as the sulfate concentration around the crystal should be in equilibrium with the free pore solution. It can explain exactly why we always observe the buffering effect from experiments: sulfate concentration is kept constant during the latent period (where no visible expansion is detected as shown in Fig. 6-1 d)), when the external sulfate reacts with the transformable aluminium-bearing hydrates in larger pores dominantly but also invade progressively into the smaller capillary and gel pores. The pressure exerted from the crystallization process stops the crystal growth until the crystal continues to grow reaching the pore wall (see Fig. 6-1 b)) so there is no damage occurring. In this process, it shows perhaps the existing maximum ettringite volume beyond which the ettringite formation in the confined space, can then expansion effectively increases. The similar idea was demonstrated in the delayed ettringite formation in [11]. In this process, it is corresponding to the elastic period of stress/strain curve where the mechanical strength of cement pastes is larger than the exerted stress from ettringite formation.

When those aluminium-bearing hydrates consume thoroughly then the sulfate concentration can be increased in pore solution, and then penetrates into smaller pores as illustrated in the case of a small pore in Fig. 6-1 c).

In the case of a crystal growing from a big pore into a small pore, a thin film  $\delta$  is assumed to remain between the crystal and the pore wall which can still feed the crystal through the ions transported from the free pore solution. The crystals at crystal-pore interface are in a non-equilibrium state as the concentration inside the small pores is higher than the large pores as discussed previously, the high supersaturation degree is satisfied in the small pore so that the crystals keep growing. When the cement pastes cannot resist anymore the pressure, micro-cracks are initiated in local pores individually. After a certain time of latency, the micro-cracks are geometrically networked in the macro-scale, and the macro-expansion or cracks can be then detected

[11]. The sulfate concentration in pore solution can be experimentally detected with increased values in this process, expansion is usually followed by the increased sulfate concentration detectable by SEM-EDS [1] or more ettringite detected by XRD [11]. Because the relatively small ettringite formed in small pores can really cause high pressure, is not virtually visible by those techniques.

Whenever the expansion can be measured on a macro-scale, most pores are seemingly filled by ettringite. The microstructural scale of expansion agglomerates into the detectable expansion, so macroscopic expansion is the reflection of the microstructural stress field that is networked through a sufficient region. Expansion is the starting point of the large fracture occurrence. As demonstrated in [8], the fracture is not caused by crystallization pressure in a single pore. One important thing is that only when the crystallization pressure is beyond the strength of the cement pastes, the large expansion with damage can then be initiated as correlated with the plastic period in the stress/strain curve. So the cement materials with higher strength usually show a lower extent of the damage.

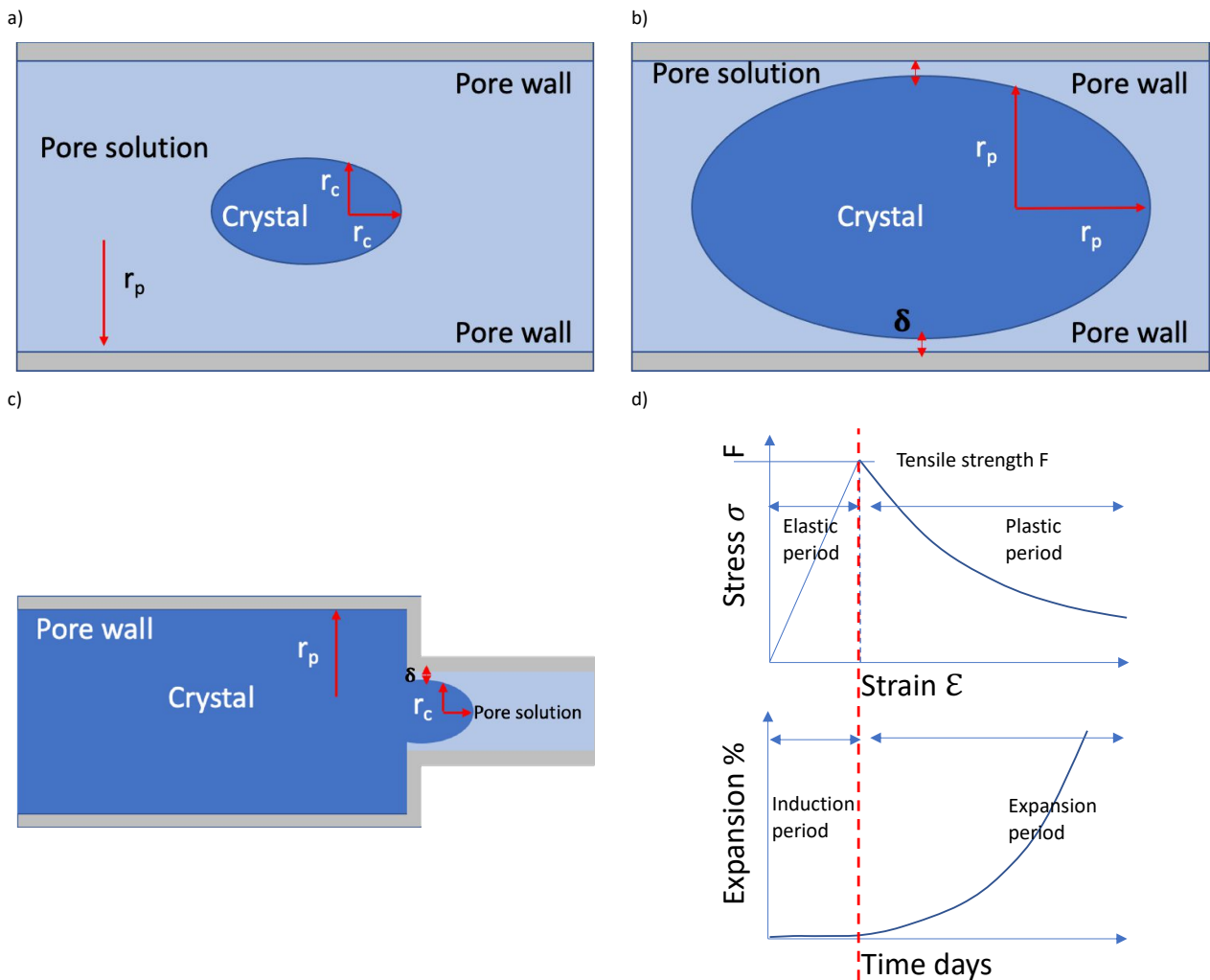


Fig. 6-1 A schematic of crystal growing inside a cylindrical pore and link to the macroscopic observations: a) a crystal grows in a relatively large pore under equilibrium, b) a crystal grows in a relatively small pore under non-equilibrium, c) expansion and stress/strain curves after sulfate

ingress. Pore radius is  $r_p$ , crystal radius is  $r_c$ ,  $r_c \ll r_p$ ,  $\delta$  is the thickness of the liquid film between the crystal and the pore wall, it is estimated to be 1 nm [8].

## 6.3 Thermodynamic modelling

The CemGEMS web app (<https://cemgems.app>) was used to calculate the phase assemblage in equilibrium condition [12]. The latest version of GEM-Selektor (GEMS v.3.9.5) [13] with the CEMDATA 18 database [14] which contains thermodynamic data of the solid phases relevant for cement systems, was carried out to simulate the saturation index. The CSHQ model developed by Kulik et al [15] was adapted to this case. The formation of ettringite30, SO4\_CO3\_AfT, and CO3\_SO4\_AfT was suppressed by setting the upper limit to 0 in the calculations, as a reason for simplicity. The chemical composition of raw cement materials (data from XRF) was defined as the inputs. The degree of cement hydration was assumed to be 80 %.

### 6.3.1 Thermodynamic calculations in equilibrium conditions

The initial hydration products were calculated and checked first, and then the ingress of the sulfate solution was set up based on the initial contents of constituents in cement and SCM materials, along with the addition of solution at a desired w/b mass ratio. It is assumed that the central part of the sample (initial “recipe” of cement paste or mortar) is hardly affected by the solution, with a very low amount (0.001 ml) of Na<sub>2</sub>SO<sub>4</sub> solution, while the outermost layer is in contact with a large amount (100 L) of Na<sub>2</sub>SO<sub>4</sub> solution. To link with the reality that CO<sub>2</sub> can be dissolved in the Na<sub>2</sub>SO<sub>4</sub> solution, 500 ppm of CO<sub>2</sub> was introduced in the simulation [16]. The same approach has been carried out in external sulfate attack to obtain the typical profiles of phase assemblages and ionic concentrations in the pore solution [5–7,17]. It was a fast approach since no transport equations need to be considered, but on the other hand, it should be noted that it is a profile imitating the real sample which is time- and depth-independent.

It must be underlined that this process assumes that the sulfate and sodium ions ingress into the sample in parallel. However, in reality, this is unlikely to happen, as the process is more likely dominated by the counter-movement of sulfate and hydroxide ions as shown in Fig. 6-2. But this is not too bad as the outwards movement of OH<sup>-</sup> in reality is imitated by raising significantly the solution volume to the amount that can similarly reduce the OH<sup>-</sup>, namely pH decreases in the exposed outer surface layer of the sample.



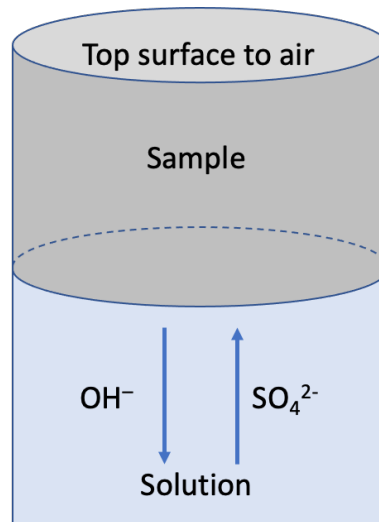


Fig. 6-2 The schematic diagram of the counter movement of sulfate and hydroxide ions in reality.

The details of the steps that have been adopted in the CemGEMS calculation for the profiles of phase assemblage are as follows:

- A. The construction of the cement pastes recipes (here is the example of PC paste, but CEM-LC3:xrf for LC<sup>3</sup> cement and CEM-III-B:xrf for slag Portland cement should be adapted when they were analysed in the simulations).
  1. Chose recipe template “CEM-I-OPC:xrf” from CemGEMS was taken, with a new name “OPC06-sulf50g\_L”.
  2. Equilibrated at 1 bar and 20 °C.
  3. Adapted to the same chemical composition as the cement used in this study. The modified cement composition according to Table 3-1.
  4. Modified SCM constituent additions according to Table 3-1, modified salts composition according to the chemical formula of Na<sub>2</sub>SO<sub>4</sub>, and salts amount to obtain 50 g/L or 3 g/L of Na<sub>2</sub>SO<sub>4</sub> at a given w/b ratio of 0.6.
  5. Equilibrated again, producing phase assemblage and C-S-H composition given in Table 6-1, and aqueous dissolved element concentrations in Table 6-2 (corresponding to 28 days hydration time).

Table 6-1 The solid phase assemblages of hydrated PC paste at w/c of 0.6.

Phase	Quantity/mol	Density g/cm <sup>3</sup>	Volume cm <sup>3</sup>	Enthalpy KJ/g	HeatCap J/K/g	Mass/g
Si-Hydrogarnet-ss	0.017	2.95	2.47	-12.23	0.98	7.31
C-N-K-S-H-ss	0.36	2.25	23.20	-14.30	1.32	52.29
Ettringite	0.0097	1.77	6.86	-13.97	1.73	12.11
monocarbonateH11	0.018	2.17	4.74	-14.52	1.54	10.28
Calcite	0.0097	2.71	0.36	-12.07	0.81	0.97
CH_Portlandite	0.32	2.24	10.67	-13.30	1.17	23.92
Hydrotalcite-OH	0.0050	2.01	1.11	-16.24	1.44	2.24

Table 6-2 Dissolved element concentrations in aqueous solution.

Species	Quantity/mol	Concentration mol/L	Mass/g
Ca <sup>2+</sup>	2.47e-5	8.54e-4	9.90e-4
K <sup>+</sup>	0.0043	0.15	0.17
Na <sup>+</sup>	0.0027	0.093	0.062
Mg <sup>2+</sup>	2.50e-12	8.63e-11	6.07e-11
OH <sup>-</sup>	0.0071	0.24	0.12
SO <sub>4</sub> <sup>2-</sup>	1.83e-5	6.33e-4	0.0018
SiO <sub>3</sub> <sup>2-</sup>	3.36e-7	1.16e-5	2.56e-5

B. The setting of process simulation steps, using the recipes mentioned above as parent systems.

1. Took process template “Leaching:Add-water” with name “OPC\_S\_50\_g\_L”.
2. Simulated the process.
3. Cloned the process, edit the sulfate solution concentration as 50 g/L by setting Na<sub>2</sub>SO<sub>4</sub> in the salts panel as 5 % mass, and H<sub>2</sub>O as 95 % mass, which gives the desired solution concentration as shown in Table 6-3.
4. Put the total amount of salt as 1 g, CO<sub>2</sub> in 500 ppm to simulate the realistic atmosphere.
5. Changed the target path from “/recipes/0/materials/2/Quantity” to “/recipes/0/materials/3/Quantity” as shown in Table 6-4.
6. Equilibrated the recipe.
7. Simulated the new process.
8. Plotted volumes of solids only (as shown in Fig. 6-3)

Table 6-3 The settings of the salt recipe.

Salts					
			1	g	1
	CO2		500	ppm	1
	Sea_salt		0	%mass	1
	NaCl		0	%mass	1
	Na2SO4		5	%mass	1
		Na2SO4	100	%mass	
	H2O		95	%mass	1
		H2O	100	%mass	

Table 6-4 The target path of the sulfate ingress process.

Process	Type	Ini Guess	Time	Stepping	Time	Time	Time	Time	Time
array ▶ 0 ▶ inputSpans ▶ 0 ▶ targetPath									
inputSpans [3]									
0 {10}									
Comment : Addition of Water from w/b = 1 to 1e4 in composition given in Water material									
InputSpan : Adding_Water									
lead : true									
numsteps : 121									
stepping : log10									
targetPath : qiao_recipes/CEM-I-OPC::xrf::Na2SO4_0.211M									
targetUnit : g									
valstart : 0.200000									
valstep : 0.040000									
valstop : 5.000000									
1 {9}									
2 {9}									
inputSpans__isExpanded : false									
parentTaskId : qiao_recipes/CEM-I-OPC::xrf::Na2SO4_0.211M									
processType : hydration									

The details of the steps that have been adopted in the GEM-Selektor calculation for the profiles of saturation index and crystallization pressure are as follows:

- C. Calculated the saturation index and then crystallization pressure.
  1. Cloned the recipe under the name “AFt-supersaturation-01”.
  2. Took the initial ettringite content in the equilibrated calculation, and suppressed the ettringite with the upper quantity limit in the process calculation.
  3. Equilibrated at 1 bar and 20 °C.
  4. Calculated SI according to the script of  $Fa[\{\text{ettringite}\}]$ .
  5. Calculated the crystallization pressure according to Equation 6-3, but replaced the SI value and the constants, the script of  $(Fa[\{\text{ettringite}\}])/0.4343*3.44$  was applied to calculate the pressure.

Fig. 6-3 shows the phase assemblages for Portland cement in contact with an increasing quantity of  $\text{Na}_2\text{SO}_4$  solution from the left to the right side. The profiles of phase assemblages and ionic concentration were obtained for these two different concentrations as used in experiments. The leaching process is imperative to simulate the sulfate degradation, as gypsum can only form in the leached zone where the pH is lower, which relates to the experimental observations. There is no gypsum formation when the process of “sulfate ingress” was applied in modelling.

Fig. 6-3 (a) and (c) show the phase assemblage simulated for the two sulfate concentrations of 10 and 50 g/L. There is a difference of the lowest sulfate concentration that can lead gypsum formation in the simulation: 10 g/L of sodium sulfate solution was the threshold instead of 3 g/L observed in the experiments.

On the left side, the initial phase composition is similarly observed as experiments in PC pastes, consisting of C-S-H, hydrotalcite, monocarbonate, portlandite, calcite, ettringite, and small amount of siliceous

hydrogarnet. It shows that there is a significant increase in the volume of ettringite precipitated when the AFm and portlandite start to be consumed. Gypsum can only form at a certain distance close to the exposed surface, when the pH is between 12 and 12.9 [18–20]. Moreover, the volume of gypsum formation is significantly higher when exposed to a highly concentrated solution. A greater amount of calcite forms on the right end where the sample surface is directly in contact with the  $\text{Na}_2\text{SO}_4$  solution as the  $\text{CO}_2$  is also introduced accompanied by the solution as the input to mimic the reality. The pH profile is also simulated, there is not much difference in the two concentrations as they are more governed by the leaching effect. pH decreases from  $\sim 13.5$  to 8 which links intimately with the presence of portlandite.

Fig. 6-3 (b) and (d) describe the ionic concentration in the pore solution as a function of the amount of sulfate solution (mimicking the depth of sulfate penetration in the experimental). The different levels of sulfate concentrations in pore solution are observed. In the exposure to 50 g/L solution, the sulfate concentration in pore solution is between 100 and 400 mmol/L in the degraded zone (starting from the maximum ettringite point to the outer surface), which can explain the more destructive fact since the high solution concentration of sulfate ions. The Ca concentration is higher in the pore solution when there is gypsum formation. In the bulk paste part where portlandite is present, there is a higher pH and lower Ca concentrations. Calcite formation from carbonation on the outer surface also increases the Ca concentrations.

However, in the exposure to 10 g/L solution (experimental 3 g/L is adapted to 10 g/L to have gypsum formation in modelling), the sulfate concentration in pore solution is all in the range of 1 to 70 mmol/L, and gypsum only forms above the concentration 50 mmol/L which is slightly higher than 10 mmol/L what was found experimentally [21,22]. Na concentration in Fig. 6-3 d) is quite constant around 100 mmol/L which is much lower than 500 mmol/L that in Fig. 6-3 b). Moreover, Ca concentration reaches higher than 10 mmol/L when the presence of small gypsum formation is observed. The thermodynamic calculations of ionic concentrations give not only the changes of sodium and sulfate concentrations, but also the other relevant elements in the pore solution which are quite important to understand the degrading processes of local chemistry.

The pore solution chemistry is of great importance to calculate the crystallization pressure of the ettringite formation, which is carried out with a different approach as introduced in the next section.

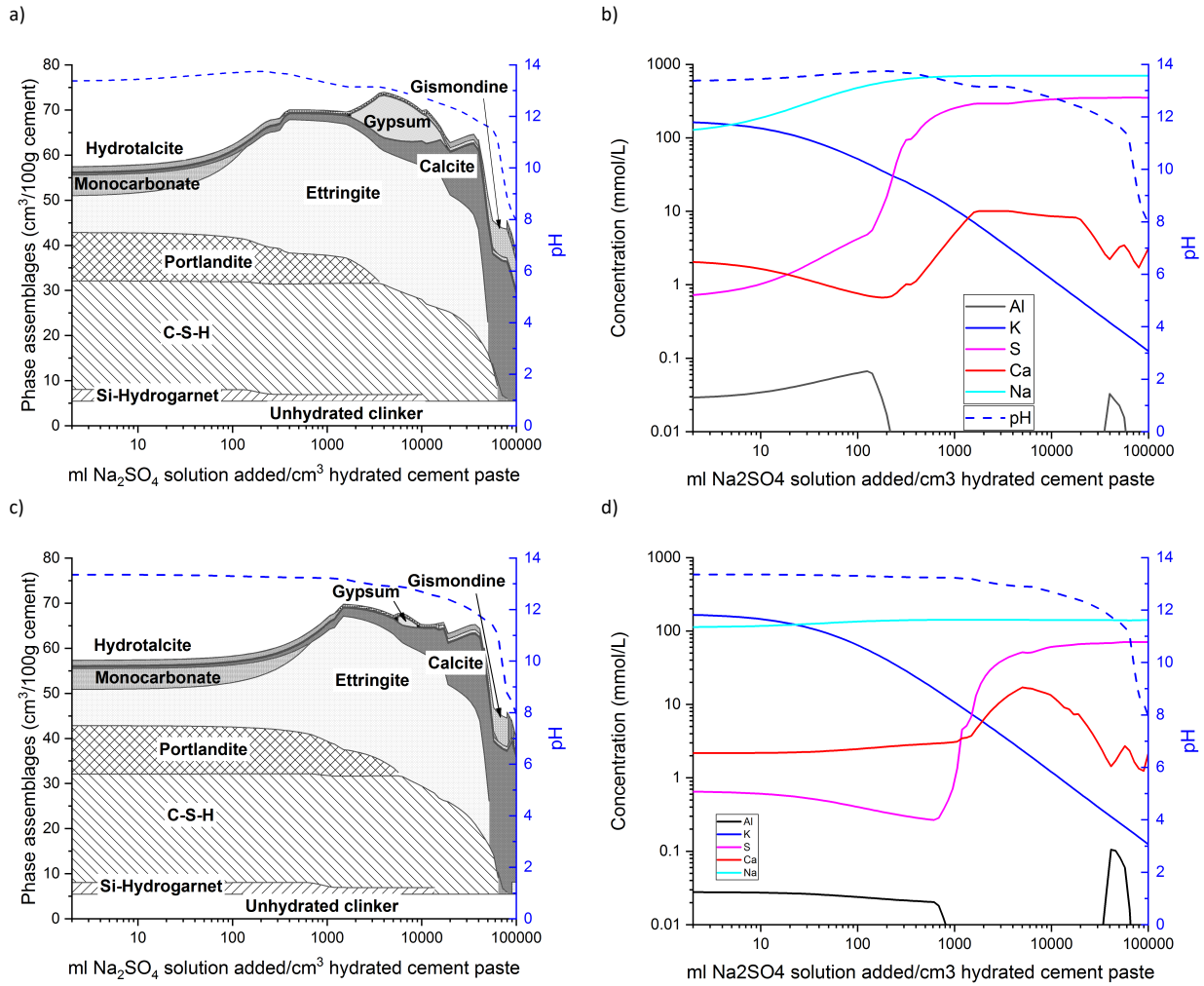


Fig. 6-3 Profiles of phase assemblages and ionic concentrations of the Portland cement paste samples contact with (a) & (b) 50 g/L Na<sub>2</sub>SO<sub>4</sub> and (c) & (d) 10 g/L Na<sub>2</sub>SO<sub>4</sub> solution, CO<sub>2</sub> concentration is 500 ppm for both cases.

### 6.3.2 Saturation index from ettringite

If we allow the phase to form freely as we described above in equilibrium conditions, there will be no saturation index of ettringite that can be simulated from GEMS.

Equation 6-1 defines the ionic activity product of ettringite IAP, and saturation index  $SI = IAP/K_{so}$ .

Equation 6-1

$$\frac{IAP}{K_{so}} = \frac{(a_{Ca^{2+}})^6 \cdot (a_{Al(OH)_4^-})^2 \cdot (a_{OH^-})^4 \cdot (a_{SO_4^{2-}})^3 \cdot (a_{H_2O})^{26}}{K_{Ettringite}}$$

But we can obtain the maximum saturation index with respect to monosulfoaluminate, the maximum activity of Ca<sup>2+</sup> and SO<sub>4</sub><sup>2-</sup> is defined by the solubility of gypsum. So the SI of ettringite can be referred as in Equation 6-2 [5]. The upper limit for the saturation index is based on the literature [14], 10<sup>6.48</sup> at 25 °C. To simulate the coexistence of gypsum and monosulfoaluminate, we should limit the ettringite formation by consuming

these two phases. In the calculation, the quantity of ettringite formation is kept constant as the initial amount before the exposure to Na<sub>2</sub>SO<sub>4</sub> solution.

Equation 6-2

$$SI_{max} = \frac{K_{Ms}K_{Gp}^2}{K_{s0,Et}} a_{H_2O}^{16} = 10^{6.48}$$

The initial hydration equilibrium state was simulated based on the cement chemical composition used in the experiments. The amount of ettringite in 0.0030 mol due to hydration was obtained. To obtain the oversaturation of ettringite while the sulfate is penetrating, this initial amount of ettringite was treated as the upper limit which does not allow any additional ettringite formation although there is more sulfate ingress in the pore solution, hence the pore solution is oversaturated with respect to ettringite.

Instead of getting a profile of increased ettringite amount from the central part to the outer surface, the constant ettringite amount equivalent to the initial state was profiled. To obtain a comparable result with the experimental, the calculation of the saturation index was consistent with the concentrations used experimentally (3 g/L and 50 g/L). Gypsum and monosulfate coexisted to provide the oversaturation with respect to ettringite in the pore solution. Moreover, the profile of logSI of ettringite was also obtained in each step and then included as blue lines in Fig. 6-4. The maximum logSI reaches 6.9 where gypsum is present. This value is slightly higher than that mentioned in Equation 6-2 because the calculation was conducted at 20 °C which is lower than the reference one which was done at 25 °C [14].

If the higher upper limit (the value 0.040 mol was obtained from the maximum ettringite amount can be detected by SEM mapping, more details can be found in appendix) was applied to the same process, the different saturation index profiles can be found as shown in Fig. 6-5. The maximum saturation index is found only with a minor difference of 1, which does not account for very different macro damage.

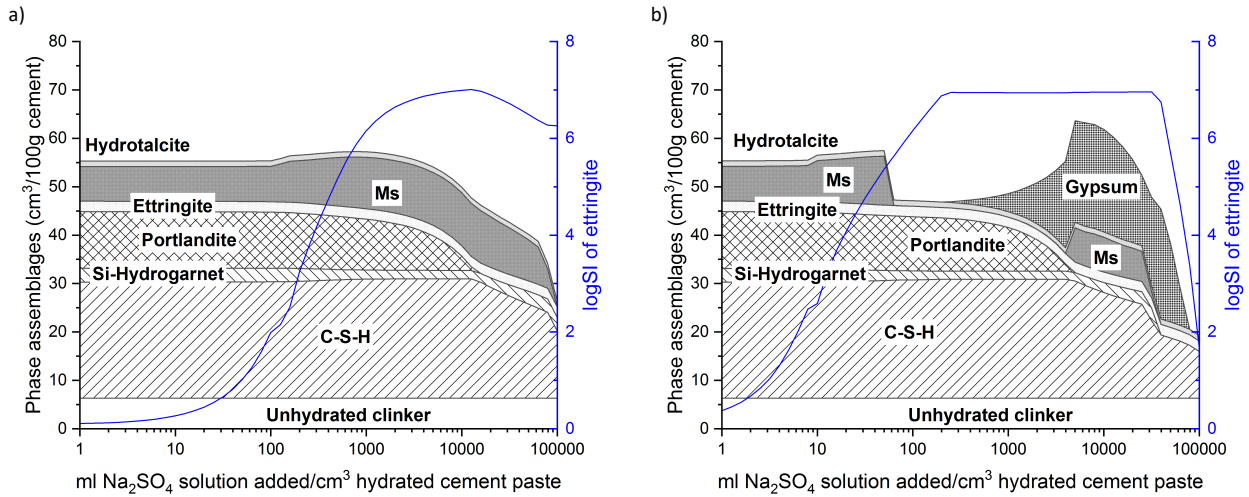


Fig. 6-4 Simulated phase assemblages and saturation index (blue lines) for a) PC exposed at 3 g/L, b) PC at 50 g/L  $\text{Na}_2\text{SO}_4$  solution, ettringite formation is suppressed by upper limit of 0.0030 mol.

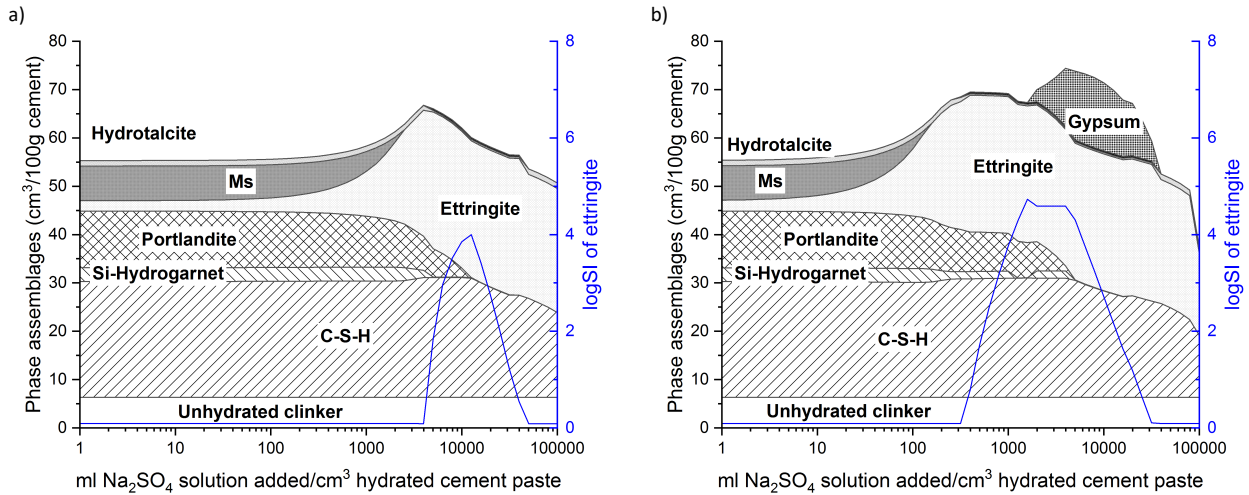


Fig. 6-5 Simulated phase assemblages and saturation index (blue lines) for a) PC exposed at 3 g/L, b) PC at 50 g/L  $\text{Na}_2\text{SO}_4$  solution, ettringite formation is suppressed by upper limit of 0.040 mol.

## 6.4 Estimation of the crystallization pressure profile of ettringite

### 6.4.1 Crystallization pressure from experimental

Experimentally, the sulfate concentration was deduced from the S/Si ratio in C-S-H using the relation between S/Si and the concentration of  $\text{SO}_4^{2-}$  [21] in pore solution as shown in Fig. 6-6. The  $\text{SO}_4^{2-}$  concentration in pore solution was deduced from the experimental data obtained from SEM-EDS analysis on C-S-H gel. It is an estimation as the pore solution chemistry cannot be practically obtained by the experimental inductively coupled plasma spectroscopy method. To simplify the calculation of supersaturation of a solution to ettringite formation as given in Equation 6-1, we assume the activity product of other relevant ions ( $\text{Ca}^{2+}$ ,  $\text{Al}(\text{OH})_4^-$ ,  $\text{OH}^-$ , and water activity) in the pore solution does not change in the sulfate ingress process. The initial concentration of  $\text{SO}_4^{2-}$  (37.5 mmol/L) in pore solution was estimated based on the same relationship (see Fig.

6-6) in the reference sample before sulfate ingress (PC06 paste at 28 days hydration). The higher  $\text{SO}_4^{2-}$  concentration (when the S/Si is more than 0.35 beyond the scale of this referred plot below) was extrapolated by the linear relationship (when the S/Si is more than 0.1) between S/Si on C-S-H and  $\text{SO}_4^{2-}$  concentration in pore solution.

Therefore,  $Q=IAP$  is given by  $[\text{current } \text{SO}_4^{2-}]^3$ , and  $K=K_{s0}$  is given by  $[\text{equilibrated } \text{SO}_4^{2-}]^3$ . Then the crystallization pressure is calculated by Equation 6-3.

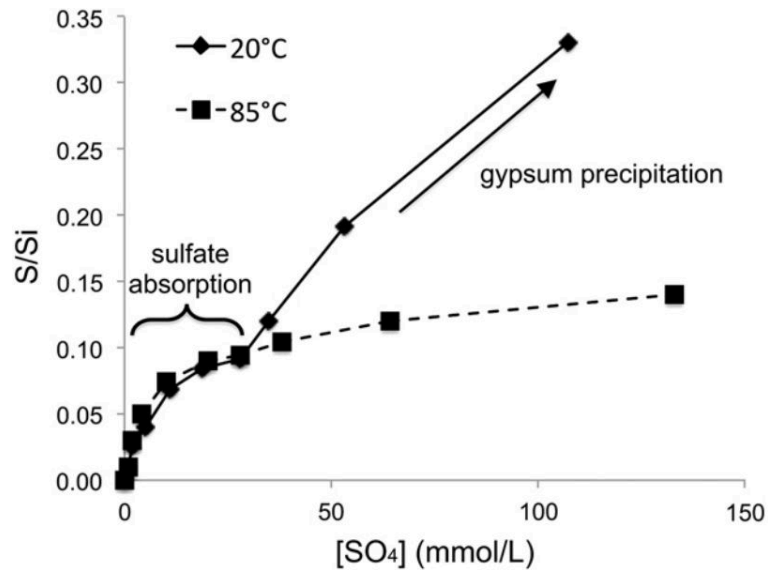


Fig. 6-6 Sulfate absorbed on synthetic C-S-H as a function of the sulfate concentration of the solution at 20 and 85 °C, adapted from [21].

Equation 6-3

$$P = \frac{R_g T}{V_{crystal}} \ln \left( \frac{IAP}{K_{s0}} \right)$$

Where the constants  $R_g$  is  $8.314 \text{ m}^3 \cdot \text{Pa} \cdot \text{K}^{-1} \cdot \text{mol}^{-1}$ ,  $T$  is the temperature in K of 293.15 K,  $V_{crystal}$  is the molar volume of ettringite of  $708 \text{ cm}^3/\text{mol}$ ,  $IAP$  is ionic activity product of ettringite,  $K_{s0}$  is solubility product of ettringite. The degree of supersaturation is defined by the ratio of  $IAP/K_{s0}$ .

Fig. 6-7 shows the example of the profile of atomic ratio S/Si on C-S-H gel in the sample of PC06-3g-148d. The grey baseline was obtained from the reference sample PC06 at 28 days of hydration.



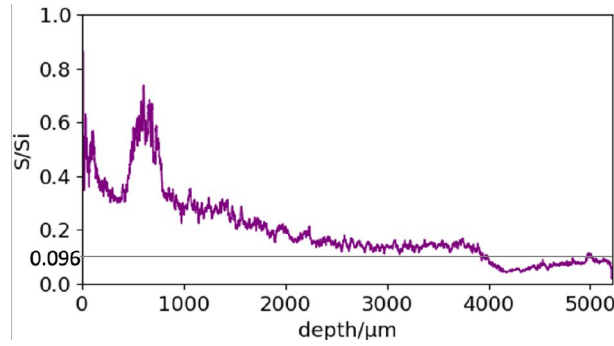


Fig. 6-7 Profile of atomic ratio of S/Si on C-S-H gel in the PC06 paste after 148 days exposure to sulfate solution with a concentration of 3 g/L.

In the example of 3 g/L solutions in PC06 as shown in Fig. 6-8,  $K_{so}$  is simplified as the  $SO_4^{2-}$  concentration in the bulk of 37.5 mmol/L in the reference sample, and IAP is simplified as  $SO_4^{2-}$  concentration of maximum at 130 mmol/L at the depth where the maximum of S/Si was obtained from C-S-H. The degree of supersaturation IAP/ $K_{so}$  is calculated as 3.5, and pressure  $P$  is calculated as 12.9 MPa. In the case of 50 g/L, the pressure profile was similarly obtained as discussed here.

$$\ln\left(\frac{IAP}{K_{so}}\right) = \ln\left(\frac{130^3}{37.5^3}\right) = 3 \times \ln\frac{130}{37.5} = 3 \times \ln 3.5, \quad P = 3.44 \times 3 \times \ln 3.5 = 12.9 \text{ MPa}$$

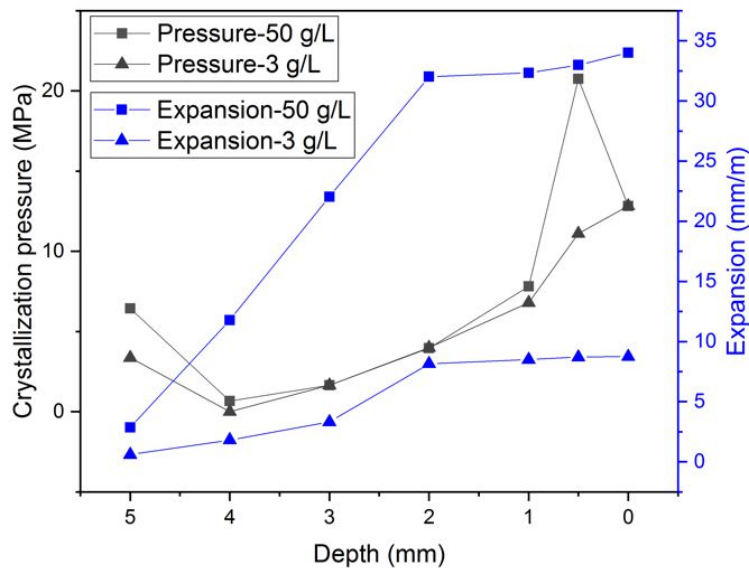


Fig. 6-8 The calculated crystallization pressure from ettringite formation by experimental in cement pastes of PC06 exposed to 3 and 50 g/L  $Na_2SO_4$  solution.

The maximum calculated pressure from 50 g/L is around 20 MPa, and the maximum pressure of 3 g/L is around 12 MPa. They are compared with the flexural strength of mortars with the same w/c of 0.6 which is 7.97 MPa. This can probably explain why the more extensive cracks are always observed in the higher concentration case, while the big cracks do not occur in the lower concentration. The pressure from crystallization will be destructive and initiate cracks only when the pressure is beyond the mechanical restraint of the materials. Large pressure leading to high expansion is the intrinsic mechanism.

### 6.4.2 Crystallization pressure calculated from saturation index

Fig. 6-9 shows the crystallization pressure profiles obtained from the modelling based on the logSI with respect to ettringite by suppressing additional ettringite formation. Two upper limits are applied here according to the calculation of saturation index in section 6.3.2.

From the simulation, the crystallization pressure was calculated by  $P = \log SI / 0.4343 * 3.44$ , based on the information of all the relevant ionic concentrations as displayed in Equation 6-1 and Equation 6-3.

The profile of the modelling result is not related directly to the depth of sulfate ingress as shown in the experimental, but it can be related to the experimental result to deduce experimental observations (i.e., maximum pressure is located at the exposed surfaces where the gypsum is present, which is associated with the experimental pressure of the depth 0 mm). In Fig. 6-9 a), the upper limit for both cases show the same level of theoretical pressure close to the outer surfaces, but they decrease quite fast towards the inner part where the sample is almost not affected by sulfate solution. However, the one with a higher sulfate concentration at 50 g/L can impact a higher distance close to the core of the sample. However, the simulated crystallization pressure profile from GEMS is way too high because it is the upper limit of the supersaturation that can be generated in the pore solution, but the real crystallization pressure is closely related to the pore size, interfacial energy, and the volume in pore network affected by crystallization stress.

In Fig. 6-9 b), the maximum exerted pressure is lower with the higher upper ettringite limit. It shows the minor difference between two sulfate concentrations, which may be not sufficient to account for the significant difference which was observed in the extent of the damage.

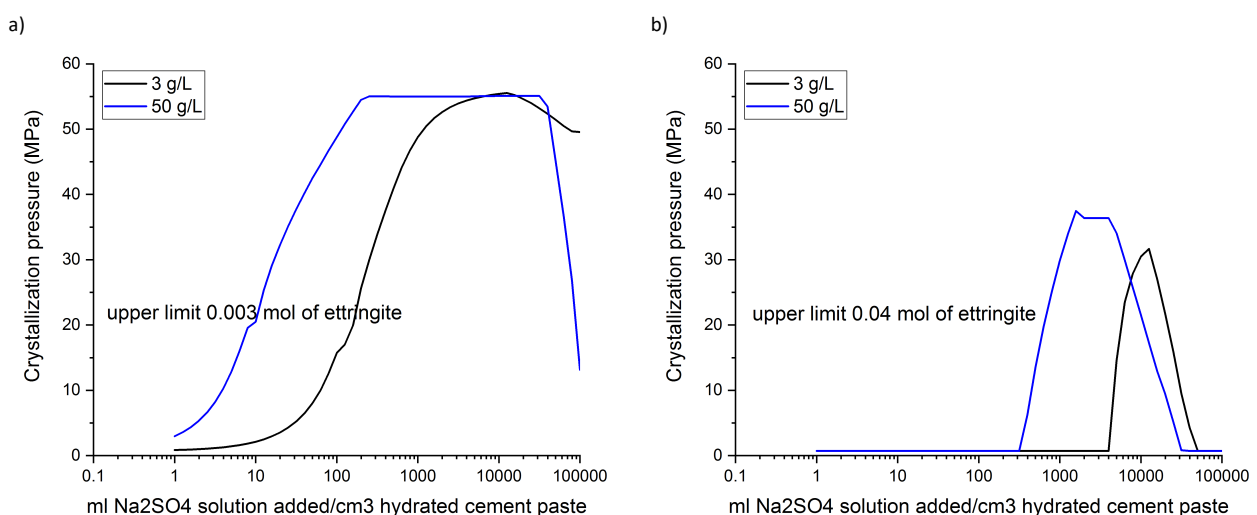


Fig. 6-9 The calculated crystallization pressure from ettringite formation by thermodynamic modelling in Portland cement pastes exposed to 3 and 50 g/L  $\text{Na}_2\text{SO}_4$  solution, a) low upper limit 0.003 mol of ettringite, b) high upper limit 0.04 mol of ettringite.

### 6.4.3 The link between crystallization pressure development and macroscopic observations

The detectable damage is not only related to the crystallization pressure that is generated from ettringite formation. The theoretical pressure is higher than the real case because that shows the upper bound on the pressure generated by a crystal inside the pores from the supersaturation. But the actual pressure exerted depends on many factors (interfacial free energy, pore size, the volume fraction of ettringite, etc). There is always free porosity which can accommodate additional ettringite without causing any damage as indicated in Equation 6-4, the supersaturation can only be maintained in the small pores which are due to the increased interfacial free energy of smaller crystals [23]. Therefore, it shows that the crystallization stress is low in large pores [8].

Equation 6-4

$$\gamma_{CL}k_{CL} = \frac{R_g T}{V_c} \ln \left( \frac{IAP}{K_{so}} \right)$$

Where  $K_{so}$  is the equilibrium solubility for a macroscopic crystal,  $IAP$  is the ion activity product with a smaller crystal,  $\gamma_{CL}$  is the interfacial free energy,  $k_{CL}$  is the curvature,  $R_g$  is the gas constant,  $T$  is the absolute temperature.

The link between expansion and the estimated pressure from theory is much more complicated than it is simply shown in Fig. 6-8. The mechanical resistance of the materials should be also considered to interpret the occurrence of the cracks in actual cases which is discussed in *Chapter 7*. A sufficient amount of ettringite has to be taken into account because the visible fracture appears only when the stress field propagates in a relatively large region (comparable in size to the strength-controlling flaws) of the network [8]. The link is shown below by the combined analysis of the phenomenological from macroscopic observations and the crystal growth theory on a microscopic scale as discussed in the theory part before.

Fig. 6-10 shows the BSE images at the different magnifications from PC06 pastes, and the microstructure of the samples before and after the large expansion is compared. In the period of low expansion corresponding to Fig. 6-10 a), the paste matrix is much densified but without parallel cracks occurring. It relates to the latent period when the microstructure is expanded (very small micro cracks in Fig. 6-10 c)) without visible detection on the macroscale. Individual cracks around the ettringite cluster are obviously seen on a micro-scale and they are quite limited present. It also implies that the dominant ettringite formation is in the non-harmful large pores so far. Therefore, it seems that the individual stress exerted from ettringite crystallization cannot significantly agglomerate yet. However, the large cracks with the presence of gypsum are observed prominently in Fig. 6-10 b), particularly, the massive connected cracks are clearly seen in the higher magnification

× 4000 Fig. 6-10 d). The large expansion is already observed in this period, it is the crystallization stress field forming in a sufficient region that can cause macro damage.

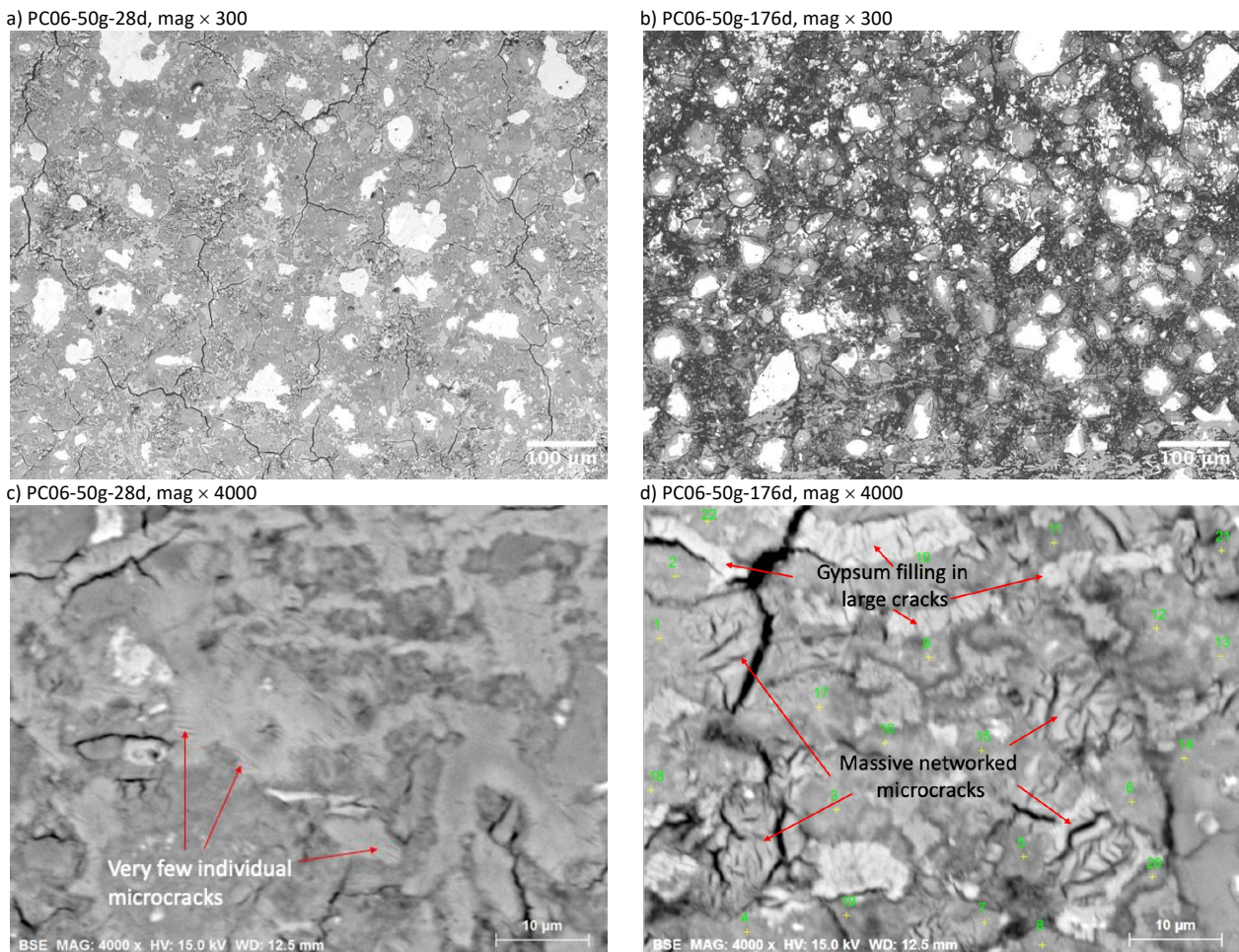


Fig. 6-10 The BSE images from SEM at the different magnification scales from PC pastes, a) before the large macroscopic expansion of PC06-28d, mag × 300, b) after the large macroscopic expansion of PC06-176d, mag × 300, c) before the large macroscopic expansion of PC06-28d, mag × 4000, d) after the large macroscopic expansion of PC06-176d, mag × 4000.

## 6.5 Salt crystallization of sodium sulfate in the carbonated and drying front

The formation of thenardite/mirabilite needs a very high concentration to precipitate from the supersaturated solution, which can be easily obtained from the evaporation process. The lower relative humidity is currently not possible to be simulated from GEMS (some thermodynamic data is still missing), so the main phase assemblages and pore solution environment were modelled to predict the susceptibility of salt crystallization in different cement pastes in the carbonated cement paste matrix.

Carbonation in the presence of sulfate solution at a concentration of 50 g/L for PC, SPC, and LC<sup>3</sup> cement pastes was simulated. The pore solution information was calculated to predict the susceptibility of salt crystallization in the similarly observed degree of carbonation found experimentally.

This section talks about the potential damage of physical sulfate attack, phase assemblages and pore solution chemistry obtained from GEMS, which are then linked to the experimental results in the drying zone. However, the important difference here is that the low RH is not simulated in GEMS which does not show exactly the same environment as we saw evaporation in experimental conditions. At the first attempt, only a normal temperature of 20 °C was considered in this section.

### 6.5.1 Susceptibility of salt crystallization in Portland cement

The phase assemblages on the drying front with CO<sub>2</sub> exposure and sulfate solution present are shown in Fig. 6-11. Phase assemblage and pore solution chemistry were obtained that can be linked with the evaporation zone in the unidirectional experimental approach. The sulfate concentration in pore solution is simulated with an increasing amount of CO<sub>2</sub> ingress (from 0 to 70 g) from interior cement paste (initial cement hydrates composition) to outer surfaces in contact with CO<sub>2</sub>. In the simulated profiles, two different sulfate concentrations were also incorporated which can link with the two experimental situations (3 and 50 g/L of Na<sub>2</sub>SO<sub>4</sub> solution).

Fig. 6-11 a) and c) show the significant phase volume changes due to carbonation in the presence of Na<sub>2</sub>SO<sub>4</sub> solution with 50 and 3 g/L, respectively. The maximum capacity of CO<sub>2</sub> bound is around 45 g/100 g cement for both cases. In the totally carbonated cement paste, most hydrates decomposed to give mainly calcite, gypsum, silica hydrates and Al-hydroxide. For the case of 50 g/L, there is a higher volume of gypsum and gismondine present than that in the case of 3 g/L.

More importantly, Fig. 6-11 c) and d) show the profiles of ionic concentrations in pore solution. The sulfate concentration in pore solution increases as more CO<sub>2</sub> is consumed by the different cement hydrates and reaches the highest concentration at 45 g CO<sub>2</sub> added when the carbonation is complete. A slight difference between the two exposed conditions was still seen: 700 mmol/L of sulfate concentration in the case of 50 g/L, and 500 – 600 mmol/L in the case of 10 g/L. The Na concentration is also higher in the case of 50 g/L: 700 mmol/L versus that in the range between 200 to 300 mmol/L in the case of 10 g/L. Therefore, the pore solution chemistry in the high concentration case is more prone to supersaturation with respect to sodium sulfate crystallization if a similar degree of carbonation is reached. The pH profile is also plotted, showing a profound drop as more CO<sub>2</sub> is introduced, which links with the phase stability. The pH continues to decrease as more calcite forms from the decomposition of hydrates, the value decreases from 13.5 to 5.

If we link this simulated phase content profile with the quantitative results from X-ray diffraction and SEM/EDS long maps, the effects of carbonation can be simulated in GEMS. Gypsum can only form above ~ 32 g of added CO<sub>2</sub> and there is a high sulfate concentration in pore solution above 100 mmol/L. However, gypsum was not identified in both cases of 3 and 50 g/L in the drying front by experimental SEM-EDS or XRD

which implies the sulfate concentration in pore solution is not able to reach saturation with gypsum (the degree of carbonation found experimentally should be lower than 32 g CO<sub>2</sub>). So it is not likely to see thenardite formation either as it is much more soluble than gypsum, which means at least gypsum forms first then thenardite might form. Evaporation is not simulated in GEMS to cause supersaturation with respect to thenardite which requires the Pitzer aqueous activity model.

Gypsum can be somehow considered as the precursor of thenardite formation, as the former needs a much lower concentration of sulfate. If there is no gypsum detected experimentally, we can deduce that thenardite must not be precipitated either. Then the damage from the physical sulfate attack is not (yet) able to occur.

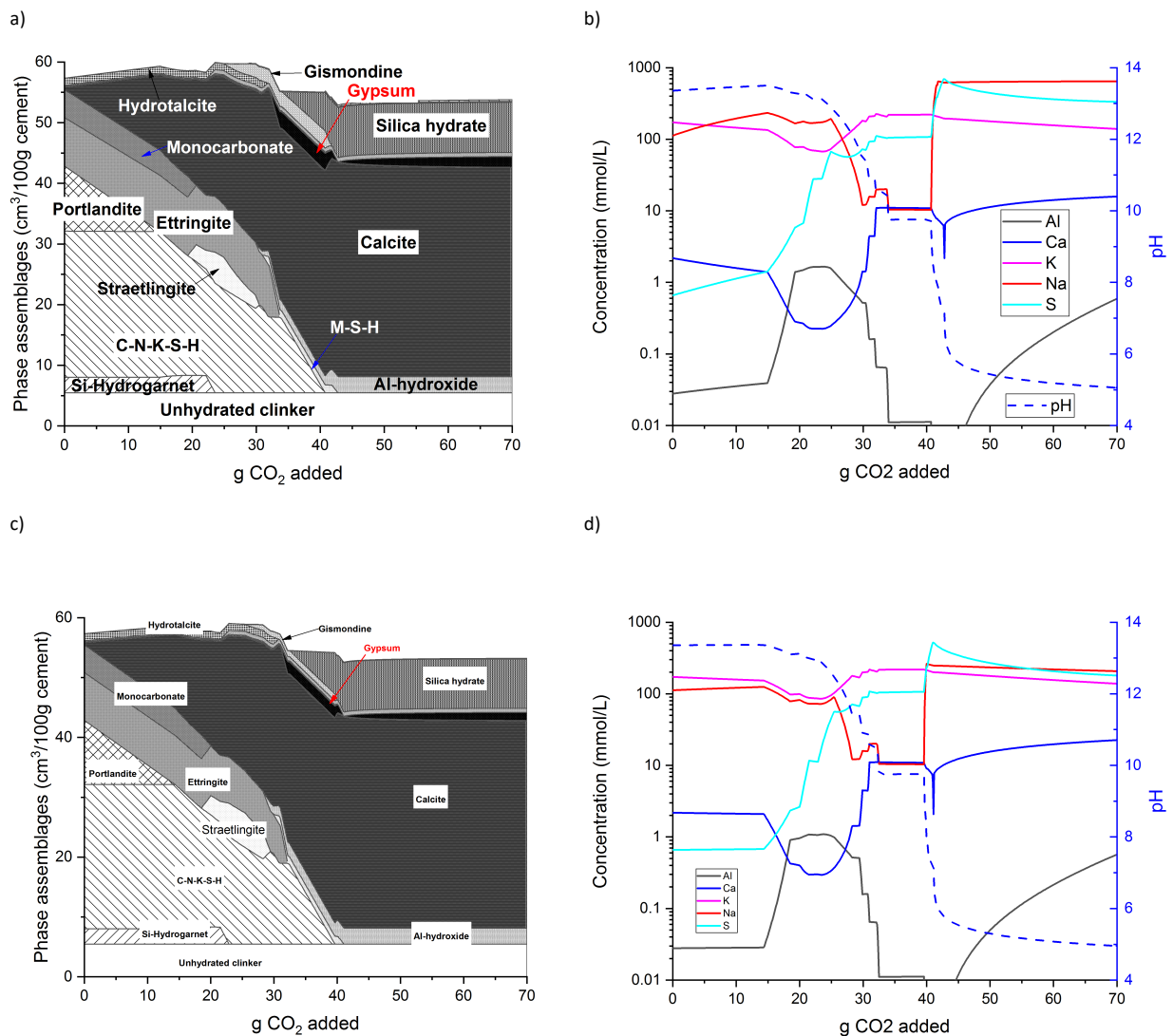


Fig. 6-11 Profiles of phase assemblages and ionic concentrations of the Portland cement paste samples contact with (a) & (b) 50 g/L Na<sub>2</sub>SO<sub>4</sub> and (c) & (d) 3 g/L Na<sub>2</sub>SO<sub>4</sub> solution with an increasing external CO<sub>2</sub> content ingress.

### 6.5.2 Comparisons between different cement pastes with 50 g/L Na<sub>2</sub>SO<sub>4</sub> in porewater

Fig. 6-12 for PC, LC<sup>3</sup> and SPC cement pastes at 20 °C. The simulation was done up to a CO<sub>2</sub> level of 70 g, sodium sulfate concentration is set as 50 g/L.

Portlandite is sometimes still found experimentally in PC systems after carbonation which shows the carbonation is not complete. Therefore, decalcification and carbonation in the calcium/sulfate-bearing phase are not that prominent, which potentially provides more sulfate in pore solution to form gypsum in PC. However, in SPC and LC<sup>3</sup> systems, because of the lack of portlandite hence the capacity to bind CO<sub>2</sub> is reduced. That can trigger the carbonation of other Ca-bearing phases, such as AFms, ettringite, and C-S-H. Therefore, the release of sulfate in the pore solution is enhanced, which provides supersaturation with respect to gypsum formation.

Gypsum formation was found experimentally in SPC and LC<sup>3</sup> cement pastes which confirms the Ca and S source in pore solution is abundant. It is consistent with the modelling results when the carbonation degree is of 20 – 25 g bound CO<sub>2</sub>. Gypsum formation in blended cement pastes that demonstrates the lack of Ca in systems incorporated with SCMs is not likely the reason to suppress the ettringite/gypsum formation and cause expansion.

If we assume the same amount of CO<sub>2</sub> (20–25 g bound CO<sub>2</sub>) is bound by calcium-bearing hydrates (which link with the gypsum presence experimentally) for these three cement pastes, the ionic concentration (particularly, Ca, S, Na) in pore solution can be compared in these different systems.

Specifically in PC cement paste as shown in Fig. 6-12 b), sulfate concentration is in the range of 6 – 70 mmol/L, Ca concentration is below 1 mmol/L, and Na concentration is between 100 and 200 mmol/L. In LC<sup>3</sup> cement paste as shown in Fig. 6-12 d), sulfate concentration is much higher in the range of 100 – 500 mmol/L (that is provided by the presence of gypsum), Ca is around 10 mmol/L, Na is in the range of 10 – 400 mmol/L (the lower limit is perhaps due to the high absorption of alkali ions on the surface of low Ca/Si in C-S-H gel). In SPC cement paste as shown in Fig. 6-12 f), sulfate concentration is in the range of 70 – 400 mmol/L which is just slightly lower than that in LC<sup>3</sup> paste, Ca is around 10 mmol/L, Na is in the range of 10 – 400 mmol/L the same as that in LC<sup>3</sup> paste. From the pore solutions, a similar aqueous environment was provided in SPC and LC<sup>3</sup> pastes hence the ultimate susceptibility of salt crystallization with respect to thenardite/mirabilite was predicted similarly.

Therefore, the susceptibility of thenardite crystallization attack is more severe in the highly concentrated pore solution with respect to Na and S because the pressure is highly dependent on the supersaturation degree that can be reached [24,25]. Finally, the exerted pressure due to thenardite/mirabilite crystallization is much higher in SPC and LC<sup>3</sup> systems than that in PC.

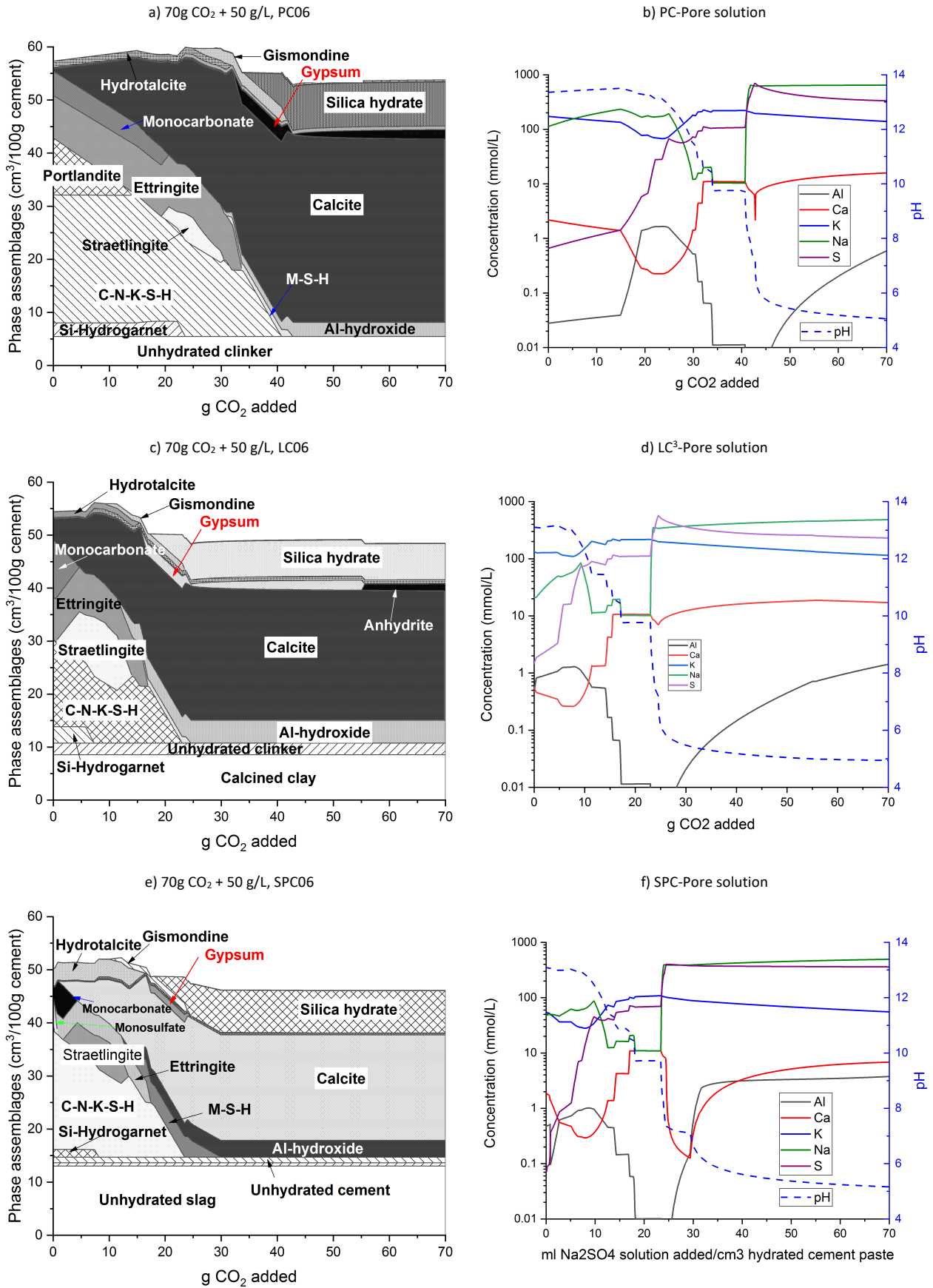


Fig. 6-12 Changes of phase assemblages and pore solution due to carbonation when 50 g/L sulfates are present in various cement pastes, a) and b) for PC paste, c) and d) for LC<sup>3</sup> paste, e) and f) for SPC paste.



## 6.6 Conclusions

- The estimation of ettringite crystallization pressure in Portland cement after sulfate exposure provides the quantitative value of  $\sim 55$  MPa (upper ettringite limit is 0.003 mol) and 36 MPa or 30 MPa (upper ettringite limit is 0.04 mol) by modelling, calculated pressure from experimental data of 20 MPa versus 12 MPa, with two sulfate concentrations. The higher pressure is predicted from GEMS because it shows the maximum supersaturation degree.
- The approach to calculate the saturation index and crystallization pressure is an estimation, but it provides a good agreement between thermodynamic modelling and the experimental observations, indicating the presence of the gypsum is a key parameter which limits the supersaturation with respect to ettringite. The massive large cracks appear when there is abundant gypsum found in the experimental observations.
- The actual expansion/damage is not simply related to the maximum crystallization pressure, but more importantly associated with the condition of ettringite formation (i.e., pore size) and sufficient ettringite volume fraction.
- Physical sulfate attack is less susceptible in Portland cement paste by the pore solution analysis of the crystallization of sodium sulfate. Gypsum presence gives the high sulfate concentration provided in the pore solution of SPC and LC<sup>3</sup> materials due to carbonation, high Na<sub>2</sub>SO<sub>4</sub> concentration provides higher Na concentration in the pore solution. The qualitative simulations by GEMS show that the susceptibility of sodium sulfate crystallization damage is higher in SPC and LC<sup>3</sup> blended cement pastes, which agrees well with the experimental findings from *Chapter 5*.

## 6.7 References

- [1] C. Yu, W. Sun, K. Scrivener, Mechanism of expansion of mortars immersed in sodium sulfate solutions, *Cement and Concrete Research*. 43 (2013) 105–111. <https://doi.org/10.1016/j.cemconres.2012.10.001>.
- [2] Jan Skalný, Jacques Marchand, Ivan Odler, *Sulfate Attack on Concrete*, London and New York, 2002. [https://www.bookdepository.com/Sulfate-Attack-on-Concrete-J.-Marchand/9780419245506?redirected=true&utm\\_medium=Google&utm\\_campaign=Base5&utm\\_source=CH&utm\\_content=Sulfate-Attack-on-Concrete&selectCurrency=CHF&w=AF72AU9SLSQSCQA803VV&pdg=pla-293946777986:kwd-293946777986:cmp-1578060869:adg-65091841852:crv-296436506046:pid-9780419245506:dev-c&gclid=EA1aIQobChMlzbvA6M-a4gIViuR3Ch0tjw8TEAYYASA-BEgJUXPD\\_BwE](https://www.bookdepository.com/Sulfate-Attack-on-Concrete-J.-Marchand/9780419245506?redirected=true&utm_medium=Google&utm_campaign=Base5&utm_source=CH&utm_content=Sulfate-Attack-on-Concrete&selectCurrency=CHF&w=AF72AU9SLSQSCQA803VV&pdg=pla-293946777986:kwd-293946777986:cmp-1578060869:adg-65091841852:crv-296436506046:pid-9780419245506:dev-c&gclid=EA1aIQobChMlzbvA6M-a4gIViuR3Ch0tjw8TEAYYASA-BEgJUXPD_BwE) (accessed May 14, 2019).
- [3] P.K. Mehta, Mechanism of expansion associated with ettringite formation, *Cement and Concrete Research*. 3 (1973) 1–6. [https://doi.org/10.1016/0008-8846\(73\)90056-2](https://doi.org/10.1016/0008-8846(73)90056-2).
- [4] M.D. Cohen, Theories of expansion in sulfoaluminate - type expansive cements: Schools of thought, *Cement and Concrete Research*. 13 (1983) 809–818. [https://doi.org/10.1016/0008-8846\(83\)90082-0](https://doi.org/10.1016/0008-8846(83)90082-0).
- [5] L. Caneda-Martínez, W. Kunther, C. Medina, M.I. Sánchez de Rojas, M. Frías, Exploring sulphate resistance of coal mining waste blended cements through experiments and thermodynamic modelling, *Cement and Concrete Composites*. 121 (2021) 104086. <https://doi.org/10.1016/j.cemconcomp.2021.104086>.
- [6] W. Kunther, B. Lothenbach, J. Skibsted, Influence of the Ca/Si ratio of the C–S–H phase on the interaction with sulfate ions and its impact on the ettringite crystallization pressure, *Cement and Concrete Research*. 69 (2015) 37–49. <https://doi.org/10.1016/j.cemconres.2014.12.002>.
- [7] B. Lothenbach, B. Bary, P. Le Bescop, T. Schmidt, N. Leterrier, Sulfate ingress in Portland cement, *Cement and Concrete Research*. 40 (2010) 1211–1225. <https://doi.org/10.1016/j.cemconres.2010.04.004>.
- [8] G.W. Scherer, Crystallization in pores, *Cement and Concrete Research*. 29 (1999) 1347–1358. [https://doi.org/10.1016/S0008-8846\(99\)00002-2](https://doi.org/10.1016/S0008-8846(99)00002-2).
- [9] W. Kunther, Investigation of Sulfate Attack by Experimental and Thermodynamic Means, PhD Thesis, EPFL, 2012. <https://doi.org/10.5075/epfl-thesis-5263>.
- [10] D. Min, T. Mingshu, Formation and expansion of ettringite crystals, *Cement and Concrete Research*. 24 (1994) 119–126. [https://doi.org/10.1016/0008-8846\(94\)90092-2](https://doi.org/10.1016/0008-8846(94)90092-2).
- [11] R.J. Flatt, G.W. Scherer, Thermodynamics of crystallization stresses in DEF, *Cement and Concrete Research*. 38 (2008) 325–336. <https://doi.org/10.1016/j.cemconres.2007.10.002>.
- [12] D.A. Kulik, F. Winnefeld, A. Kulik, G.D. Miron, B. Lothenbach, CemGEMS – an easy-to-use web application for thermodynamic modelling of cementitious materials, *RILEM Technical Letters*. 6 (2021) 36–52. <https://doi.org/10.21809/rilemtechlett.2021.140>.
- [13] K. Dmitrii, Gibbs Energy Minimization Software for Geochemical Modeling, (n.d.). <https://gems.web.psi.ch/>.
- [14] B. Lothenbach, D.A. Kulik, T. Matschei, M. Balonis, L. Baquerizo, B. Dilnesa, G.D. Miron, R.J. Myers, Cemdata18: A chemical thermodynamic database for hydrated Portland cements and alkali-activated materials, *Cement and Concrete Research*. 115 (2019) 472–506. <https://doi.org/10.1016/j.cemconres.2018.04.018>.
- [15] D.A. Kulik, Improving the structural consistency of C–S–H solid solution thermodynamic models, *Cement and Concrete Research*. 41 (2011) 477–495. <https://doi.org/10.1016/j.cemconres.2011.01.012>.
- [16] Characteristic lengths of the carbonation front in naturally carbonated cement pastes: Implications for reactive transport models, *Cement and Concrete Research*. 134 (2020) 106080. <https://doi.org/10.1016/j.cemconres.2020.106080>.
- [17] W. Kunther, B. Lothenbach, K. Scrivener, Influence of bicarbonate ions on the deterioration of mortar bars in sulfate solutions, *Cement and Concrete Research*. 44 (2013) 77–86. <https://doi.org/10.1016/j.cemconres.2012.10.016>.
- [18] R. Ragoug, O.O. Metalssi, F. Barberon, J.-M. Torrenti, N. Roussel, L. Divet, J.-B. d’Espinose de Lacaillerie, Durability of cement pastes exposed to external sulfate attack and leaching: Physical and chemical aspects, *Cement and Concrete Research*. 116 (2019) 134–145. <https://doi.org/10.1016/j.cemconres.2018.11.006>.
- [19] K. Sotiriadis, M. Hlobil, A. Viani, P. Mácová, M. Vopálenský, Physical-chemical-mechanical quantitative assessment of the microstructural evolution in Portland-limestone cement pastes exposed to magnesium sulfate attack at low temperature, *Cement and Concrete Research*. 149 (2021) 106566. <https://doi.org/10.1016/j.cemconres.2021.106566>.
- [20] F.E. -mail: frank bellmann@bauing.uni-weimar.de Bellmann, B. Moeser, J. Stark, Influence of sulfate solution concentration on the formation of gypsum in sulfate resistance test specimen, *Cement and Concrete Research*. 36 (2006). <https://doi.org/10.1016/J.CEMCONRES.2005.0>.
- [21] R. Barbarulo, H. Peycelon, S. Leclercq, Chemical equilibria between C–S–H and ettringite, at 20 and 85 °C, *Cement and Concrete Research*. 37 (2007) 1176–1181. <https://doi.org/10.1016/j.cemconres.2007.04.013>.
- [22] M.A. González, E.F. Irassar, Ettringite formation in low C3A Portland cement exposed to sodium sulfate solution, *Cement and Concrete Research*. 27 (1997) 1061–1071. [https://doi.org/10.1016/S0008-8846\(97\)00093-8](https://doi.org/10.1016/S0008-8846(97)00093-8).
- [23] G.W. Scherer, Stress from crystallization of salt, *Cement and Concrete Research*. 34 (2004) 1613–1624. <https://doi.org/10.1016/j.cemconres.2003.12.034>.
- [24] C. Rodriguez-Navarro, E. Doehne, Salt weathering: influence of evaporation rate, supersaturation and crystallization pattern, *Earth Surface Processes and Landforms*. 24 (1999) 191–209. [https://doi.org/10.1002/\(SICI\)1096-9837\(199903\)24:3<191::AID-ESP942>3.0.CO;2-G](https://doi.org/10.1002/(SICI)1096-9837(199903)24:3<191::AID-ESP942>3.0.CO;2-G).
- [25] C. Rodriguez-Navarro, E. Doehne, E. Sebastian, How does sodium sulfate crystallize? Implications for the decay and testing of building materials, *Cement and Concrete Research*. 30 (2000) 1527–1534. [https://doi.org/10.1016/S0008-8846\(00\)00381-1](https://doi.org/10.1016/S0008-8846(00)00381-1).

# Chapter 7 Discussion

## Contents

<b>7.1</b>	<b>Introduction .....</b>	<b>155</b>
<b>7.2</b>	<b>Porosity measured by mercury intrusion porosimetry (MIP) .....</b>	<b>156</b>
<b>7.3</b>	<b>Mechanical strength .....</b>	<b>159</b>
<b>7.4</b>	<b>The interaction between porosity and strength in controlling expansion/cracking.....</b>	<b>162</b>
<b>7.5</b>	<b>Water adsorption and desorption .....</b>	<b>163</b>
7.5.1	Sulfate ingress versus water adsorption .....	165
<b>7.6</b>	<b>The interplay between chemical and physical attack.....</b>	<b>165</b>
<b>7.7</b>	<b>Comments on the observed physical sulfate attack in this project .....</b>	<b>166</b>
<b>7.8</b>	<b>References.....</b>	<b>167</b>

## 7.1 Introduction

In this Chapter, the physical properties of cement pastes/mortars on porosity, mechanical strength, and water adsorption/desorption are discussed. We try to link these to the degradation behaviour that we found experimentally and in the thermodynamic modelling.

Capillary porosity contributes to the capillary rise action which is the dominant mechanism of sulfate degradation considered in this project. It was found that the concrete with a low w/c ratio showed higher sulfate resistance [3–7] as they slow down effectively the sulfate ingress, which supports the prescription of low w/c ratio in standards [8]. It is likely that the strength of the concrete also plays a big role in resisting the expansive stress and reducing the damage [9–11]. However, the interaction between these two factors, porosity and strength, is not yet well understood. It is not clear if one or the other is dominant in affecting sulfate degradation.

Porosity was characterised on cement paste samples by MIP, as pastes can be measured more reliably and the interaction with sulfate ions mainly concerns the cement paste (aggregates are inert in the process of sulfate ingress). Mechanical strength (EN 196-1) and water adsorption/desorption (ASTM C1585-13) were carried out on mortar samples as required by standard methods, and the details can be found in the experimental *Chapter 3*. In *Chapter 4*, it was shown that Portland cement mortars and pastes show similar degradation patterns. We also found that physical attack had similar features in mortars and pastes: the spalling started from a relatively small region, then it propagated over the entire surface and at greater depths from the outer surface. However spalling damage was greatly delayed if the mortars were used instead of pastes due to the two times of sample thickness. This indicates that the use of pastes for the characterisation of porosity is reasonable.

The relative water adsorption and desorption rates were conducted in cementitious mortars in a one-dimensional approach. It gives a qualitative indication of the susceptibility to subflorescence or efflorescence which takes place inside or outside the materials. The simple characterization of intrinsic physical property of mortars is discussed in terms of the potential for physical sulfate attack.

As discussed in *Chapter 6*, we know that porosity is a very important factor affecting the crystallization pressure and the continuous propagation of the stress field in the network before creating any visible cracking. However, the role of cement strength on the occurrence of expansion and cracks is still not clearly understood and not decoupled from porosity. As the inclusion of SCMs in blended systems and even more complexity, the effect of porosity and strength of PC systems are discussed in this chapter.

## 7.2 Porosity measured by mercury intrusion porosimetry (MIP)

In this chapter, four cement systems are discussed in terms of two aspects: chemical and physical sulfate attack. The terminologies included such as Portland cement (PC), sulfate-resisting cement (HS), slag Portland cement (SPC), and limestone calcined clay cement (LC<sup>3</sup>).

Fig. 7-1 a) shows the total porosity by MIP for the different systems with w/c ratios of 0.4 and 0.6. The capillary pores vary from diameters of 10 nm to 1  $\mu\text{m}$  (pore size classification based on [12]). The total porosity increased in the order PC03 (9.29 %), PC04 (15.57 %), HS04 (16.24 %), SPC04 (16.27 %), LC04 (17.17 %), PC06 (25.05 %), LC06 (29.71 %), HS06 (31.74 %), SPC06 (34.99 %). The trend at w/b=0.4 shows how SPC and LC<sup>3</sup> materials have finer capillary porosity compared with PC pastes, although the total porosity in the blended system is higher.

Fig. 7-1 b) shows the critical pore entry diameters that are the most frequently occurring radius for the interconnected pores that allow percolation of chemical species through the cement pastes [13]. It is the radius of the largest sphere that can freely pass through the cement paste so that it controls the permeability of the cement pastes [14]. In the same cement paste, the critical pore size decreases as the w/c ratios decrease. The critical pore size in blended systems shows smaller values than in PC pastes. The critical pore size should play a key role in the build-up of crystallization pressure, which leads to cracking as suggested by Scherer [15], an interconnected network must build sufficient stress to permit the crystals to pass through the smaller pores. Therefore, the pore size distribution can influence the kinetics of sulfate ingress and the ultimate extent of deterioration.

The porosity shows a similar effect on sulfate expansion and degradation as the factor of strength which is discussed in the next part, with finer porosity of cement pastes, a lower extent of degradation was found. However, porosity and strength are coupled factors (low porosity shows high strength), and the question of which one is the dominant factor in controlling sulfate expansion and damage is discussed in the next sections.

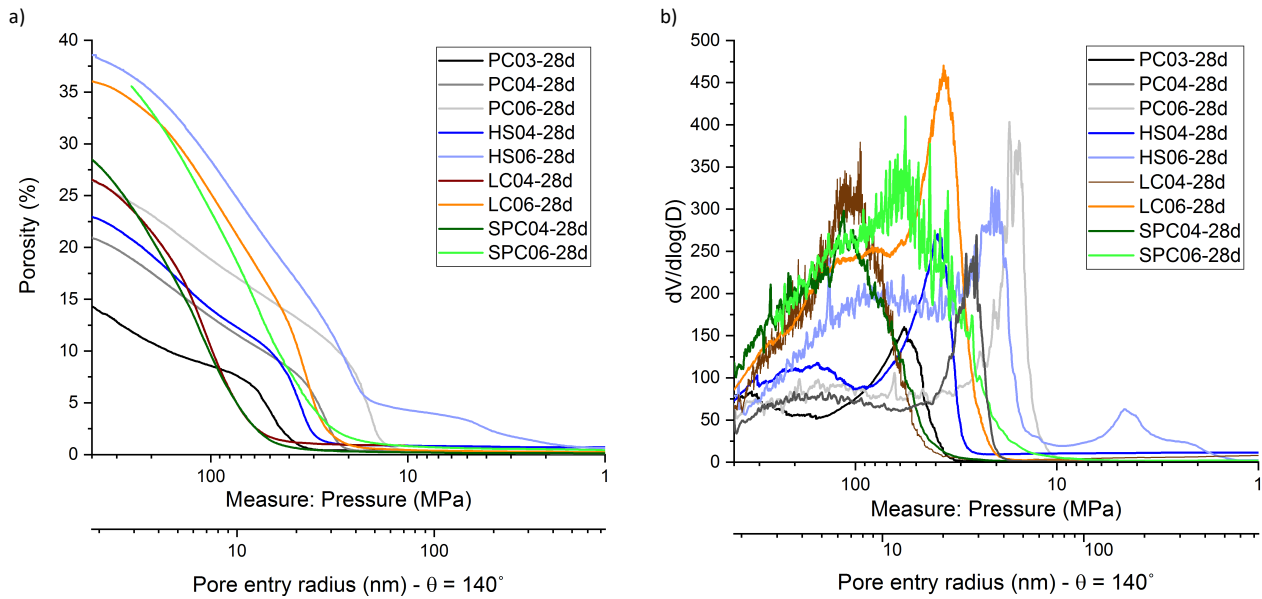


Fig. 7-1 Pore size distribution of different cement pastes with various w/c ratios, a) cumulative porosity, b) differential distribution curves.

First of all, if we link the sulfate ingress with the role of porosity, we can see the qualitative and quantitative sulfur fronts as shown in Fig. 7-2.

The images of sulfate ingress front are compared for different w/c ratios at 3 g/L  $\text{Na}_2\text{SO}_4$  solution in Fig. 7-2. The sulfate ingress depth increases as the increase of w/c ratio, and the thicker gypsum band is observed at the higher w/c ratio. This indicates the sulfate advances more easily and penetrates deeper into the sample to react with the AFm hydrates in the case of w/c ratio of 0.6. There is little cracking in any of these systems at this stage, which indicates that strength does not play a role. The dominant factor is higher total porosity and larger critical pore size, faster sulfate ingress.

Before we see large cracks, the sulfate ingress is not only controlled by porosity, but also by the transformable AFm phase content available in the bulk, this binding effect is often overlooked.

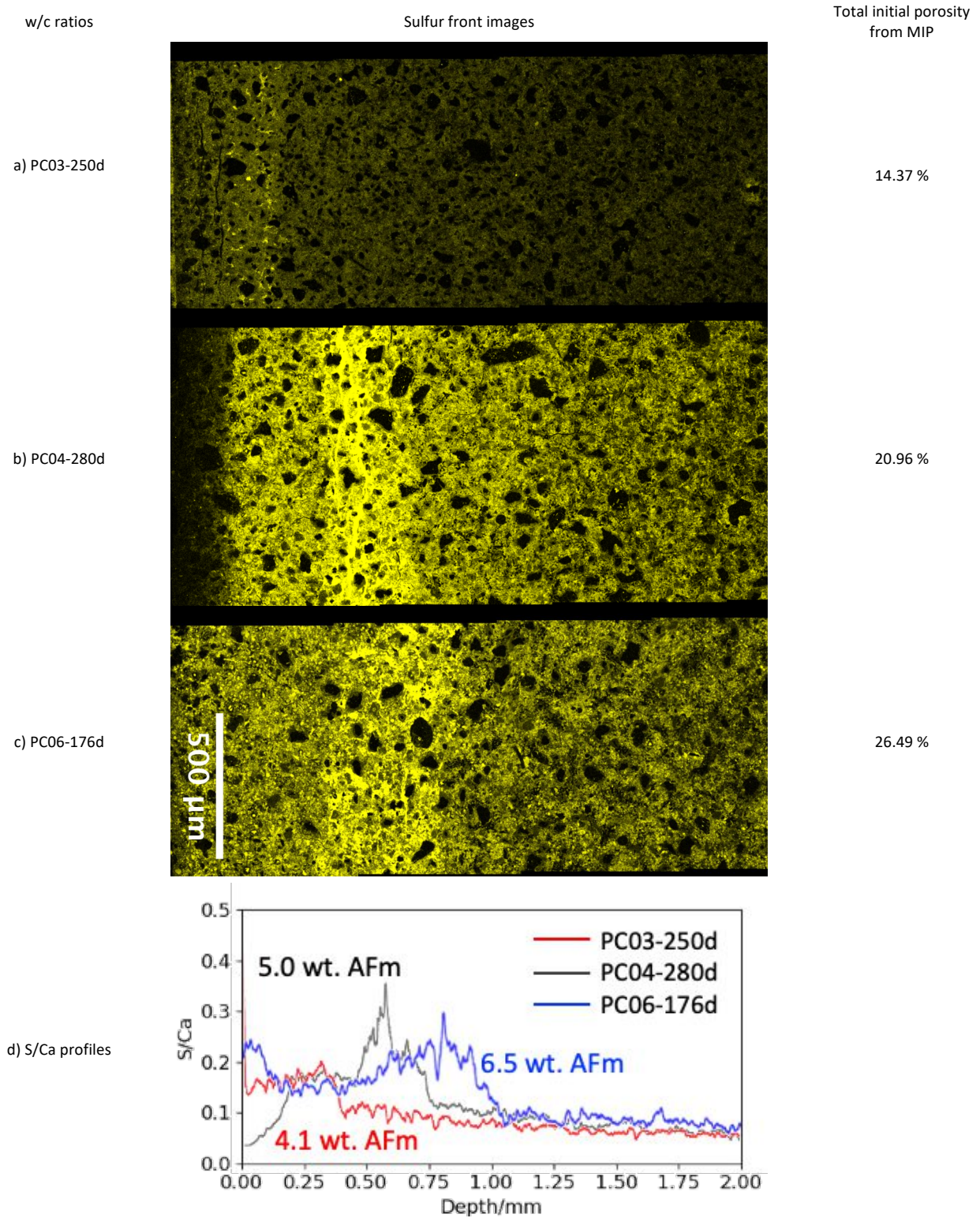


Fig. 7-2 The sulfate penetration graphs and profiles on the bottom layer of depth of ~0-2 mm from Portland cement pastes with different w/c ratios at the same sulfate concentration of 3 g/L. a) PC03-250d, b) PC04-280d, c) PC06-176d, d) sulfate penetration profiles as S/Ca ratios of these three systems.

The transformable AFm hydrates can slow down the sulfate ingress because only when they are completely consumed by external sulfates, the sulfate can again penetrate further through the pore solution. The AFm

mass contents for these three PC systems are 4.1, 5.0, and 6.5 wt. % as indicated in Fig. 7-2 d). Although there is not much difference among them, it is expected to show an increasing order of sulfur buffering capacity: PC03 < PC04 < PC06. However, from the sulfate ingress profile shown in Fig. 7-2 d), the effect of the sulfur buffering capacity by AFm content is outweighed by the higher porosity, which shows the increasing ingress depth as the porosity increases from PC03 (0.3 mm) to PC06 (1.1 mm). Moreover, the somewhat shorter exposure age at 176 days of PC06 still shows higher ingress depth than the other samples with lower w/c ratios at 250 and 280 days, which strengthens the conclusion that the porosity plays a larger role than the transformable AFm contents do.

### 7.3 Mechanical strength

Fig. 7-3 shows the mechanical strength of different mortar samples at 28 days. The lower w/c gives the higher mechanical strength. Mortar samples with a w/c of 0.6 show a similar flexural strength in all systems which implies it is less dependent on the cement compositions.

With a low w/c ratio, the detectable damage from either chemical sulfate attack or from salt crystallization attack is largely suppressed in the cement paste samples. But does the damage suppression come from the lower porosity or higher strength in the lower w/c ratio? In this section, we look at the samples exposed to the higher sulfate concentration as these cases show more damage.

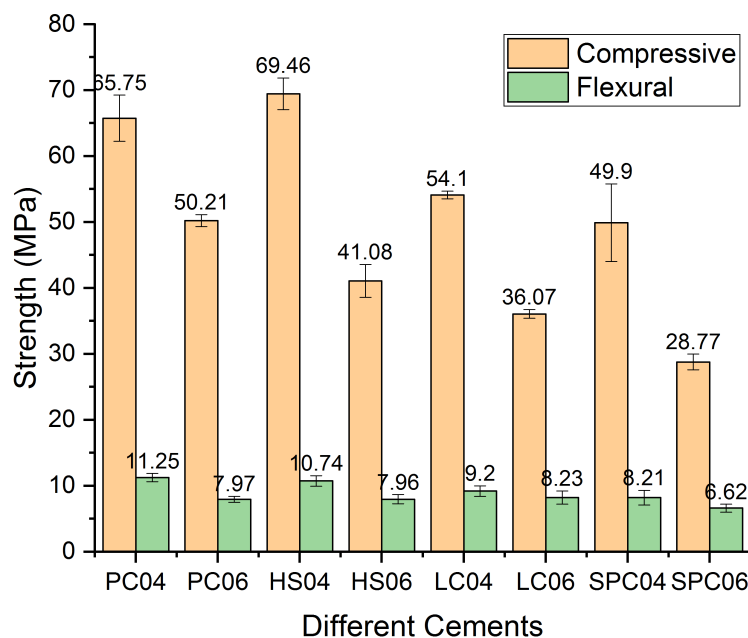


Fig. 7-3 Compressive and flexural strength at 28 days for mortar samples made with different cements.

First of all, the damage extent observed visually from the appearance is discussed. There are some photos shown in Fig. 7-4 to demonstrate the extent of the cracking in PC and HS cement systems, only the samples



exposed to 50 g/L are taken for the comparison. At the same w/c ratio of 0.6, showing the appearance of cracks after sulfate exposure as the similar flexural strength in these two mortars are present, which provides similar mechanical restraint against the exerted pressure by ettringite. The low w/c ratio of 0.4 shows that higher strength results in lower damage with less extensive cracks. The smaller expansion and damages observed from chemical sulfate attack in blended systems complicates the understanding of the role of the strength factor on the damage extent. Therefore, the discussion of the factor strength is based on the PC pastes only.

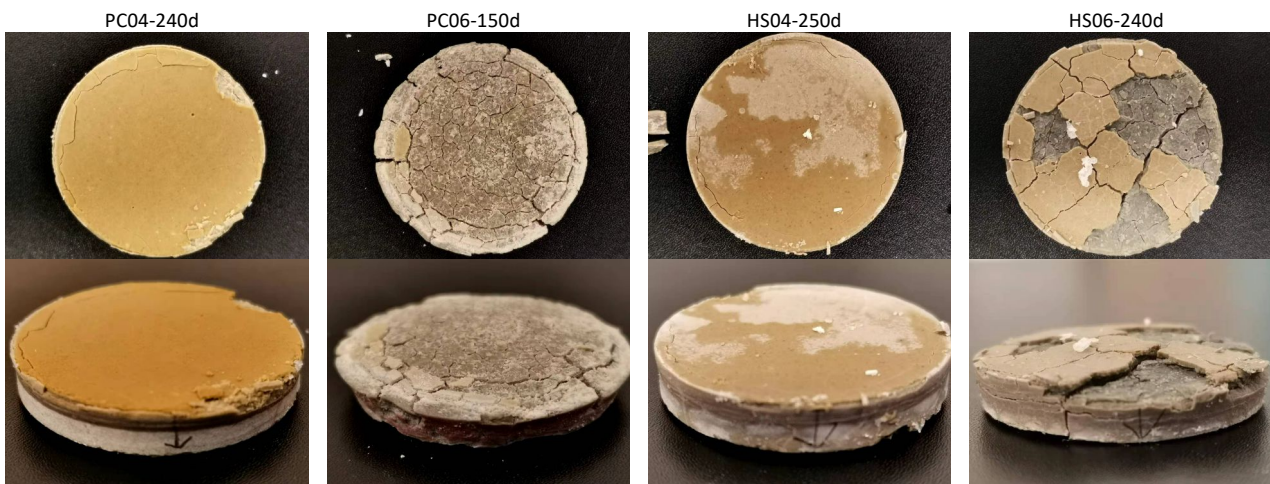


Fig. 7-4 The comparison of cracking extent of the bottom surfaces in PC04 and PC06 pastes after sulfate exposure.

Fig. 7-5 shows sulfate ingress profiles of the PC samples at the different w/c and the high sulfate exposure solution. It also shows the higher S/Ca ratio above 0.4 as observed in Fig. 7-5 d), which implies that the higher sulfate concentration at each depth layer is bound in the gypsum and ettringite phases in the case of high concentration. More interestingly, at the lowest w/c of 0.3 the sulfate ingress is still limited (same as in the 3 g/L case), but there is much more extensive cracking due to the higher crystallisation pressure. The comparison of the 0.4 and 0.6 w/c indicates these have similar depths of sulfate ingress, but the 0.6 sample shows much more extensive cracking due to its lower flexural strength.

The depth that sulfate penetrated at 50 g/L in PC06 increases from 1.1 mm which was observed at 3 g/L to 1.5 mm, which is due to the newly formed perpendicular cracks that facilitate further the sulfate ingress apart from the initial high porosity effect. The cracks perpendicular to the surface connecting the parallel cracks are only observed in PC06 system indicating that the mechanical integrity of the material is lost and cracks grow and connect relatively free. Parallel cracks are also observed in PC03 and PC04, but they are still in a quite good shape which does not allow the material to fall apart attributed to the higher mechanical restraint. Particularly, PC03 shows the lowest cracking in a relatively thin and small region (still quite close to the

bottom surfaces in contact with the solution). Because the lower porosity and higher strength of PC03 control the sulfate ingress and cracking growth, respectively.

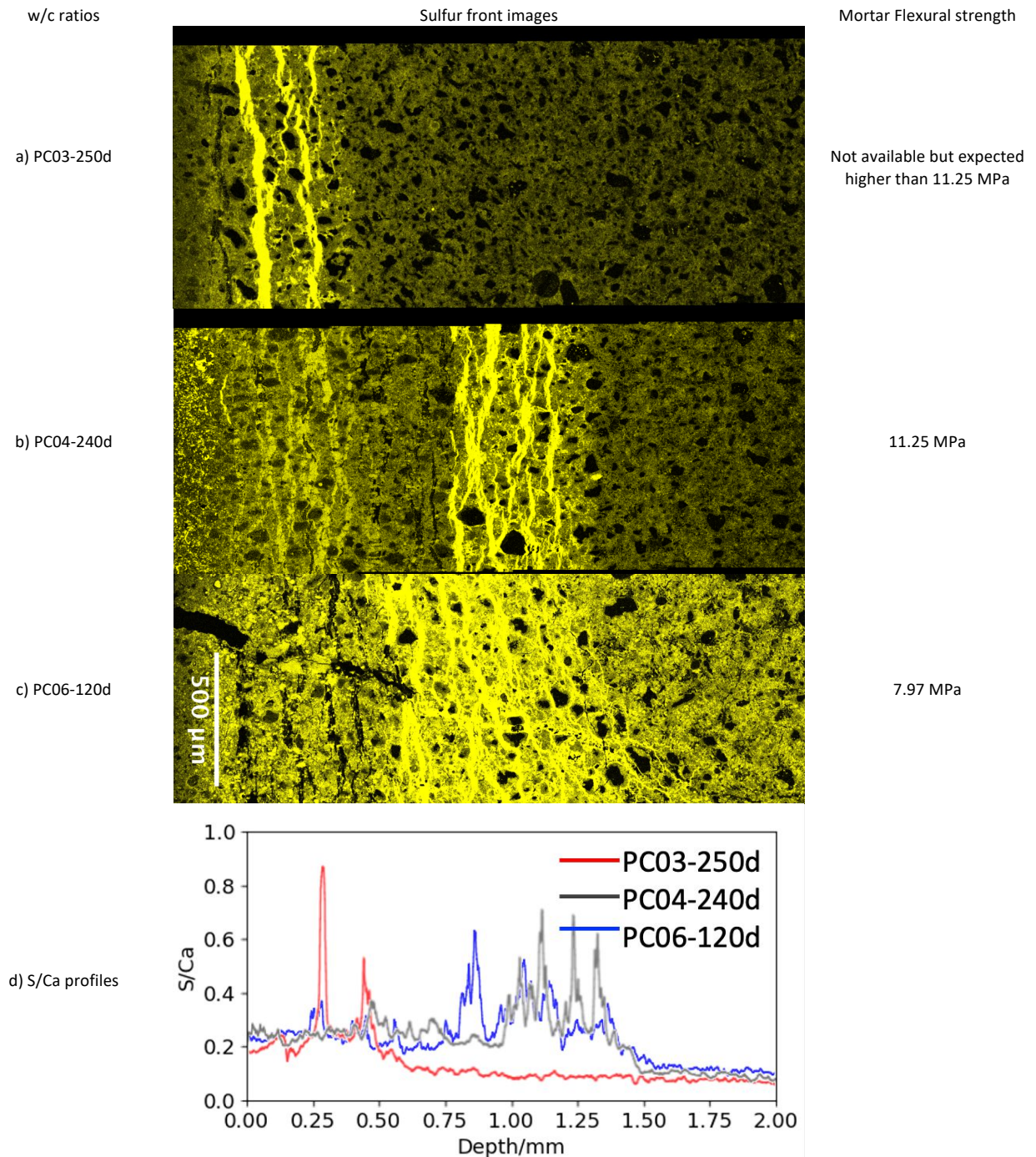


Fig. 7-5 The sulfate penetration graphs and profiles on the bottom layer of depth of ~0-2 mm from Portland cement pastes with different w/c ratios at the same sulfate concentration of 50 g/L. a) PC03-250d, b) PC04-240d, PC06-120d d) sulfate penetration profiles as S/Ca ratios of these three systems.

## 7.4 The interaction between porosity and strength in controlling expansion/cracking

Attention should be paid to interpreting the sulfate ingress fronts under external sulfate attack, as these are complicated by the formation of cracks which allow unimpeded ingress of sulfate. Damage will also depend on the overall size of the specimen as the expanding parts of a paste sample have to overcome the restraint from the interior unaffected parts before we see a significant expansion and cracking [16].

Based on the previous discussion on the factor of porosity and strength, they are interacting in the process of sulfate degradation. In this section, we observe these two factors together in a more comprehensive way and link them with the macro damage from the experiment.

Fig. 7-6 shows the depth that sulfate penetrated in the PC and HS cement pastes versus the detected expansion. Sulfate ingress depth increases as the exposure time increases in the same cement systems, but the time is not shown in the plot for the less complexity. Sulfate ingress is associated with the transformable AFm hydrates and porosity. When sulfate penetrates into the cement in pore solution, it can react with the transformable AFm hydrates and slow down the sulfate ingress until all the AFm hydrates are transformed into ettringite. Then the sulfate concentration in the pore solution is increased and sulfate ions continue penetrating further.

From graph Fig. 7-6 below, the expansion seems to increase when the sulfate has penetrated to a certain depth at  $\sim 3$  mm. No matter what is the w/c (i.e., different porosity), expansion starts increasing significantly as sulfate penetrates further above the depth of 3 mm at this stage. The porosity is a key factor to control the expansion under a relatively low level because the affected layer (3 mm in this case) is key to triggering the expansion and more points below 3mm are associated with the systems of w/c ratio 0.4.

Before the large expansion ( $> 10$  mm/m), the small sulfate ingress depth ( $< 3$  mm) can suppress the expansion because the bulk inner unaffected zone provides the restraint to expansion. It shows the importance of sufficient affected depth from the surface to initiate the expansion.

After the depth of  $\sim 3$  mm, the larger expansion ( $> 10$  mm/m) can be triggered, usually, the cracks appear in this stage. In these larger expanded samples, the cracks appear as the crystallization pressure surpasses the strength of the cement material. It is consistent with the concept that was proposed in *Chapter 6* where the crystal growth kinetics were discussed, the expansion initiation needs a sufficient stress field that is networked from the microstructure to the macro-scale. After the expansion initiation point, the extent of the cracking is only dependent on the mechanical restraint from the host materials. Higher expansion accompanied with larger cracking is observed only in the cement pastes with lower strength. The samples with high strength (such as PC04 and HS04) can indeed expand when the sulfate ingress surpasses 3 mm, but they show

much less expansion because there are fewer extensive cracks occurring in these systems. Therefore, in this period, strength is more important than porosity to control the further dramatic degradation. Because low porosity in the samples with w/c of 0.4 cannot stop the further ingress above 3 mm, which is the threshold depth the cracking can be triggered.

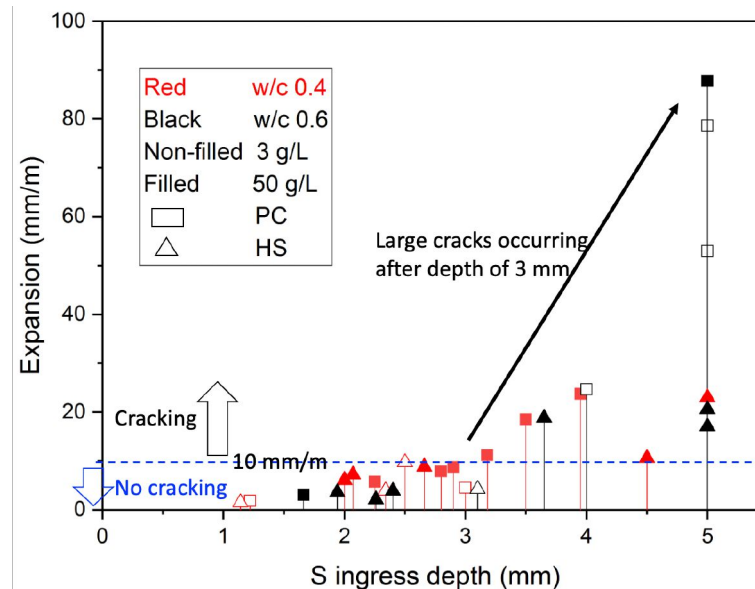


Fig. 7-6 The depth of sulfate penetration versus the expansion in Portland cement and HS cement pastes at w/c ratios of 0.4 and 0.6.

All these samples cracked as shown in Fig. 7-4 and located in the zone above the cracking line shown in Fig. 7-6, but the cracking extent is totally different as the strength varies in the samples with different w/c ratios. It demonstrates that strength can control the propagation of the cracks, so the ultimate damage is largely suppressed in PC04 and HS04.

Therefore, these two interacting factors in the sulfate degradation process between porosity and strength are well decoupled. Porosity mainly influences the sulfate ingress and thus controls the expansion initiation. Strength plays a big role in controlling the propagation of cracking.

## 7.5 Water adsorption and desorption

Fig. 7-7 a) shows the water adsorptive (data measured after the first day was used) in these four types of cement mortars, and b) shows the water evaporation with the same four cement types. Two w/c ratios were conducted with 0.4 and 0.6. Generally, cement mortars with a high w/c ratio show high adsorptive and drying rates. More importantly, there is a clear difference between the cement types that are used.

The water adsorption rate is consistent with the capillary porosity order from PC06 to HS06. The systems with similar capillary porosity have similar adsorption, such as HS04 (16.24 %) and LC04 (17.17 %). There is one exception, the PC systems are out of the trend, lower capillary porosity in PC04 and PC06 exceptionally

shows higher adsorption than other blended systems which contain more capillary porosity. It perhaps can be attributed to the pore connectivity in blended systems being lower than PC.

PC shows a higher water adsorption rate while LC<sup>3</sup> indicates the lower capacity of water adsorption. Interestingly, the drying rate does not follow the same trend of adsorption, SPC shows a faster drying rate than LC<sup>3</sup> systems no matter what the w/c ratios are. The high drying rate of SPC systems usually gives the shrinkage cracking that can be observed from microscopy as discussed in *Chapter 5*. However, it is more interesting to compare each system between adsorption and desorption which determines the location of the dry/wet interface. It directly impacts the ultimate result of salt crystallization whether as efflorescence or as subflorescence.

HS06 has a considerably lower drying rate than adsorption and consequently shows a large amount of efflorescence outside the sample. SPC and LC<sup>3</sup> systems show a higher drying rate than adsorption, HS04 shows the same trend but just with a slight rate difference. It gives a lot of information which could explain the observed spalling damage discussed in *Chapter 5*, at least there is a greater potential for salt crystallization in the fast-drying systems of LC<sup>3</sup> and SPC.

Fast drying is the main factor that determines the occurrence of subflorescence. However, the appearance of spalling damage is also dependent on the degree of crystallization pressure exerted which is another big factor that controls the occurrence of damage as discussed in *Chapter 6* by thermodynamic modelling. For the systems in which at least ~ two fold of drying rate than adsorptive is more sufficient to ensure the dry/wet interface located inside the sample, which is exactly the LC06 and SPC06 with an extensive spalling was talked about previously. Other systems with just a slightly higher drying rate show limited flaked pieces in HS04 and LC04, as it is meanwhile restricted by the higher mechanical strength as shown similarly in Fig. 7-3.

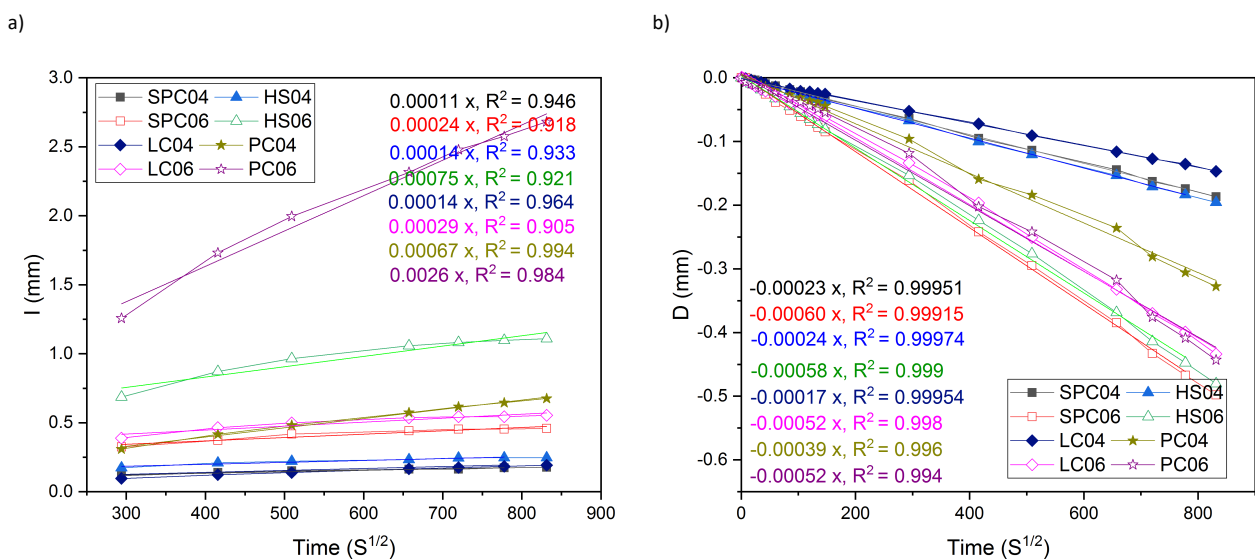


Fig. 7-7 Water adsorptive and drying rate of various cement mortars with w/c ratios of 0.4 and 0.6, a) adsorption, b) desorption.

### 7.5.1 Sulfate ingress versus water adsorption

The adsorption is not the same as the sulfate ingress rate. PC shows higher adsorptive than LC<sup>3</sup>, but the ingress rate is slower in PC paste due to the slowing down by the chemical binding of ettringite and gypsum as well as lower porosity than LC<sup>3</sup>. Therefore, with the same exposure time scale between PC and LC<sup>3</sup> cement pastes, LC<sup>3</sup> cement paste can allow more S ingress continuously to the other side of the samples than PC, meanwhile, LC<sup>3</sup> cement samples have a higher drying speed than water adsorptive that causing the accumulation of salts inside the materials. This effect of subflorescence is more possible in LC<sup>3</sup> rather than PC.

SPC cement systems seemly have the same property as LC<sup>3</sup> because the high chemical resistance and fast drying property are sufficient to satisfy the favourable conditions of salt crystallization inside the materials. It is consistent with the chemical phase profiles talked about in *Chapter 5* that LC<sup>3</sup> and SPC systems have thenardite formation and more potentially result in visible spalling damage.

Therefore, the sulfate ingress rate is not only related to the water adsorptive, but it is also dependent on the sulfate chemical resistance (depends on cement types). However, the sulfate ingress rate in the same cement system follows the same trend as water adsorptive: a high w/c system has a high adsorptive and sulfate ingress rate. After all, sulfate penetrates by the carry of water in the capillary rise process. Based on the sulfate ingress rate accompanied by the results from drying properties, the susceptibility of salt crystallization damage is able to be predicted. If the factors of low mechanical strength and high supersaturation are also favourable, probably the damage can be observed.

## 7.6 The interplay between chemical and physical attack

This new unidirectional approach was successfully applied in this sulfate project to understand the overlooked interplay between the well-known chemical sulfate attack and the less-studied physical sulfate attack. The most representative situation for field samples is that the two attacks occur simultaneously.

Chemical sulfate attack is present in Portland cement which shows the large sulfate binding capacity by cement hydrates. The destructive force comes from the ettringite crystallization pressure when it forms from AFms finely mixed with C-S-H gel. Usually, the sulfate concentration gradient along the depth within C-S-H gel can be observed. The chemical attack consumes the most sulfate that ingresses from the external solution and accumulates in the pore solution. Accordingly, very little sulfate progresses to the other surface to contribute to the physical sulfate attack.

Physical sulfate attack was found to take place more often in blended cementitious materials (only when a very high concentration sulfate solution was used) which is a more complicated process than chemical sulfate attack. Contrary to the case of Portland cement, it was shown that very little sulfate can be consumed by the lower amount of transformable aluminium-bearing hydrates along the ingress path before reaching to the

drying zone prone to physical attack. There were no or very few AFm phases dispersed in the C-S-H, thus the contribution from this expansive ettringite formation in C-S-H is not significant to cause detectable expansion. The capillary rise continues to deliver the abundant sulfate to the drying front through the pore solution without demonstrating a typical sulfate concentration gradient as seen in PC systems. On the other hand, the susceptibility to physical attack is increased as more sulfate is accumulated in the pore solution below the surface. The spalling appears when the supersaturation to salt  $\text{Na}_2\text{SO}_4 \cdot 10\text{H}_2\text{O}/\text{Na}_2\text{SO}_4$  is obtained.

## 7.7 Comments on the observed physical sulfate attack in this project

For the blended systems, no significant expansion and cracking from chemical sulfate attack was seen at both w/c ratios and sulfate concentrations. For spalling damage, Slag Portland cement of w/c 0.6 shows a quite early occurrence of spalling damage after only 28 days of exposure to 50 g/L  $\text{Na}_2\text{SO}_4$  solutions, because the flexural strength is as low as 6.62 MPa which is probably below the crystallization force that sodium sulfate salt can generate.

The possible driving mechanism of salt crystallization takes place under constant condition is maybe due to the combination of fast evaporation (fast drying in SPC and LC<sup>3</sup> cement mortars were determined by the water desorption test) and dissolution of thenardite and reprecipitate as mirabilite with respect to supersaturation in the solution as suggested in [17]. In the unidirectional capillary rise, the possible relative humidity gradient inside the samples can be sustained: higher RH close to the solution side decreases as it goes deeper until near the surface exposed to the environment [18]. So the dissolution of salts can take place inside wherever the dry/wet interface is below the exposing surfaces. Both processes contribute to the high degree of supersaturation.

The case of evaporation-driven crystallization can only happen with high evaporation rates which is the case of the cyclic exposure (RH at 33 % accelerates the evaporation), the supersaturation can only be high close to the sample's surface [17]. Therefore, decreased defects are observed in cyclic conditions than when the thenardite dissolution is the main source of crystallization under constant conditions. The very small and thin layer of salt forming below the surfaces was clearly shown by the phase profiles in LC06-50g-cycle.

It was indeed found that the disintegration propagated much deeper under constant conditions, the deep spalling of the surfaces was found in both LC<sup>3</sup> mortar and pastes in the case of 50 g/L. Moreover, the dissolution of thenardite can only take place inside the materials when the prerequisite is met that the evaporation is faster than capillary rise which allows thenardite to form inside previously, dissolution takes place when the solution enters and reaches the salts. The high concentration of sulfate is closely associated with carbonation which was not considered in the past study. Otherwise, there is no salt crystallization pressure can be generated in any form of supersaturation (evaporation-driven or dissolution of thenardite driven),

such as in PC and HS06 systems which have been observed without any spalling damage as their drying rates are slower than capillary rise.

The spalling can happen only when the subflorescence is preferred in a specific cement material (can be determined by water adsorption and desorption tests), relatively low mechanical restraint, high sulfate concentration can be sustained by the external sulfate solution and the carbonation, and in cement which can inhibit chemical sulfate attack sufficiently.

## 7.8 References

- [1] N. Ghafoori, I. Batilov, M. Najimi, Influence of Nanosilica on Physical Salt Attack Resistance of Portland Cement Mortar, *MJ*. 117 (2020) 67–80. <https://doi.org/10.14359/51725779>.
- [2] H. Haynes, M.T. Bassuoni, Physical Salt Attack on Concrete, *CI*. 33 (2011) 38–42.
- [3] P.J.M. Monteiro, Scaling and saturation laws for the expansion of concrete exposed to sulfate attack, *Proc. Natl. Acad. Sci. U.S.A.* 103 (2006) 11467–11472. <https://doi.org/10.1073/pnas.0604964103>.
- [4] Tixier Raphaël, Mobasher Barzin, Modeling of Damage in Cement-Based Materials Subjected to External Sulfate Attack. I: Formulation, *Journal of Materials in Civil Engineering*. 15 (2003) 305–313. [https://doi.org/10.1061/\(ASCE\)0899-1561\(2003\)15:4\(305\)](https://doi.org/10.1061/(ASCE)0899-1561(2003)15:4(305)).
- [5] M.L. Nehdi, A.R. Suleiman, A.M. Soliman, Investigation of concrete exposed to dual sulfate attack, *Cement and Concrete Research*. 64 (2014) 42–53. <https://doi.org/10.1016/j.cemconres.2014.06.002>.
- [6] R. Ragoug, O.O. Metalsi, F. Barberon, J.-M. Torrenti, N. Roussel, L. Divet, J.-B. d’Espinose de Lacaillerie, Durability of cement pastes exposed to external sulfate attack and leaching: Physical and chemical aspects, *Cement and Concrete Research*. 116 (2019) 134–145. <https://doi.org/10.1016/j.cemconres.2018.11.006>.
- [7] M. Moranville, S. Kamali, E. Guillon, Physicochemical equilibria of cement-based materials in aggressive environments—experiment and modeling, *Cement and Concrete Research*. 34 (2004) 1569–1578. <https://doi.org/10.1016/j.cemconres.2004.04.033>.
- [8] Jan Skalny, Jacques Marchand, Ivan Odler, *Sulfate Attack on Concrete*, London and New York, 2002. [https://www.bookdepository.com/Sulfate-Attack-on-Concrete-J.-Marchand/9780419245506?redirected=true&utm\\_medium=Google&utm\\_campaign=Base5&utm\\_source=CH&utm\\_content=Sulfate-Attack-on-Concrete&selectCurrency=CHF&w=AF72AU9SLSQSCQA803VV&pdg=pla-293946777986:kwd-293946777986:cmp-1578060869:adg-65091841852:crv-296436506046:pid-9780419245506:dev-c&gclid=EAlalQobChMizbvA6M-a4g1ViuR3Ch0tjw8TEAYASA-BEgJUXPD\\_BwE](https://www.bookdepository.com/Sulfate-Attack-on-Concrete-J.-Marchand/9780419245506?redirected=true&utm_medium=Google&utm_campaign=Base5&utm_source=CH&utm_content=Sulfate-Attack-on-Concrete&selectCurrency=CHF&w=AF72AU9SLSQSCQA803VV&pdg=pla-293946777986:kwd-293946777986:cmp-1578060869:adg-65091841852:crv-296436506046:pid-9780419245506:dev-c&gclid=EAlalQobChMizbvA6M-a4g1ViuR3Ch0tjw8TEAYASA-BEgJUXPD_BwE) (accessed May 14, 2019).
- [9] N. Tsui, R.J. Flatt, G.W. Scherer, Crystallization damage by sodium sulfate, *Journal of Cultural Heritage*. 4 (2003) 109–115. [https://doi.org/10.1016/S1296-2074\(03\)00022-0](https://doi.org/10.1016/S1296-2074(03)00022-0).
- [10] R.M. Espinosa-Marzal, G.W. Scherer, Advances in Understanding Damage by Salt Crystallization, *Acc. Chem. Res.* 43 (2010) 897–905. <https://doi.org/10.1021/ar9002224>.
- [11] R.J. Flatt, G.W. Scherer, Thermodynamics of crystallization stresses in DEF, *Cement and Concrete Research*. 38 (2008) 325–336. <https://doi.org/10.1016/j.cemconres.2007.10.002>.
- [12] P.K. Mehta, *CONCRETE. STRUCTURE, PROPERTIES AND MATERIALS*, (1986). <https://trid.trb.org/view/273357> (accessed June 29, 2022).
- [13] D.N. Winslow, S. Diamond, A MERCURY POROSIMETRY STUDY OF THE POROSITY IN PORTLAND CEMENT, *Journal of Materials*. (1970). <https://trid.trb.org/view/96627> (accessed July 19, 2022).
- [14] N. Nishiyama, T. Yokoyama, Permeability of porous media: Role of the critical pore size, *Journal of Geophysical Research: Solid Earth*. 122 (2017) 6955–6971. <https://doi.org/10.1002/2016JB013793>.
- [15] G.W. Scherer, Crystallization in pores, *Cement and Concrete Research*. 29 (1999) 1347–1358. [https://doi.org/10.1016/S0008-8846\(99\)00002-2](https://doi.org/10.1016/S0008-8846(99)00002-2).
- [16] W. Kunther, Investigation of Sulfate Attack by Experimental and Thermodynamic Means, PhD Thesis, EPFL, 2012. <https://doi.org/10.5075/epfl-thesis-5263>.
- [17] R.J. Flatt, Salt damage in porous materials: how high supersaturations are generated, *Journal of Crystal Growth*. 242 (2002) 435–454. [https://doi.org/10.1016/S0022-0248\(02\)01429-X](https://doi.org/10.1016/S0022-0248(02)01429-X).
- [18] S. Zhutovsky, R. Douglas Hooton, Experimental study on physical sulfate salt attack, *Mater Struct.* 50 (2016) 54. <https://doi.org/10.1617/s11527-016-0936-z>.



# Chapter 8 Sulfate-resisting cement mortar in full immersion test

## **Abstract**

This study aims to understand the effect of elevated temperatures on the hydration phase assemblages and the distribution of the aluminium-bearing hydrates (AFm and AFt) which are mainly responsible for the expansion due to the external sulfate attack. Mortars were prepared from Ordinary Portland (PC) and sulfate resisting (HS) cements with a w/c ratio of 0.5. These were cured at 20 °C, 40 °C and 60 °C before full immersion in sodium sulfate solutions. The results showed that higher temperature curing shortens the latent period of expansion in both PC and HS systems. The expansion took place much later in HS mortar due to the lower content of C<sub>3</sub>A even though aluminium content was higher due to the presence of slag. The high-temperature curing changed the intermix of phases in the C-S-H matrix, which accelerated the expansion and degradation.

## Contents

<b>8.1</b>	<b>Introduction .....</b>	<b>170</b>
<b>8.2</b>	<b>Materials and methods.....</b>	<b>171</b>
8.2.1	Types of cement .....	171
8.2.2	Methods .....	172
<b>8.3</b>	<b>Results and discussion .....</b>	<b>175</b>
8.3.1	Expansion .....	175
8.3.2	Effect of temperature on initial hydrates and distribution .....	175
8.3.3	Effect of curing temperature on sulfate ingress.....	179
8.3.4	Comparison of C-S-H compositions before and after expansion .....	181
<b>8.4</b>	<b>Conclusions.....</b>	<b>183</b>
<b>8.5</b>	<b>References.....</b>	<b>185</b>

## 8.1 Introduction

Sulfate-resisting cement has been prescribed in standards for many years. However, the mechanism of its resistance to sulfate attack remains unclear, since the initial concern was only to reduce the  $C_3A$  content in the clinker. The role of the ferrite phase that also contains aluminium has not been well considered. Most studies have shown that sulfate-resisting cement has much-reduced expansion compared to normal Portland cements [1,2]. However, the long-term performance of HS cements has not been well studied.

Previous studies [3,4] showed that even when the low  $C_3A$  content ( $< 5\%$ ) cement was exposed to sulfate, the expansion still happened after 10 years because the content of  $C_4AF$  was high at  $13\%$  which could perhaps contribute to the long latent period as ferrite hydrated rather slowly [5,6]. The mechanisms of this long-delayed expansion were not clearly investigated.

Gollop and Taylor [7] studied sulfate-resisting Portland cement in the 1990s and suggested that decreased ettringite formation and decreased decalcification could be attributed to the low content of aluminium in hydrates. Much of the aluminium was already present in ettringite before exposure to sulfate solution [8]. One important application field of this type of ferrite-rich cement is high-temperature marine environments because the slow hydration and low hydration heat can be beneficial in such cases.

In some special environments where the concrete serves in a high temperature in the field, and a large temperature difference exists in massive marine concrete, not only the attack from sulfate and chloride is concerned, but also the influence of the high temperature on the durability in realistic conditions [1,9]. Kalousek and Adams were the first to describe cement chemistry after high-temperature treatment [10]. Al and S can be incorporated into the structure of the C-S-H phase because there are more Al and S dissolved in the pore solution. Sulfate concentration can be as high as  $\sim 200$  mM in pore solution after high-temperature curing, which is ten times more than cement pastes cured under room temperature. S is incorporated into C-S-H by adsorption, while Al is incorporated by substituting Si in C-S-H to form C-A-S-H [10]. Upon heat curing, a more heterogeneous distribution of hydration products, and a coarser porosity can be observed compared to pastes cured under ambient conditions [11,12].

However, literature is scarce on the aspects of sulfate resistance of ferrite-rich cement incorporated with slag after it undergoes an elevated curing temperature. This study compares the sulfate resistance between normal PC and slag blended HS cement mortars cured under 20, 40 and 60 °C and then in the long-term exposure to sodium sulfate solution for 3 years. The initial phase compositions are analysed by SEM-EDS in the C-S-H and the aluminium bearing hydrates distribution is compared between 20 °C and 60 °C cured samples. The sulfur concentration profiles before and after expansion initiation are tracked, which gives

information on the rate of sulfate ingress. Finally, the mechanism of delayed expansion of HS samples cured at 60 °C is discussed.

## 8.2 Materials and methods

### 8.2.1 Types of cement

Normal Portlandite cement CEM I 42.5 (PC) and high sulfate-resisting cement (HS) were used in this study. The chemical composition and main clinker phases according to a Rietveld analysis are shown in Table 8-1. The slag content measured with the external standard method is 17 %.

Table 8-1 Chemical composition and phase composition of Portland cement and HS cement.

Oxides wt.%	PC	HS	Phase composition wt.%	PC	HS
SiO <sub>2</sub>	20.4	24.4	C <sub>3</sub> S	63.8	49.5
Al <sub>2</sub> O <sub>3</sub>	5.1	6.5	C <sub>2</sub> S	13.9	13.1
Fe <sub>2</sub> O <sub>3</sub>	1.9	2.7	C <sub>3</sub> A	10.6	3.3
CaO	64.2	55.1	C <sub>4</sub> AF	1.9	6.9
MgO	1.0	3.7	Anhydrite	4	1.3
SO <sub>3</sub>	2.9	4.6	Calcite	5.2	0.6
Na <sub>2</sub> O	0.4	0.3	Gypsum	0.6	8.3
K <sub>2</sub> O	0.7	0.9	Slag		17
TiO <sub>2</sub>	0.2	0.3			
P <sub>2</sub> O <sub>5</sub>	0.2	0.2			
LOI	1.67	1.29			

Fig. 8-1 shows the particle size distribution of PC and HS cement pastes as measured by laser diffractometry, which was performed as described below. First, 0.1 g cement was dispersed in 50 ml isopropanol to avoid possible hydration during the measurement. The suspension was dispersed with an ultrasonic probe for 15 minutes while at the same time being stirred with a magnetic stirrer. After the suspension was ready, a pipette was used to transfer the solution into the measuring zone, which was also rinsed and homogenized by isopropanol for three times, the transfer was carried out slowly until a 12 % obscuration was reached. The distribution curve was finally obtained by an average of three measurements.

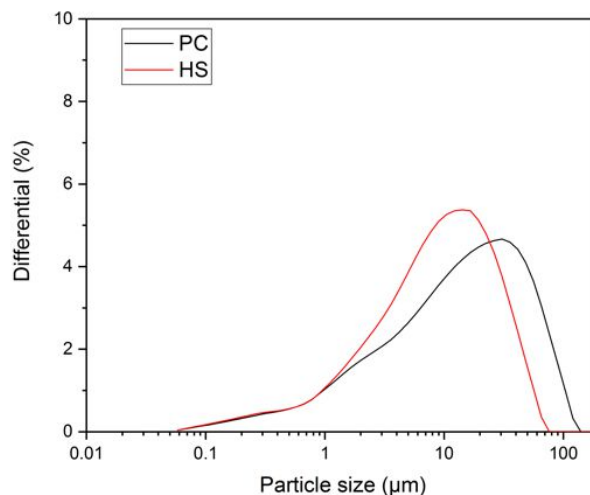


Fig. 8-1 Particle size distribution of the raw materials used in this study.

## 8.2.2 Methods

### Sodium sulfate solution

A chemical grade pure salt containing more than 99 %  $\text{Na}_2\text{SO}_4$  solid was used as the external sulfate source.

### Sample preparations

Mortar prisms were cast according to the standard test EN 196-1 with a w/c of 0.5. For each mix, 1 part of cement (491 g) to 2.75 parts of sand (1350 g) by mass was used. They were cured under the saturated lime solution for 28 days with different temperatures of 20 °C, 40 °C and 60 °C. The mortar samples were immersed under lime solution in a sealed container during the curing period. For each system, three mortar prisms were prepared with the studs adhered on the two ends for the expansion test and one prism for the microstructural test. The full immersion test was done in  $\text{Na}_2\text{SO}_4$  solution with a concentration of 50 g/L as indicated by the standard [13] and the solution was refreshed every month to control the sufficient constant sulfate concentration. The setup was kept at room temperature around 20 °C.

### XRD Rietveld method with the external standard method

The phase assemblages after 28 days of curing under different temperatures were measured on fresh slices. X-ray diffraction (XRD) analyses were done with a Philips X'Pert Pro PANalytical ( $\text{CuK}\alpha$ ,  $\lambda = 1.54$ ) working in Bragg–Brentano geometry over a  $2\theta$ -range of 5–65°. Quantitative Rietveld analyses were achieved with the HighScore Plus software and the external standard method (titanium dioxide as crystalline standard, rutile Kronos 2300).

### Expansion and SEM test

Expansion measurements were carried out every two weeks [13]. Microstructural test samples on SEM were cut perpendicularly to obtain a cross-section slice with a thickness of around 5 mm, as shown in Fig. 8-2. The sampling times were chosen depending on the expansion, as the samples were taken at the time before the expansion “take off” as well as after expansion. The slices were taken at least 10 mm from the ends of the sample. Samples were impregnated in epoxy and polished with diamond spray suspension of 9  $\mu\text{m}$ , 3 $\mu\text{m}$  down to 1  $\mu\text{m}$ .

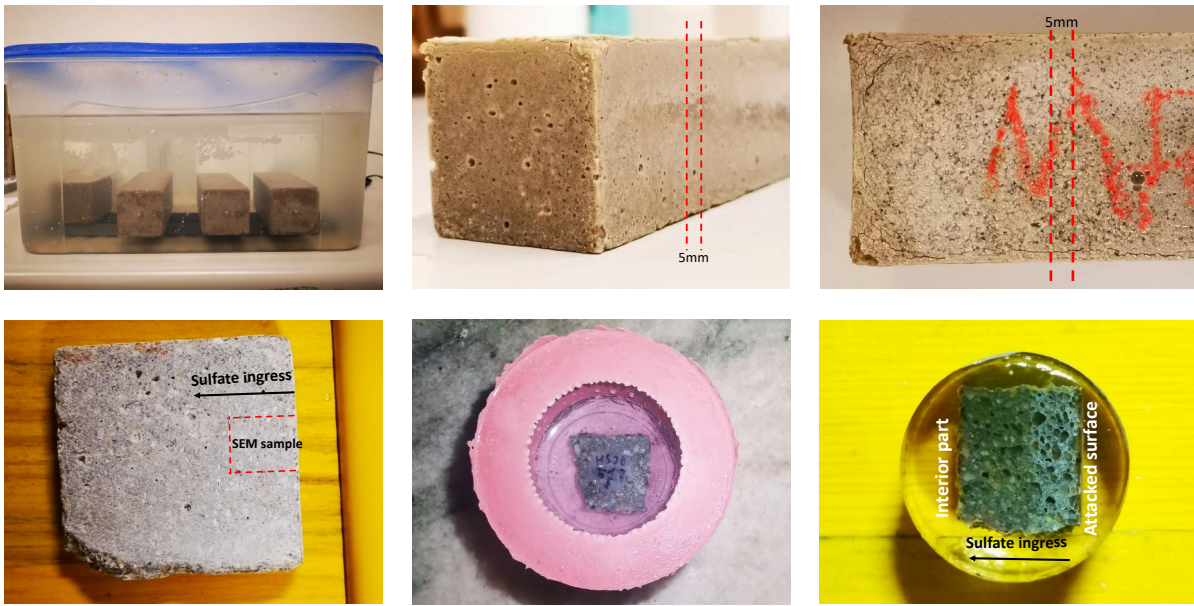


Fig. 8-2 SEM sample preparation process.

Energy dispersive spectroscopy (EDS) point analyses were made on the polished section in the scanning electron microscopy (FEI Quanta 200). Elemental hyper mappings were also obtained to get the relative sulfur concentration from the outer surface to the interior. The accelerating voltage was 15.0 kV, with a working distance of 12.5 mm. For point analysis, the points were selected carefully from the outer C-S-H phase of cement paste parts of mortars. The operator’s expertise is needed to select the points avoiding portlandite, ettringite, AFm and aggregates as much as possible. More detail on proper point selection from a typical BSE image is discussed in [14]. 200 points for each sample were selected at the same distance from the exposed surface. An example is shown in Fig. 8-3, from the morphology and grey level of different phases, outer C-S-H can be distinguished. The aggregates, large size of AFm and AFt, clinker, and portlandite are indicated and should be avoided while selecting the phase of interest.

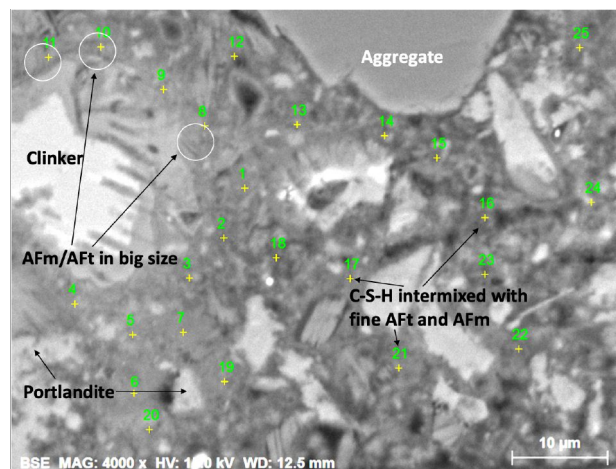


Fig. 8-3 Example of EDS point analysis on outer C-S-H phase for PC mortar sample.

For hyper mapping, a scanned map was set from the sulfate-exposed surface (initial position) to the inner part (final position) with a given step and mapping overlap. Each mapping area was about  $1720 \times 1290 \mu\text{m}$  (nominal magnification  $150\times$ ) with a resolution of  $1000 \times 750$  pixels (pixel size of  $1.72 \mu\text{m}$ ). For each sample, a depth of 10 mm was imaged in 10 steps. The Esprit 1.9 software was used to quantify the hypermaps after calibration with standards for each element of interest. The 10 individual maps were stitched together with ImageJ [15]. Eventually, a long BSE map and elemental information over the whole analysed depth can be obtained. After processing, the mappings were quantitatively analysed by using the EDXIA approach developed by Georget et al. [16]. The example of a stitched long BSE image is shown in Fig. 8-4. The left-hand side is the solution-exposed surface and the right-hand side is the interior part.

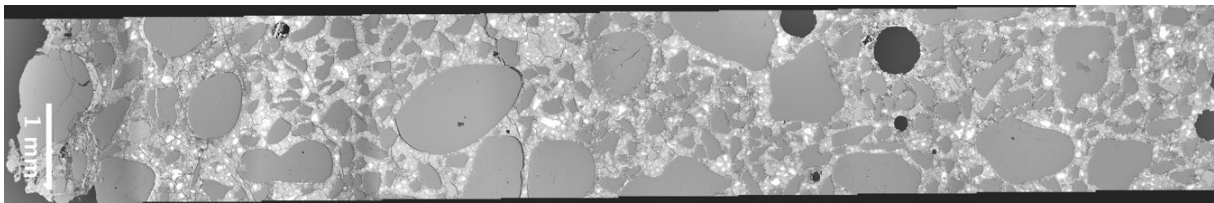


Fig. 8-4 Example of stitched long BSE image for PC mortar after sulfate attack with a depth around 10 mm.

### Thermodynamic modelling

The CemGEMS web app (<https://cemgems.app>) was used to model cement hydration. The mineralogical phase composition of the cement was obtained by the XRD Rietveld method, was used as input of the modelling. The initial equilibrium condition was obtained with the recipe, and then the process of cement hydration was simulated based on the modified Parrot and Killoh model (mP&K) until reaching 1000 hours of hydration. The evolution of phase assemblage over the hydration time was obtained. The details of the steps that have been adopted in the CemGEMS calculation for the profiles of phase assemblage are as follows:

A. The construction of the cement mortar recipes (here is the example of PC mortar at  $20^\circ\text{C}$ , but CEM-I-SR:min for sulfate-resisting cement and temperatures of  $40^\circ\text{C}$  and  $60^\circ\text{C}$  should be also adapted).

1. Chose recipe template “CEM-I-OPC:min” from CemGEMS, with a new name “OPC06-20C”.
2. Equilibrated at 1 bar and  $20^\circ\text{C}$ .
3. Adapted to the same chemical composition as the cement used in this study. The modified cement composition according to Table 8-1.
4. Equilibrated again, producing phase assemblage and C-S-H composition.

B. The settings of process simulation steps, using the recipes mentioned above as parent systems.

1. Took the process template “Hydration-MPK:Time-log” with the name “OPC-Hydration-20C”

2. Simulated the process.
3. Plotted volumes of solids only as shown in Fig. 8-7.

## 8.3 Results and discussion

### 8.3.1 Expansion

The expansion was measured up to almost 3 years, as shown in Fig. 8-5. A large difference can be seen between the samples cured at different temperatures. Generally, the expansion “takes off” earlier in the samples cured at higher temperatures in both PC and HS mortars. However, the latent period before significant expansion is very different between the two systems: expansion started in PC-60 °C at about 56 days, but HS-60 °C was delayed to about 600 days. The expansion of PC mortar cured at 60 °C presents a higher ultimate expansion than that cured at 20 °C.

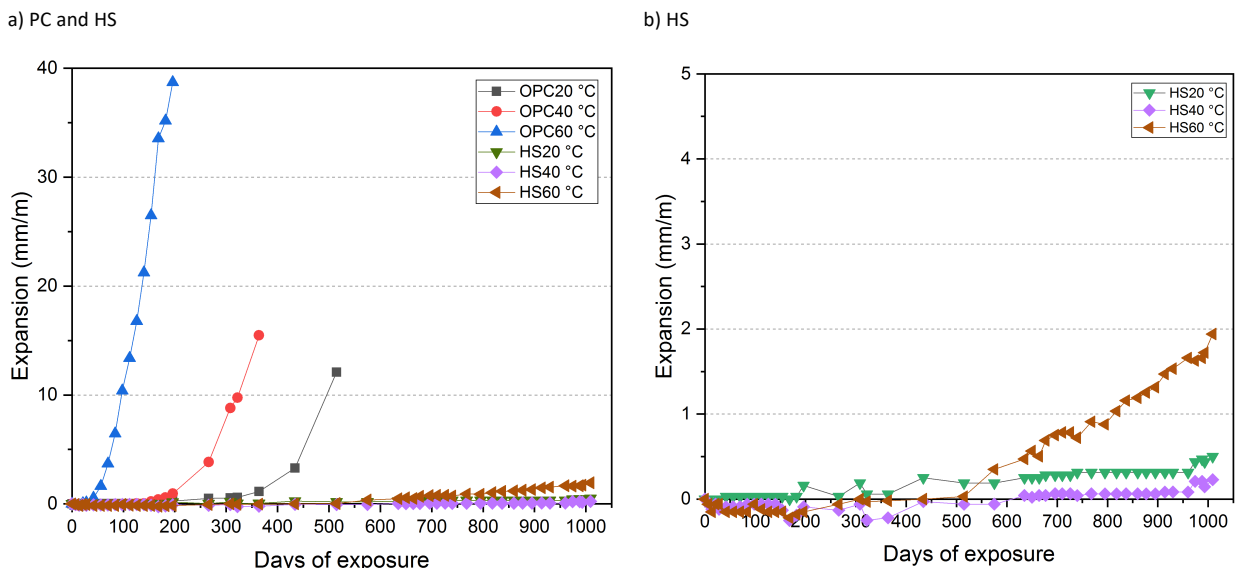


Fig. 8-5 Sulfate expansion evolution over time under different curing temperatures of PC and HS mortars.

### 8.3.2 Effect of temperature on initial hydrates and distribution

The cement phase assemblages after hydration are shown in Fig. 8-6, as characterized by XRD-Rietveld method. For HS cements, the Al-bearing phase content is increasing as the curing temperature is higher, namely, most Al-bearing phases (in hydrotalcite form in HS hydrates) were found in HS-60 °C. Al-bearing phases in HS-20 °C were not easily detected by XRD and almost all the sulfate was present in the ettringite phase under 20 °C cured condition. Al-bearing phase content is most in PC04-20 °C, which is even more than the 60 °C cured HS sample. The decreased ettringite formation agrees well with the experimental TGA results [12] and thermodynamic modelling results [17,18]. However, the monosulfate phase was not found in XRD measurements, the possible poorly crystalline monosulfate leads to the limitation of detecting the specific phase in the XRD characterization [19].



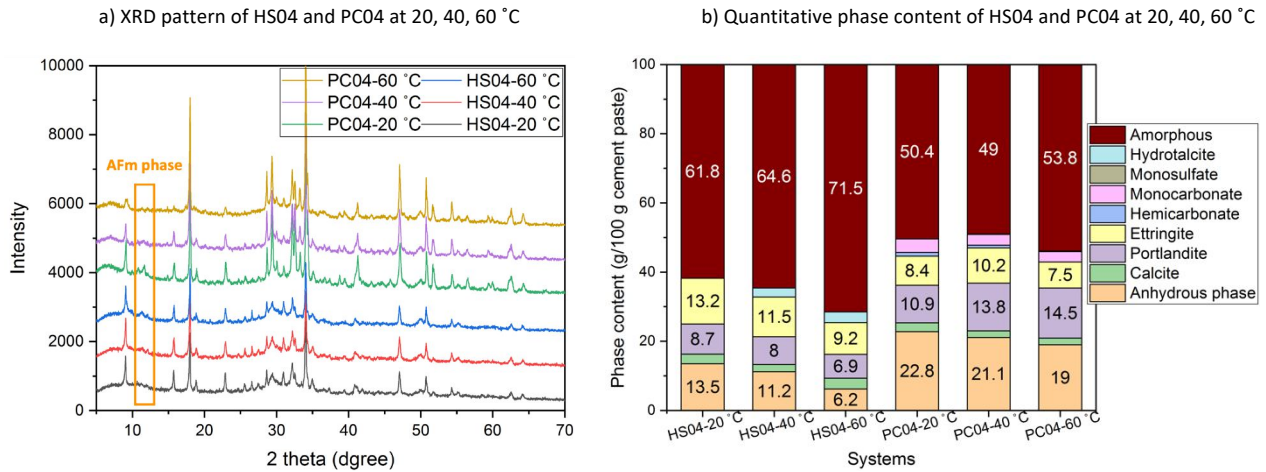
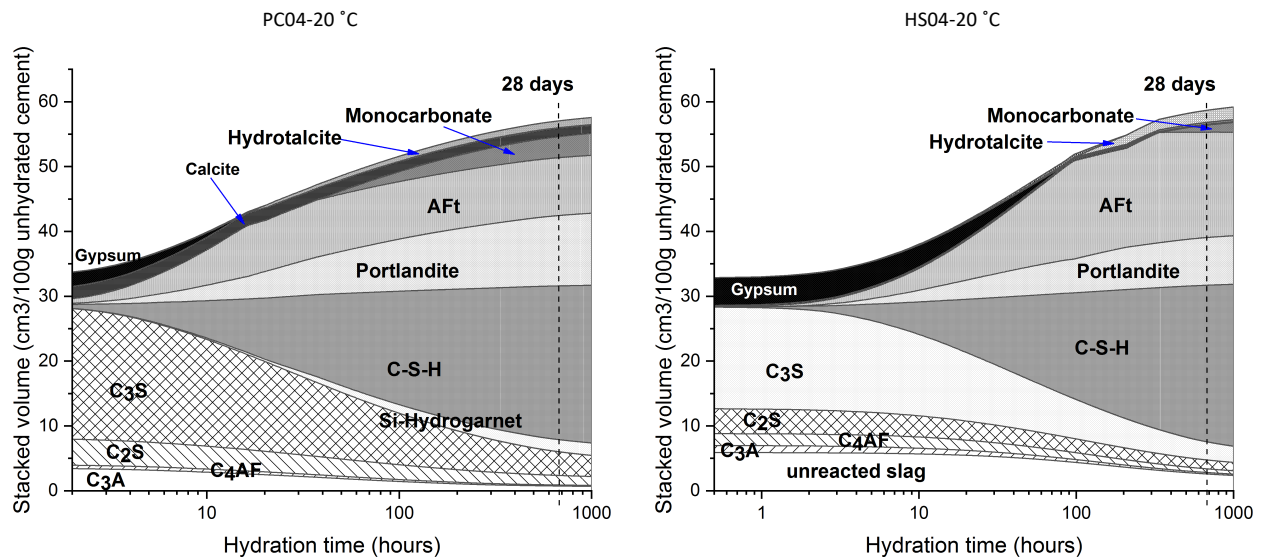


Fig. 8-6 Phase contents after hydration after 28 days of curing under different temperatures.

The phase assemblages were also simulated by thermodynamic modelling, as shown in Fig. 8-7. The examples of 20 °C and 60 °C were conducted to check the forms of aluminium expected in the hydrates. At elevated curing temperature (more than 20 °C), ettringite is more soluble hence other forms of aluminate-bearing AFms can precipitate: monosulfate forms in PC, while, The ettringite is more stable at 60 °C in the HS system and monocarbonate forms. More ettringite forms in HS hydrates, which agrees with the cement composition (more aluminate and more SO<sub>3</sub> content in HS cement). The modelling results correspond to the expected phase transformation, although it was not detected similarly in XRD.



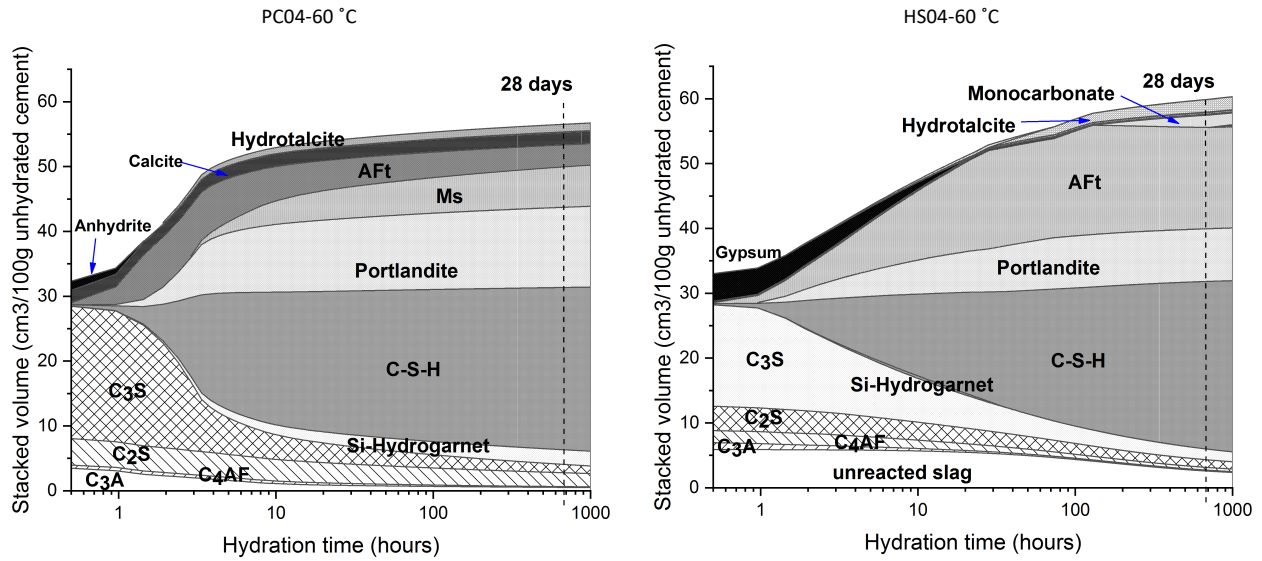


Fig. 8-7 Phase assemblages of HS and PC cement hydration modelled in CemGEMS under 20 °C and 60 °C cured conditions.

Fig. 8-8 is an example showing the segmentation of aluminium phases of the HS cement paste by EDXIA [16]. Hydrotalcite is present due to the slag grains incorporated in HS cement. Monosulfate with very few Mc/Hc is detected by SEM. All these phases are mixed with C-A-S-H which is mapped with different colours in Fig. 8-8 d): Ht (in orange) is the hydrate of slag located in the circumferential rims of slag grains, monosulfate (in cyan) is the relatively big size in micrometres that can be detected by SEM, C-A-S-H phase (in purple) is inter-mixed with the finely distributed phase and binds the hydrates together. These results confirm that the main aluminate-bearing phase is monosulfate. The presence of AFm is also confirmed by the morphology of the typical feature in the segmented monosulfate particles in Fig. 8-8 d).

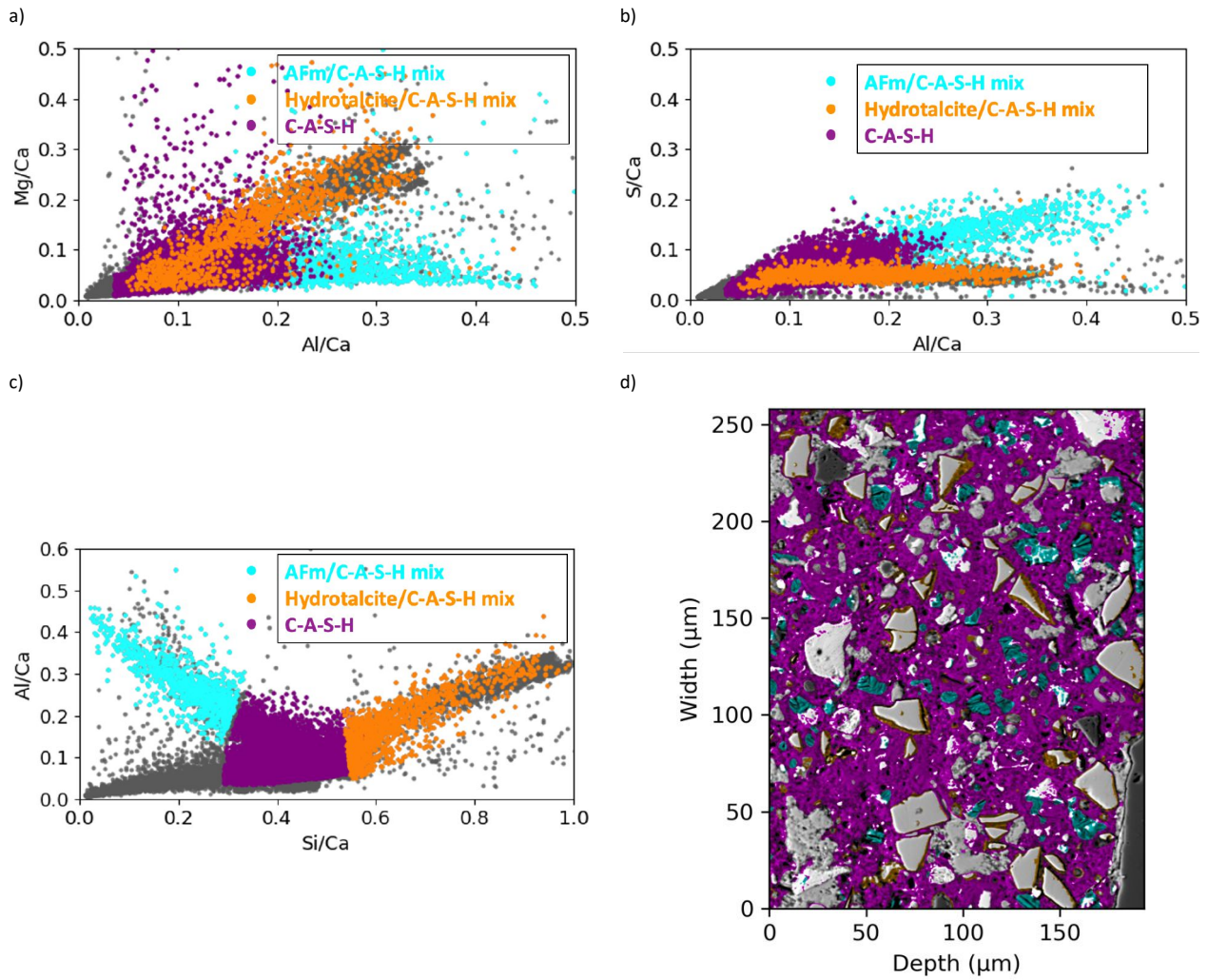


Fig. 8-8 Aluminium-bearing phase segmentation of HS 20 °C mortar by EDXIA: Ms, hydrotalcite, C-A-S-H phases.

Fig. 8-9 shows the initial AFm hydrate content after hydration of 28 days under 20 ° and 60 °C. The AFm phase was segmented from EDXIA [16] and mapped with BSE images in a different colour. High-temperature curing leads to higher contents of AFm in both PC and HS cement pastes. It is consistent with the results from the XRD Rietveld method. Also, the PC system cured under 20 °C even has a higher AFm content than HS cement paste cured at 60 °C. In HS at 20 °C, the AFm phase detected by EDS is a mixture of mainly monosulfate and minor content of Hc/Mc, which was not found by the XRD method (maybe due to the low intensity of monosulfate in the refinement). It seems that the increase of aluminium phase in HS only comes from the AFm, Ht was found constant at both curing temperatures. The S/Ca ratios of the C-(A)-S-H phase is also shown for each system and treated as the background of the reference sample after 28 days of curing, which is used in the next sections. S/Ca ratios are slightly increased in the heat-cured samples.

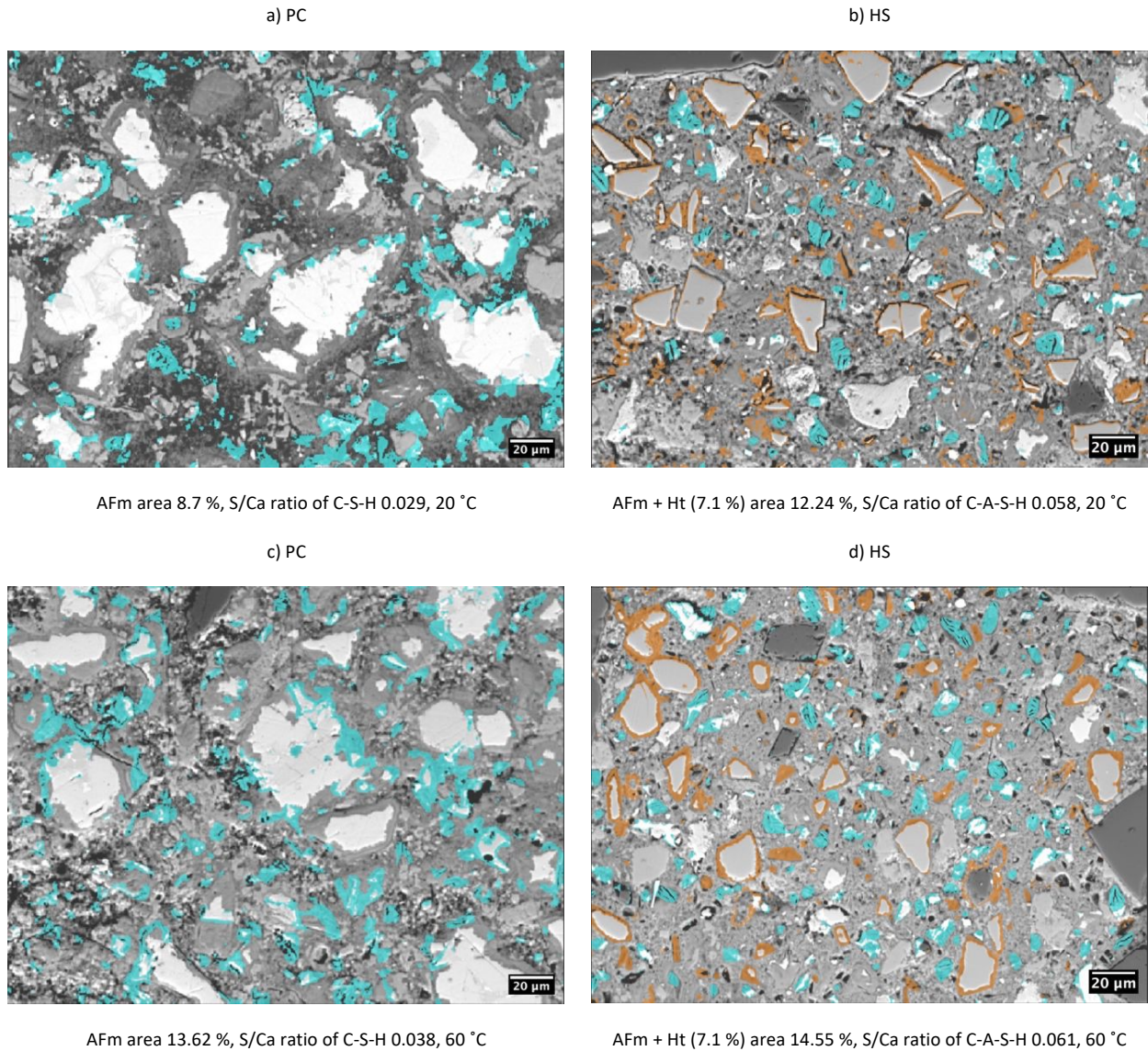


Fig. 8-9 BSE maps of a) and c) for PC mortars, b) and d) for HS mortars with AFm phases mapped in cyan and Ht in orange, after 28-day curing at 20 °C and 60 °C.

### 8.3.3 Effect of curing temperature on sulfate ingress

#### Portland cement mortar

Fig. 8-10 shows the profiles of S/Ca within C-S-H of PC mortars after sulfate solution exposure is obtained from mappings: the concentration gradient from the exposed surface to the interior depth of 10 mm has a decreasing trend. At 20 °C, sulfate ingress reaches about 6 mm and S/Ca increases after expansion. The peak moves from 0.5 mm to 2 mm of the bottom surface, which shows the progressive layer degradation. The peak of S/Ca corresponds to the gypsum band that forms in the cracks or the interfacial zone between aggregates and pastes. At 60 °C, sulfate can ingress to a depth of about 6 mm, but with a much shorter period of exposure, which demonstrates the heat cured samples allow a faster sulfate penetration. Expansion occurred in both cases as long as the S/Ca is higher than 0.2, no matter how long the exposure time was.

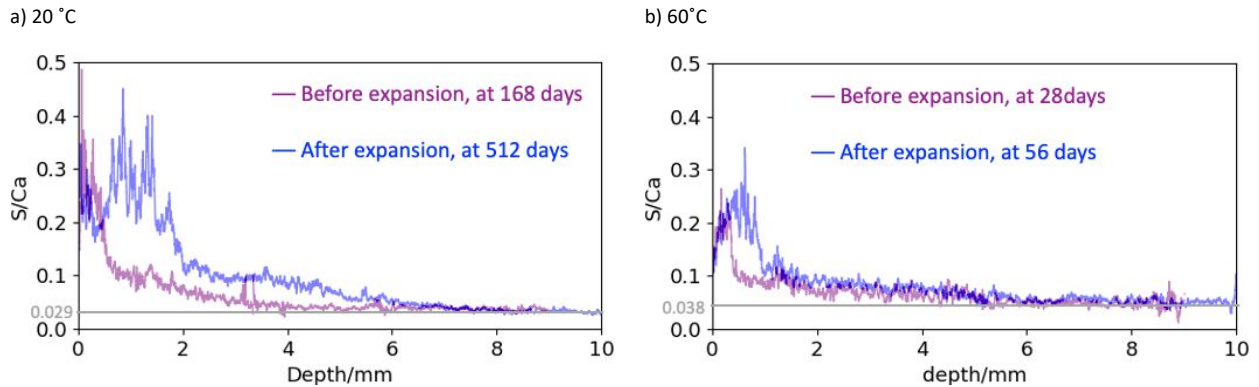


Fig. 8-10 S/Ca profiles obtained by hyper mappings in C-S-H phase before and after expansion for sample curing at a) 20 °C and b) 60 °C.

### Sulfate-resisting cement mortar

Similar profiles of S/Ca within C-S-H were obtained from HS mortars, as shown in Fig. 8-11. Sulfate ingress depth (> 5 mm) at 60 °C is obviously higher than that of samples cured at 20 °C (4 mm). However, the S/Ca ratio in HS cement cannot reach beyond 0.2 within a wide region, which is contrary to PC cement where it reached beyond 0.3 in the sample after expansion. This result implies that less gypsum is present in HS systems. Gypsum is considered to be a guarantee of high expansion because its presence ensures the high supersaturation condition with respect to the ettringite formation [20–22]. Therefore, the HS still does not expand after approximately 1000 days of exposure at 20 °C.

High-temperature curing shows a faster penetration through the microstructure, which is explained by a more heterogeneous distribution of hydration products and a weakening of the paste to aggregate bond. However, the depth of sulfate ingress does not change much before and after expansion, which implies that the sulfate ingress is quite slow in HS mortars. The decreased sulfate diffusion in HS can be interpreted by the slow reaction kinetics between sulfates and transformable AFm, only those aluminium source is depleted and the high sulfate concentration can then be built up to trigger the further diffusion [23]. The S/Ca ratio in the expanded zone can reach over 0.2 with a wide depth of ~ 0.5 mm after expansion in PC. However, in HS mortars, the S/Ca does not change considerably before and after expansion, which shows that the concentration of sulfate in the pore solution is not that different. It also implies that there is no abundant gypsum that can form.

However, in the case of 60 °C, the S/Ca profile above the depth of 2 mm is still the same concentration which shows that further penetration was still not triggered as the sulfate did not consume the transformable aluminium completely in the zone below the depth of 2 mm. It suggests somehow the slow kinetics of sulfate expansion in HS systems is partly due to the slow sulfate binding reaction in ettringite and/or gypsum.

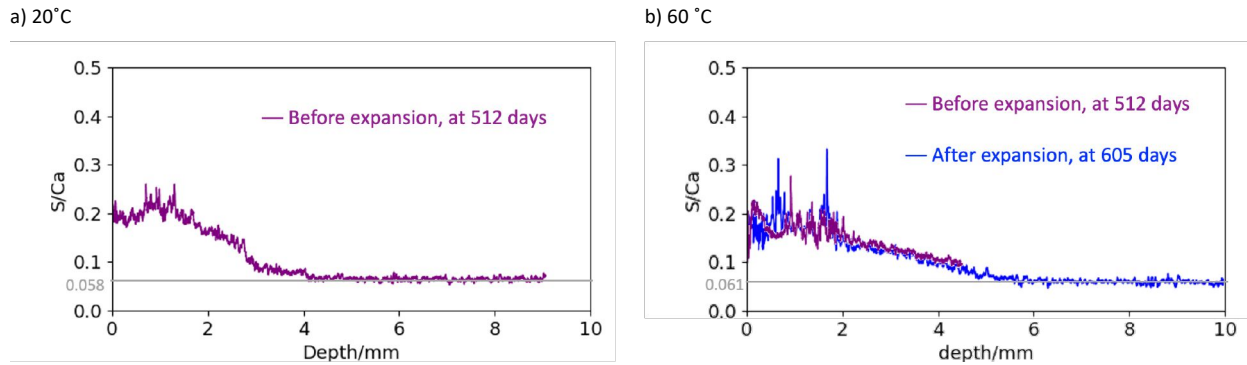


Fig. 8-11 S/Ca profiles in C-S-H phase as obtained by hyper mapping before and after expansion for sample curing at a) 20 °C and b) 60 °C.

### 8.3.4 Comparison of C-S-H compositions before and after expansion

#### Portland cement

Chemical point analyses on the outer C-S-H phase were done for PC systems on the reference sample cured for 28 days, a sample just before expansion and a sample after expansion, as shown in Fig. 8-12. We already knew from the phase composition characterization that AFm is present in higher quantities in heat-cured samples, which is consistent with the observed trend that the outer C-S-H cluster shifts towards monosulfate.

In the PC mortar, the small crystals of Ms/Hc and Mc intermixed within the outer C-S-H phase can be transformed into ettringite which can cause the expansion [14]. Both for 20 and 60 °C, there is a clear trend that the monosulfate phase is already partly transformed into ettringite in the sample just before expansion. In the sample after expansion, the monosulfate is somewhat all transformed into ettringite. However, there may still be some large monosulfate grains left at 20 °C (i.e., not in the C-S-H), but they are not believed to be responsible for the expansion. The significant expansion started around 300 days when all monosulfate has transformed into ettringite. It implies that the latent period is related to the relative content of small crystals of Ms intermixed in the C-S-H matrix, and the microstructure which impacts the reaction kinetics. As shown in Fig. 8-5, the expansion started with the same mechanism for samples cured at 20 and 60 °C, but the initial phase compositions of C-S-H were different and led to different developments of expansion. This shows that the expansion is associated with the location where ettringite forms, but not with the overall ettringite amount.

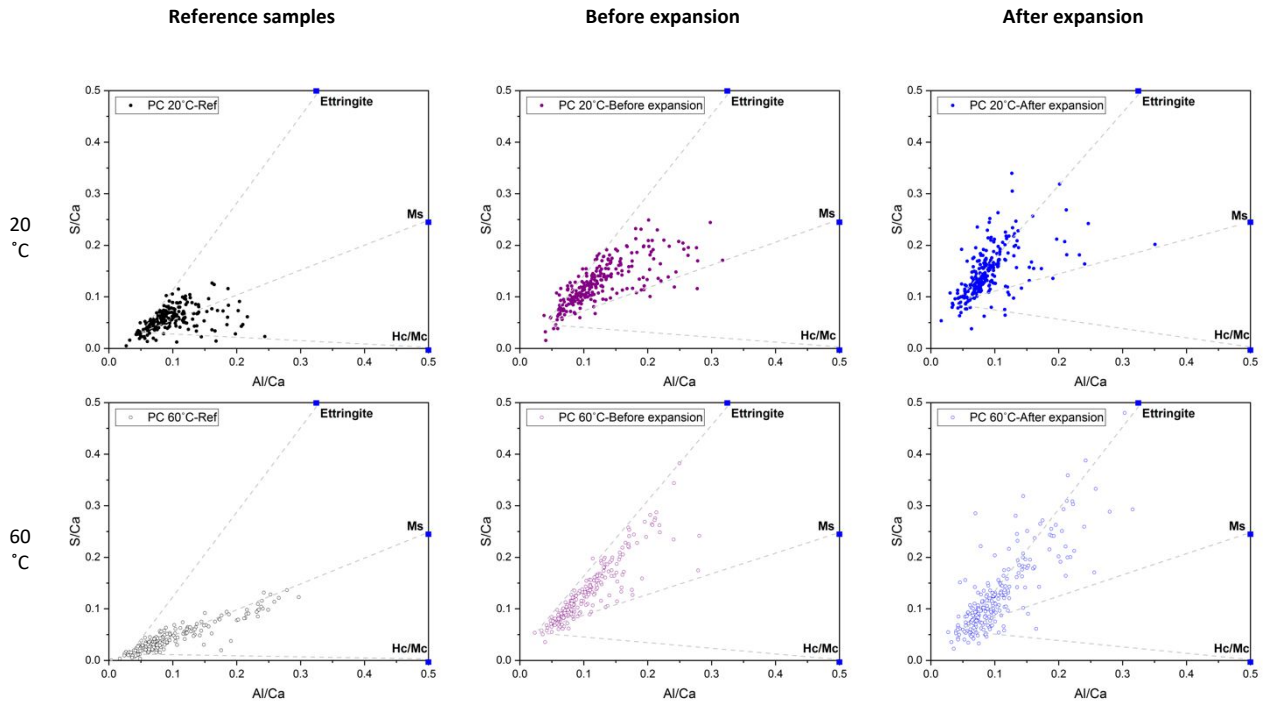


Fig. 8-12 Atomic ratios of S/Ca versus Al/Ca of the outer C-S-H cluster before and after expansion in PC-20 °C and PC-60 °C at the depth of 0.5mm.

### Sulfate-resisting cement

The phase composition changes of HS mortar are shown in Fig. 8-13. The AFm phase and ettringite are both intermixed with outer C-S-H in the reference 28-day sample. Some extent of sulfate is already embedded in ettringite, meaning that less monosulfate is mixed with C-S-H, which is potentially less problematic to sulfate expansion when the transformation of AFm in C-S-H is initiated. This agrees with the XRD-Rietveld results which showed that sulfates are mainly in ettringite in HS cement systems (see the XRD results in Fig. 8-6). Because of this, the precipitation rate of ettringite in the small pores (which needs supersaturation) is very slowly happening and the expansion still does not take off until 1000 days (even though we observe the partial conversion, the main cluster is located between monosulfate and ettringite lines).

The high-temperature curing changes the microstructure and the reaction kinetics of the ferrite phase may be accelerated. The ettringite phase is partially replaced by monosulfate as we observe in reference samples in Fig. 8-13. In the samples just before we observe expansion, the points are scattered somewhere around the lines of ettringite and Ms, which means the transformation starts and there is still some Ms left. There is a significant amount of large ettringite grains forming in those latent periods, and they are observed from the microscopy analyses. After the expansion has initiated, the points in the cluster are more concentrated to the ettringite trend line, and barely any such points are going towards Ms anymore. All the points mentioned above were taken from a depth of around 0.5 mm distance from the sulfate exposed surface.

The latent period is depending on the cement material, the relative amount of Ms, and the reaction kinetics of transformation between Ms and ettringite. It was largely delayed in HS mortar systems before the expansion was detected, there was no obvious expansion until 600 days. This is a very long latent period compared to the PC system where it was only around 56 days. Apart from the much lower content of the  $C_3A$  phase and the pre-existing ettringite, the low reaction kinetics of the ferrite phase that also contains an aluminium source can perhaps contribute to the expansion, which could be an additional explanation for the expansion does not start in the 20 °C cured sample.

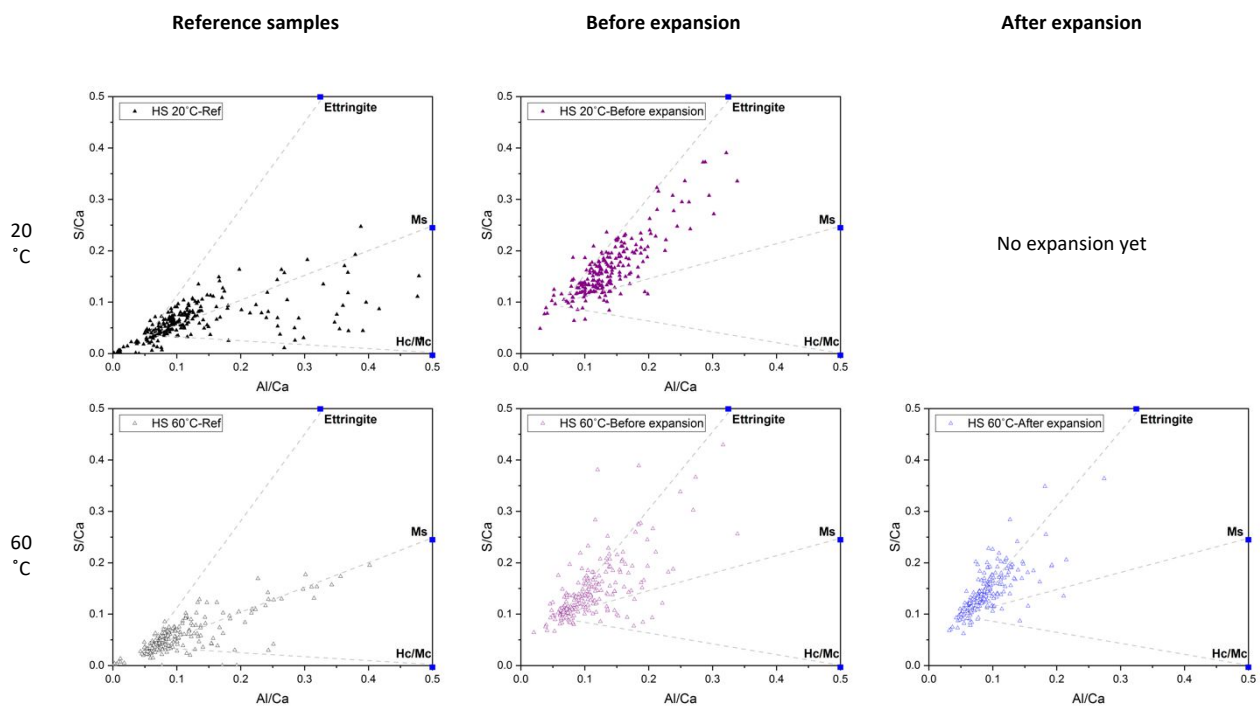


Fig. 8-13 Atomic ratios of S/Ca versus Al/Ca of the outer C-S-H cluster before and after expansion in HS 20 °C and HS-60 °C at the depth of 0.5 mm.

## 8.4 Conclusions

This chapter provided further understanding of the effect of the elevated curing temperature on the sulfate resistance in full immersed HS cement mortars. Based on the results presented in this study, the following conclusions can be drawn:

1. Expansion of mortar is higher when cured at 60 °C than when cured at 20 °C. Expansion of HS cement is much slower than that of PC cement, and is also less affected by higher curing temperature.
2. In PC paste, aluminium hydrates occur in the form of ettringite + hemicarbonate/monocarbonate/monosulfate (AFm can transform into ettringite upon sulfate exposure). In HS paste, aluminium hydrates occur in the form of ettringite + hydrotalcite + monosulfate.
3. For PC cured at 60 °C, ettringite is more soluble and its content is thus lower compared to normal curing, while AFm content increases (with a higher potential of expansion upon sulfate exposure).



For HS cured at 60 °C, ettringite content reduces and hydrotalcite+monosulfate content increases. Less Al for AFt/AFm leads to less potential expansion upon sulfate exposure.

4. In PC, sulfate is found in C-S-H and monosulfate before exposure, then moves into ettringite before expansion and then into C-S-H with higher S/Ca (ettringite +  $\text{CaSO}_4$ ) after expansion. In HS, most sulfate is in C-A-S-H (with only a very limited amount in monosulfate) which shows much slower kinetics for ettringite transformation from monosulfate within C-A-S-H. Hydrotalcite was found to be stable before and after expansion, thus it does not contribute to expansion.

## 8.5 References

- [1] H.M. Yang, S.M. Zhang, L. Wang, P. Chen, D.K. Shao, S.W. Tang, J.Z. Li, High-ferrite Portland cement with slag: Hydration, microstructure, and resistance to sulfate attack at elevated temperature, *Cement and Concrete Composites*. 130 (2022) 104560. <https://doi.org/10.1016/j.cemconcomp.2022.104560>.
- [2] P.J. Tikalsky, D. Roy, B. Scheetz, T. Krize, Redefining cement characteristics for sulfate-resistant Portland cement, *Cement and Concrete Research*. 32 (2002) 1239–1246. [https://doi.org/10.1016/S0008-8846\(02\)00767-6](https://doi.org/10.1016/S0008-8846(02)00767-6).
- [3] P.J.M. Monteiro, K.E. Kurtis, Experimental Asymptotic Analysis of Expansion of Concrete Exposed to Sulfate Attack, *ACI Materials Journal*. 105 (2008) 62–71.
- [4] P.J.M. Monteiro, Scaling and saturation laws for the expansion of concrete exposed to sulfate attack, *Proc. Natl. Acad. Sci. U.S.A.* 103 (2006) 11467–11472. <https://doi.org/10.1073/pnas.0604964103>.
- [5] H.F.W. Taylor, *Cement Chemistry*, Thomas Telford, 1997.
- [6] S. Han, J. Zhong, W. Ding, J. Ou, Strength, hydration, and microstructure of seawater sea-sand concrete using high-ferrite Portland cement, *Construction and Building Materials*. 295 (2021) 123703. <https://doi.org/10.1016/j.conbuildmat.2021.123703>.
- [7] R. Gollop, H. Taylor, Microstructural and microanalytical studies of sulfate attack III. Sulfate-resisting portland cement: Reactions with sodium and magnesium sulfate solutions, (1995). [https://doi.org/10.1016/0008-8846\(95\)00151-2](https://doi.org/10.1016/0008-8846(95)00151-2).
- [8] R.S. Gollop, H.F.W. Taylor, Microstructural and microanalytical studies of sulfate attack III. Sulfate-resisting portland cement: Reactions with sodium and magnesium sulfate solutions, *Cement and Concrete Research*. 25 (1995) 1581–1590. [https://doi.org/10.1016/0008-8846\(95\)00151-2](https://doi.org/10.1016/0008-8846(95)00151-2).
- [9] A.M. Hossack, M.D.A. Thomas, The effect of temperature on the rate of sulfate attack of Portland cement blended mortars in Na<sub>2</sub>SO<sub>4</sub> solution, *Cement and Concrete Research*. 73 (2015) 136–142. <https://doi.org/10.1016/j.cemconres.2015.02.024>.
- [10] T. Ramlochan, M.D.A. Thomas, R.D. Hooton, The effect of pozzolans and slag on the expansion of mortars cured at elevated temperature: Part II: Microstructural and microchemical investigations, *Cement and Concrete Research*. 34 (2004) 1341–1356. <https://doi.org/10.1016/j.cemconres.2003.12.026>.
- [11] H. Haynes, Sulfate Attack on Concrete: Laboratory vs. Field Experience, *CI*. 24 (2002) 64–70.
- [12] B. Lothenbach, F. Winnefeld, C. Alder, E. Wieland, P. Lunk, Effect of temperature on the pore solution, microstructure and hydration products of Portland cement pastes, *Cement and Concrete Research*. 37 (2007) 483–491. <https://doi.org/10.1016/j.cemconres.2006.11.016>.
- [13] C01 Committee, Test Method for Potential Expansion of Portland-Cement Mortars Exposed to Sulfate, ASTM International, 2019. <https://doi.org/10.1520/C0452-19>.
- [14] C. Yu, W. Sun, K. Scrivener, Mechanism of expansion of mortars immersed in sodium sulfate solutions, *Cement and Concrete Research*. 43 (2013) 105–111. <https://doi.org/10.1016/j.cemconres.2012.10.001>.
- [15] S. Preibisch, S. Saalfeld, P. Tomancak, Globally optimal stitching of tiled 3D microscopic image acquisitions, *Bioinformatics*. 25 (2009) 1463–1465. <https://doi.org/10.1093/bioinformatics/btp184>.
- [16] F. Georget, W. Wilson, K.L. Scrivener, edxia: Microstructure characterisation from quantified SEM-EDS hypermaps, *Cement and Concrete Research*. 141 (2021) 106327. <https://doi.org/10.1016/j.cemconres.2020.106327>.
- [17] B. Lothenbach, T. Matschei, G. Möschner, F.P. Glasser, Thermodynamic modelling of the effect of temperature on the hydration and porosity of Portland cement, *Cement and Concrete Research*. 38 (2008) 1–18. <https://doi.org/10.1016/j.cemconres.2007.08.017>.
- [18] W. Wilson, J.N. Gonthier, F. Georget, K.L. Scrivener, Insights on chemical and physical chloride binding in blended cement pastes, *Cement and Concrete Research*. 156 (2022) 106747. <https://doi.org/10.1016/j.cemconres.2022.106747>.
- [19] K. Scrivener, R. Snellings, B. Lothenbach, eds., *A Practical Guide to Microstructural Analysis of Cementitious Materials*, CRC Press, Boca Raton, 2017. <https://doi.org/10.1201/b19074>.
- [20] W. Kunther, B. Lothenbach, Improved volume stability of mortar bars exposed to magnesium sulfate in the presence of bicarbonate ions, *Cement and Concrete Research*. 109 (2018) 217–229. <https://doi.org/10.1016/j.cemconres.2018.04.022>.
- [21] W. Kunther, B. Lothenbach, K. Scrivener, Influence of bicarbonate ions on the deterioration of mortar bars in sulfate solutions, *Cement and Concrete Research*. 44 (2013) 77–86. <https://doi.org/10.1016/j.cemconres.2012.10.016>.
- [22] M.A. González, E.F. Irassar, Ettringite formation in low C3A Portland cement exposed to sodium sulfate solution, *Cement and Concrete Research*. 27 (1997) 1061–1071. [https://doi.org/10.1016/S0008-8846\(97\)00093-8](https://doi.org/10.1016/S0008-8846(97)00093-8).
- [23] R. Ragoug, O.O. Metalssi, F. Barberon, J.-M. Torrenti, N. Roussel, L. Divet, J.-B. d’Espinose de Lacaillerie, Durability of cement pastes exposed to external sulfate attack and leaching: Physical and chemical aspects, *Cement and Concrete Research*. 116 (2019) 134–145. <https://doi.org/10.1016/j.cemconres.2018.11.006>.

# Chapter 9 Conclusions

## Contents

9.1	Feasibility of the new unidirectional semi-immersion test (Chapter 4) .....	187
9.2	Macroscopic and microscopic findings (Chapter 5 and Chapter 8) .....	187
9.3	General discussion (Chapter 6 and Chapter 7) .....	189
9.4	Perspectives .....	190

The sulfate attack on cement mortars and pastes was comprehensively investigated through this thesis. A better understanding of the whole degradation process was obtained by the application of the unidirectional semi-immersion approach. Fundamental insights on the interaction between chemical sulfate attack and salt crystallization attack were obtained with a combination of experimental testing and thermodynamic modeling. The objectives of the thesis were achieved and the main conclusions are presented here, according to the research questions which were raised from the state of the art in *Chapter 2*. Finally, perspectives are given in the end.

## 9.1 Feasibility of the new unidirectional semi-immersion test (Chapter 4)

To evaluate the viability of the proposed approach, aggressive exposure conditions were selected in *Chapter 4* and the degradation behaviours were compared between mortars and pastes. The main conclusions are the following:

- The study confirmed the layer-by-layer process. With this methodology, 4 zones were identified in both PC cement mortars and pastes: two chemical sulfate attack zones (a bottom leached zone and a densified/expanded subsurface zone), a central zone without visible damage, and a carbonated top zone susceptible to salt crystallization attack.
- The comparison between Portland cement mortars and pastes showed that the degradation follows a very similar pattern in both cases. Paste samples can be used to accelerate the degradation process.

## 9.2 Macroscopic and microscopic findings (Chapter 5 and Chapter 8)





The core of the thesis addressed in *Chapter 5* three main sets of parameters which impact the sulfate attack. *Chapter 8* showed the effect of the curing temperature on the expansion mechanism in submerged HS cement mortars. Each set of parameters were investigated to answer the research questions and the findings are summarized as follows:

1. The effect of the w/c ratio and sulfate concentration on the progressive layer-by-layer damage.
  - Sulfate ingress was very slow at w/c of 0.3 when samples are exposed to 3 g/L Na<sub>2</sub>SO<sub>4</sub> solution, no expansion and damage were detected after one year. The large expansion and cracking damage were found in the case of w/c of 0.6.
  - The extensive degradation was found to be related to the presence of gypsum.
  - The sulfate concentration is a key factor changing the latent time and the degradation extent.
2. The effect of the binder type on the degradation.

- In PC systems, the expansion and cracking from the chemical sulfate attack was the main sulfate degradation, no visible damage on the drying surface was found.
  - In SPC and LC<sup>3</sup> cement systems, spalling damage on the drying surface was observed more preferentially under a sulfate concentration of 50 g/L in constant conditions.
  - Gypsum was found in the carbonated zone of blended cement pastes, which could imply that a high sulfate concentration was reached. It shows more susceptibility to salt crystallization attack as the local chemistry is more likely satisfied.
  - In LC<sup>3</sup> cement pastes, no surface damage by sodium sulfate crystallization pressure was observed under a low sulfate concentration (3 g/L) until nearly 2.5 years of sulfate exposure.
  - In sulfate-resisting cement mortars, detectable expansion can be also measured for the samples cured at 60 °C, but only in the long term after 1.5 years in the full-immersion test.
3. The comparison of constant and cyclic exposure conditions.
- Sulfate ingress was accelerated in the cyclic exposure and the degradation progressed more rapidly.
  - The salt crystallization attack happened much faster in constant conditions compared to cyclic conditions.
  - The ultimate appearance of spalling damage is intimately related to the water adsorption and desorption. Subflorescence was found in SPC and LC<sup>3</sup> cement samples, whereas efflorescence was observed in PC and HS cement pastes.

Table 9-1 summarizes the effect of different factors involved in the whole sulfate attack degradation process. It visually presents the rankings of damage with respect to individual parameters.

Table 9-1 The rankings of sulfate degradation on two aspects – chemical sulfate attack and salt crystallization attack

Chemical sulfate attack			Salt crystallization attack	
Expansion and cracking of exposed surfaces			Spalling and efflorescence of drying surfaces	
Cement mortar	Cement paste		PC systems	Blended systems
3 g/L Na <sub>2</sub> SO <sub>4</sub> concentration	50 g/L Na <sub>2</sub> SO <sub>4</sub> concentration		High strength	Low strength
W/C=0.3	W/C=0.4	W/C=0.6	3 g/L Na <sub>2</sub> SO <sub>4</sub> concentration	50 g/L Na <sub>2</sub> SO <sub>4</sub> concentration
				
Low degree	Medium degree	High degree	No visible spalling yet	High degree of spalling
Extent of cracking damage			Extent of spalling	
				
Bottom surfaces in contact with solution			Top surfaces in contact with environment	

### 9.3 General discussion (Chapter 6 and Chapter 7)

Thermodynamic modelling was applied in *Chapter 6* to estimate the pore solution chemistry in both chemical sulfate attack and salt crystallization attack. Results were then used to evaluate the maximum saturation index with respect to ettringite in the pore solution. A general discussion was presented in *Chapter 7* to link the macroscopic and microscopic findings with other relevant physical properties. The main findings are summarized below:

- Thermodynamic modelling can be used to predict the maximum saturation index by setting an upper limit of ettringite content, which can allow the coexistence of monosulfate and gypsum. Crystallization pressure profiles from modelling and experiments were similar but with a magnitude difference.

- Porosity mainly influences the sulfate ingress and thus controls the expansion initiation. Strength plays a big role in controlling the propagation of cracking.
- Salt crystallization attack was found more susceptible in high sulfate concentration and in the blended cement samples. The high S and Na concentrations in the pore solution can explain the spalling damage from sodium sulfate crystallization. The experimental results agree with the simulation that the presence of gypsum is not only an indicator of a large expansion in the chemical sulfate attack, but also as an indicator of favourable conditions for salt crystallization attack.

## 9.4 Perspectives

The whole thesis was carried out over 4 years and provided new insights on different aspects of sulfate attacks. However, 4 years is not long enough to obtain degradation in some specific conditions which require longer-term studies. Moreover, new directions were kept out of the scope of this thesis and could include:

- The interesting observation is that blended cement samples showed negligible damage at 3 g/L sodium sulfate solution, which would benefit from monitoring for decades. This can probably give quite important insights relevant to field cases.
- Other sulfate solutions may also be interesting to be studied. The link between the type of solution and salt crystallization attack needs to be further investigated.
- Investigating the effect of the combined sulfate and chloride ions in the external solution would be of interest.
- The evaporation rate could be increased by applying an airflow system to learn more about the salt crystallization damage.
- A combination of other disturbances exists in the field, which should also be considered, such as freeze-thaw, wind, sun, rain flush, latex painting, etc. The synergetic effect on top of the salt crystallization attack may be useful to link with the spalling damage found in real situations.

# Appendix

The detailed content is included in the shared database platform at Zenodo, it can be accessed via the link below:

[www.doi.org/10.5281/zenodo.7072784](http://www.doi.org/10.5281/zenodo.7072784)



# Curriculum Vitae



**Qiao WANG**

qiao.wang@epfl.ch/mrwujiaxian@gmail.com

## PERSONAL INFORMATION

Born	15 June 1993
Nationality	Chinese, Swiss type B permit residence
Language	Chinese (native), English (fluent), French (B1)
Status	Married
Professional address	EPFL – STI – IMX – LMC – MXG 235 (Bâtiment MXG) Station 12 CH-1015 Lausanne / Switzerland
Telephone	+41 21 693 28 21
Mobile	+41 78 955 0922

## EMPLOYMENT HISTORY

2016 – 2017	Internship at China Academy of Building Research (CABR), Beijing, China <ul style="list-style-type: none"><li>• Preparation and Characterization of High Strength Wet – mixed Shotcrete</li><li>• Draftsman of Standard for test method of mechanical and physical performance on concrete, GB/T 50081-2019</li><li>• Draftsman of Natural zeolite powder used in concrete and mortar, JG/T 3048</li></ul>
-------------	--

## EDUCATION

2018 – 2022	PhD in École polytechnique fédérale de Lausanne (EPFL) Laboratory of Construction Materials (LMC), Switzerland Materials Science and Engineering
-------------	--

*Resistance of cementitious materials to sulfate attack: quantifying performance with a reliable unidirectional approach*

- 2015 – 2018      Master in Chongqing University, China  
Materials Science and Engineering  
*High performance shotcrete*
- 2011 – 2015      Bachelor in Hebei University of Engineering, China  
Inorganic non-metallic materials science and engineering
- 2005 – 2011      Primary and secondary school  
Bazhong Zhongxue (school name), Bazhong city, Sichuan province, China

#### **AWARDS AND GRANTS**

- 2019      Winning award on the 14<sup>th</sup> Chunhui Cup of Chinese overseas students on Innovation and Entrepreneurship Competition
- 2018      Four years funding from China Scholarship Council (2018–2022)
- 2017      Scholarship and excellent postgraduate student of Chongqing University

#### **PUBLICATIONS**

Published peer-reviewed journal paper

- 2018      Hong Huang, **Qiao Wang**, Xuerun Li, et al. Sulfate adjustment for cement with triisopropanolamine: Mechanism of early strength enhancement, construction and Building Materials, 2018. DOI: 10.1016/j.conbuildmat.2018.06.123.

Submitted peer-reviewed journal paper

- 2022      **Qiao Wang**, William Wilson, Karen Scrivener. Unidirectional penetration approach for characterizing sulfate attack mechanisms on cement mortars and pastes, submitted to Cement and Concrete Research.

Published peer-reviewed conference papers

- 2022                    **Qiao Wang**, William Wilson, Karen Scrivener. A novel uniaxial penetration approach to investigate sulfate attack on cement-based materials, ICRCs, Kyoto, in Japan.
- 2021                    **Qiao Wang**, William Wilson, Karen Scrivener. Unidirectional sulfate ingress in limestone calcined clay cement (LC<sup>3</sup>) pastes under cyclic exposure, Microdurability, Hague, in Netherlands.
- 2021                    **Qiao Wang**, William Wilson, Karen Scrivener. Investigating dual sulfate attack mechanisms using unidirectional penetration approach, ICCM, Toulouse, in France.
- Patent
- 2018                    A New High Strength and Low Rebound Rate Shotcrete and placement Technology (In China)

**PROFESSIONAL MEMBERSHIPS**

- 2021                    Member of RILEM TC 285 TMS
- 2021                    Member and subgroup leader of RILEM TC 298 EBD

**INTERESTS**

Sing,  
Hip-pop dance,  
Hiking,  
Biking,  
Badminton,  
Table tennis.